TUM

Modeling Extraction for Better Taste and Aroma: Espresso Coffee Extraction and Supercritical Fluid Extraction

Verena Bernadette Pannusch

Complete reprint of the dissertation approved by the TUM School of Life Sciences

of the Technical University of Munich for the award of

Doktorin der Ingenieurwissenschaften (Dr.-Ing.).

Chair: Prof. Dr.-Ing. Marius Henkel

Examiners:

    1.   Prof. Dr.-Ing. Heiko Briesen

    2.   Prof. Dr.-Ing. Mirjana Minceva

The dissertation was submitted to the Technical University of Munich on 02.02.2024

and accepted by the TUM School of Life Sciences on 21.06.2024.

Abstract

Extraction represents an important process to separate value-adding food and beverage ingredients from plants. Among the most common *green* extraction methods are aqueous solid-liquid extraction and supercritical fluid extraction. From an engineering perspective, optimization of efficiency and product quality is the main goal. State-of-the-art research in this field focused so far on maximizing the yield of total extract or selective extraction of bioactive compounds. There is, however, a lack of knowledge when it comes to the question of how different operating conditions influence the ratio of taste- and odor-active molecules contributing to human sensory perception. Although mechanistic modeling of the extraction process has been shown to accurately describe the extraction kinetics of solutes, little is known about the relation between operating conditions and model parameters and just as little about how the extraction kinetics and the sensitivity towards operating conditions vary for different molecules.

In this publication-based dissertation, mechanistic modeling of extraction processes combined with parameter estimation was applied to predict the extraction kinetics of different key components contributing to the taste and aroma of the extract. Two common use cases were investigated: (1) espresso coffee extraction (articles 1, 2, and 3), and (2) supercritical CO_2 extraction of essential oil from hops (article 4). In both processes, a solvent flows through a packed bed by forced convection; the variable operating conditions to be controlled are temperature, flow, pressure, and the properties of the solid material, i.e., particle size distribution and swelling. The latter was elucidated in the first article, which proved the occurrence of swelling and particle erosion during coffee extraction. Microscopic images revealed a quick progression of swelling when particles are surrounded by laminar flow at extraction temperature. In the second article, the extraction kinetics of caffeine, trigonelline, chlorogenic acid, and total dissolved solids were examined experimentally for different flow rates ranging from 1 to 3 mL s^{-1} and for temperatures between 80 and 98 °C. Based on the results, a mechanistic model was developed and parameterized in article no. 3 and a new espresso brewing control chart was presented. The fourth article about supercritical CO_2 extraction from hops deals with predicting the yield of seven volatile aroma components under different temperature (40-50 °C) and pressure (90-110 bar) conditions. The results of that study showed that modeling enables the manipulation of the ratio of the dominant aroma components β-myrcene and α-humulene and thereby optimizing the process toward a target flavor.

The high predictive performance of the presented models with respect to both types of extraction processes underlines the applicability of mechanistic modeling for optimization and process development as well as the transferability to other extraction processes and raw materials.

Zusammenfassung

Extraktion stellt einen wichtigen Prozess zur Abtrennung wertgebender Inhaltsstoffe für Lebensmittel und Getränke aus Pflanzen dar. Zu den am häufigsten verwendeten *grünen* Extraktionsmethoden zählen die wässrige Fest-Flüssig-Extraktion und die Extraktion mittels überkritischen Fluiden. Von einem ingenieurwissenschaftlichen Standpunkt aus ist die Optimierung von Effizienz und Produktqualität das Hauptziel. Die moderne Forschung auf diesem Gebiet konzentrierte sich dabei bisher auf die Maximierung der Extrakt-Ausbeute oder der selektiven Extraktion bioaktiver Verbindungen. Wissenslücken bestehen jedoch im Hinblick auf die Frage wie unterschiedliche Prozessbedingungen das Verhältnis geschmacks- und geruchsaktiver Moleküle beeinflussen, welche maßgeblich an der humansensorischen Wahrnehmung beteiligt sind. Obwohl gezeigt werden konnte, dass die mechanistische Modellierung des Extraktionsprozesses sich für die Beschreibung der Extraktionskinetik von Gelöststoffen eignet, ist wenig über die Zusammenhänge zwischen Prozessbedingungen und Modellparametern bekannt und ebenso wenig darüber, wie sich die Extraktionskinetiken und die Sensitivität gegenüber den Prozessbedingungen für verschiedene Moleküle unterscheiden.

In dieser publikationsbasierten Dissertation wurde mechanistische Modellierung von Extraktionsprozessen, kombiniert mit Parameterschätzung, dazu genutzt die Extraktionskinetiken verschiedener Schlüsselkomponenten, die zum Geschmack und Aroma des Extrakts beitragen, vorherzusagen. Zwei übliche Anwendungsfälle wurden behandelt: (1) Espresso-Kaffee-Extraktion (Artikel 1, 2 und 3) und (2) Extraktion ätherischer Öle mittels überkritischem CO_2 aus Hopfen (Artikel 4). Bei beiden Prozessen durchströmt ein Lösemittel ein Festbett durch erzwungene Konvektion; die variablen zu steuernden Betriebsbedingungen sind dabei die Temperatur, die Durchflussrate, der Druck und die Eigenschaften des Feststoffes, z. B. Partikelgrößenverteilung und Quellvermögen. Letzteres wurde im ersten Artikel durchleuchtet, in dem das Auftreten von Quellung und Partikelerosion während der Extraktion nachgewiesen wurde. Mikroskopische Aufnahmen ergaben einen schnellen Verlauf der Quellung bei laminarer Strömungsumgebung und Extraktionstemperatur. Im zweiten Artikel wurden die Extraktionskinetiken von Koffein, Trigonellin, Chlorogensäure und der Gesamtmenge an Gelöststoffen experimentell für unterschiedliche Durchflussraten von 1 bis 3 mL s^{-1} und Wassertemperaturen zwischen 80 und 98 °C untersucht. Auf der Grundlage dieser Ergebnisse wurde in Artikel Nr. 3 ein mechanistisches Modell entwickelt und parametriert und ein neues Steuerungsdiagramm für die Espressozubereitung präsentiert. Der vierte Artikel zur Extraktion mittels überkritischem CO_2 aus Hopfen beschäftigt sich mit der Vorhersage der Ausbeute von sieben flüchtigen Aromastoffen bei unterschiedli-

chen Temperaturen (40-50 °C) und Drücken (90-110 bar). Die Ergebnisse dieser Studie zeigten, dass Modellierung die Möglichkeit bietet, das Verhältnis der dominanten Aromastoffe β-Myrcen und α-Humulen gezielt zu verändern und damit den Prozess hinsichtlich eines Ziel-Aromaeindrucks zu optimieren.

Die hohe Vorhersagegenauigkeit der präsentierten Modelle für beide Extraktionsprozesse unterstreichen die Anwendbarkeit mechanistischer Modellierung zur Optimierung und Prozessentwicklung sowie die Übertragbarkeit auf diverse Extraktionsprozesse und Rohmaterialien.

Danksagung

Hinter einem persönlichen Erfolg steckt aus meiner Sicht nie nur die Leistung einer einzelnen Person, sondern auch all derer, die zur Umsetzung und zum Erfolg der Arbeit beigetragen haben. In erster Linie danke ich hochachtungsvoll meinem Doktorvater und Mentor Prof. Heiko Briesen, der mir die Möglichkeit zur Promotion gegeben hat und mich während der gesamten Zeit stets auf professioneller und persönlicher Ebene exzellent unterstützt hat. Vor allem danke ich Heiko für sein wertschätzendes Feedback, das mich immer wieder motiviert hat am Ball zu bleiben. Außerdem danke ich Prof. Mirjana Minceva für ihre überragende Unterstützung bei der Anfertigung unserer gemeinsamen Veröffentlichungen sowie bei der Zusammenarbeit im Forschungsprojekt. Heikos und Mirjanas hohe Zuverlässigkeit und Sorgfalt beim Korrekturlesen sowie ihre Hilfsbereitschaft in sämtlichen Angelegenheiten verdienen meinen allergrößten Dank und Respekt. Auch meinem Mentor Luciano Navarini danke ich für den wertvollen fachlichen Austausch und die Bereitschaft zur Mentorschaft.

Meinen Teamkolleg*innen Benedikt Schmieder, Nina Cleve und Jan Mühlenweg danke ich von Herzen für die Leidenschaft und Aufopferungsbereitschaft, mit der sie sich in unserem gemeinsamen Projekt eingebracht haben. Die Zusammenarbeit mit ihnen hat mir großen Spaß gemacht und mich immer wieder motiviert und inspiriert. Ein besonderer Dank gilt außerdem meinem Betreuer und Kollegen Michael Kuhn. Zum einen wäre ohne Michael das Forschungsprojekt zur Kaffeeextraktion wohl nicht zustande gekommen. Michael ist aber auch bereits seit meiner Bachelorarbeit, die er nebenbei hervorragend betreut hat, ein Vorbild für mich gewesen und hat mich zur Arbeit in der Forschung inspiriert. Während der Doktorarbeit hatte er für mich immer ein offenes Ohr und mir insbesondere den Einstieg in die Thematik dank seiner Erfahrung und Hilfsbereitschaft erleichtert. Des Weiteren danke ich all den (ehemaligen) Student*innen, die mich mit besonderem Fleiß unterstützt haben: Lara Vannieuwenhuyse, Lukas Viebahn, Charlotte Deffur, Abror Yakubov, Chams-Eddine Bouaziz, Amelie Ochs, Deborah Kracheletz, Moritz Aulepp, Nicolas Salcedo Prieto, Stefan Lang, Ingrid Nono Nougang und Linshuo Du. Auch wenn hier nicht namentlich genannt, danke ich natürlich auch den Student*innen, die von meinen Kolleg*innen Benedikt, Nina und Jan betreut wurden und zum Erfolg unseres Gemeinschaftsprojekts beigetragen haben. Selbstverständlich danke ich auch all meinen Kolleg*innen am Lehrstuhl für Systemverfahrenstechnik: den wissenschaftlichen Mitarbeitern, den Labormitarbeitern, den Mitarbeitern der Werkstatt, der IT, des Projektmanagements und der Teamassistenz. Das positive Arbeitsklima sowie die gemeinsamen Mittagspausen, Ausflüge und Feste haben mir ei-

nen unvergesslich schönen Lebensabschnitt ermöglicht, auf den ich gerne zurückblicke.

Zu guter Letzt möchte ich den wichtigsten Menschen in meinem Leben danken, durch die ich der Mensch geworden bin, der ich heute bin: meinem Ehemann Philipp, meinen Eltern Ursula und Peter und meiner Schwester Patricia. Philipp war während dieses nervenaufreibenden Abenteuers Doktorarbeit (und natürlich weit darüber hinaus) immer mein rettendes Ufer und treuer Gefährte. Er hat mich getröstet und aufgerichtet, wenn ich frustriert war, mir in den schwierigsten Phasen Mut und Selbstvertrauen geschenkt und mich zum Lachen gebracht, wenn ich mal wieder alles zu ernst genommen habe. Ich kann in Worten nicht ausdrücken, wie dankbar und glücklich ich bin dich, lieber Philipp, an meiner Seite zu haben. Weiterhin danke ich meiner Mutter Ursula und meinem Vater Peter, auf die ich immer zählen konnte und die immer für mich da waren, egal ob wir Erfolge gefeiert haben oder ich mit Schwierigkeiten zu kämpfen hatte. Ich bin euch beiden unendlich dankbar, dass ihr mein Leben lang immer an mich geglaubt habt, mir den Rücken gestärkt habt und mir Vertrauen und Fürsorge geschenkt habt. Zum Abschluss danke ich meiner lieben Schwester und Seelenverwandten Patricia, die mir unglaublich viel bedeutet und mit der ich über alles reden kann. Ich blicke mit einem breiten Lächeln auf all die gemeinsamen Mittagspausen am Campus zurück und auf unsere langen Gespräche und Spaziergänge, die mir aus sämtlichen Motivationstiefs geholfen haben. Du hast mich gelehrt achtsam mit mir selbst zu sein und bist immer für mich da, wenn ich Hilfe brauche.

Danke!

„So thank you for taking a chance on me
I know it isn't easy
But I hope to be worth it."
Imagine Dragons – *„Next To Me"*

Table of Contents

List of Abbreviations

T

1 Motivation

Extraction from solid plant material is a widely applied process in the food and beverage industry. It is used to either isolate desired food and beverage ingredients and additives, bioactive compounds, and flavors or to remove undesired compounds such as contaminants or off-flavors from agricultural crops (Tzia 2003, p. 172). Previous research has been focusing on maximizing the yield of target compounds or groups of compounds such as proteins and vegetable oils (Tzia 2003, pp. 172–175), flavors and aroma compounds (Capuzzo et al. 2013; Saffarionpour and Ottens 2018), and bioactive compounds with health-promoting properties (Chemat et al. 2020; Wijngaard et al. 2012). In the case of solid-liquid extraction, maximizing the yield of a specific compound can be achieved by proper grinding of the solid material, the selection of a suitable solvent, an adequate process temperature and pressure, and the modification of flow (percolation or immersion, flow rate, etc.) (Tzia 2003, p. 170). Novel processes additionally incorporate technologies enhancing mass transfer such as microwaves, ultrasound, and high-speed mixers (Chemat 2015, pp. 115–122). Regarding supercritical fluid extraction which is predominantly used for the extraction of aroma and flavors, the main process variables are the selection of the solvent, the operating pressure and temperature, the mass flow rate, and the properties of the solid material (bulk density, pre-treatment, grind size) (Tzia 2003, p. 171). Although maximizing yield is often the highest aim from an economical perspective, it does not always suffice for optimal process performance when the extract, a multi-component mixture, is used as a food ingredient or beverage without any further purification or separation. Additional requirements need to be met in that case including (1) food safety, (2) the preservation of health-promoting substances, and (3) reaching a desired sensory quality. Health hazards and environmental concerns of organic solvents have been encouraging process engineers in the past decades to transfer to "green" solvents like water or carbon dioxide. Both solvents exhibit GRAS (generally recognized as safe) status, which means that they do not harm the human body when consumed, and are hence not subject to any limit of intake. On top of the requirement of safety, preserving essential vitamins and antioxidants induces limits to the use of high temperatures. Processes need to be operated below temperatures at which valuable compounds would start to degrade or harmful compounds would be formed, which mostly limits the range of applicable temperatures to low or moderate temperatures below 100 °C. Beside food safety and nutritional value, the aspect of sensory quality is of particular interest in food engineering because taste and aroma is a key buying criterion and determines the value and acceptability of a product. Common human sensory tests are done by a trained sensory

panel and are evaluated by multivariate analysis (Stampanoni Koeferli et al. 1998). Optimizing taste by means of selecting the right operating conditions is, however, a challenging task due to the high complexity and subjectivity of human sensory perception, which makes the results strongly dependent on the panel constitution and performance. To substitute sensory analyses, the ratio of key compounds contributing to taste and odor can serve as a target variable. With regard to the aroma, e. g., a recombination of key aroma compounds could be shown to closely imitate the aroma of real coffee extract (Kirsch 2019), which demonstrates the applicability of this approach. Optimizing the extraction process with respect to those key taste- and aroma-active compounds, thus, represents an alternative to conventional sensory studies and may improve the predictability of the extraction process in terms of product sensory quality.

Prediction, optimization, and control of extraction remains to be a trial-and-error procedure if mathematical models are lacking that describe the system's physics. Mechanistic modeling offers the possibility to describe the transport phenomena of extraction processes and hence to predict mass transfer rates and yield of key compounds in dependence of the process variables. Combining experiments with mechanistic modeling can support the process understanding and may help to overcome challenges on the way towards taste-optimal processes. This particularly applies to processes that are characterized by simultaneous extraction of desired and undesired compounds, e.g., nutrients or pleasant aroma compounds vs. bitter compounds or off-flavors. Coffee is a prime example of this issue as the sensory quality of a coffee beverage is a complex balance of bitter, sour, and astringency intensity as well as an aroma balance of various impressions like "roasty", "caramel-like", "fruity", or "cocoa-like". Only slight perturbations from the ideal balance can reduce consumer acceptance. Furthermore, an important prerequisite for model-based process optimization is the existence of tunable process variables that are suitable for manipulating the content of key flavors. Supercritical fluid extraction is a prime technology for this purpose. By controlling pressure and temperature, the fluid density and viscosity are manipulated, which enables a more selective dissolution and extraction of specific molecules. The idea arises that not only essential oil can be isolated at higher purity (van Opstaele et al. 2012a) but also that its composition and aroma profile can be tuned towards certain notes (van Opstaele et al. 2012b).

This thesis aims at modeling and investigating the extraction kinetics of key taste- and aroma-active compounds in dependence of the process variables to predict the dynamic change of the extract composition during process time. Two characteristic use cases are investigated: coffee extraction, a typical example for solid-liquid extraction, and

supercritical CO_2 extraction of essential oil from hops. Regarding coffee extraction, the scope of this thesis is limited to espresso coffee extraction as it is to date much less understood than immersion brewing and still has potential for optimization. An appropriate description of the process by a mathematical model including the effects of process variables on the model parameters is an important step to pave the way for optimization and optimal control. The thesis begins with a literature review on solid-liquid extraction and supercritical fluid extraction (basics and models), followed by the methodologies of experiments, simulations, and parameter estimation. The results comprise the summaries of four research papers added, which can be found in Appendix B, and are followed by a discussion, conclusion, and outlook.

2 State of Knowledge

2.1 Solid-Liquid Extraction

The following section focuses on the general aspects and modeling of solid-liquid extraction with a final focus on espresso coffee extraction. For theoretical background on supercritical fluid extraction, the reader is referred to Section 2.2, which deals with supercritical fluid extraction with the same structure of content as done in this section. Solid-liquid extraction is a process with a long history and is commonly applied in the food industry to isolate food components from solid plant matrices. The origins of this process date back to the Bronze Age in around 3500 BC (Chemat 2015, p. 102). Solid-liquid extraction involves the dissolution and mass transfer of solutes into the liquid solvent with the rate-controlling mechanism usually being the liquid-phase diffusive transport in the pore space of the solid plant material (Tzia 2003, p. 37). Common examples for the application in foods are the extraction of "sucrose in cane or beets, lipids from oilseeds, proteins in oilseed meals, phyto-chemicals from plants, and functional hydrocolloids from algae" (Tzia 2003, p. 35). Further applications are the production of beverages like coffee and tea as well as the extraction of bioactive pharmaceuticals or nutraceuticals (Chemat 2015, p. 102) and the removal of contaminants or toxins (Tzia 2003, p. 35). In the field of application for food and beverages, common solvents are water, ethanol, hexane, and CO_2 with a trend towards natural and harmless solvents like water, water-ethanol mixtures, and CO_2 (Tzia 2003, pp. 35–36).

2.1.1 Process Variables of Solid-Liquid Extraction

When designing a solid-liquid extraction process, there are some general aspects to consider for ensuring high yield and product quality. Those considerations include the type of equipment, the type of solvent, and the mechanical and thermal treatment of both solvent and solid.

I.   Choice of Equipment

First, an appropriate method and type of equipment needs to be selected starting with the decision for a batch vs. a continuous process. Batch processes are usually classic maceration processes in which the solid and liquid are mixed in a stirred vessel until concentration equilibrium is reached and the solid is subsequently separated by filtration. This type of process is often conducted in a multi-stage manner where fresh solvent is added in each step to allow full leaching (Chemat 2015, p. 105). In continuous

processes, in contrast, the solid and liquid are transported with a specific throughput, either in cocurrent or countercurrent direction. Continuous processes result in shorter extraction times than when using batch processes. The contact between solid and liquid can be either an immersion type with the solid dispersed in the liquid (transported for example by screw conveyors) or a percolation type where the solid material is arranged as a fixed bed and perfused by the liquid (Chemat 2015, p. 106). In this thesis, espresso coffee extraction is investigated which can be classified as a small-scale percolation batch processes.

II.   Solubility and Operating Conditions

The solvent needs to be selected carefully taking into account the following criteria as described in (Tzia 2003, p. 37): (1) Solubility: the compounds to be extracted must be miscible in the solvent according to the principle "likes dissolves like" (Zhuang et al. 2021). In coffee extraction, only hydrophilic components including carbohydrates, acids and alkaloids are dissolved in water, whereas hydrophobic lipids are extracted as emulsified droplets (Illy and Viani 2005, pp. 292–293) at relatively low yield (Moeenfard et al. 2015). (2) Recovery: if partial or complete removal of the solvent is required after extraction, the enthalpy of vaporization and vapor pressure must be taken into consideration. This aspect would be of interest for instant coffee production where extraction is followed by drying but it is not relevant for this thesis as no subsequent separation of the solvent is desired. (3) Interfacial tension and viscosity: those properties determine the wetting behavior and the penetration of pores which can additionally result in swelling of the plant matrix. In this thesis, the change of these properties with temperature are of special interest which is part of our model presented in Section 4.3. (4) Safety and environmental aspects such as toxicity, chemical inertness, flammability, environmental impact, and cost. Bottled mineral water was used for espresso coffee extraction in this thesis which is safe and harmless for people and environment and available at low cost (depending on the desired water quality).

As in many other food processes, the operating temperature is an essential factor for solubility. Depending on the molecule, a change in temperature leads to a change in its solubility (Tzia 2003, p. 170). In coffee extraction, for instance, the solubility of many compounds increases with a rise in temperature (Angeloni et al. 2019). Moreover, temperature influences the density and viscosity of a liquid, which can improve wetting and mass transfer. Nevertheless, a too high temperature should often be avoided due to possible negative effects like simultaneous extraction of undesirable solutes, or degradation and evaporative loss of sensitive and volatile target components (Tzia 2003,

p. 170). With regard to espresso extraction, e.g., Andueza et al. (2003) reported an increase of caffeine concentration with water temperature but a decrease of chlorogenic acid and trigonelline concentration (two major compounds in coffee) with an increase above 92 °C, which the authors attributed to thermal degradation of the molecules. Although the effect of water temperature on espresso coffee extraction has been studied in the past showing an increase of several solutes with a rise in temperature (Andueza et al. 2003; Albanese et al. 2009) as well as effects from applying temperature gradients (Salamanca et al. 2017), recent studies reported inconsistent or no influences of water temperature on solute extraction and taste (Batali et al. 2020; Angeloni et al. 2023). Unveiling the role of water temperature in coffee extraction physics, hence, is one of the main goals of this thesis.

III. Preparation of Solid Material

Another important aspect is the preparation and prior treatment of the solid material. Before extraction, the plant seeds or leaves are subjected to comminution by grinding, crushing, cutting, or flaking (Tzia 2003, p. 170). This size reduction and partial breakage of plant cells constituting the seeds or leaves is critical as it increases the surface area of the solid material and the access to intracellular solutes resulting in shorter extraction time and higher yield. Grinding too fine, on the other hand, can be problematic for filtration because smaller particles often exhibit a higher packing density which is mostly accompanied by smaller channels and hence lead to a strong increase in hydraulic resistance. Espresso coffee extraction, e.g., is strongly influenced by the grind size where recent studies have shown that too fine grinds can lead to partial blocking and inhomogeneous flow resulting in lower yield (Cameron et al. 2020). To prevent such difficulties, a compromise must be found between high surface area and filterability. Additionally, natural ground plant materials usually exhibit a broad and multimodal size distribution of non-spherical porous particles. Therefore, not only the mean particle size must be taken into consideration but also the fractions of different fine and coarse particles as well as their sphericity and porosity. The influence of different grind levels (same grinder, different settings from fine to coarse) on the extraction kinetics of representative compounds in espresso brewing is investigated in this thesis. To evaluate the effects of particle surface area and contact time separately, the flow was decoupled from the grind size by flow rate control through the pump.

IV. Flow Rate and Extraction Time

There is one more criterion to be considered when working with percolation extraction processes: the flow through the porous fixed bed. When percolation is only driven by

gravitation, the contact time between solvent and solid material depends solely on the packed bed permeability, i.e., the higher the permeability, the shorter the contact time for a certain amount of solvent. If an additional pressure gradient is applied by a pump, the pump capacity and control together with the bed permeability determine the flow rate. The flow rate influences the contact time between solid and liquid and the external mass transfer rate from the surface of particles into the fluid. It should be high enough to accelerate molecular diffusion from the particle surface into the bulk fluid phase but also low enough to allow sufficient contact time regarding intra-particle diffusion limitation. Coffee bed permeability has been in the focus of previous espresso coffee research (Corrochano et al. 2015; Vaca Guerra et al. 2023b), which demonstrated its high complexity in espresso coffee. Due to the high variability, difficult prediction, and time-dependence of permeability, we pursued a different approach in this thesis than usually practiced in espresso brewing: the flow rate was maintained by adjusting the pump pressure and thus different extraction times could be evaluated for the same grind.

2.1.2 Mathematical Modeling of Solid-Liquid Extraction

In the scope of this doctoral thesis, batch-wise extraction by percolation is investigated. The relevant mass transport phenomena in this process are (I) intra-particle diffusion and (II) convection.

Target molecules are initially located either inside the parenchyma cells (storage cells) of the plant tissue or in the intercellular space between cells (Tzia 2003, p. 38; Britannica 2019). Due to the low permeability of intact cell walls, diffusion is slow inside the plant tissue, especially for large molecules (Tzia 2003, p. 38). By breakage and disruption through grinding, a larger fraction of the molecules is extracted more quickly from broken cells located at the particle surface, thereby increasing the overall mass transfer rate and yield (Tzia 2003, p. 38); this decrease in diffusion resistance by reducing the grind size has been demonstrated, e.g., for caffeine extraction from roasted coffee (Spiro and Selwood 1984). Scanning electron microscopy images revealed those broken cells at the particle surface of ground coffee (Corrochano 2015, p. 110). Hence, extraction from ground plant tissue can involve both extraction from broken cells at the surface of the ground plant tissue and extraction from intact cells via hindered liquid-phase diffusion. In the beginning of extraction, the plant material is wetted by the solvent. A network of conducting tissue called phloem and xylem (serve the plant as transport channels for nutrients and water, respectively (Britannica 2022; Petruzzello 2023)) facilitates the solvent uptake so that the solvent can penetrate the solid by capillary forces and pressure gradients. Mechanical relaxation of cell walls due to swelling

can furthermore accelerate the distribution of the solvent in the plant matrix. The step of wetting including the replacement of air by the solvent and swelling of the tissue is a very complex multi-phase process and strongly depends on the composition of the biological material. Thus, the initial state of an extraction model is assumed to be fully saturated and that all pores are filled by the solvent at the beginning of the process. Accordingly, intra-particle mass transport happens by molecular diffusion in the liquid through the cellular pore network, the driving force being the concentration gradient between the solvent bulk phase surrounding the particle and the particle center. An illustration of the mass transport phenomena in solid-liquid extraction from ground plant tissue at the scale of a single particle is provided in Figure 2.1. The path of a solute from a plant cell to the solvent bulk phase is indicated by arrows and involves internal diffusion, adsorption, external diffusion, and convection. If additional liquid phases, that are not miscible with the solvent, are at a mass fraction low enough to be disregarded, the system can be described as a porous two-phase system as follows. The two phases are: (1) the solid phase s (liquid phase in the pore space of the solid particles) and (2) the liquid phase l (liquid phase in the pore space between the particles). The reader is advised that mass transport in the solid phase is usually assumed to occur in the liquid filling the pore network of the solid plant tissue and not in the solid material itself.
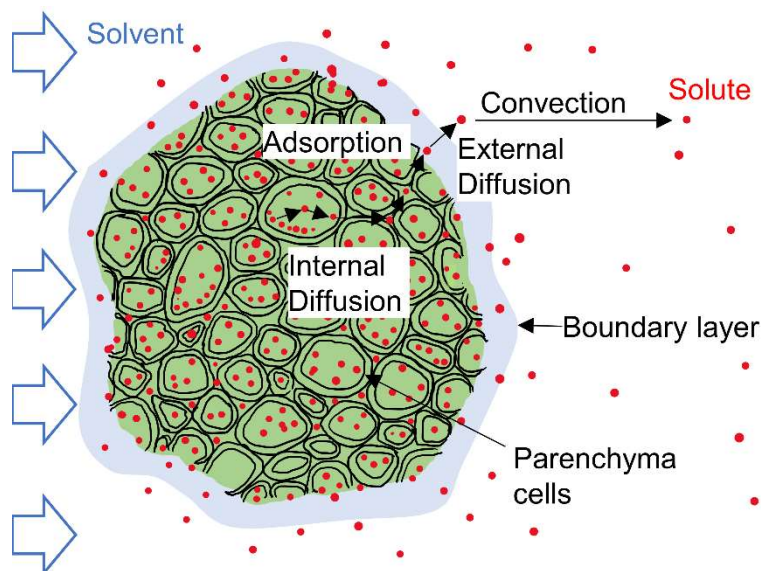
Figure 2.1. Illustration of solute mass transport phenomena in solid-liquid extraction from ground plant material.

The general model for solid-liquid percolation extraction including the transport phenomena illustrated in Figure 2.1 is shown below in Eq. 2.1.1 to Eq. 2.1.5. A detailed derivation of this multi-scale model is provided in Appendix A. Eq. 2.1.1 and Eq. 2.1.2 represent the mass balances of a solute in the liquid phase and in the solid phase, re-

spectively. Liquid-phase transport phenomena (Eq. 2.1.1) include mass transport by convection (first term on right-hand side) in the direction of flow z and longitudinal dispersion (second term on right-hand side) as well as mass transport by longitudinal diffusion (third term on right-hand side). Solid-phase transport phenomena (Eq. 2.1.2) are limited by radial diffusive transport in the particle from the center. Both equations are coupled by the boundary condition at the particle surface ($r = R$) shown in Eq. 2.1.3, which assumes equal flux in both phases at the interphase. Eq. 2.1.4 and Eq. 2.1.5 show the boundary conditions for the radial particle coordinate r and for the unidirectional water flow z. The latter is the Danckwerts boundary condition and means that convective flux equals diffusive flux across the inlet plane (z = 0). When longitudinal dispersion can be disregarded, the concentration at the inlet simplifies to $\bar{c}_i^l(z = 0) = 0$. The meanings of symbols and respective units are included in Table 2.1.

$$\varepsilon \frac{\partial \bar{c}_i^l}{\partial t} = -\varepsilon \left(v_{l,z} \frac{\partial \bar{c}_i^l}{\partial z} - D_L \frac{\partial^2 \bar{c}_i^l}{\partial z^2} \right) + D_{i,eff,b} \frac{\partial^2 \bar{c}_i^l}{\partial z^2} + a_V k_{sl} \left(K_i \bar{c}_i^s|_R - \bar{c}_i^l \right) \qquad \text{Eq. 2.1.1}$$

$$\phi \frac{\partial \bar{c}_i^s}{\partial t} = \frac{D_{i,eff}}{r^2} \frac{\partial}{\partial r} \left(r^2 \frac{\partial \bar{c}_i^s}{\partial r} \right) \qquad \text{Eq. 2.1.2}$$

$$-D_{i,eff} \frac{\partial \bar{c}_i^s}{\partial r}|_{r=R} = a_v k_{sl} \left(K_i \bar{c}_i^s|_R - \bar{c}_i^l \right) \qquad \text{Eq. 2.1.3}$$

$$\frac{\partial \bar{c}_i^s}{\partial r}|_{r=0} = 0 \qquad \text{Eq. 2.1.4}$$

$$v_{l,z} \bar{c}_i^l - D_L \frac{\partial \bar{c}_i^l}{\partial z} - D_{i,eff,b} \frac{\partial \bar{c}_i^l}{\partial z} = 0 \ , \ z = 0 \qquad \text{Eq. 2.1.5}$$

$$\frac{\partial \bar{c}_i^f}{\partial z}|_{z=L} = 0 \qquad \text{Eq. 2.1.6}$$

Different simplifications and extensions can be done to the model above depending on its application. Those are elaborated in the subsequent section for espresso coffee extraction, the solid-liquid application of interest in this thesis.

Table 2.1. List of model symbols.

Symbol	Description	Dimension
$\overline{c}_i^{\,l}$	Intrinsic average concentration of a solute i in the liquid phase l	$M\,L^{-3}$
$\overline{c}_i^{\,s}$	Intrinsic average concentration of a solute i in the pore liquid of solid phase s	$M\,L^{-3}$
t	Time	T
z	Coordinate in flow direction	L
r	Radial coordinate of solid particles	L
$v_{l,z}$	Average velocity of liquid phase l in z direction	$L\,T^{-1}$
ε	Bulk porosity of packed bed	1
ϕ	Particle porosity	1
$D_{i,eff}$	Effective diffusion coefficient of solute i in porous particles	$L^2\,T^{-1}$
$D_{i,eff,b}$	Effective diffusion coefficient of solute i in packed bed	$L^2\,T^{-1}$
D_L	Longitudinal dispersion coefficient	$L^2\,T^{-1}$
k_{sl}	Mass transfer coefficient of solute i at the solid-liquid interface	$L\,T^{-1}$
K_i	Solid-liquid phase distribution constant of solute i	1
a_V	Volume-specific surface area of solid-liquid interface	L^{-1}
R	Average particle radius	L
L	Packed-bed height	L

2.1.3 Espresso Coffee Extraction Modeling

Modeling the extraction kinetics of different components is particularly useful when the ratio or balance of those components influence the sensory quality of the product. A prime example of this problem is espresso coffee extraction. Whether a consumer likes or dislikes the extracted beverage strongly depends on the balance of bitter and sour taste as well as on the overall taste and aroma intensity. Unsurprisingly, mechanistic modeling of espresso extraction has become a topic of high interest in the past decade as it is expected to contribute to innovations in the development of espresso machines. Mathematical modeling of the percolation extraction process supports the understanding of physical transport phenomena, which enables engineering of the process on a theoretical basis rather than applying trial-and-error strategies. This will enable manufacturers of espresso machines and users to standardize operating conditions appropriately and counteract variations in coffee quality. Especially in fully automated machines, simulation data can be applied and be used for optimizing machine programs.

The timeline of espresso extraction modeling up to date can be divided into three phases: Phase 1: First mass balance equations and model assumptions were developed and validated by extraction kinetics data of total dissolved solids (TDS, total mass of solutes). Phase 2: Different representative single components and intragranular diffusion were taken into consideration. Phase 3: Models were modified for investigating

different extraction process variables. Table 2.2 gives a chronological overview of existing espresso extraction models as well as some key aspects for comparison including the transport phenomena considered, the experimental data used for parameter estimation, and the process variables investigated where applicable.

Before the 21st century, coffee extraction was majorly modeled for infusion brewing rather than for percolation like espresso extraction. The first researchers presenting an espresso coffee extraction model were Fasano et al. (1992). They developed a convection-diffusion model for the liquid phase and described the interphase mass transfer by a first-order kinetic. In their further studies, they assumed that fine particles were carried with flow to the bottom of the filter basket where those particles formed a compact layer (Fasano and Talamucci 2000a, 2000b). They extended their model accordingly by distinguishing between the main packed bed and a compact layer at the bottom where diffusion phenomena occurred besides convection. Some drawbacks, however, limited the applicability of the model including the lack of experimental extraction kinetics data for validation, the scarcity of model derivations and justifications of assumptions, as well as the fact that their suggested particle migration theory was not validated experimentally by particle measurements. A first multi-scale model was presented by Melrose et al. (2012) and Corrochano (2015). They proposed a two-grain model, i.e., mass transfer was assumed to occur from particles of two characteristic grain sizes: fine and coarse. Corrochano (2015) furthermore compared modeled and experimentally obtained extraction kinetics of TDS at different particle size distributions (PSD), packed-bed densities, and flow rates. Moroney et al. (2015) presented another multi-scale model for both drip coffee and espresso extraction. They described the model derivation by volume averaging as well as their assumptions and simplifications in detail in their study. The authors leaned their one-dimensional model on a common model in supercritical fluid extraction, the Broken and Intact Cells (BIC) model by Sovová (1994). Accordingly, interphase mass transfer was assumed to occur from broken cells (fine particles) and intact cells (coarse particles) simultaneously. For the intact cells, they applied volume averaging over the particle volume, whereas interphase mass transfer from the broken cells was assumed to occur from a saturated layer on the particle surface. In a subsequent publication, Moroney et al. (2016) conducted an asymptotic analysis of the espresso model in (Moroney et al. 2015) in which longitudinal diffusion and dispersion, disregarded in (Moroney et al. 2015), were considered along with convection. Although Melrose et al. (2012), Corrochano (2015), and Moroney et al. (2015) created an important foundation for following studies, they compared their mod-

els with extraction kinetics data of TDS only, i.e., no single components were evaluated. This left potential for further improvements.

New extraction models were proposed between 2015 and 2020 introducing data of different representative single components for comparison and applying different simplifications to the general mass balance equations as well as different solution approaches. A study by Kuhn et al. (2017) compared their model with extraction kinetics data of the two components caffeine and trigonelline. Thereby, Kuhn and colleagues were the first who modeled the extraction of single components. Moreover, they investigated the effect of different PSDs obtained by sieving and different tamping forces. They showed that the ratio of caffeine and trigonelline was influenced by the PSD and that tamping force had no significant impact on the extracted concentrations of the analyzed solutes. The solution of the model was, however, strongly simplified as the liquid-phase PDE was not solved numerically but reduced to an ordinary differential equation (ODE) by assuming a linear concentration gradient in the packed bed. In contrast, a numerical solution was presented by Melrose et al. (2018) who additionally considered intragranular diffusion along the radial coordinate of fine and coarse particles as shown in Eq. 2.1.2. As already mentioned above, a downside of their study was that they investigated no single components but only TDS. Sano et al. (2019) developed a 3D model of PDEs but instead of solving the system of equations numerically, they strongly simplified their model to obtain an ODE which they solved analytically. This way, the authors circumvented the use of a mesh such as finite differences applied in (Moroney et al. 2015) and (Melrose et al. 2018). Ellero and Navarini (2019) pursued a different approach using smoothed particle hydrodynamics (SPH), a meshfree Langrangian method. Diffusion was modeled by assigning interparticle diffusion coefficients to fluid- and solid-phase particles. The extraction kinetics predicted by the model were compared to data of caffeine, trigonelline, and chlorogenic acid.

Around 2020, new extraction models focused on describing and comparing different process variables. Moroney et al. (2019) compared a conical and a cylindrical geometry of the extraction chamber as well as a single-grain vs. a two-grain model in 1D and 3D. They proved the admissibility of the reduction towards a 1D model by CFD simulations and the superiority of the two-grain model by Melrose et al. (2018) over the single-grain model. Giacomini et al. (2020) were the first who investigated the effect of water temperature and water pressure by using modeling. They compared their model predictions to caffeine and chlorogenic acids data. However, their study has two major drawbacks: (1) the process variables were related to the mass transfer rate by a mixed exponential and quadratic function without taking into consideration physical effects of

the process variables on the solute behavior like adsorption or flow-mass-transfer relations. (2) The authors did not analyze extraction kinetics of the solutes experimentally but only the concentration in a final beverage amount of 40 g in duplicate. The same applies to Cameron et al. (2020) who only measured TDS in 40 g which is insufficient when one is interested in other beverage volumes or coffee-to-water ratios. Cameron et al. examined the effects of grinding levels and coffee mass. Similar to Moroney et al. (2019), they described separate mass transfer rates for fine and coarse particles applying different surface areas estimated from experimental data. In a recent study by Angeloni et al. (2023), the same model as presented in (Giacomini et al. 2020) was used with the only difference that the correlation function for the dependence of mass transfer rate from temperature and pressure was slightly modified. The exponential term was removed from the function leaving a quadratic multilinear regression with respect to temperature and pressure. Additionally, three different grinding levels were compared, which was captured in the model by different porosity values. Although the authors investigated many components, the same drawbacks remain as stated above for (Giacomini et al. 2020) because no extraction kinetics were analyzed and the fact that experiments were done only in duplicates makes an evaluation of statistical significance difficult. Other phenomena which are suggested to contribute to extraction are swelling and mechanical erosion of coffee particles. Both might affect the porosity and permeability of the packed bed. Swelling, which leads to an expansion of particles and their pores, might additionally influence the intragranular diffusion resistance of coarse particles leading to a change in mass transfer rate. Mo et al. (2022) modeled swelling applying an SPH model and found that its influence on the space between particles could lead to an increased yield of compounds according to their simulation. In (Mo et al. 2021), the authors moreover investigated the progression of particle erosion, where fine particles are disrupted from the surface of coarse particles by flow. They found an stronger porosity increase in the lower part of the coffee bed than in the upper part and a connection to channeling which itself affects the homogeneity of flow and hence extraction. They moreover proved their findings by µ-Computed Tomography (µ-CT) scans in a recent study (Mo et al. 2023). The appearance of phenomena like swelling and particle erosion should, thus, be taken into consideration when investigating espresso coffee extraction because both phenomena might influence permeability and flow. For the purpose of capturing flow inhomogeneity caused by too fine grinding, a "two pathway model" was recently developed by Lee et al. (2023), in which flow was suggested to be split into two possible pathways with different permeability. The authors compared their simulations to the experimental data by Cameron et al. (2020) and could show that the modeled change in extraction yield with a change in grinding

level qualitatively matched experimental data. Lee et al. (2023) used the Kozeny-Carman equation for packed beds of spherical particles to determine the permeability from the bed porosity. An alternative approach considering not only the porosity but also the shape of the PSD was proposed by Vaca Guerra et al. (2023b). They developed a modified Kozeny-Carman equation by introducing a size uniformity parameter and several empirical constants which they fitted to experimental data. The good agreement between calculated and experimental permeability values achieved using their modified equation demonstrates the importance of considering not only the mean particle size but rather the shape of the PSD for understanding the impact of different grind levels on espresso extraction. In their subsequent study, Vaca Guerra et al. (2023a) proved a correlation of different compounds' extraction rate with the ratio of coarse and fine particles' mean diameters and hence an increase in the extraction rate with a rise in the specific surface area. They moreover reported a dependence of this correlation on molecular polarity as higher changes with PSD were observed for trigonelline than for the less polar compounds caffeine and chlorogenic acid. However, Vaca Guerra et al. (2023a) did not conduct mechanistic modeling to determine the extraction rates but fitted a simple hyperbolic function to their experimental data. A parameterized mechanistic model would, however, help to understand why extraction rates changed to a different extent for molecules of different polarity and to include polarity into calculations using, e.g., molecule-specific distribution constants. Mo et al. (2024) furthermore continued their research on the effect of swelling on espresso extraction. The authors incorporated a particle-level swelling model (geometric expansion resulting in changes of the intragranular and intergranular porosity) with a 1D extraction model (based on the two-grain model by Melrose et al. (2018)). Their modeling results indicated that swelling enhances the coffee yield when constant pressure control is applied and that the effect is more pronounced the finer the grinding level. However, when the flow rate is kept constant, swelling had a small effect on the yield. The authors concluded that constant flow rate control is recommendable to avoid variability from swelling in espresso preparation. Mo et al. (2024) also compared their model results with experimental TDS extraction kinetics data at different fixed flow rates and grinding levels. The yield was observed to increase slightly with a decrease in flow rate (attributed to the longer residence time), and with finer grinding (attributed to the larger specific surface area). Although the model matched experimental data well in the first half of extraction, the predicted yield deviated significantly from experiments at a beverage mass above 30 g, thus leaving space for improvement.

The contribution of this thesis to espresso extraction research can be summarized as follows:

- Investigating the occurrence and extent of swelling and particle erosion as possible influencing factors of espresso coffee extraction.

- Developing a model including the effects of the process variables water temperature, flow rate/pressure, and grind level on the model parameters.

- Validating the model for different representative components to enable a better understanding of: a) the impact of the above process variables on the beverage composition, b) the dependence of extraction on molecular properties.

- Ensuring the applicability of results for practitioners by implementing a new brewing control chart and app for espresso coffee.

Table 2.2. Espresso coffee extraction mechanistic models for simulating the concentration of solutes in the cup.

Model	Liquid-phase transport	Solid-phase transport	Interphase mass transfer	Experimental data	Extraction process variables
Fasano et al. (1992)	Convection (1D).	No intragranular diffusion.	First-order kinetic.	In-cup concentration, not presented.	Not investigated.
Fasano and Talamucci (2000a), Fasano and Talamucci (2000b)	Convection (1D) in packed bed; convection (1D) and diffusion (1D) in compact layer.	No intragranular diffusion.	Functions of flow velocity and solid-phase concentration.	Not presented.	Not investigated.
Melrose et al. (2012)	Convection (1D).	Intragranular radial diffusion (1D, sphere).	Two mass transfer rates from fine and coarse particles; $K_i = 1$.	Not presented.	Not investigated.
Corrochano (2015)	Convection (1D).	Intragranular radial diffusion (1D, sphere).	Two mass transfer rates from fine and coarse particles; K_i estimated from experiments.	Total dissolved solids (yield) extraction kinetics (0-80 s, 10 s intervals).	Particle size distribution, flow rate, bed density.
Moroney et al. (2015)	Convection (1D).	Volume average diffusion.	Mass transfer from intact-cell particles, mass transfer from broken cells, constant saturation concentration at surface of broken cells.	Total dissolved solids, extraction kinetics (0-1 kg, 30 g steps).	Not investigated.
Moroney et al. (2016)	Convection (1D), longitudinal diffusion, longitudinal dispersion.	Volume average diffusion.	Mass transfer from intact-cell particles, mass transfer from broken cells, constant saturation concentration at surface of broken cells.	Total dissolved solids, extraction kinetics (0-30 s, 15 samples).	Not investigated.

Kuhn et al. (2017)	Convection (1D), linear concentration profile along bed length assumed.	Volume average diffusion.	One mass transfer rate, K_i estimated from experiments.	Caffeine, trigonelline, extraction kinetics (0-26 s, 16 samples).	Particle size distribution, tamping force.
Melrose et al. (2018)	Convection (1D).	Intragranular radial diffusion (1D, sphere).	Two mass transfer rates from fine and coarse particles; $K_i = 1$.	Total dissolved solids, extraction kinetics (0-70 s, 7 samples).	Not investigated.
Sano et al. (2019)	Convection (3D), dispersion (3D), diffusion (3D).	Intragranular diffusion (3D).	Mass transfer from solid phase to liquid phase.	Caffeic acid (30 s, 3 s steps, 10 samples).	Not investigated.
Ellero and Navarini (2019)	Convection (3D), diffusion (3D), interparticle diffusion coefficient for liquid phase.	Intragranular diffusion (3D), interparticle diffusion coefficient for solid phase.	Interparticle release coefficient.	Caffeine, trigonelline, chlorogenic acid (0-60 s, 10 samples).	Not investigated.
Moroney et al. (2019)	Convection (1D and 3D).	Volume average diffusion.	Two mass transfer rates from fine and coarse particles; $K_i = 1$.	Total dissolved solids, extraction kinetics (0-230 s, 21 samples).	Conical vs. cylindrical extraction chamber, fine vs. coarse grinding level.
Giacomini et al. (2020)	Convection (3D), diffusion (3D), dispersion (3D).	No intragranular diffusion.	Dissolution rate (analogous to global mass transfer coefficient) as mixed exponential and quadratic function of temperature, pressure, and porosity.	Caffeine, chlorogenic acids[1], fine solid particles; no extraction kinetics but concentration in 40 ± 2mL in duplicates.	Water temperature (88, 93, 98 C), water pressure (7, 9, 11 bar), tamping force (10, 15, 20, 30 kgF).
Cameron et al. (2020)	Convection (1D), diffusion (1D).	Intragranular radial diffusion (1D, sphere) for fine and coarse particles, coupled with interphase transfer.	Two mass transfer rates: One mass transfer coefficient, two surface areas[2] for fine and coarse particles; no partition coefficient	Total dissolved solids; no extraction kinetics but concentration in 40.05 g, 5 replicates per experiment.	Grinding levels (1.1-2.3 on Mahlkoenig EK43), mass of coffee (16-24 g), water pressure (4-10 bar).

			but product of concentrations[3].		
Angeloni et al. (2023)	Convection (3D), diffusion (3D), dispersion (3D).	No intragranular diffusion.	Dissolution rate (analogous to global mass transfer coefficient) as quadratic function of temperature and pressure.	Total dissolved solids, total lipids, caffeine, trigonelline, chlorogenic acids[3], ferulic acid, acetic acid, citric acid, tartaric acid; no extraction kinetics but concentrations in 40 ± 2 g in duplicate.	Grinding levels (fine, standard, coarse), water temperature (88, 93, 98 °C), water pressure (6, 9, 12 bar), Arabica and Robusta.
Lee et al. (2023)	Convection (1D).	Volume average diffusion.	One mass transfer rate from solid phase (no distinction between coarse and fine particles); constant saturation concentration at particle surface; two flow pathways with different permeability.	Experimental data by (Cameron et al. 2020).	Grinding levels (1.1-2.3 on Mahlkoenig EK43).
Mo et al. (2024)	Convection (1D).	Intragranular radial diffusion (1D, sphere).	Two mass transfer rates from fine and coarse particles; K_i estimated from experiments.	Total dissolved solids (yield) extraction kinetics (80 g, 6 samples).	Flow rate (2, 3, 4 mL s^{-1}), grinding levels ($d_{32} = 76\ \mu m$ to $d_{32} = 201\ \mu m$).

[1] 3-caffeoylquinic acid, 5-caffeoylquinic acid, 3,5-dicaffeoylquinic acid

[2] surface area from Brunauer-Emmett-Teller isotherm but measurements unsuccessful, hence, surface areas estimated from extraction data

[3] $G_i = k\, c_{si}(c_{si} - c_l^*)(c_{sat} - c_l^*)$

2.2 Supercritical Fluid Extraction

Supercritical Fluid Extraction (SFE) has been used since the second half of the 20th century for the extraction of biomolecules from plants (Paul and Wise 1971; Schneider 1980). Fluids are at supercritical state when the operating temperature and pressure are above the critical point of the fluid in the pressure-temperature diagram (Williams and Clifford 2000, p. 2). If conditions are slightly below the critical point, the fluid is called "near-critical", otherwise the term "subcritical" is used (Williams and Clifford 2000, p. 2). Each chemical substance has a characteristic critical point, i.e., a critical temperature, pressure, and molar volume (Poling et al. 2001, p. 25). Supercritical fluids have special features in comparison to liquids making them preferable solvents for many applications. Their density (Span and Wagner 1996), viscosity (Laesecke and Muzny 2017), and dielectric constant (Hourri et al. 1998) can be tuned significantly between liquid-like and gas-like properties by only small variations of temperature and pressure. As a result, diffusion coefficients can be increased by orders of magnitude compared to the liquid state (McHugh and Krukonis 1994, p. 15). Although a variety of solvents exhibit viable critical points for supercritical applications (Tzia 2003, p. 62), supercritical carbon dioxide ($SCCO_2$) is usually the solvent of choice due to its low critical temperature of 31 °C and critical pressure of 74 bar. Moreover, it is recognized a "green" solvent, i.e., complying with the twelve principles of green chemistry (Calvo-Flores et al. 2018), and exhibits GRAS status (U. S. Food and Drug Administration 1979). An impact on climate change as a greenhouse gas can furthermore be avoided by recycling the gas using a condenser instead of emitting it to the atmosphere after use (Chemat et al. 2019). Typical applications in the food industry are the decaffeination of coffee and the processing of hops for the beer industry besides the production of flavors, specialty oils, natural pigments, and antioxidants (Tzia 2003, pp. 58–59).

2.2.1 Process Variables of Supercritical Fluid Extraction

As described for solid-liquid extraction in Section 2.1.1., also the process conditions of SFE must be selected carefully to achieve a desired product yield and quality. The main aspects to be considered and process variables to be selected when optimizing SFE processes are summarized below.

I. Choice of Equipment

SFE with $SCCO_2$ is usually a fixed-bed batch process. CO_2 gas is transformed into a liquid state by cooling, then pumped through a heat exchanger to reach the desired operating temperature, and subsequently passes an extraction vessel from bottom to

top loaded with a packed bed of the solid material (Pronyk and Mazza 2009). The pressure in the extraction vessel is controlled via a backpressure regulator at the out-flow. After $SCCO_2$ has passed the pressure regulator, the extract can either directly be collected in a collection vessel by reducing the pressure to atmospheric pressure or the $SCCO_2$-compound mixture enters one or more separators, each set to a certain pressure between operating and atmospheric pressure (Pronyk and Mazza 2009). Such downstream separators fulfill the goal of fractionating different components of the extract by making use of different molecular vapor pressures. Additional fractionation makes particular sense for applications where the target components are co-extracted with undesired components like, e.g., cuticular waxes (Baldino et al. 2018). Besides classical batch processes, continuous processes exist for large industrial scales. Those include countercurrent liquid-liquid pressurized extractors, quasi-continuous solid-liquid pressurized extractors, and continuous countercurrent solid-liquid pressurized extractors (Pronyk and Mazza 2009). Another possible extraction process type is fractional extraction using fractionation columns (Dunford and King 2000; Terada et al. 2010). Whatever pilot-scale or industrial-scale extractor is selected, experiments on a laboratory scale are always necessary to determine mass transfer limitations and phase equilibria of target compounds for the investigated plant material and to optimize operating conditions accordingly (Pronyk and Mazza 2009). Those parameters as well as lab-scale superficial velocity, flow-to-solid or solvent-to-solid ratios can then be taken into consideration for scale-up (Pronyk and Mazza 2009).

II.   Solubility and Operating Conditions

In the supercritical state, fluid properties are highly sensitive towards changes in operating temperature and pressure. Just as at liquid state, an increase in temperature causes a decrease in both density and viscosity of $SCCO_2$ whereas an increase in pressure leads to an increase in density and viscosity. Those changes of fluid properties influence the diffusivity and solubility of compounds. A change in fluid density influences intermolecular interactions between the solute and the solvent resulting in a large influence of the density on the solubility of compounds. Chrastil (1982) proposed a solubility model for different compounds depending on $SCCO_2$ density and showed good agreement with experimental values. Solubility furthermore depends on the molecular structure. Polar groups as well as C-C double bonds are known to contribute to solubility (Stahl et al. 1988; Wong and Johnston 1986). Besides solubility, extraction is limited by intragranular diffusion for which the pressure plays an important role. Raising the pressure leads to an increase in viscosity and density of $SCCO_2$. While the density reaches a value close to liquid-state CO_2, viscosity keeps below a liquid-state value,

which enhances diffusivity and motility of compounds in the pores of the plant matrix (Tzia 2003, p. 64). It therefore depends on the rate-limiting phenomenon which pressure-temperature combination is favorable for a certain target compound in a certain plant. High temperatures and pressures are often favorable for maximum yield but can lead to decomposition of sensitive aroma compounds and to co-extraction of undesired compounds, which makes a targeted selection of conditions and an understanding of the chemical structures and their sensitivities necessary.

III.   Preparation of Solid Material

Like in solid-liquid extraction, the size reduction of plant material plays an important role for successful extraction. Grinding or shredding disrupts cells and increases the surface area, thereby enhancing accessibility and mass transfer rate. The same applies as described for solid-liquid extraction in section 2.1.1: the target particle size should not fall below a critical value at which the bulk density and porosity of the packed bed would become too low resulting in flow inhomogeneity. Additionally, the type of size-reduction process such as grinding, chopping, or flaking, previous decortication as well as subsequent pelletization needs to be considered (Tzia 2003, p. 80; Ivanovic et al. 2014). The moisture content should be well controlled to avoid a barrier to diffusion for unpolar compounds on the one hand or to enable an enhanced extraction of polar compounds on the other hand (Gopalakrishnan and Narayanan 1991). Swelling of the plant material leading to a reduction in diffusion resistance should also be considered (Stamenic et al. 2010).

IV.   Flow Rate and Extraction Time

Another process variable influencing $SCCO_2$ extraction is the flow rate of the fluid. If the flow rate is sufficiently high, diffusion in the solid is rate limiting, whereas a slow flow rate in the same range as intragranular diffusion is solely limited by external diffusion within a laminar boundary layer. In the former case, an increase in flow rate would increase the extraction rate (Pronyk and Mazza 2009). This naturally only applies if flow is homogeneous. The flow rate does not only affect the mass transfer rate but also the extraction time. A flow rate that is high enough that only internal mass transfer is limiting can reduce the necessary extraction time to reach a certain yield. If neither external nor internal mass transfer are limiting, e.g., when a compound is distributed freely on the particle surface, the extraction rate can be limited by solubility only. In this case, changing the flow rate has no effect on the almost constant extraction rate. Selecting an appropriate extraction time is important to receive a satisfactory yield on the one hand and a certain composition on the other hand as extract composition changes con-

tinuously during extraction. A possibility to achieve both is fractional extraction receiving fractions with different composition (Dunford and King 2000; Terada et al. 2010).

2.2.2 Mathematical Modeling of Supercritical Fluid Extraction

The general mass transport phenomena of SFE are the same as in solid-liquid extraction. Accordingly, the general diffusion model, presented in Eq. 2.2.1 to Eq. 2.2.3 below, is based on the same mass balances as in solid-liquid extraction (Eq. 2.1.1 to Eq. 2.1.3). The only difference is that diffusion in the pore phase between particles is in general disregarded. This can be explained by a study of del Valle and Catchpole (2005) who developed a correlation for the ratio of longitudinal dispersion coefficient D_L and molecular (binary) diffusion coefficient D_i in SCCO$_2$ based on a collection of experimental data (del Valle and Catchpole 2005; del Valle et al. 2010, p. 422). They showed that the ratio of D_L/D_i increased exponentially at convection-controlled conditions (Peclet number $Pe_d > 1$) from around 1 by four orders of magnitude in the investigated range ($Pe_{d,max} \approx 1000$). Considering the fact that $D_{i,eff,b} < D_i$ and that most SFE processes are in the convection-dominant regime (del Valle et al. 2010, p. 422), diffusion in the bulk pore phase can be disregarded. The following one-dimensional model follows, which is the same as in (del Valle et al. 2010, p. 399) but with some different symbols to keep the notation consistent within this thesis:

$$\varepsilon \frac{\partial \bar{c}_i^f}{\partial t} = -\varepsilon \left(v_{l,z} \frac{\partial \bar{c}_i^f}{\partial z} - D_L \frac{\partial^2 \bar{c}_i^f}{\partial z^2} \right) + a_V \, k_{sf} \, (K_i \, \bar{c}_i^s|_R - \bar{c}_i^f) \qquad \text{Eq. 2.2.1}$$

$$\phi \frac{\partial \bar{c}_i^s}{\partial t} = \frac{D_{i,eff}}{r^2} \frac{\partial}{\partial r} \left(r^2 \frac{\partial \bar{c}_i^s}{\partial r} \right) \qquad \text{Eq. 2.2.2}$$

$$-D_{i,eff} \frac{\partial \bar{c}_i^s}{\partial r}\Big|_{r=R} = a_v \, k_{sf} \left(K_i \, \bar{c}_i^s|_R - \bar{c}_i^f \right) \qquad \text{Eq. 2.2.3}$$

The boundary conditions for $r = 0$, $z = 0$ and $z = L$ are:

$$\frac{\partial \bar{c}_i^s}{\partial r}\Big|_{r=0} = 0 \qquad \text{Eq. 2.2.4}$$

$$v_{l,z} \, \bar{c}_i^f - D_L \frac{\partial \bar{c}_i^f}{\partial z} = 0 \quad , \quad z = 0 \qquad \text{Eq. 2.2.5}$$

$$\frac{\partial \bar{c}_i^f}{\partial z}\Big|_{z=L} = 0 \qquad \text{Eq. 2.2.6}$$

The same symbols have been used as for the solid-liquid extraction model listed in Table 2.1 but the index for the fluid in the bulk pore phase is changed from l for liquid to f for fluid. For more details on the model assumptions and derivation, the reader is referred to Appendix A and (del Valle et al. 2010).

In SFE modeling, different simplified forms of the general diffusion model (Eq. 2.2.1 to Eq. 2.2.3) have been established and applied for different raw materials and target components. The reviews by Oliveira et al. (2011) and del Valle et al. (2010) provide comprehensive information and comparisons of the common models. For the sake of brevity, the presentation of those models is hereafter confined to a concise summary of model assumptions and the types of raw material they have been validated for. The reader is referred to (Oliveira et al. 2011) and (del Valle et al. 2010) for more details, references, and equations. The models can mainly be classified by the way how mass transport inside the solid plant material and mass transfer from solid phase to fluid phase is described. The most common SFE models according to (Oliveira et al. 2011; del Valle et al. 2010) are listed in Table 2.3.

Frequently used models are the linear driving force model, and the broken and intact cells model as can be seen from the various applications in Table 2.3. The type of model chosen for a system depends on the rate-limiting phenomenon. The linear driving force is applicable when the residual solute concentration profile is approximately parabolic (del Valle et al. 2010, p. 409). The desorption-dissolution-diffusion model requires the availability of various parameters (Goto et al. 1993), thus, the material to be investigated should be well understood and analyzed. When solutes are present at high concentrations so that solubility is the driving force, the shrinking core model is applicable (del Valle et al. 2010, p. 407). In cases, where a significant fraction of the ground material is broken cells, two stages of extraction kinetics can often be distinguished by using the broken and intact cells model (Sovová 1994): an early stage at quick mass transfer rate and a second stage at slow mass transfer rate. This model, however, requires many parameters to be estimated because an additional state variable is introduced (Sovová 2005). The internal or external mass transfer limitation models (another term often used is internal/external mass transfer control model), reduce mass transfer to the one which is rate limiting. For the internal mass transfer limitation model, e.g., it is assumed that the concentration at the surface of a particle is the same as in the bulk fluid, whereas for the external mass transfer limitation model, the average concentration of the particle is assumed to be the same as at the particle surface, thereby disregarding intragranular diffusion (del Valle et al. 2010).

Table 2.3. Common supercritical fluid extraction models (Oliveira et al. 2011; del Valle et al. 2010, pp. 400–411).

Model	Description	Examples of application
Linear driving force model	Solute mass flux in a particle is approximated by a linear concentration gradient between the average solute concentration in the particle and the concentration at the particle surface which is in equilibrium with the fluid phase concentration.	Essential oil from clove bud / pennyroyal / rosemary / oregano / peppermint leaves, black pepper / fennel / sage / celery / coriander / parsley seeds. Caffeine from coffee.
Desorption-dissolution-diffusion model	Solute is adsorbed (e.g., linear, Langmuir, Freundlich, or Brunauer-Emmet-Teller isotherm) to the solid plant matrix inside the particle, then diffuses through the pores of the solid particle to the surface of the particle where it is released from the surface to the fluid phase (external mass transfer).	Essential oil from peppermint / valerian / spearmint leaves, clove buds.
Shrinking core model	Particle is divided into a core un-extracted region at solubility concentration and an extracted outer region with a sharp moving boundary in between. During extraction, the volume of the core region shrinks and so does the average concentration of the particle until the center of the particle is reached and the average solid-phase concentration approaches zero. This model is valid for solutes that are present in the solid at concentrations close to solubility, i.e., when solubility is limiting the extraction rate.	Oil from rapeseeds. Essential oil from nutmeg, camphor, lavender flowers, hops.
Broken and intact cells model	It is assumed that grinding the plant material produces particles consisting of intact cells with broken cells on the surface. Mass transfer occurs from intact to broken cells at a slow mass transfer rate due to intracellular diffusion hindrance and from broken to fluid phase at a fast mass transfer rate (external diffusion across a laminar boundary layer).	Essential oil from spearmint / chamomile / *Lippia sidoides* Cham. / vetiver / rosemary leaves, clove, hops, nutmeg, sage / parsley / caraway / ani- / celery seeds, black pepper, orange peel, carqueja. Oleoresins from marigold, ginger.
Internal mass transfer limitation model	Internal mass transfer in the solid particle is considered rate limiting, external mass transfer is disregarded.	Essential oil from black pepper, basil.
External mass transfer limitation model	External mass transfer in the laminar boundary layer (fluid phase) is considered rate limiting, internal mass transfer is disregarded.	Essential oil from black pepper, chamomile flower heads.

2.2.3 Supercritical CO₂ Extraction from Hops

One of the most common applications of SFE in food engineering is $SCCO_2$ extraction from hops. The industrially relevant variety is *Humulus lupulus* L., the "common" hop, whose secondary metabolites are demanded in the beer industry due to their popular sensory attributes as well as their technological and nutritional functionalities. Those target compounds are divided into bitter compounds, essential oil containing volatile aroma compounds, and polyphenols (Biendl et al. 2015, p. 51). Brewers are particularly interested in the taste- and aroma-relevant bitter components and the essential oil, present in the lupulin of hop cones (sticky secretion contained in glands) (Biendl et al. 2015, p. 51). The bitter components are divided into hard resins (not soluble in hexane) and soft resins (soluble in hexane), the latter containing the important α-acids (2-20 %) and β-acids (3-10 %) (Biendl et al. 2015, p. 62). The alpha-acids' chemical derivatives produced during wort boiling, the iso-alpha acids, are the main components imparting bitterness to beer (Biendl et al. 2015, p. 64). Besides their bitter taste, alpha-acids contribute to the formation and stability of the beer foam (Biendl et al. 2015, pp. 70–71) and to microbial preservation due to their antibacterial properties (Biendl et al. 2015, p. 73). The essential oil in hop consists of aroma-relevant volatiles which are responsible for the characteristic hoppy, spicy, and floral aroma of many beer types. A classic example, where the hop aroma is strongly pronounced, is the "Indian Pale Ale" which is dry hopped directly before filling. For dry hopping, hop cones or pellets are added to the beer in cold state directly before filling, thereby many volatiles are preserved that would otherwise be lost during classic hopping (usually addition during wort boiling process). Different groups of aroma compounds can be distinguished: the major components monoterpenes (40 %), sesquiterpenes (40 %), carboxylic acid esters (15 %), and the minor components (each <= 1%) including aliphatic hydrocarbons, carboxylic acids, monoterpene oxides, sesquiterpene oxides, aldehydes, ketones, and thiols (Biendl et al. 2015, p. 54). Sensorially important are especially the monoterpenes β-myrcene ("spicy" (The Good Scents Company 1988b, myrcene)), α-/β-pinene ("herbal"(The Good Scents Company 2000, alpha-pinene)), and limonene ("citrus" (The Good Scents Company 1988a, dipentene)) and the sesquiterpenes β-caryophyllene ("spicy" (The Good Scents Company 1999, beta-caryophyllene)) and α-humulene ("woody" (The Good Scents Company, alpha-humulene)) (Biendl et al. 2015, pp. 55–56).

Common $SCCO_2$ processes to extract bitter compounds and essential oils from hops are conducted by batch-extraction from hop pellets (ground dried cones pressed to pellets) in a cylindrical extraction vessel followed by one or two downstream separators (Biendl et al. 2015, pp. 168–171). Typical extraction conditions are in the range 200-

250 bar and 40-60 °C (Biendl et al. 2015, p. 168). In the first separator, the pressure is reduced to 100-120 bar at which part of the resins become insoluble while essential oils stay dissolved. In the second separator, the pressure is reduced to subcritical conditions so that CO_2 becomes gaseous and the residual extract is collected (Biendl et al. 2015, p. 171). The result is a resin-rich fraction (46.5 % α-acids and 1.7 % essential oil) and an oil-rich fraction (33.5 % α-acids and 29.3 % essential oil) (Biendl et al. 2015, p. 172). To further modify the essential oil composition or purify target compounds, the oil-rich extract needs to be fractionated by an additional extraction, e.g., liquid-liquid countercurrent extraction (Biendl et al. 2015, pp. 171–172) or solid phase extraction (van Opstaele et al. 2012a).

Instead of extracting all compounds and subsequently purifying them at the cost of additional equipment at energy-intensive operating conditions, selective $SCCO_2$ extraction can be applied. By simply adjusting operating pressure and temperature (CO_2 density and viscosity), certain target components can be extracted at higher yield based on their molecular structure without any further fractionation. This objective has been of interest in the research community for the last 30 years. An overview of the relevant studies published about SFE from hops is provided in Table 2.4. Early studies showed that varying pressure and temperature conditions in $SCCO_2$ extraction had a significant impact on the extract composition with regard to resins and essential oil (Langezaal et al. 1990; Verschuere et al. 1992; del Valle et al. 2003; Zekovic et al. 2007; van Opstaele et al. 2012a). van Opstaele et al. (2012b) first demonstrated that pressure and temperature conditions affected not only the content of total essential oil but also the essential oil composition. They proposed a two-step process where the first step yielded higher fractions of "floral" aroma compounds at lower pressure (90 bar) and the second step yielded higher fractions of "spicy" aroma compounds at higher pressure (110 bar). After having added both extracts to beer, a trained sensory panel could discriminate between the beer with the extract from the first step characterizing it as "floral, hoppy, and citrus" and the beer with the extract from the second step which was classified as more "herbal and hoppy". Several other studies followed that focused on maximizing yield (Nagybákay et al. 2021) and the comparison of different solvents for the extraction of resins, essential oil and polyphenols (Bizaj et al. 2021, 2022). Although essential oil composition was analyzed in most of the studies in Table 2.4, a lack of knowledge remained about the influence of different pressure-temperature combinations on the extraction kinetics of single compounds. Essential oil composition was either only analyzed for the total extract (Verschuere et al. 1992; Zekovic et al. 2007; del Valle et al. 2003; Nagybákay et al. 2021; Bizaj et al. 2022) or kinetics were only presented for one

or few pressure-temperature combinations (Langezaal et al. 1990; van Opstaele et al. 2012a, 2012b). Extraction kinetics data are, however, necessary to model and understand the rate-controlling mechanisms and to apply model-based optimization.

A first modeling study about $SCCO_2$ extraction from hops was published by Kupski et al. (2017). The authors compared three different models: the equilibrium model by Reverchon (1996), the shrinking core model by Goto et al. (1996) and the broken and intact cells model by Sovová et al. (1995). They estimated the respective model parameters from extraction data for total extract at different temperature-pressure conditions and concluded that the broken and intact cells model was preferable for modeling SFE from hops. As Kupski et al. (2017) estimated model parameters for total extract only, their study did not allow predicting and understanding how aroma composition changes during extraction at different pressures and temperatures. Experiments were done with ground hop pellets instead of intact hop pellets which limits the transferability of results to industrial use because mass transfer rates of ground pellets are known to be different from those of intact pellets (del Valle et al. 2003). Furthermore, model parameters were fitted to single extraction curves at different conditions instead of including the influence of temperature and pressure in the model via constitutive equations.

This thesis builds on previous research on SFE from hops and extends it as follows:

- Modeling $SCCO_2$ extraction from hop pellets comparing possible models commonly used (see Table 2.3).

- Including the effects of the process variables operating temperature and pressure in the model based on extraction data of various aroma compounds.

- Validating the model for different temperature-pressure conditions in a practically relevant range.

- Identifying process variables and extraction times for tuning the extract in a certain direction and derive recommendable measures for the brewing industry.

Table 2.4. Overview of studies on supercritical fluid extraction from hops.

Study	Main results	Analyzed components	Process variables	Mathematical modeling
Langezaal et al. (1990)	Yield and composition influenced by pressure and temperature conditions, highest yield at 40 °C/200 bar.	Resins: α-/ β-acids. Essential oil: β-myrcene, β-caryophyllene, α-humulene, γ-/δ-cadinene, β-caryophyllene epoxide.	Temperature: 40/60 °C. Pressure: 125/200/275 bar. Sampling: fractional, 1/2/3 h. Material: cones/leaves.	None.
Verschuere et al. (1992)	Selective extraction of essential oil at low density (0.2 g mL^{-1}) and short extraction time (15 min).	Resins: α-/ β-acids. Essential oil: humulene, myrcene, β-caryophyllene.	Temperature: 50 °C. CO_2 density: 0.05-1 g cm^{-3}. Sampling: fractional, 15/30 min. Material: dried and ground.	None.
del Valle et al. (2003)	Increase in yield with increase in pressure up to 200 bar. Increase in yield and selective extraction of resins with decrease in temperature (max. 40 °C) but only at low pressure (120 bar). Faster extraction for milled than for whole pellets.	Total solids. Resins: α-/ β-acids. Essential oils: content summarized in aroma index.	Temperature: 40/50/60 °C. Pressure: 120/160/200/240/280 bar. Sampling: 30/60/90/120/150/180/210/240 min. Material: pellets.	None.
Zekovic et al. (2007)	Highest α-acids content in bitter variety (Magnum cultivar).	Resins: α-/ β-acids. Essential oil: α-humulene, β-caryophyllene.	Two steps: A: 40 °C/150 bar for 2.5 h B: 40 °C/300 bar for 2.5 h. Material: dried cones.	None.
van Opstaele et al. (2012a)	110 bar/50 °C best for selective isolation of essential oils with all kinds of aroma compounds, polar hop essence obtained by SPE[1] fractionation, extract vs. fractionated extract changed sensory flavor profile of beer significantly; essential oil profile changes during extraction.	Essential oil: marker components for 1) "floral" aroma: linalool, 2-undecanone, methyl 4-decenoate 2) sesquiterpene hydrocarbons: α-copaene, β-caryophyllene, α-humulene, β-selinene	SFE coupled with SPE[1] for fractionation of essential oil. Temperature: 40/50/60 °C. Pressure: 80/85/90/95/100/105/110 bar. Sampling: stop after 25.0 L CO_2 consumption, kinetics at 50 °C/110 bar: 10/20/30/45/60/75/90 min.	None.

		3) "spicy" aroma: caryophyllene oxide, humulene epoxide I&II, humulenol II, unidentified sesquiterpenoid.	Material: pellets.	
van Opstaele et al. (2012b)	First step at low pressure yielded higher fraction of "floral" aroma compounds, second step at higher pressure yielded higher fraction of "spicy" compounds; extract from first step caused "floral, hoppy, and citrus" aroma in beer, extract from second step caused "herbal/hoppy" aroma.	Essential oil: marker components for 1) "floral" aroma: linalool, 2-undecanone, methyl 4-decenoate 2) sesquiterpene hydrocarbons: α-copaene, β-caryophyllene, α-humulene, β-selinene 3) "spicy" aroma: caryophyllene oxide, humulene epoxide I&II, humulenol II, unidentified sesquiterpenoid.	Two steps: 1) 50 °C/90 bar 2) 50 °C/110 bar. Sampling: stop after 25.0 L CO_2 consumption each, kinetics: 10/20/30/40 L CO_2 for groups of "floral", "sesquiterpene hydrocarbon" and "spicy" compounds for both steps. Material: pellets.	None.
Kupski et al. (2017)	Highest yield at 55 °C/200 bar, best goodness of fit for broken and intact cells model, estimated mass transfer coefficients depended on temperature and pressure.	Total extract (kinetics). Resins: lupulone (β-acid). Essential oil (no kinetics): humulene, humulene epoxide. Others: betamethasone valerate, stigmasterol.	Temperature/Pressure combinations: 35 °C/100 bar, 45 °C/150 bar, 35 °C/200 bar, 55 °C/200 bar, 55 °C/100 bar. Sampling: stop after ~3 h, 17 samples. Material: ground and sieved pellets.	Equilibrium model[2], shrinking core model[3], broken and intact cells model[4].
Nagybákay et al. (2021)	Maximum yield (Response Surface Methodology) was achieved at 370 bar/43 °C/80 min with high content of α- and β-acids. Total content of carotenoid and chlorophyll was	Total extract (incl. kinetics). Resins: α-/β-acids Chlorophyll and carotenoid content.	Central Composite Design for: Temperature: 40-60 °C. Pressure: 250-450 bar. Extraction time: 30-90 min. Sampling for extraction kinetics at	None.

	negligibly small.	Essential oil (no kinetics): main compounds β-pinene, β-myrcene, α-/β-humulene, α-selinene, methyl-4-decenoate and many others.	100/125/150 bar, 40 °C: 15/30/45/60/90/120/150/180/210/ 240/270/300 min.	
Bizaj et al. (2021)	Comparison of solvents CO_2, sulfur hexafluoride, and low-/high-density dimethyl ether; yield of bitter acids influenced by type of solvent. For CO_2: highest yield of α-acids: 40 °C/150 bar, β-acids: 20 °C/150 bar, total extract: 40 °C/150 bar.	Total extract (kinetics). Resins: α-/β-acids.	Temperatures: 20/40/60/80 °C. Pressures: 50/100/150 bar. Sampling: every 10 kg CO_2/kg material, stop at max. 240 kg CO_2/kg material or 9 h (kinetics only for yield), resins determined in final extracts.	Two-site kinetic model (ODE, modified Crank's hot ball diffusion model).
Bizaj et al. (2022)	Comparison of solvents CO_2, propane, dimethyl ether; highest content of linalool, β-caryophyllene, and α-humulene with CO_2, higher content of other compounds using propane; CO_2: highest essential oil content at 60 °C/150 bar.	Essential oil: myrcene, linalool, geraniol, β-caryophyllene, α-humulene, farnesene, α-selinene, δ-cadinene. Polyphenol: xanthohumol.	Temperatures: 20/40/60/80 °C. Pressures: 100/150 bar. Sampling: total extract after 90 min (no kinetics).	None.

[1] Solid Phase Extraction (with octadecylsilica and ethanol/water mixtures)
[2] (Reverchon 1996)
[3] (Goto et al. 1996)
[4] (Sovová et al. 1995)

3 Methods

3.1   Experimental Methods

Extraction models contain different parameters of the porous medium that need to be determined before conducting simulations. Those include the density of the fluid, the specific surface area and wetting behavior of the solid, and the solid density and porosities of the packed bed and the porous particles. In this thesis, the fluid density and its correlation with temperature and pressure were approximated by the available solvent data from literature, e.g., the density of water reported in (VDI-Wärmeatlas 2006) for espresso extraction and the density of CO_2 from (Span and Wagner 1996) for $SCCO_2$ extraction. The specific surface area was estimated via PSD analyses and the wetting and swelling of particles was determined by microscopy. The bulk porosity was derived from the packing density and particle porosity.

I.   Particle Size Distribution (PSD) Analysis

In this thesis, laser diffractometry was used to determine the volume distribution of coffee particles. The respective methods are described in detail in (Hargarten et al. 2020) and (Schmieder et al. 2023). Selecting this method was based on the high accuracy and reproducibility of laser diffractometry and on the intention of comparing our results to earlier publications by different authors. Vibrational sieving followed by air jet sieving was used to fractionate coarse and fine particles as a preparation step for laser diffractometry measurements (see (Hargarten et al. 2020)).

II.   Microscopy

When the temporal change of the particle size is of interest, e.g., during swelling, measuring the PSD as described above does not allow tracking different states of the same particle. Light microscopy was used to investigate the progress of particle swelling. Details about the method are available in (Hargarten et al. 2020). In brief, videos during the first minutes of wetting the particles were taken by a camera, the obtained images were processed, and the projection area of each particle was analyzed. To eliminate errors from particle movements and gas bubbles, the particles were fixed in a custom-made flow cell made from acrylic glass and connected to a peristaltic pump. An image of the used flow cell is provided in Figure 3.1. The constant flow produced by the pump enabled the removal of most gas bubbles and full penetration of water into the pores. Remaining gas bubbles were removed from the particle outline in the image by

image processing. Water temperature was kept close to extraction temperature around 80 °C during the measurement by isolating the flow cell and the connecting tubes (see Figure 3.1). Tilting and turning of particles during the measurement was avoided by fixing the particles on a thin layer of adhesive.
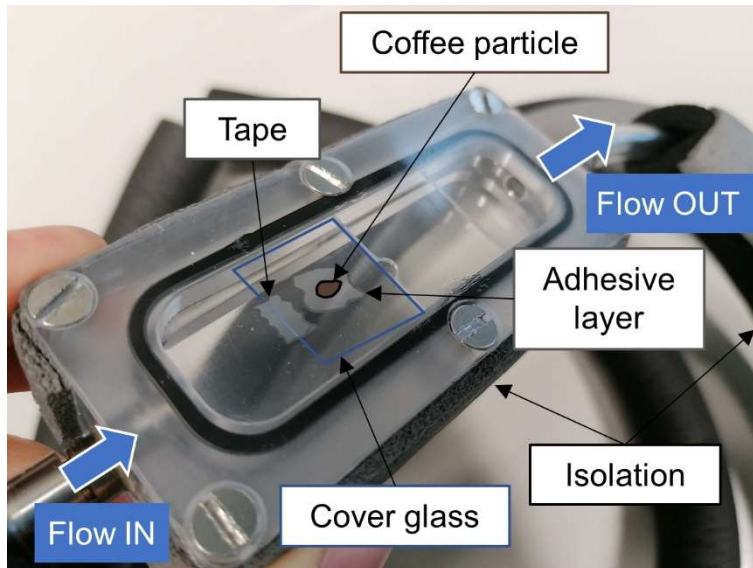

Figure 3.1. Flow cell used for microscopy analyses.

III.   Solid Density

The solid density was determined by helium pycnometry as described in (Pannusch et al. 2023). A schematic diagram of the pycnometry setup is shown in Figure 3.2. The volume occupied by the solid in the cell chamber was determined from the gauge pressures at open and closed expansion valve via the ideal gas law and the solid density ρ_s was obtained dividing the sample mass by the measured volume.
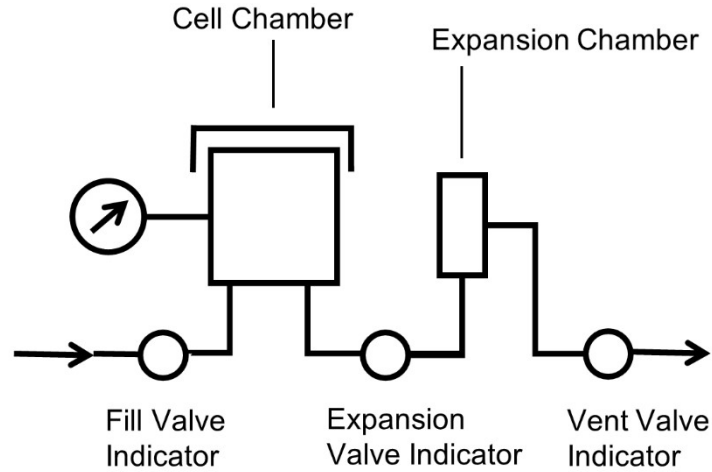
Figure 3.2. Schematic diagram of helium pycnometry setup, based on (Micromeritics Instrument Corporation 2005, p. 9).

IV.   *Porosity Estimation*

The total porosity of a packed bed consisting of porous particles is the sum of intragranular porosity ϕ and bulk porosity ε_{bulk} *(pore space between particles):*

$$\varepsilon_{tot} = \varepsilon_{bulk} + (1 - \varepsilon_{bulk})\phi$$

Eq. 3.1.1

The intragranular porosity ϕ can be derived in different ways. An option for simple geometries like pellets is measuring the mass, diameter, and length of single pellets and determining the mean value from a random sample (described in (Pannusch et al. 2023)). For more complex geometries like coffee particles, µ-CT scans can be used as in (Pittia et al. 2011) or mercury porosimetry as in (Corrochano et al. 2015). To determine an estimate for bulk porosity, the method by Corrochano et al. (2015) is applicable. They derived the bulk porosity by:

$$\varepsilon_{bulk} = 1 - \frac{\rho_{bulk}}{\rho_{particle}}$$

Eq. 3.1.2

In this thesis, the method in (Corrochano et al. 2015) was followed for espresso coffee as described in (Pannusch et al. 2024). For SFE from hop pellets, Eq. 3.1.2 was used to determine the bulk porosity. The total porosity was then calculated using Eq. 3.1.1 (details in (Pannusch et al. 2023)).

3.2 Simulation and Parameter Estimation

3.2.1 Numerical Solution of Partial Differential Equations

An analytical solution of PDEs yielding an explicit form of the state variable is not possible (Quarteroni 2017, p. 3). Instead, a numerical solution is the common practice to approximate the exact solution. Appropriate numerical solutions converge to the exact solution when the resolution of the discretization mesh tends to infinity (Quarteroni 2017, p. 4).

The *Method of Lines* used in this thesis is a common method to solve PDEs and consists of two steps (Vande Wouwer et al. 2014, p. 125): (I) the spatial derivatives are approximated yielding a system of semi-discrete equations (ODEs: discrete in space, continuous in time). (II) The system of ODEs is solved via time integration.

I. Spatial derivative approximation

Different methods are distinguished for the approximation of the spatial derivative. The most common are the following:

- *Finite Difference Method (FDM):* the simplest method. Continuous spatial coordinates are replaced by a grid of discrete points at which the derivative is derived from a Taylor series expansion (Vande Wouwer et al. 2014, p. 126).

- *Finite Volume Method (FVM):* the spatial domain is subdivided into finite cells or control volumes (Le Dret and Lucquin 2016, p. 345). The differential equation is integrated over each cell applying Gauss divergence theorem, i.e., the volume integral of a derivative can be replaced by its solution at the cell surface (Quarteroni 2017, p. 214). This results in a set of piecewise constant functions (average values for all cells). The derivatives are approximated using Taylor series expansions of adjacent cells (Le Dret and Lucquin 2016, p. 346).

- *Methods of Weighted Residuals (MWR)*: makes use of a *truncated Fourier series* that approximates the exact solution of the PDE using basis functions (Vande Wouwer et al. 2014, p. 215). Weighting functions are determined which make the inner product of weighting functions and the residuals between the exact and the approximate time derivative (weighted residuals) become zero (Vande Wouwer et al. 2014, p. 212). Two common MWR methods are:

- *Finite Element Method (FEM):* A common method is the Galerkin method, where the weighting functions are the same as the basis functions (Vande Wouwer et al. 2014, pp. 212–214).

- *Spectral Method (SM) and Spectral Element Method (SEM)*: Use global polynomials (SM) or local/piecewise polynomials (SEM) as basis functions (Quarteroni 2017, p. 225).

Which one of the above methods is best to be selected for a specific model depends on the type of PDE and the temporal and spatial system behavior. In this thesis, the espresso coffee extraction model based on Eq. 2.1.1, Eq. 2.1.2, and Eq. 2.1.3 was simplified by neglecting dispersion and diffusion in the liquid phase (Eq. 2.1.1) and averaging the solid-phase solute concentration over the particle volume applying Gauss' divergence theorem (Pannusch et al. 2024). The same simplifications were applicable for the SFE model in Eq. 2.2.1, Eq. 2.2.2, and Eq. 2.2.3 (Pannusch et al. 2023). Convection therefore dominates in both cases which means that both PDEs can be classified as hyperbolic (Quarteroni 2017, p. 5). Moreover, both percolation extraction models are reduced to one dimension in the z direction of flow assuming unidirectional and uniform flow (see Section 2.1.2 and Section 2.2.2). For this kind of 1D convection equation, FDM has proven to be applicable (Moroney et al. 2015; Moroney et al. 2019; Kupski et al. 2017). Other methods like FEM would be preferable if the problem would have to be formulated in 2D or 3D (where the assumption of uniform flow would no longer be valid). Having chosen FDM for the solution, the differentiation scheme remains to be selected. Vande Wouwer et al. (2014, p. 158) recommend a five-point biased-upwind scheme for calculating the first-order spatial derivative of the state variable $\frac{dx}{dz}$ at a location z_i in convection equations:

$$\frac{dx}{dz}\Big|_{z_i} = \frac{-x_{i-3} + 6x_{i-2} - 18x_{i-1} + 10x_i + 3x_{i+1}}{12\Delta z} + O(\Delta z^4) \qquad \text{Eq. 3.2.1}$$

Together with the boundary points proposed in (Bickley 1941), the differentiation matrix D_1 used in (Pannusch et al. 2024) and (Pannusch et al. 2023) was:

$$D_1 = \begin{bmatrix} -25 & 48 & -36 & 16 & -3 & 0 & \ldots & \ldots & 0 \\ -3 & -10 & 18 & -6 & 1 & 0 & \ldots & \ldots & 0 \\ 1 & -8 & 0 & 8 & -1 & 0 & \ldots & \ldots & 0 \\ -1 & 6 & -18 & 10 & 3 & 0 & \ldots & \ldots & 0 \\ & & & & \ldots & & & & \\ 0 & 0 & -1 & 6 & -18 & 10 & 3 & 0 & 0 \\ & & & & \ldots & & & & \\ 0 & \ldots & \ldots & 0 & -1 & 6 & -18 & 10 & 3 \\ 0 & \ldots & \ldots & 0 & 3 & -16 & 36 & -48 & 25 \end{bmatrix} \qquad \text{Eq. 3.2.2}$$

II. Time integration

Conventional ODE solvers can be used to integrate the ODE obtained from spatial approximation. In MATLAB, common ODE solvers are *ode45* and *ode15s*. The solver *ode45* is based on an "explicit Runge-Kutta (4,5) formula" (MathWorks, Documentation R2023a, ode45) whereas *ode15s* is a "variable-step, variable-order (VSVO) solver based on the numerical differentiation formulas (NDFs) of orders 1 to 5" (MathWorks, Documentation R2023a, ode15s). The selection of the solver depends on the stiffness of the problem. In general, *ode15s* can be used for stiff problems, i.e., when there are large differences in the inherent time constants, but *ode45* is only accurate for non-stiff problems. Furthermore, *ode15s* is applicable for the solution of differential algebraic equations which was required for the interphase boundary condition in Eq. 2.1.3 and in Eq. 2.2.3. Hence, the solver *ode15s* was used in (Pannusch et al. 2024) and (Pannusch et al. 2023).

3.2.2 Parameter Estimation

Several parameters are necessary to describe the extraction kinetics of a solute during the extraction process accurately. Some of them are not measurable directly or accessible from literature data, e.g., the mass transfer coefficient. Other parameters cannot be easily determined due to the high complexity of natural multiphase, multicomponent systems, e.g., the distribution constant or the initial concentration in the solid phase. Therefore, these parameters were estimated from experimental extraction kinetics data using mathematical optimization, i.e., by minimizing or maximizing a cost function representing the deviation of experimental values and model predictions.

Different cost functions exist for parameter estimation, the most common being the *least squares* and *maximum likelihood* cost functions. In this thesis, least-squares minimization was used. The respective minimization problem based on the notation in (Walter and Pronzato 1997, p. 38) is:

$$\min_{\boldsymbol{p}} \sum_k \sum_{t_{i_k}} w_k \left(\hat{y}_k(t_{i_k}, \boldsymbol{p}) - y_k(t_{i_k}) \right)^2 \qquad \text{Eq. 3.2.3}$$

The elements of the parameter vector $\boldsymbol{p}$ are the parameters to be estimated. The symbols $\hat{y}_k$ and y_k specify the state variables predicted by the model and obtained from experiments, respectively, at discrete times t_{ik} of a single experiment k. y_k was the mass concentration in case of espresso coffee extraction (Pannusch et al. 2024), and the accumulated mass in case of SFE from hops (Pannusch et al. 2023). The factor w_k

is a weighting coefficient, which shall improve the performance of the optimization. For espresso coffee extraction w_k was specified as $w_k = 1/y_k(t_{1k})^2$ (Pannusch et al. 2024) whereas for SFE from hops it was set to 1, i.e., no weighting was applied.

If $\hat{y}_k(t_{ik}, \boldsymbol{p})$ is linear in the parameters, the explicit form of the model can be substituted in Eq. 3.2.3 and the least squares solution can be determined analytically as described in (Aster et al. 2019, pp. 25–26). If the model term is not linear in the parameters, an analytical solution is not possible. Instead, the solution is determined numerically applying iterative optimization algorithms. In (Pannusch et al. 2024) and (Pannusch et al. 2023), the model solution $\hat{y}_k(t_{ik}, \boldsymbol{p})$ was computed using spatial discretization and numerical ODE integration as described in Section 3.2.1. Different methods exist to find the minimum of the cost function which shall not be discussed in detail here for the sake of brevity. For the interested reader, an excellent overview is provided in (Nocedal and Wright 2006).

In this thesis, the MATLAB function *lsqnonlin*, a least-squares solver for nonlinear functions, was used (MathWorks, Documentation R2023a, lsqnonlin). The *trust-region-reflective algorithm* was selected which is described in detail in (MathWorks, Documentation R2023a, Least-Squares (Model Fitting) Algorithms). This type of optimization algorithm defines an approximation of the cost function (subproblem) by a quadratic Taylor series expansion within a trust region around the current iterate. The step to the next iterate is set to the step which minimizes the subproblem within the trust region. If a step is not acceptable, the trust region is reduced and the minimization of the subproblem is repeated for the reduced trust region. The minimization of each subproblem requires the definition of the Jacobian (first partial derivatives) and the Hessian matrix (matrix of second partial derivatives) of the cost function. Those are approximated numerically using, by default, finite forward differences (MathWorks, Documentation R2023a, lsqnonlin). To obtain good approximations of the finite-difference derivative, the step size should be selected small enough but not too small to avoid roundoff errors (Aster et al. 2019, pp. 246–247). In *lsqnonlin*, the square root of the floating-point relative accuracy is used by default. If problems occur when using the forward scheme, alternative schemes such as a centered scheme or complex step differentiation (Lyness and Moler 1967; Squire and Trapp 1998) can be used whose local errors are proportional to the squared step size ($O(h^2)$) (Vande Wouwer et al. 2014, 126–127, 193), which makes them more accurate than the Euler forward scheme (local error of first order ($O(h)$)) (Vande Wouwer et al. 2014, p. 20). The default forward scheme was, however, selected for our studies (Pannusch et al. 2024) and (Pannusch et al. 2023) because it was sufficiently accurate while requiring less computation time.

Theoretically, a local minimum is reached when the optimality conditions are fulfilled. The first-order necessary condition or first-order optimality is fulfilled when the first derivative of the cost function becomes zero (Papageōrgiu et al. 2012, p. 20), which is investigated in MATLAB by calculating the infinity norm of the Jacobian (MathWorks, Documentation R2023a, First-Order Optimality Measure). The second-order sufficient condition or second-order optimality for a local minimum is reached when the second derivative of the cost function is greater than or equal to zero (Papageōrgiu et al. 2012, p. 20). In (Pannusch et al. 2024) and (Pannusch et al. 2023), it was ensured that the function tolerance, step tolerance, or optimality tolerance was reached, as all of those three stopping criteria indicate a flat region close to a local minimum, i.e., fulfilling the first-order optimality condition.

Although the first-order and second-order optimality conditions enable to identify a local minimum, they do not guarantee that a global minimum is achieved (smallest of all local minima within the constrained space). Difficulties arise when the cost function exhibits multiple local minima (nonconvex), discontinuities in the first derivative, or when it exhibits a "flat bottom" (Aster et al. 2019, p. 248). Regardless which of those cases occur, one obtains different optimal solutions depending on the initial guess values (start points). Global optimization procedures exist which involve the selection of a variety of start points (multistart method) and define the best of the obtained set of solutions as the global optimum (Aster et al. 2019, pp. 248–250). This procedure starting from several initial guess values for the mass transfer coefficients was done in (Pannusch et al. 2023). To facilitate the selection of guess values (no suitable values were available from literature or previous studies), an initialization procedure was pursued in (Pannusch et al. 2023) and (Pannusch et al. 2024): mass transfer coefficients and equilibrium parameters were estimated for single experiments and the parameters correlating mass transfer and equilibrium to the process variables were estimated from that dataset of estimated parameters at different conditions, yielding the guess values for the main parameter estimation with all experimental data. Despite the availability of global optimization algorithms, identifying the true parameters of a model can still be challenging when parameters correlate with each other yielding a loss of identifiability (Aster et al. 2019, p. 252). Parameter correlations can be eliminated by determining some of the parameters from other analyses or using an experimental design that reduces correlations. If this is not possible, a workaround for this issue is to not estimate the correlating parameters simultaneously but rather pursuing sequential estimation steps, where one parameter is kept constant at a realistic order of magnitude and the other one is estimated (relaxed) using the same or a different set of experiments. This

kind of procedure was conducted in (Pannusch et al. 2024) to determine flow and temperature dependent parameters and particle-size dependent parameters separately.

The parameter optima depend not only on the problem formulation but also on the experimental data used. Two replicates of the same experiment will yield different optimum values due to error propagation. Local estimates of the parameter variances and their confidence intervals can be calculated by the linear Taylor approximation at the optimum point. The variance-covariance matrix of a parameter thus is (Aster et al. 2019, p. 243):

$$Cov(\boldsymbol{p}^*) = s^2 \big(\boldsymbol{J}(\boldsymbol{p}^*)^T \boldsymbol{J}(\boldsymbol{p}^*)\big)^{-1}$$

<div align="right">Eq. 3.2.4</div>

With s being the mean standard deviation of the experiments (assuming that the errors of all individual experiments are approximately equal to the mean error of all experiments) and $\boldsymbol{J}(\boldsymbol{p}^*)$ being the jacobian matrix of the optimum vector of parameters $\boldsymbol{p}^*$. The diagonal elements of Cov represent the variances of the parameters which can be used to calculate the confidence intervals of parameters and evaluate accuracy. Non-diagonal elements are the covariances of parameters with elements close to zero indicating no correlation of parameters whereas positive or negative elements close to one indicate strong correlations of two parameters (Aster et al. 2019, p. 252). The variance-covariance matrix can be used to specify the accuracy of parameter solutions, to identify parameter correlations, and to conduct model-based optimal design of experiments (Franceschini and Macchietto 2008). In (Pannusch et al. 2024), we used the approximate variance-covariance matrix to determine a reasonable number of decimals for the identified parameters.

4 Results

4.1 Swelling Properties of Roasted Coffee Particles (Hargarten et al. 2020)

4.1.1 Summary

Since the particle size influences both the permeability of the coffee puck and the mass transfer of solutes, it is a critical aspect when optimizing espresso coffee extraction. In the beginning of extraction, the dry roasted coffee particles are wetted and take up water due to capillary forces. Consequently, the hydrostatic pressure in the cells and the chemical hydration of the cell wall polysaccharides lead to an expansion of the insoluble cell network. This process is called swelling. Understanding wetting and swelling of the coffee grains in water is important to verify our model assumptions. First, the occurrence of swelling would mean that the intragranular pores are completely saturated with water before extraction begins and that diffusion takes place in the intragranular water phase. Second, a progression of swelling during extraction might counteract the porosity increase from the dissolution of particles which would support the assumption of constant porosity. Previous literature reported contradictory results about swelling, some reported an increase in particle volume, but others refuted the appearance of swelling. This study was meant to provide clarity about: (1) whether roasted coffee particles are subjected to swelling, (2) by which extent the particle size changes, and (3) how quick swelling takes place to understand its impact on espresso coffee extraction.

Particles were analyzed in bulk by laser diffractometry and individually by light microscopy. Measuring the PSD was intended to clarify if the initial particle size (fine vs. coarse particles) had an influence on swelling. Microscopy analyses of single particles were used to identify the progression and total time of swelling and to verify PSD measurements. PSD measurements were conducted for ground coffee at different grinding levels in two manners: (1) bimodal distributions including fine and coarse particles and (2) monomodal distributions of fine and coarse particle fractions separately. The latter was achieved using preliminary sieving. Particles were measured in dry and wet dispersion (water) and the distributions were compared. An increase in the fines content with wetting was observed for the bimodal distributions, which was traced to particle erosion, i.e., a release of fine particles and fragments from the surface of coarse particles during wetting. An increase of the water temperature was found to significantly enhance this effect. Monomodal distributions significantly shifted towards

larger particle sizes after wetting, which was observed for all coarse fractions at different grinding levels. No significant change was, however, observed for the fine particle fraction. On average, a change in the particle diameter by 15 % was quantified and the same applied for medium- and light-roast coffee. Microscopy was used to take videos of fixed particles surrounded by laminar flow and the particle size was quantified from the projection areas. Since the degree of swelling strongly varied for different particles, a quantitative verification of the PSD measurements was not possible. However, the images revealed a quick increase in diameter within the first 30 s of wetting and that swelling was mostly completed after 4 min.

Based on the results, roasted coffee particles can be expected to swell during preinfusion (initial wetting phase) and espresso coffee extraction. For this reason, a consistent preinfusion step is essential to allow comparability of experiments. It should be taken care for espresso extraction that a change in permeability during extraction is not only influenced by dissolution of solids but also by particle erosion and swelling which would both lead to a decrease in permeability. On the one hand, fine particles from erosion may migrate to the bottom of the filter basket and either form a compact layer or be carried into the beverage. On the other hand, swollen particles may fill the increasing pore space caused by dissolution of solids, which would lead to a lower or no increase in porosity and permeability. Swelling might furthermore influence intragranular diffusion resistance, which was modeled in a study by Mo et al. (2022).

4.1.2 Author Contribution

VB Hargarten and M Kuhn conceptualized the study and planned the experiments. VB Hargarten developed the experimental methods and procedures and conducted the experiments (PSD and microscopy analyses). VB Hargarten evaluated the data including statistical analyses. VB Hargarten, M Kuhn, and H Briesen interpreted the data. VB Hargarten wrote the manuscript; M Kuhn and H Briesen reviewed the manuscript.

4.2 Influence of Flow Rate, Particle Size, and Temperature on Espresso Extraction Kinetics (Schmieder et al. 2023)

4.2.1 Summary

Espresso coffee extraction has experienced a rising interest by engineers and scientists from various research groups during the past decade. However, optimizing the taste and aroma of the beverage by means of changing the extraction parameters, e.g., water temperature, flow rate or pressure, brew ratio, and grinding level, still belonged to the skills of a barista, and was considered rather an art than a scientific optimization problem. Based on sensory studies and quantifications of representative component concentrations, several authors already showed that taste and aroma can be significantly changed through adjustments of the above parameters. The concentrations of those key components had only been measured in the final beverage, but no extraction kinetics were compared at different extraction conditions. The goal of this study was to analyze the effects of influencing parameters on the extraction kinetics of key components to explain sensory perceptions and to quantify changes in the solute concentrations.

The extraction kinetics of TDS, caffeine (bitter), trigonelline, and chlorogenic acid (sour) were determined by fractionated sampling of the coffee beverage using a specifically designed sampling wheel with adjustable rotation velocity. TDS was determined via measuring the refractive index of the solution, and caffeine, trigonelline, and chlorogenic acid were quantified via High Performance Liquid Chromatography (HPLC). The extraction kinetics curves were approximated by fitting an exponential function to the experimental data points with respect to each individual experiment. The cup concentrations were then estimated for three brew ratios – 1/1, 1/2, and 1/3 – by integrating the exponential function. The estimated cup concentrations were used for response surface methodology with a second-order model to identify and compare the influences of the different extraction parameters. The same qualitative effects applied: an increase in the cup concentrations of all components was observed with a decrease in flow rate (longer extraction time) at brew ratios 1/1 and 1/2 whereas the temperature effect showed no consistent trend. A slightly reduced solute mass was observed at the finest grind level which was hypothesized to be caused by flow inhomogeneity accompanied by a higher pressure. Overall, the concentration differences at different temperatures and flow rates were by far smaller than expected from literature. In contrast, the brew ratio was found to have the largest impact on the solute concentrations as well as on the ratio of components due to differences in the molecules' extraction kinetics.

The results suggest that water temperature and flow rate (extraction time) have a lower impact on the taste of espresso coffee than concluded in the previous literature. The deviation from former results might be explained by an interdependence of water temperature and flow rate or flow inhomogeneity when controlling constant pressure, which was systematically prevented in this study (constant flow rate control). The brew ratio was however found to be of high interest as the shape of extraction kinetics curves differed for molecules of different polarity, which may be used to quantify and predict the balance of taste attributes for different stages of extraction. The data in this paper served the parameterization of an extraction model for single compounds in the subsequent study (Section 4.3).

4.2.2 Author Contribution

VB Pannusch and BKL Schmieder conceptualized the study and selected the experimental design. VB Pannusch and BKL Schmieder developed the experimental methods of espresso extraction, sampling, and sample preparation. VB Pannusch developed the experimental methods for TDS and PSD analysis, BKL Schmieder developed the experimental method for HPLC analysis. VB Pannusch conducted the espresso preparation and sampling, TDS analysis, and PSD analysis. VB Pannusch, BKL Schmieder, and L Vannieuwenhuyse collaborated on sample preparation for HPLC and TDS analysis. L Vannieuwenhuyse and BKL Schmieder conducted the HPLC analyses. VB Pannusch evaluated the TDS, PSD, and scale data. BKL Schmieder and L Vannieuwenhuyse evaluated the HPLC data and BKL Schmieder conducted the statistical evaluation of results by exponential fitting and response surface methodology. BKL Schmieder, VB Pannusch, H Briesen, and M Minceva interpreted the results. BKL Schmieder wrote the manuscript. VB Pannusch, M Minceva and H Briesen reviewed the manuscript.

4.3 Model-Based Kinetic Espresso Brewing Control Chart for Representative Taste Components (Pannusch et al. 2024)

4.3.1 Summary

As described in Section 2.1.3, several different models had previously been proposed to describe mass transport of espresso coffee extraction. Those models were, however, lacking relations between the extraction kinetics of different solutes and the parameters of espresso preparation. Using the experimental data obtained in the scope of our previous article (Section 4.2), a model was developed and parameterized, which incorporated the influences of water temperature and flow rate and enabled the prediction of espresso composition for different beverage volumes.

The model by Moroney et al. (2019) was extended by constitutive equations that relate the model parameters to flow velocity, water temperature, and PSD. This model, originating from the work of Melrose et al. (2018), described the ground coffee as a bi-disperse bulk of spherical particles, i.e., the bimodal PSD of coffee was simplified by reducing it to only two representative particle sizes (fine and coarse). The volume fractions and sizes of those representative particles were estimated from PSD measurements by laser diffractometry. The mass transfer coefficient was related to flow velocity and temperature by a function of Reynolds number and Schmidt number. A van't-Hoff-type equation was used to capture the dependence of the distribution constant from temperature. The parameters were estimated by nonlinear least-squares minimization using the extraction kinetics data of TDS, caffeine, trigonelline, and chlorogenic acid from our previous study (Section 4.2). A sequential estimation procedure was pursued to avoid parameter correlations. The parameterized model was observed to match the experimental data well for all analytes based on the mean absolute percentage error. The model was validated by comparing model predictions of TDS, caffeine, trigonelline, and chlorogenic acid concentrations to additional experimental data at constant temperatures and flow rates. Furthermore, dynamic temperature gradients and flow gradients were compared to evaluate the impact of time-varying conditions. The time variation was motivated by a previous study by Salamanca et al. (2017) who had reported significant differences in TDS and caffeine concentrations between upward and downward gradients. The model results showed good agreement with experimental data except for chlorogenic acid, which can be explained by an unintentional difference in roasting. However, the differences in cup concentrations, comparing the different constant and dynamic temperature and flow rate profiles, were not statistically significant but, if so, caused by a variance in the beverage volume.

Based on the good practicality of the widely known coffee brewing control chart (created for drip coffee), an espresso brewing control chart was proposed which maps the yield of a component, predicted by the model, against temperature and flow rate at different beverage volumes. The control chart was additionally implemented as a MATLAB App to facilitate exploring and comparing the extraction behavior of different compounds at different extraction conditions. The chart visualized well how effects and extraction kinetics differ with respect to the investigated molecules. Especially noteworthy is the observed connection of extraction kinetics to the molecular polarity, which verified findings from other studies on aroma and bitter compounds that the more polar a compound, the quicker it is extracted.

We presented a model in this study which relates relevant molecule-specific features such as the distribution constant and the diffusion coefficient to the influencing factors water temperature and flow rate. Thus, the model supports the understanding of physical phenomena inside the coffee puck that regulate solute mass transfer and reveals the sensitivity of those limiting phenomena towards perturbations in temperature and flow rate. The new espresso brewing control chart is suitable to compare different compounds and influencing variables. It represents a tool to understand and optimize espresso coffee extraction and can be extended by additional data and influencing factors in the future.

4.3.2 Author Contribution

VB Pannusch conceptualized the study. VB Pannusch conducted the modeling part, developed the parameter estimation procedure, and developed the methods of espresso preparation, TDS analysis, and porosity estimation. BKL Schmieder and L Vannieuwenhuyse developed the HPLC analysis method. VB Pannusch conducted the parameter estimations and model simulations, and designed and programmed the espresso brewing control app. VB Pannusch and L Vannieuwenhuyse collaborated on espresso preparation, sampling, and sample preparation. VB Pannusch conducted and evaluated the TDS analyses, L Vannieuwenhuyse conducted and evaluated the HPLC analyses. VB Pannusch evaluated and interpreted the results including statistical analyses. BKL Schmieder, M Minceva, and H Briesen contributed to interpreting the results. VB Pannusch wrote the manuscript; H Briesen and M Minceva reviewed the manuscript.

4.4 Predicting the Essential Oil Composition in Supercritical Carbon Dioxide Extracts from Hop Pellets Using Mathematical Modeling (Pannusch et al. 2023)

4.4.1 Summary

$SCCO_2$ extraction is a common process to extract hop compounds for beer hopping, which was so far mainly used to extract bitter acids. Nevertheless, the main advantage of this process has not yet been fully exploited: the capability to selectively extract target compounds by adjusting CO_2 density while preserving sensible aroma molecules at the typically moderate process temperatures. Since the popularity of hop aroma is rising with the global craft beer movement, recent scientific studies have been focusing on a selective extraction of the aroma-active essential oil. The principal idea of this study is to systematically reach a specific extract composition with targeted aroma characteristics (spicy, floral, citrus, etc.) by adjusting the extraction pressure and temperature. Mathematical modeling was used to predict the temperature- and pressure-dependent extraction kinetics of 7 key aroma compounds: β-myrcene, α-humulene, β-caryophyllene, 2-methylbutyl isobutyrate, undecanone, linalool, and α-pinene.

$SCCO_2$ experiments were conducted in a lab-scale extractor at all combinations of the extraction pressures 90/100/110 bar and the temperatures 40/45/50 °C. The concentration of each aroma component was analyzed via gas chromatography from samples taken in 15 min time intervals up to a total extraction time of 135 min. To identify an appropriate model, we compared two possible models from literature: the Broken and Intact Cells (BIC) model (Sovová 2005) and the Internal Mass Transfer Control (IMTC) model (Del Valle et al. 2000). At first, we estimated the model parameters of both models for each individual experiment. Using the modified Akaike criterion considering the residual sum of squares and the number of parameters estimated, the IMTC model was found to be preferable over the BIC model. Thus, the IMTC model was selected for describing thereupon the influence of temperature and pressure on extraction kinetics. Correlation functions defined how the mass transfer coefficient, the solid-fluid phase distribution, and the initial solid-phase concentration depended on temperature and pressure. For the equilibrium concentration in the fluid phase, the model by Chrastil (1982) was used, whereas the intragranular diffusion resistance, called microstructural factor, and the initial solid-phase concentration were described by second-order response surface models. The respective parameters of those correlation equations were estimated using the extraction kinetics data of the 7 components and of the total extract

mass. The IMTC model, extended by the correlation equations, was able to describe the extraction kinetics of the different analytes and changes with temperature and pressure conditions correctly. The most accurate model predictions were obtained at high pressures (110 bar) and low temperatures (40 °C). Our experiments revealed that the yield of all analyzed aroma compounds increased with a decrease in temperature and an increase in pressure. To validate the predictive performance of the model, the extraction of essential oil components was predicted for three additional experimental conditions in between the pressure-temperature conditions used for parameter estimation. Excellent results were obtained for the sesquiterpenes and total mass, whereas the yields of monoterpenes β-myrcene and α-pinene were overpredicted, possibly due to evaporation losses during storage. The essential oil composition could, however, be predicted accurately for different extraction times and pressure-temperature combinations.

We proved by this study that tuning the essential oil composition and hence the aroma quality of hop extracts by means of mathematical modeling is possible. Especially pressure and extraction time were shown to influence the ratio of monoterpenes and sesquiterpenes to a considerable extent. For industrial applications, we recommend conducting upscaling experiments, as the results in this study were validated for a laboratory scale only. Tailored hop aroma extracts may be produced and optimized based on our study. Those extracts may be used for beer flavoring and entail additional ecological advantages: by reusing the hop pellets after $SCCO_2$ aroma extraction in classic hopping (addition during wort boiling step) and adding the optimized aroma-rich extract to the cool beer before filling, the consumption of hops to produce craft beer may be reduced.

4.4.2 Author contribution

VB Pannusch conceptualized the modeling part of the study, L Viebahn, and M Minceva conceptualized the experimental part of the study. L Viebahn planned the experiments for the parameter estimation, VB Pannusch and L Viebahn planned the experimental design for the model validation experiments. VB Pannusch conducted and evaluated the modeling and simulation, parameter estimation, and the porosity measurements. H Briesen contributed to the modeling part. L Viebahn conducted and evaluated the SFE experiments and GC analyses. VB Pannusch interpreted the simulation results in comparison with the experimental data and was advised by L Viebahn, M Minceva, and H Briesen. L Viebahn interpreted the experimental results concerning molecular differences in extraction kinetics. VB Pannusch wrote the Abstract and Conclusion (100%), and the Introduction, Results, and Methods sections (~80%) together

with L Viebahn who contributed state of knowledge, methods, and results focusing on the experimental part. M Minceva and H Briesen reviewed the manuscript.

5 Discussion

When comparing the studies on espresso coffee extraction and supercritical CO_2 extraction from hops, it is noticeable that, despite the similarity of both models regarding the basic mass balance equations, the models differed substantially in the influence of the process variables on solute concentrations. A change of the solvent temperature by 10 °C did not have a significant influence on the concentrations of compounds in the case of espresso extraction but it caused a considerable change in the solute extraction in $SCCO_2$ extraction. This chapter shall demonstrate the similarities and differences between modeling solid-liquid extraction and supercritical fluid extraction and help to understand the transferability and limitations of our findings. In Section 5.1, we take a closer look on the sensitivity of both extraction processes towards changes in the investigated process variables temperature, pressure, and flow rate. Section 5.2 deals with the connections between molecular structure and extraction kinetics considering the representative taste compounds in coffee extraction and the representative aroma compounds in essential oil extraction.

5.1   Influence of Process Variables on Extract Composition

In Sections 2.1.1 and 2.2.1, the influencing variables of solid-liquid and supercritical fluid extraction were briefly summarized. Both extraction processes depend on (I) the selection of the process, (II) the selection of the solvent and the operating conditions influencing solubility, (III) the preparation of the solid material such as grinding, moisture content, etc. , and (IV) the solvent flow rate or extraction time. Hereafter, we focus on the fluid properties and consider the solid properties such as the surface area to be constant. First, one needs to consider the physical phenomena determining the extraction yield of a single solute. In the beginning of extraction, a certain amount of a compound is dissolved in the solvent, which is represented in our extraction models by the initial equilibrium concentration in the fluid phase. Accordingly, solubility, which depends on the intermolecular forces of fluid and solute, is the first aspect to investigate. Second, extraction of a solute is limited by intragranular diffusion in the solid pore network, which is affected by properties of the fluid and of the solid alike. Hence, the second part of our discussion will focus on the time required to extract a compound. When one understands those two criteria with respect to key sensory components in a certain solid-fluid system, it becomes possible to systematically optimize the process towards a certain sensory quality or to understand the limitations and causality of experiences.

5.1.1 Equilibrium Concentration vs. Solubility

The following section is divided into two subsections. (I) A short summary of fundamental aspects and initial hypotheses regarding solubility in espresso extraction and SFE to support the understanding of the subsequent section. (II) The discussion of hypothesized solubility changes based on the studies presented in this thesis.

I. Fundamental Aspects of Solubility and Initial Hypotheses

Solubility is the maximum concentration at which a molecule is dissolvable in a solvent, it characterizes an equilibrium state. Since the field of solubility research is too large to cover all theories and influencing factors in this thesis, the following discussion limits to the most important phenomena and variables. An old but until today well-known fact about solubility is the latin phrase "similia similibus solvuntur" (Hildebrand 1936, p. 2), nowadays often known as "like dissolves like". This phenomenon can often be related to the polarity of molecules. A simple measure to characterize the polarity of a solvent is, e.g., the dielectric constant (Hildebrand 1936, pp. 78–79). More sophisticated approaches are thermodynamic equilibrium models such as Quantitative Structure Property Relationship (QSPR) models that predict the solubility of a molecule based on molecular descriptors (structural properties such as functional groups) (Klamt and Smith 2007, pp. 301–302). A common method based on those QSPR descriptors is the Conductor-like Screening Model for Realistic Solvation (COSMO-RS) (SCM 2023; Klamt 2018). COSMO-RS models are helpful to understand the different solubilities of individual molecules in a binary molecule-solvent mixture and to investigate a solvent's suitability for selective extraction of a certain molecule.

Having a closer look at SFE, there are several common models to predict the solubilities of compounds in $SCCO_2$. One of the most common models is the semiempirical model by Chrastil (1982) which had also been used in (Pannusch et al. 2023):

$$c^* = \rho_{SCCO_2}^{k} \exp\left(\frac{a}{T} + b\right)$$

Eq. 5.1.1

Here, c^* is the equilibrium concentration, ρ_{SCCO_2} is the density of $SCCO_2$, and T is the temperature. The coefficients k, a, and b are estimated from experiments. Eq. 5.1.1 indicates that solubility depends on temperature and CO_2 density and hence pressure (density increases with pressure). Besides Chrastil's model, equations of state models have been presented, e.g., the Peng-Robinson equation (Peng and Robinson 1976). QSPR models are applicable for $SCCO_2$ as well, e.g., to parameterize Chrastil's model as done in (Valenzuela et al. 2014). In contrast to liquid solvents like water whose den-

sity barely changes with temperature and pressure, SFE depends on the density of the supercritical fluid.

In the coffee literature, it has been stated that the influence of water temperature on taste is mainly caused by its influence on the solubility of compounds (Folmer 2017, pp. 365–368; Cordoba et al. 2020). With regard to SFE, the solubility of essential oil components changes significantly with pressure and temperature (Berna et al. 2000; da Cruz Francisco and Sivik 2002). This change can limit the extraction yield based on model investigations by Ajchariyapagorn et al. (2009). Thus, the initial hypotheses of this thesis can be summarized as follows: the solubility of taste molecules in espresso extraction can be manipulated by a change in water temperature based on solvation thermodynamics; the solubility of aroma molecules in $SCCO_2$ extraction is additionally influenced by the CO_2 density.

II. *Equilibrium Concentrations in Espresso Extraction and Supercritical Fluid Extraction*

To compare the influence of temperature and pressure (in case of SFE) on solubility in the scope of the espresso coffee (Pannusch et al. 2024) and hop extraction (Pannusch et al. 2023) modeling study, the initial state of extraction is investigated. From the estimated distribution constants K_i of a solute i and the initial mass fractions of a solute $x_{0,i}$ in the solid material, the mass fraction of a solute in the fluid phase $y_{0,i}^*$ was predicted:

$$y_{0,i}^* = K_i\, x_{0,i}$$

Eq. 5.1.2

This mass fraction at equilibrium $y_{0,i}^*$ was then normalized by the mass fraction at the lowest temperature of the investigated range and the respective pressure to enable comparability between solutes, which yielded for espresso extraction:

$$y_{0,i,rel}^* = \frac{y_{0,i}^*\left(x_{0,i},\ T\right)}{y_{0,i}^*\left(x_{0,i}, 80\,°C\right)}$$

Eq. 5.1.3

And for $SCCO_2$ extraction from hops:

$$y_{0,i,rel}^* = \frac{y_{0,i}^*\left(x_{0,i},\ p, T\right)}{y_{0,i}^*\left(x_{0,i}, p, 40\,°C\right)}$$

Eq. 5.1.4

The curves of this relative equilibrium mass fraction are plotted in Figure 5.1 for espresso extraction and in Figure 5.2 for SFE from hops. It can be seen from Figure 5.1

that the predicted equilibrium mass fractions of the coffee components caffeine, trigonelline, and chlorogenic acids decrease by less than 5 % with an increase in temperature, whereas the equilibrium mass fractions of the aroma oil components plotted in Figure 5.2 decrease by up to 37 % at 110 bar and 57 % at 90 bar at a temperature rise from 40 to 50 °C. The reader is advised that, regarding espresso extraction, the changes in equilibrium concentration with a temperature change from 80 to 100 °C were in the same range as the mean experimental error indicating a lack of significance, as concluded in (Pannusch et al. 2024). The negative correlation with temperature observed could accordingly be a result of experimental error rather than molecular physics. The same lack of solubility change was observed for the total mass of solutes, the TDS, indicating that this observation is not only limited to the three analyzed compounds but applies to most soluble non-volatile components in espresso extraction. It is concluded that a change by 10 °C leads to a considerable change in solubility in SFE but does barely influence the solubility of non-volatiles in espresso extraction. This difference in sensitivity may be explained by the fluid properties of water and $SCCO_2$. Figure 5.3 shows the temperature dependence of the density and dielectric constant of water. Both properties decrease only slightly with temperature in the investigated range. However, the density of $SCCO_2$ changes drastically as visible in Figure 5.4. It decreases with increasing temperature and increases with an increase in pressure. It is moreover noteworthy that even the shapes of the density curves at 90 bar and 110 bar are similar to the curves of the equilibrium mass fraction in Figure 5.2: a higher slope is observable in the lower temperature region for 90 bar than for higher pressures. Our results for SFE indicate that density strongly influences the equilibrium concentration in $SCCO_2$ extraction and that a higher temperature reduces the solubility of essential oil components in hops. The same was observed in a study by Berna et al. (2000) for limonene and linalool data, which verifies the qualitative prediction of our model parameters. The dielectric constant of $SCCO_2$ behaves similar as the density: it increases with an increase in pressure and decreases with an increase in temperature. The changes are however small according to data reported by Zhang et al. (2005) where the dielectric constant decreased from 1.25 at 40 °C to 1.13 at 60 °C, at a pressure of 90 bar, and from 1.40 at 40 °C to 1.20 at 60 °C, at a pressure of 110 bar.
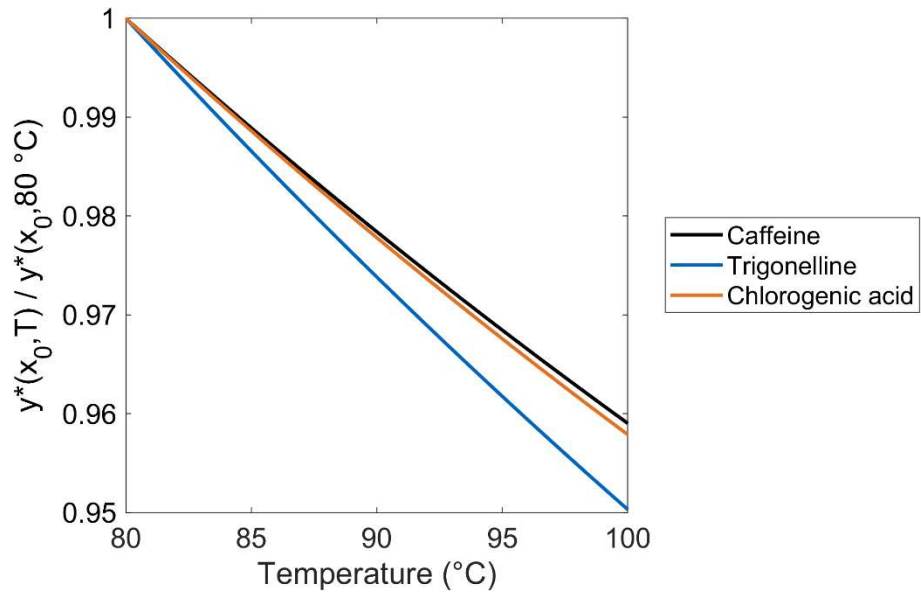
Figure 5.1. Relative initial equilibrium mass fraction in water against temperature based on model parameters in (Pannusch et al. 2024).
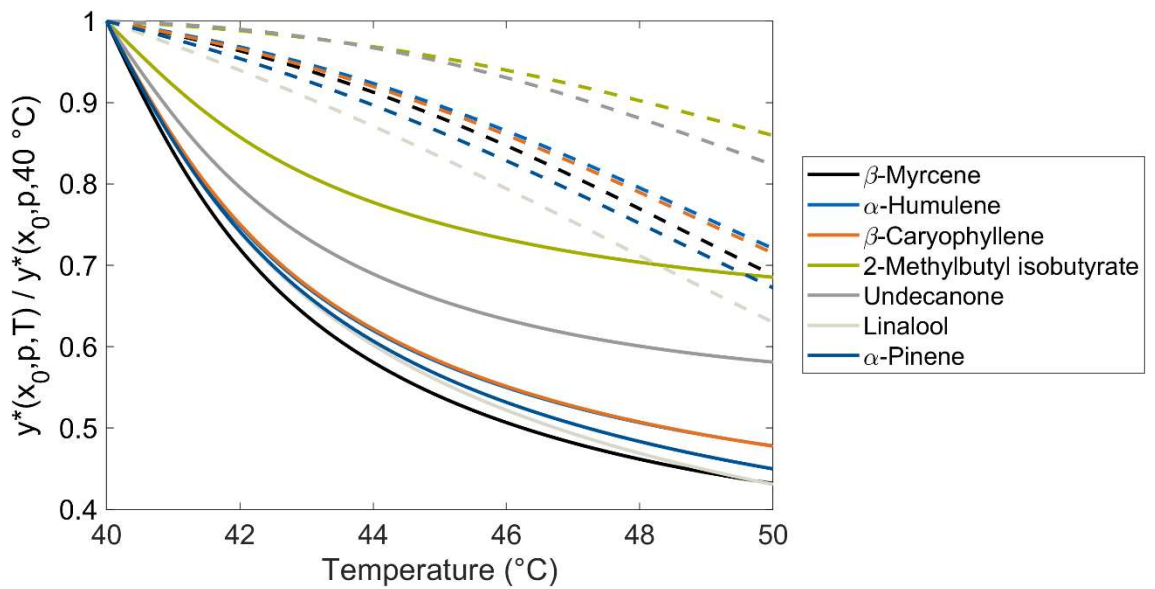

Figure 5.2. Relative initial equilibrium concentration in SCCO$_2$ against temperature at extraction pressures 90 bar (solid lines) and 110 bar (dashed lines) based on model parameters in (Pannusch et al. 2023).
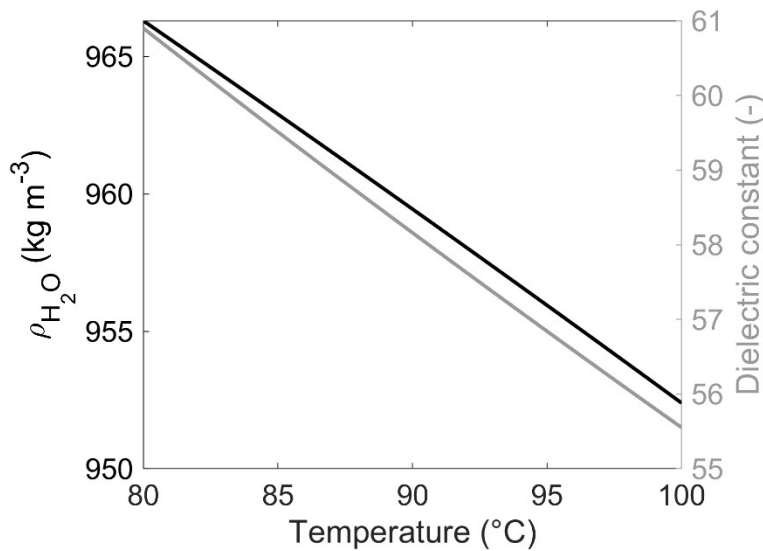
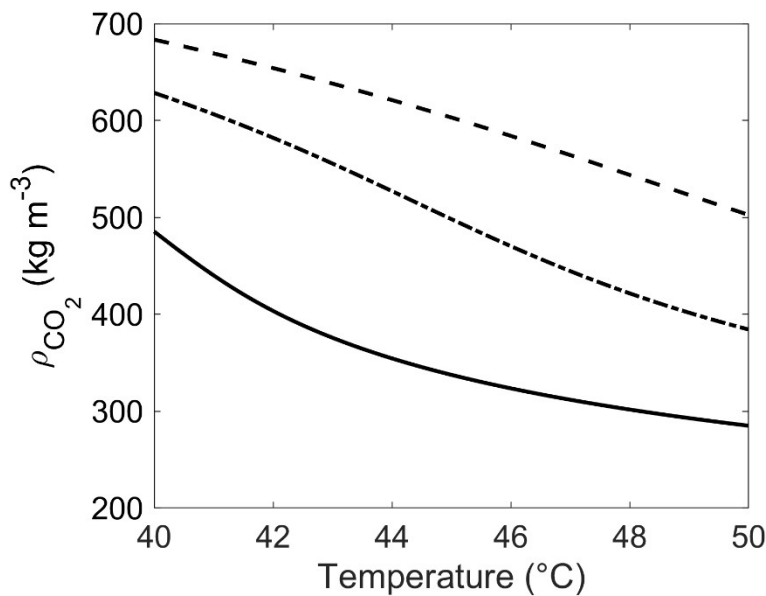Figure 5.3. Density (VDI-Wärmeatlas 2006) and dielectric constant (Archer and Wang 1990) of water against temperature.

Figure 5.4. Density of SCCO$_2$ against temperature at 90 bar (solid line), 100 bar (dash-dotted line), and 110 bar (dashed line).

Besides the fluid properties, the concentrations of the components play an important role in evaluating the impact of temperature on espresso extraction. It is probable that the solid-phase concentration of most polar compounds is far below their solubility concentration at espresso extraction temperatures. A good example is caffeine which exhibits a solubility of 182 mg mL^{-1} (The Merck index 2013, p. 289) which is almost 20 times higher than the initial concentrations observed in our study. If the concentration of a compound is by far lower than its solubility concentration (saturation), it should be released completely into the fluid phase if not physically or chemically adsorbed to the

solid material. Although the solubility of caffeine increases strongly between 80 and 100 °C (The Merck index 2013, p. 289), it does not influence the extraction of caffeine from the solid coffee particles during espresso extraction. Previous assumptions that the influence of temperature on espresso coffee extraction is caused by a change in molecular solubility are therefore refuted. A lack of temperature effect on taste and TDS was also observed by Batali et al. (2020) in a recent study on drip coffee extraction, which confirms our conclusion that solubility has no significant impact in the hot brew range above 80 °C. Solubility plays, however, a role in cold-brew coffee, as, with a reduction of temperature to <10 °C, the equilibrium concentrations of taste compounds may fall to the same range or below their contents in the coffee bean (e.g. caffeine solubility at 20 °C is 22 mg mL^{-1} (The Merck index 2013, p. 289)).

5.1.2 Diffusion Time Scale vs. Extraction Time

Both solid-liquid and supercritical fluid extraction processes are in some cases limited by intra-particle diffusion. Understanding diffusion from the solid phase in that case is critical to select an appropriate extraction time. Dimensionless numbers are useful to investigate and optimize a process and to compare different processes. One number of this type is the Fourier number Fo which relates a characteristic time such as the process time to a characteristic diffusion time scale (Bear 2018, p. 250). Based on the model and parameters presented in (Pannusch et al. 2024), we define the diffusion time scales of a compound i for fine particles (subscript 1) and coarse particles (subscript 2) in espresso extraction as:

$$t_{COF,1,dif} = \frac{d_{s1}}{6\,(1-\varepsilon)\,k_{sl1,i}} \quad ; \quad t_{COF,2,dif} = \frac{d_{s2}}{6\,(1-\varepsilon)\,k_{sl2,i}}$$

Eq. 5.1.5

The characteristic extraction time is selected as the time at which a beverage volume of 60 mL is reached at a given flow rate Q:

$$t_{COF,E} = \frac{60\,mL}{Q}$$

Eq. 5.1.6

With regard to SCCO$_2$ extraction from hops, the diffusion time scale was calculated from the parameters determined in (Pannusch et al. 2023):

$$t_{SFE,dif} = \frac{d_s}{2\,(1-\varepsilon)\,k_{sf,i}}$$

Eq. 5.1.7

The characteristic extraction time was set to the final process time: $t_{SFE,E} = 135 \cdot 60\,s = 8100\,s$. From those characteristic time scales, Fo was calculated in each case by:

$$Fo = \frac{t_{c,E}}{t_{c,dif}}$$
<div align="right">Eq. 5.1.8</div>

Figure 5.5 shows the values of Fo for espresso extraction against flow rate within the investigated range. Solid lines represent the Fo values of fine particles, dashed lines are the Fo values of coarse particles. At all conditions, fine particles exhibit a $Fo > 1$, whereas $Fo < 1$ is observed for coarse particles, valid for all three components. This observation indicates that in a typical extraction time between 20 and 60 s for brewing 60 mL of espresso, diffusion from coarse particles (diameter of 330 µm in this case) has barely taken place. In contrast, diffusion from fine particles of 24 µm in diameter considerably influenced extraction in the respective time scale. It is furthermore observable that Fo reduces with increasing flow rate. This means that the effect of the predicted increase of the mass transfer coefficient with a rise in flow rate (Sherwood function in (Pannusch et al. 2024)) is less than the effect of the respective decrease in extraction time. The difference is furthermore higher between 1 and 2 mL s^{-1} than it is between 2 and 3 mL s^{-1} and the ratio of the caffeine and chlorogenic acid Fo changed as well. Figure 5.5 stresses the importance of the fine particle fraction for espresso coffee extraction. Although a change in the size of coarse particles may influence permeability and flow homogeneity, a sufficient amount of fine particles is key for espresso extraction yield and composition. Based on Figure 5.5 and the espresso brewing control chart presented in (Pannusch et al. 2024), a change in the flow rate should affect the extraction yield and composition in an extraction time range between 30 and 60 s but barely influences the beverage between 20 and 30 s.
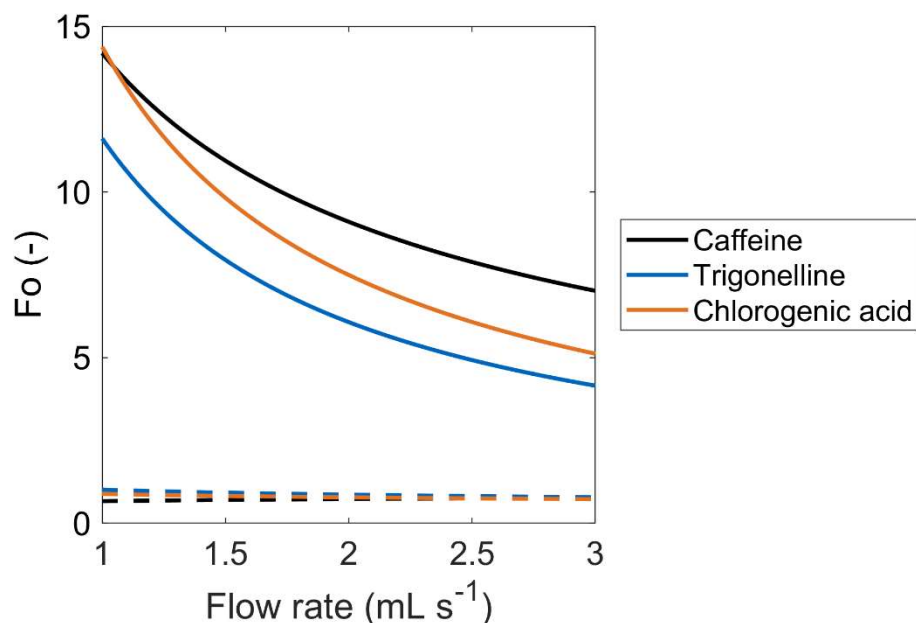
Figure 5.5. Fourier number (Fo) of different compounds vs. flow rate based on parameters from (Pannusch et al. 2024) for fine particles (solid lines) and coarse particles (dashed lines).

Figure 5.6 presents Fo versus the applied pressure in SCCO$_2$ extraction from hops. For the sake of better visibility, only the major oil components β-myrcene, α-humulene, β-caryophyllene, and 2-Methylbutyl isobutyrate (2-MBIB) are plotted. The curves of the other analytes undecanone, linalool, and α-pinene are very similar to the ones of 2-MBIB. It can be seen in Figure 5.6 that $Fo \gg 1$, which confirms that the chosen process time is long enough that diffusion of all compounds takes place to a significant extent. The Fo of the monoterpene β-myrcene is by factor 4 lower than the ones of all other compounds, which is due to a lower estimated value of the microstructural factor F_M (diffusion resistance, see (Pannusch et al. 2023)). This means that effective diffusion of β-myrcene is predicted to be slower than diffusion of other aroma compounds. Nevertheless, β-myrcene was extracted faster due to its higher predicted equilibrium concentration (Pannusch et al. 2023). All curves are plotted at two different temperatures: 40 °C (solid lines) and 50 °C (dashed lines). In general, the relative changes of Fo values with a change in pressure and temperature are only marginal compared with the changes of coffee components in Figure 5.5 (factor > 2). Fo values change in the same way with a change in pressure and temperature for all compounds except β-myrcene whose Fo decreases with increasing pressure at low temperature and behaves contrarily at higher temperature. This distinction of β-myrcene from the other components matches the differently shaped F_M plot of β-myrcene, seen in (Pannusch et al. 2023). Changes of F_M with pressure and temperature may be related to changes in wetting and penetration of the fluid into the solid material due to changes in the SCCO$_2$ viscosi-

ty and surface tension. Another possible reason, discussed in (Pannusch et al. 2023), is the co-extraction of cuticular waxes which act as a barrier.
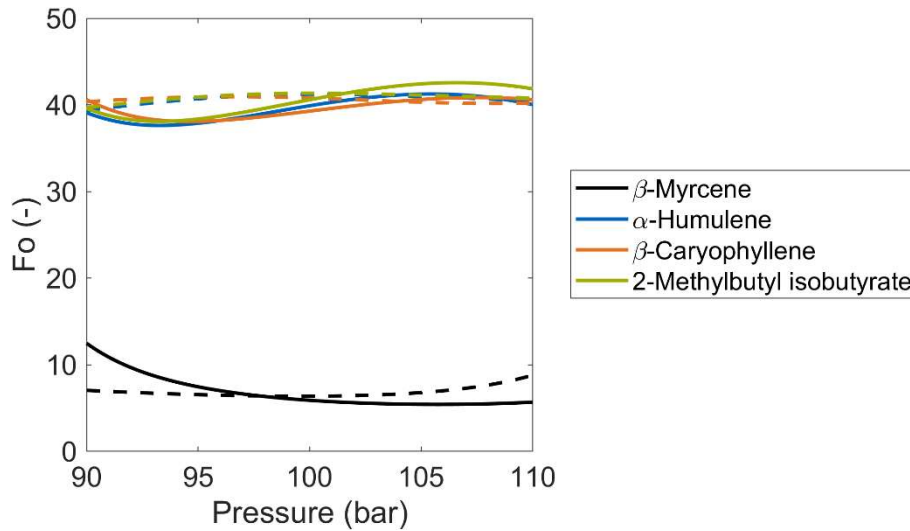

Figure 5.6. Fourier number of major compounds vs. extraction pressure based on parameters from (Pannusch et al. 2023) at 40 °C (solid lines) and 60 °C (dashed lines).

Table 5.1. Diffusion time scales of compounds at medium conditions: espresso extraction at 2 mL s^{-1} and 90 °C and supercritical fluid extraction of hop oil at 100 bar and 40 °C.

Espresso extraction		Supercritical CO2 extraction from hops	
Component	$t_{c,dif}$ / s	Component	$t_{c,dif}$ / s
Fine particles		β-Myrcene	1,270
Caffeine	14	α-Humulene	196
Trigonelline	21	β-Caryophyllene	198
Chlorogenic acid	17	2-MBIB	196
Coarse particles		Undecanone	196
Caffeine	176	Linalool	196
Trigonelline	147	α-Pinene	196
Chlorogenic acid	163		

In Table 5.1, the diffusion time scales are listed with respect to espresso extraction and SCCO$_2$ from hops at medium flow rate and pressure, respectively. The time scales of coarse coffee particles, which consist of intact cells, are by one order of magnitude higher than the time scales of fine particles (broken cells). To extract components from coarse coffee particles, extraction times of more than 2.5 min are required, as applied in immersion brewing or drip coffee brewing. It is noteworthy that the diffusion time scales of taste compounds from coarse particles are in the same range as the diffusion time scales of aroma compounds in SCCO$_2$ extraction. Those relatively high time scales indicate intragranular diffusion limitation for both coarse coffee particles and hop pellets. We conclude from the above observations that the diffusion time scales and

Fourier numbers based on model predictions not only help to select an appropriate extraction time and flow rate but also to better understand the tunability and limitations of extraction processes.

5.2 Extraction Kinetics of Taste and Aroma Compounds – A Question of Polarity and Molecular Mass

Both modeling studies, (Pannusch et al. 2024) and (Pannusch et al. 2023), showed that the extraction kinetics of taste and aroma compounds are crucial criteria that differentiate components from one another and that determine the extract composition. To relate extraction kinetics with the molecular properties, the estimated solid-fluid distribution constants K of all analyzed compounds were investigated in comparison with their molecular structures and properties. Investigating a molecule's solubility based on its structural properties belongs to the field of thermodynamic equilibrium modeling, a broad field of research. As described previously in this section, QSPR models including structural descriptors to predict Gibbs free energy of solvation can be used, e.g., to predict the aqueous solubility of organic compounds (Meftahi et al. 2021). Predicting, however, the dissolution equilibrium of a molecule from a solid mixture of various components into an aqueous solution containing a variety of solutes as well as dispersed fine particles and oil droplets, would not be possible without oversimplifying assumptions. Hence, a simple comparison of parameters and easily available molecular data (octanol-water partition coefficients and molecular mass) is subsequently applied to identify molecular descriptors that are useful for estimating and distinguishing compound-specific extraction kinetics in espresso coffee extraction and $SCCO_2$ extraction of essential oil from hops. The reader is advised that the comparison hereafter is limited to the experimental data presented in (Schmieder et al. 2023) and (Pannusch et al. 2023), and should rather be interpreted as an attempt of facilitating process understanding and knowledge transferability than a general rule.

Figure 5.7 shows the chemical structures, the octanol-water coefficients log K_{OW} (indicator of polarity) and the molecular mass of caffeine, chlorogenic acid, and trigonelline. Trigonelline, which forms a zwitterion in aqueous solution, is the most polar of the three compounds with a log K_{OW} = -2.53. The estimated distribution constants K reflect this phenomenon since the values of caffeine and chlorogenic acid are less than the value of trigonelline. The fact that the order of K matches conversely the order of log K_{OW}, with the least polar compound caffeine exhibiting the lowest K, shows that polarity is an important molecular property to explain extraction kinetics of non-volatile solutes in

espresso extraction. The molecular mass (see Figure 5.7) has, in contrast, no noticeable impact in this case; despite the significantly larger size of chlorogenic acid than caffeine, the K values of both molecules do not differ much. It has been shown in (Pannusch et al. 2024) that trigonelline was extracted significantly faster than caffeine and chlorogenic acid. Our finding that more polar taste compounds are extracted faster than less polar molecules confirmed earlier studies by Blumberg et al. (2010), Mestdagh et al. (2014), and Vaca Guerra et al. (2023a). Based on this knowledge, the distribution constant in the mass transport model presented in (Pannusch et al. 2024) may be used in the future for quickly estimating the extraction behavior of similar taste compounds.

a) Caffeine[1] **c) Chlorogenic acid[2]** **b) Trigonelline[3]**

K = 0.80
log K_{OW} = -0.07
M = 194.19 g mol⁻¹

K = 0.94
log K_{OW} = -0.356
M = 354.31 g mol⁻¹

K = 1.36
log K_{OW} = -2.53
M = 137.14 g mol⁻¹
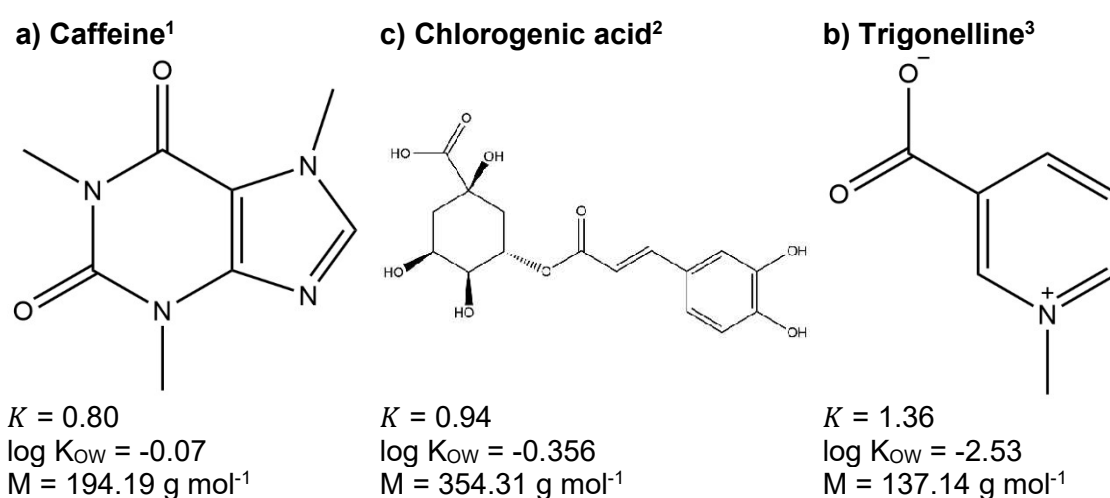
Figure 5.7. Molecular structures, model distribution constants at 87 °C (Pannusch et al. 2024), octanol-water partition coefficients, and molecular mass of coffee components.

The molecular data and K values are depicted for the seven analyzed aroma compounds of hop essential oil in Figure 5.8: the monoterpenes β-myrcene and α-pinene, the sesquiterpenes α-humulene and β-caryophyllene, the ketone undecanone, and the more polar compounds 2-MBIB and linalool. The monoterpenes, sesquiterpenes, and undecanone are much less polar than the compounds 2-MBIB and linalool. This can be seen from the polar ester and hydroxyl group in the chemical structure of the latter and their log K_{OW} values of below 3 (log K_{OW} > 4 for the other compounds). In contrast to the results received for espresso extraction (Figure 5.7) no correlation is observed between the values of log K_{OW} and K. However, a similar order can be seen for K and the molecular mass M. The smallest molecule β-myrcene exhibits the highest value of K followed by compounds of intermediate molecular mass (2-MBIB, linalool, and undecanone), and are least for the largest molecules, the sesquiterpenes α-humulene
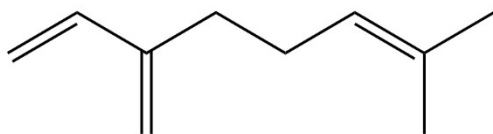
---

[1] Molecule data from https://pubchem.ncbi.nlm.nih.gov/compound/2519, checked on 5/13/2023
[2] Molecule data from https://pubchem.ncbi.nlm.nih.gov/compound/1794427, checked on 5/13/2023
[3] Molecule data from https://pubchem.ncbi.nlm.nih.gov/compound/5570, checked on 5/13/2023

and β-caryophyllene. The only exception is α-pinene which exhibits a small value of K although it has the same molecular mass as β-myrcene. An explanation for this difference might be its hexagonal ring conformation or a larger error in parameter estimation, because concentrations of α-pinene were small and exhibited large errors, which lead to comparatively low prediction accuracy of the model (Pannusch et al. 2023).
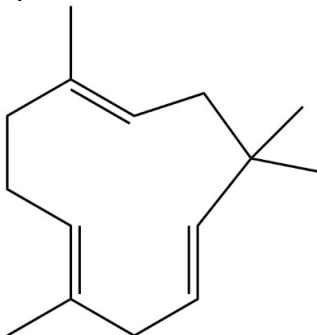
a) β-Myrcene[1]

K = 1.26
log K_{OW} = 4.33
M = 136.23 g mol^{-1}

b) α-Pinene[2]
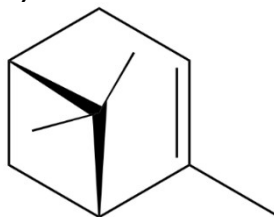
K = 0.20
log K_{OW} = 4.83
M = 136.23 g mol^{-1}

c) α-Humulene[3]

K = 0.24
log K_{OW} = 4.5
M = 204.35 g mol^{-1}

d) β-Caryophyllene[4]
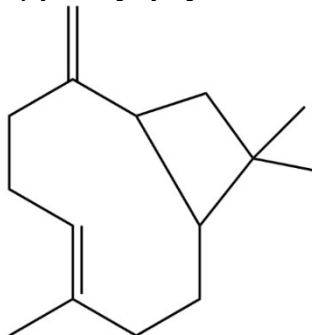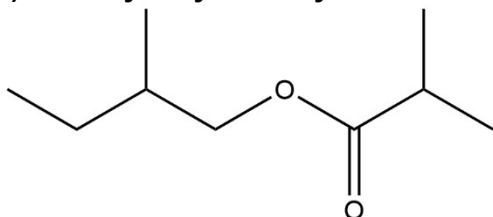
K = 0.25
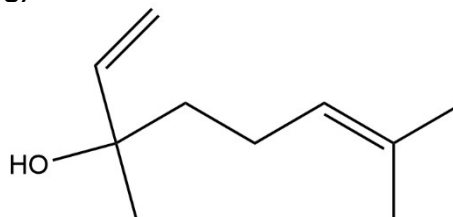log K_{OW} = 4.4
M = 204.35 g mol^{-1}

e) Undecanone[5]
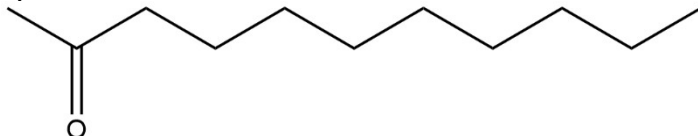
K = 0.27
log K_{OW} = 4.09
M = 170.29 g mol^{-1}

f) 2-Methylbutyl isobutyrate[6]

K = 0.38
log K_{OW} = 2.8
M = 158.24 g mol^{-1}

g) Linalool[7]

K = 0.30
log K_{OW} = 2.97
M = 154.25 g mol^{-1}

Figure 5.8. Molecular structures, model distribution constants at 40 °C and 110 bar (Pannusch et al. 2023), octanol-water partition coefficients, and molecular mass of hop essential oil components.

[1] Molecule data from https://pubchem.ncbi.nlm.nih.gov/compound/31253, checked on 5/13/2023

[2] Molecule data from https://pubchem.ncbi.nlm.nih.gov/compound/6654, checked on 5/13/2023

[3] Molecule data from https://pubchem.ncbi.nlm.nih.gov/compound/5281520, checked on 5/13/2023

[4] Molecule data from https://pubchem.ncbi.nlm.nih.gov/compound/5281515, checked on 5/13/2023

[5] Molecule data from https://pubchem.ncbi.nlm.nih.gov/compound/8163, checked on 5/13/2023

[6] Molecule data from https://pubchem.ncbi.nlm.nih.gov/compound/97883, checked on 5/13/2023

[7] Molecule data from https://pubchem.ncbi.nlm.nih.gov/compound/6549, checked on 5/13/2023

The model-based extraction kinetics of the aroma compounds are plotted in a normalized form in Figure 5.9 for maximum-yield conditions (40 °C, 110 bar). Comparing the order of the curves from left to right with the distribution constants K in Figure 5.8 clarifies that K determines the different extraction kinetics of the components. The higher K, the faster a component is extracted. In contrast to espresso extraction, K is – when comparing essential oil compounds – not influenced by the molecules' polarity but rather by their molecular mass, i.e., the smaller an aroma compound, the faster it is extracted. Accordingly, molecular mass may serve as a criterion for differentiating extraction kinetics in SCCO$_2$ extraction of aroma compounds from hop pellets and for predicting the extract composition at different extraction times. Regarding potential applications, fractional extraction, where the extract is, e.g., collected at different time intervals to achieve different extract compositions, may benefit from this model-based evaluation. Optimal times of fraction collections may be obtained through predicting the change of the composition with time by using a parameterized mass transport model as the one presented in (Pannusch et al. 2023). In combination with the selection of optimal pressure-temperature combinations, SFE processes may be optimized to develop new products, improved product quality, or higher contents of target compounds.
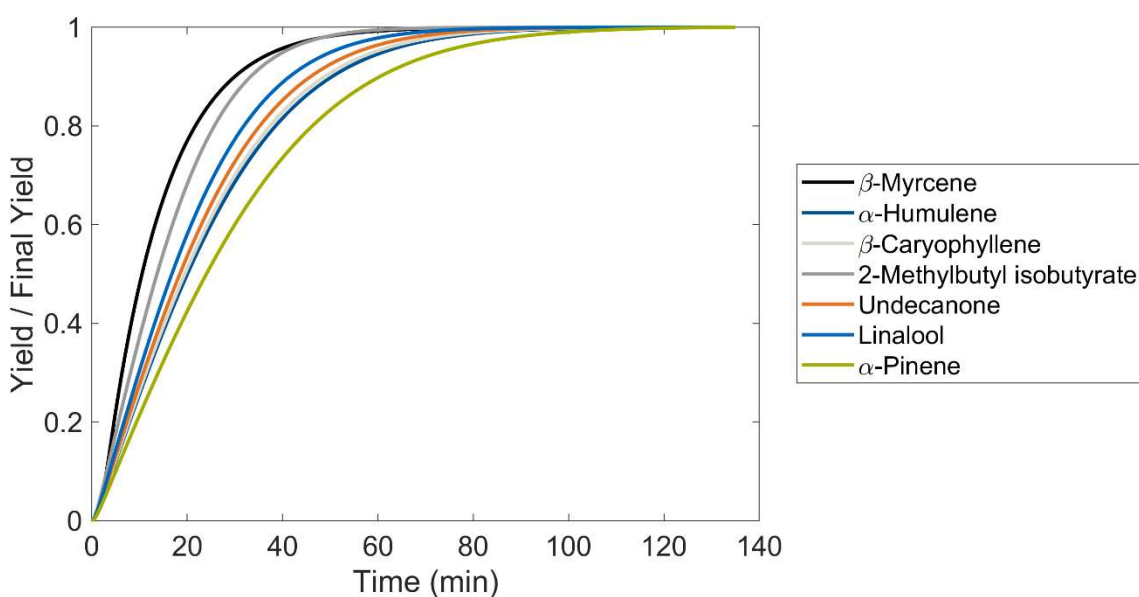

Figure 5.9. Normalized extraction kinetics of hop essential oil components as predicted by the IMTC model for 40 °C and 110 bar (Pannusch et al. 2023).

6 Conclusion & Outlook

It is evident from the results of this thesis that mathematical modeling and simulation contributes to unveiling relevant physical phenomena and predicting the extract composition for different types of percolation extractions such as solid-liquid extraction (espresso coffee extraction) and supercritical fluid extraction ($SCCO_2$ extraction from hops). The remaining question is: what are the general benefits and limits of the presented research and what kinds of applications do our conclusions imply? The following section shall summarize the main findings and achievements and how they may contribute to future research and innovations.

In both espresso extraction and SFE from hops, the parameterized mechanistic models successfully predicted the analyzed compounds' extraction kinetics, i.e., how extract composition changes over process time. Furthermore, different molecule-specific extraction kinetics were observed, which could be captured by the model parameters. These general findings entail various possible applications. To optimize espresso taste, the kinetic espresso brewing control chart may be used to find an optimal brew ratio considering bitter and sour components along with TDS (representing overall strength). Replacing trial-and-error strategies by such model-based approach may direct innovations in espresso machine technology and may be used for training professionals and end users. In supercritical fluid extraction, a fractionated extract collection aiming for a certain aroma composition may allow enhanced and targeted extract quality without the need of additional separation steps. For manipulating the aroma profile by collecting separate fractions during extraction, one may rely on the difference in extraction kinetics between monoterpenes, such as β-myrcene, and sesquiterpenes, such as α-humulene. This way, extracts with higher content of target compounds or characteristic sensory properties may be produced without the need of additional purification operations.

An important feature of our models is the introduction of correlation functions that relate kinetic and equilibrium model parameters to the investigated process variables, i.e., solvent temperature, flow rate, pressure, and particle size distribution. Those correlations are parameterized from experimental data (extraction kinetics) at different process conditions. On the one hand, this means that the parameters obtained from parameter estimation lack physical meaning and generality, because they are not based on physical theory or material constants and prone to data quality and quantity. On the other hand, a data-based approach enables predictions at relatively high accuracy de-

spite the natural plant materials' complex composition. To improve generality and enable extrapolation of results in the long term, automated experiments to create large datasets combined with data-driven models, such as machine learning, are recommended. The result would be a hybrid model consisting of mechanistic balance equations and data-based correlations. It should, however, be considered that data-driven models strongly depend on the type and amount of available data, which represents the most important limitation of this approach. In addition to extraction kinetics data, experimental data from high-resolution imaging, e.g., micro-computed tomography, may be used in the future to quantify dynamic changes in the porous medium properties and fluid dynamics.

When it comes to the practical application of our results, one should consider the processes' sensitivity towards the investigated process variables:

I.   Espresso coffee extraction

It was demonstrated experimentally that a change in water temperature above 80 °C did not have a significant effect on extract composition and TDS. Based on the experimental data of caffeine, trigonelline, and chlorogenic acid, the brew ratio had the largest effect on the beverage composition. Our results indicate that an optimization of the brew ratio and a precise control of the beverage volume, by using, e.g., a scale instead of a timer for stopping the espresso brewing process, would be more effective than adjusting the water temperature or flow rate within the investigated range. The question of how those process variables influence other components among the thousands of volatile and non-volatile coffee ingredients cannot be answered by this study. However, the basic coffee brewing control chart might be extended by additional data in the future to obtain a more comprehensive picture about the relations between process variables and sensory profile. One question that could not yet be answered by this thesis is the role of the PSD. The relation between PSD properties, specific surface area and pressure loss require further research to improve the model's practical applicability. Furthermore, flow inhomogeneity as well as dynamic changes in the bed porosity and fine particle migration require further research to shade more light on the (gradually shrinking) black box of espresso coffee extraction.

II. $SCCO_2$ extraction of essential oil from hops

A key finding of this thesis was the varying pressure and temperature sensitivity comparing the investigated aroma compounds. Not only did the pressure-temperature conditions influence the overall essential oil yield but they additionally affected the oil's

composition. Being able to predict those sensitivities by having a parameterized model at hand raises the idea of applying numerical optimization and optimal control. If one aimed for a certain target composition to reach a desired sensory profile, the model could be used for nonlinear optimization algorithms, which would determine a pressure-temperature combination that minimizes the difference from this target composition. Even dynamic optimal pressure and temperature profiles might be feasible using optimal control theory, provided that time-varying control was technically feasible. Another downside: the results from optimization and optimal control would only be applicable for the same experimental setup and raw material that has been used for parameter estimation. Due to the limited amount of data, model predictions should furthermore not be extrapolated beyond the experimental design space. These limitations do, however, not mean that the general methodology cannot be replicated for other experimental data and raw materials. An example of current interest is the selective extraction of cannabinoids from cannabis using supercritical fluid. In that context, our study might provide a direction towards selecting an appropriate model for optimizing process conditions and maximizing cannabinoid yield and purity.

7 References

Ajchariyapagorn, Araya; Kumhom, Thippawan; Pongamphai, Suwassa; Douglas, Supaporn; Douglas, Peter L.; Teppaitoon, Wittaya (2009): Predicting the extraction yield of nimbin from neem seeds in supercritical CO2 using group contribution methods, equations of state and a shrinking core extraction model. In *The Journal of Supercritical Fluids* 51 (1), pp. 36–42. DOI: 10.1016/j.supflu.2009.06.022.

Albanese, D.; Di Matteo, M.; Poiana, M.; Spagnamusso, S. (2009): Espresso coffee (EC) by POD: Study of thermal profile during extraction process and influence of water temperature on chemical–physical and sensorial properties. In *Food Research International* 42 (5-6), pp. 727–732. DOI: 10.1016/j.foodres.2009.02.027.

Andueza, S.; Maeztu, L.; Pascual, L.; Ibáñez, C.; Peña, M. P. de; Cid, C. (2003): Influence of extraction temperature on the final quality of espresso coffee. In *J. Sci. Food Agric.* 83 (3), pp. 240–248. DOI: 10.1002/jsfa.1304.

Angeloni, Giulia; Guerrini, Lorenzo; Masella, Piernicola; Innocenti, Marzia; Bellumori, Maria; Parenti, Alessandro (2019): Characterization and comparison of cold brew and cold drip coffee extraction methods. In *J. Sci. Food Agric.* 99 (1), pp. 391–399. DOI: 10.1002/jsfa.9200.

Angeloni, Simone; Giacomini, Josephin; Maponi, Pierluigi; Perticarini, Alessia; Vittori, Sauro; Cognigni, Luca; Fioretti, Lauro (2023): Computer Percolation Models for Espresso Coffee: State of the Art, Results and Future Perspectives. In *Applied Sciences* 13 (4), p. 2688. DOI: 10.3390/app13042688.

Archer, Donald G.; Wang, Peiming (1990): The Dielectric Constant of Water and Debye-Hückel Limiting Law Slopes. In *Journal of Physical and Chemical Reference Data* 19 (2), pp. 371–411. DOI: 10.1063/1.555853.

Aster, Richard C.; Borchers, Brian; Thurber, Clifford H. (2019): Parameter estimation and inverse problems. Third edition. Amsterdam, Oxford, Cambridge, MA: Elsevier. Available online at https://www.sciencedirect.com/science/book/9780128046517.

Baldino, Lucia; Adami, Renata; Reverchon, Ernesto (2018): Concentration of Ruta graveolens active compounds using SC-CO2 extraction coupled with fractional separation. In *The Journal of Supercritical Fluids* 131, pp. 82–86. DOI: 10.1016/j.supflu.2017.09.008.

Batali, Mackenzie E.; Ristenpart, William D.; Guinard, Jean-Xavier (2020): Brew temperature, at fixed brew strength and extraction, has little impact on the sensory profile of drip brew coffee. In *Scientific reports* 10 (1), p. 16450. DOI: 10.1038/s41598-020-73341-4.

Bear, Jacob (2018): Modeling phenomena of flow and transport in porous media. Cham: Springer (Theory and applications of transport in porous media, Vol. 31).

Bear, Jacob; Bachmat, Yehuda (1991): Introduction to modeling of transport phenomena in porous media. Dordrecht: Kluwer Academic (Theory and applications of transport in porous media, 4).

Bear, Jacob; Whitaker, Stephen (1999): The Method of Volume Averaging. Dordrecht: Springer Netherlands (13).

Berna, Angel; Cháfer, Amparo; Montón, Juan B. (2000): Solubilities of essential oil components of orange in supercritical carbon dioxide. In *Journal of Chemical & Engineering Data* 45 (5), pp. 724–727. DOI: 10.1021/je9903101.

Bickley, W. G. (1941): Formulae for Numerical Differentiation. In *Math. Gaz.* 25 (263), pp. 19–27. DOI: 10.2307/3606475.

Biendl, Martin; Engelhard, Benhard; Forster, Adrian; Gahr, Andreas; Lutz, Anton; Mitter, Willi et al. (2015): Hops: their cultivation, composition and usage: Fachverlag Hans Carl (1).

Bizaj, Katja; Škerget, Mojca; Košir, Iztok Jože; Knez, Željko (2021): Sub-and supercritical extraction of slovenian hops (Humulus lupulus L.) aurora variety using different solvents. In *Plants* 10 (6), p. 1137. DOI: 10.3390/plants10061137.

Bizaj, Katja; Škerget, Mojca; Košir, Iztok Jože; Knez, Željko (2022): Hop (Humulus lupulus L.) Essential Oils and Xanthohumol Derived from Extraction Process Using Solvents of Different Polarity. In *Horticulturae* 8 (5), p. 368. DOI: 10.3390/horticulturae8050368.

Blumberg, Simone; Frank, Oliver; Hofmann, Thomas (2010): Quantitative studies on the influence of the bean roasting parameters and hot water percolation on the concentrations of bitter compounds in coffee brew. In *Journal of agricultural and food chemistry* 58 (6), pp. 3720–3728. DOI: 10.1021/jf9044606.

Britannica, The Editors of Encyclopaedia (2019): parenchyma. Edited by Encyclopedia Britannica. Available online at https://www.britannica.com/science/parenchyma-plant-tissue, updated on 9/6/2019, checked on 8/14/2023.

Britannica, The Editors of Encyclopaedia (2022): phloem. Edited by Encyclopedia Britannica. Available online at https://www.britannica.com/science/phloem, updated on 2/3/2022, checked on 8/14/2023.

Calvo-Flores, Francisco G.; Monteagudo-Arrebola, María José; Dobado, José A.; Isac-García, Joaquín (2018): Green and Bio-Based Solvents. In *Topics in current chemistry (Cham)* 376 (3), p. 18. DOI: 10.1007/s41061-018-0191-6.

Cameron, Michael I.; Morisco, Dechen; Hofstetter, Daniel; Uman, Erol; Wilkinson, Justin; Kennedy, Zachary C. et al. (2020): Systematically Improving Espresso: Insights from Mathematical Modeling and Experiment. In *Matter* 2 (3), pp. 631–648. DOI: 10.1016/j.matt.2019.12.019.

Capuzzo, Andrea; Maffei, Massimo E.; Occhipinti, Andrea (2013): Supercritical fluid extraction of plant flavors and fragrances. In *Molecules* 18 (6), pp. 7194–7238. DOI: 10.3390/molecules18067194.

Chemat, Farid (Ed.) (2015): Green extraction of natural products. Theory and practice. Weinheim: Wiley-VCH.

Chemat, Farid; Abert Vian, Maryline; Fabiano-Tixier, Anne-Sylvie; Nutrizio, Marinela; Režek Jambrak, Anet; Munekata, Paulo E. S. et al. (2020): A review of sustainable and intensified techniques for extraction of food and natural products. In *Green Chem.* 22 (8), pp. 2325–2353. DOI: 10.1039/C9GC03878G.

Chemat, Farid; Abert Vian, Maryline; Ravi, Harish Karthikeyan; Khadhraoui, Boutheina; Hilali, Soukaina; Perino, Sandrine; Tixier, Anne-Sylvie Fabiano (2019): Review of Alternative Solvents for Green Extraction of Food and Natural Products: Panorama, Principles, Applications and Prospects. In *Molecules* 24 (16). DOI: 10.3390/molecules24163007.

Chrastil, Josef (1982): Solubility of solids and liquids in supercritical gases. In *The Journal of Physical Chemistry* 86 (15), pp. 3016–3021. DOI: 10.1021/j100212a041.

Cordoba, Nancy; Fernandez-Alduenda, Mario; Moreno, Fabian L.; Ruiz, Yolanda. (2020): Coffee extraction: A review of parameters and their influence on the physico-chemical characteristics and flavour of coffee brews. In *Trends in Food Science & Technology* 96, pp. 45–60. DOI: 10.1016/j.tifs.2019.12.004.

Corrochano, B. R. (2015): Advancing the Engineering Understanding of Coffee Extraction. Dissertation. The University of Birmingham, Birmingham. School of Chemical Engineering.

Corrochano, B. R.; Melrose, J. R.; Bentley, A. C.; Fryer, P. J.; Bakalis, S. (2015): A new methodology to estimate the steady-state permeability of roast and ground coffee in packed beds. In *Journal of Food Engineering* 150 (25), pp. 106–116. DOI: 10.1016/j.jfoodeng.2014.11.006.

da Cruz Francisco, José; Sivik, Björn (2002): Solubility of three monoterpenes, their mixtures and eucalyptus leaf oils in dense carbon dioxide. In *The Journal of Supercritical Fluids* 23 (1), pp. 11–19. DOI: 10.1016/S0896-8446(01)00131-0.

del Valle, Jos M.; Rivera, Oscar; Teuber, Osvaldo; Palma, M. Teresa (2003): Supercritical CO2 extraction of Chilean hop (Humulus lupulus) ecotypes. In *J. Sci. Food Agric.* 83 (13), pp. 1349–1356. DOI: 10.1002/jsfa.1547.

del Valle, José M.; Catchpole, Owen J. (2005): Transferencia de masa en lechos empacados operando con fluidos supercríticos. I. Correlación de coeficientes de dispersión axial. In : XVI Congreso Chileno de Ingeniería Química. XVI Congreso Chileno de Ingeniería Química. Pucón, Chile.

del Valle, José M.; Juan, C.; Uquiche, Edgar; Zetzl, Carsten; Brunner, Gerd (2010): Mass transfer and equilibrium parameters on high-pressure CO2 extraction of plant essential oils. In : Food engineering interfaces: Springer, pp. 393–470.

Del Valle, J. M.; Napolitano, P.; Fuentes, N. (2000): Estimation of relevant mass transfer parameters for the extraction of packed substrate beds using supercritical fluids. In *Industrial & Engineering Chemistry Research* 39 (12), pp. 4720–4728. DOI: 10.1021/ie000034f.

Delgado, J. M. P. Q. (2006): A critical review of dispersion in packed beds. In *Heat Mass Transfer* 42 (4), pp. 279–310. DOI: 10.1007/s00231-005-0019-0.

Dunford, N. T.; King, J. W. (2000): Phytosterol Enrichment of Rice Bran Oil by a Supercritical Carbon Dioxide Fractionation Technique. In *J Food Science* 65 (8), pp. 1395–1399. DOI: 10.1111/j.1365-2621.2000.tb10619.x.

Ellero, M.; Navarini, L. (2019): Mesoscopic modelling and simulation of espresso coffee extraction. In *Journal of Food Engineering* 263, pp. 181–194. DOI: 10.1016/j.jfoodeng.2019.05.038.

Fasano, A.; Primicerio, M.; Baldini, G. (1992): Mathematical models for espresso coffee preparation. In Michiel Hazewinkel, Helmut Neunzert, Alan Tayler, Frank Hodnett (Eds.): Proceedings of the Sixth European Conference on Mathematics in Industry August 27–31, 1991 Limerick, vol. 8. Wiesbaden: Vieweg+Teubner Verlag, pp. 137–140.

Fasano, A.; Talamucci, F. (2000a): A Comprehensive Mathematical Model for a Multispecies Flow Through Ground Coffee. In *SIAM J. Math. Anal.* 31 (2), pp. 251–273. DOI: 10.1137/S0036141098336698.

Fasano, A.; Talamucci, F. (2000b): The Espresso Coffee Problem. In Nicola Bellomo, Antonio Fasano (Eds.): Complex Flows in Industrial Processes. Boston, MA: Birkhäuser Boston, pp. 241–280.

Folmer, Britta (2017): The craft and science of coffee. London, United Kingdom: Academic Press/Elsevier.

Franceschini, Gaia; Macchietto, Sandro (2008): Model-based design of experiments for parameter precision: State of the art. In *Chemical Engineering Science* 63 (19), pp. 4846–4872. DOI: 10.1016/j.ces.2007.11.034.

Giacomini, Josephin; Khamitova, Gulzhan; Maponi, Pierluigi; Vittori, Sauro; Fioretti, Lauro (2020): Water flow and transport in porous media for in-silico espresso coffee. In *International Journal of Multiphase Flow* 126, p. 103252. DOI: 10.1016/j.ijmultiphaseflow.2020.103252.

Gopalakrishnan, Narayanan; Narayanan, Cadavallur S. (1991): Supercritical carbon dioxide extraction of cardamom. In *Journal of agricultural and food chemistry* 39 (11), pp. 1976–1978. DOI: 10.1021/jf00011a018.

Goto, Motonobu; Roy, Bhupesh C.; Hirose, Tsutomu (1996): Shrinking-core leaching model for supercritical-fluid extraction. In *The Journal of Supercritical Fluids* 9 (2), pp. 128–133. DOI: 10.1016/S0896-8446(96)90009-1.

Goto, Motonobu; Sato, Masaki; Hirose, Tsutomu (1993): Extraction of Peppermint Oil by Supercritical Carbon Dioxide. In *Industrial & Engineering Chemistry Research* 26 (4), pp. 401–407. DOI: 10.1252/jcej.26.401.

Hargarten, Verena Bernadette; Kuhn, Michael; Briesen, Heiko (2020): Swelling properties of roasted coffee particles. In *J. Sci. Food Agric.* 100 (10), pp. 3960–3970. DOI: 10.1002/jsfa.10440.

Hildebrand, Joel Henry (1936): Solubility of non-electrolytes. 2nd ed. New York: Reinhold Publishing Corporation. Available online at https://hdl.handle.net/2027/mdp.39015006391653.

Hourri, A.; St-Arnaud, J. M.; Bose, T. K. (1998): Solubility of solids in supercritical fluids from the measurements of the dielectric constant: Application to CO2–naphthalene. In *Review of Scientific Instruments* 69 (7), pp. 2732–2737. DOI: 10.1063/1.1149007.

Illy, Andrea; Viani, Rinantonio (Eds.) (2005): Espresso coffee. The science of quality. 2nd ed. Amsterdam, Heidelberg: Elsevier Academic Pr. Available online at http://www.loc.gov/catdir/enhancements/fy0726/2004113615-d.html.

Ivanovic, Jasna; Meyer, Florian; Stamenic, Marko; Jaeger, Philip; Zizovic, Irena; Eggers, Rudolf (2014): Pretreatment of Natural Materials Used for Supercritical Fluid Extraction of Commercial Phytopharmaceuticals. In *Chem. Eng. Technol.* 37 (9), pp. 1606–1611. DOI: 10.1002/ceat.201300715.

Kirsch, Sarah Lara (2019): Impact of hot water extraction methods on key aroma compounds in beverages from differently roasted coffees and studies on the influence of single aroma compounds on the overall coffee aroma. Dissertation. Technische Universität München; Verlag Dr. Hut.

Klamt, Andreas (2018): The COSMO and COSMO-RS solvation models. In *WIREs Comput Mol Sci* 8 (1), Article e1338. DOI: 10.1002/wcms.1338.

Klamt, Andreas; Smith, Brian J. (2007): Challenge of Drug Solubility Prediction. In Raimund Mannhold (Ed.): Molecular Drug Properties: Wiley (Methods and Principles in Medicinal Chemistry), pp. 283–311.

Kuhn, Michael; Lang, Sandra; Bezold, Franziska; Minceva, Mirjana; Briesen, Heiko (2017): Time-resolved extraction of caffeine and trigonelline from finely-ground espresso coffee with varying particle sizes and tamping pressures. In *Journal of Food Engineering* 206 (5–6), pp. 37–47. DOI: 10.1016/j.jfoodeng.2017.03.002.

Kupski, Sérgio Carlos; Klein, Elissandro Jair; da Silva, Edson Antônio; Palú, Fernando; Guirardello, Reginaldo; Vieira, Melissa Gurgel Adeodato (2017): Mathematical modeling of supercritical CO2 extraction of hops (Humulus lupulus L.). In *The Journal of Supercritical Fluids* 130, pp. 347–356. DOI: 10.1016/j.supflu.2017.06.011.

Laesecke, Arno; Muzny, Chris D. (2017): Reference correlation for the viscosity of carbon dioxide. In *Journal of Physical and Chemical Reference Data* 46 (1). DOI: 10.1063/1.4977429.

Langezaal, Carlos R.; Chandra, Amitabh; Katsiotis, Stavros T.; Scheffer, Johannes J. C.; Haan, Andre B. de (1990): Analysis of supercritical carbon dioxide extracts from cones and leaves of a Humulus lupulus L cultivar. In *J. Sci. Food Agric.* 53 (4), pp. 455–463. DOI: 10.1002/jsfa.2740530404.

Le Dret, Hervé; Lucquin, Brigitte (2016): Partial Differential Equations: Modeling, Analysis and Numerical Approximation. Cham: Springer International Publishing (168).

Lee, W. T.; Smith, A.; Arshad, A. (2023): Uneven extraction in coffee brewing. In *Physics of Fluids* 35 (5), Article 054110. DOI: 10.1063/5.0138998.

Lyness, J. N.; Moler, C. B. (1967): Numerical Differentiation of Analytic Functions. In *SIAM Journal on Numerical Analysis* (4), Article 2, pp. 202–210. Available online at https://www.jstor.org/stable/2949389.

MathWorks: First-Order Optimality Measure. Documentation R2023a. Available online at https://de.mathworks.com/help/optim/ug/first-order-optimality-measure.html, checked on 5/3/2023.

MathWorks: Least-Squares (Model Fitting) Algorithms. Available online at https://de.mathworks.com/help/optim/ug/least-squares-model-fitting-algorithms.html, checked on 4/19/2023.

MathWorks: lsqnonlin. Documentation R2023a. Available online at https://de.mathworks.com/help/optim/ug/lsqnonlin.html, checked on 5/3/2023.

MathWorks: ode15s. Documentation R2023a. Available online at https://de.mathworks.com/help/matlab/ref/ode15s.html, checked on 4/18/2023.

MathWorks: ode45. Documentation R2023a. Available online at https://de.mathworks.com/help/matlab/ref/ode45.html, checked on 4/18/2023.

McHugh, Mark A.; Krukonis, Val J. (1994): Supercritical Fluid Extraction. Principles and Practice. 2nd ed. Stoneham: Butterworth-Heinemann.

Meftahi, Nastaran; Walker, Michael L.; Smith, Brian J. (2021): Predicting aqueous solubility by QSPR modeling. In *Journal of molecular graphics & modelling* 106, p. 107901. DOI: 10.1016/j.jmgm.2021.107901.

Melrose, J. R.; Corrochano, B. R.; Norton, M.; Silanes-Kenny, J.; Fryer, P.; Bakalis, S. (2012): Optimising Coffee Brewing Using a Multiscale Approach. In ASIC - Association for science and information on coffee (Ed.): Proceedings of the 24th International Conference on Coffee Science. 24th International Conference on Coffee Science. San José, Costa Rica.

Melrose, John; Roman-Corrochano, Borja; Montoya-Guerra, Marcela; Bakalis, Serafim (2018): Toward a New Brewing Control Chart for the 21st Century. In *Journal of agricultural and food chemistry* 66 (21), pp. 5301–5309. DOI: 10.1021/acs.jafc.7b04848.

Mestdagh, Frédéric; Davidek, Tomas; Chaumonteuil, Matthieu; Folmer, Britta; Blank, Imre (2014): The kinetics of coffee aroma extraction. In *Food Research International* 63, pp. 271–274. DOI: 10.1016/j.foodres.2014.03.011.

Micromeritics Instrument Corporation (2005): AccuPyc 1330 Pycnometer. Operator's Manual V3.03. Part No. 133-42808-01. Available online at https://www.micromeritics.com/Repository/Files/AccuPyc_1330_Pycnometer_Operators_Manual_V3.03.pdf, checked on 4/17/2023.

Mo, Chaojie; Johnston, Richard; Navarini, L.; Ellero, M. (2021): Modeling the effect of flow-induced mechanical erosion during coffee filtration. In *Physics of Fluids* 33 (9), p. 93101. DOI: 10.1063/5.0059707.

Mo, Chaojie; Johnston, Richard; Navarini, Luciano; Liverani, Furio Suggi; Ellero, Marco (2023): Exploring the link between coffee matrix microstructure and flow properties

using combined X-ray microtomography and smoothed particle hydrodynamics simulations.

Mo, Chaojie; Navarini, Luciano; Liverani, Furio Suggi; Ellero, Marco (2022): Modeling swelling effects during coffee extraction with smoothed particle hydrodynamics. In *Physics of Fluids* 34 (4), p. 43104. DOI: 10.1063/5.0086897.

Mo, Chaojie; Navarini, Luciano; Liverani, Furio Suggi; Ellero, Marco (2024): Modelling swelling effects in real espresso extraction using a 1-dimensional coarse-grained model. In *Journal of Food Engineering* 365, p. 111843. DOI: 10.1016/j.jfoodeng.2023.111843.

Moeenfard, Marzieh; Silva, José Avelino; Borges, Nuno; Santos, Alejandro; Alves, Arminda (2015): Diterpenes in espresso coffee: impact of preparation parameters. In *Eur Food Res Technol* 240 (4), pp. 763–773. DOI: 10.1007/s00217-014-2381-y.

Moroney, K. M.; Lee, W. T.; Brien, S. B. G. O'; Suijver, F.; Marra, J. (2016): Asymptotic Analysis of the Dominant Mechanisms in the Coffee Extraction Process. In *SIAM J. Appl. Math.* 76 (6), pp. 2196–2217. DOI: 10.1137/15M1036658.

Moroney, K. M.; Lee, W. T.; O'Brien, S. B. G.; Suijver, F.; Marra, J. (2015): Modelling of coffee extraction during brewing using multiscale methods: An experimentally validated model. In *Chemical Engineering Science* 137 (2), pp. 216–234. DOI: 10.1016/j.ces.2015.06.003.

Moroney, K. M.; O'Connell, K.; Meikle-Janney, P.; O'Brien, S. B. G.; Walker, G. M.; Lee, W. T. (2019): Analysing extraction uniformity from porous coffee beds using mathematical modelling and computational fluid dynamics approaches. In *PloS one* 14 (7), e0219906. DOI: 10.1371/journal.pone.0219906.

Nagybákay, Nóra Emilia; Syrpas, Michail; Vilimaite, Vaiva; Tamkute, Laura; Pukalska, Audrius; Venskutonis, Petras Rimantas; Kitryte, Vaida (2021): Optimized supercritical CO2 extraction enhances the recovery of valuable lipophilic antioxidants and other constituents from dual-purpose hop (Humulus lupulus L.) variety ella. In *Antioxidants* 10 (918). DOI: 10.3390/antiox10060918.

Nocedal, Jorge; Wright, Stephen J. (2006): Numerical optimization. Second edition. New York, NY: Springer (Springer series in operations research and financial engineering). Available online at https://ebookcentral.proquest.com/lib/kxp/detail.action?docID=6315051.

Ogata, Akio; Banks, R. B. (1961): A solution of the differential equation of longitudinal dispersion in porous media: US Geological Survey (Professional Paper). Available online at http://dx.doi.org/10.3133/pp411A.

Oliveira, Eduardo L.G.; Silvestre, Armando J.D.; Silva, Carlos M. (2011): Review of kinetic models for supercritical fluid extraction. In *Chemical Engineering Research and Design* 89 (7), pp. 1104–1117. DOI: 10.1016/j.cherd.2010.10.025.

Pannusch, Verena Bernadette; Schmieder, Benedikt Karl Leonhard; Vannieuwenhuyse, Lara; Minceva, Mirjana; Briesen, Heiko (2024): Model-based kinetic espresso brewing control chart for representative taste components. In *Journal of Food Engineering* (367), Article 111887. DOI: 10.1016/j.jfoodeng.2023.111887.

Pannusch, Verena Bernadette; Viebahn, Lukas; Briesen, Heiko; Minceva, Mirjana (2023): Predicting the essential oil composition in supercritical carbon dioxide extracts from hop pellets using mathematical modeling. In *Heliyon* 9 (2), e13030. DOI: 10.1016/j.heliyon.2023.e13030.

Papageōrgiu, Markos; Leibold, Marion; Buss, Martin (2012): Optimierung. Statische, dynamische, stochastische Verfahren für die Anwendung. 3., neu bearb. und erg. Aufl. Berlin, Heidelberg: Springer Vieweg (Lehrbuch).

Paul, P. M. F.; Wise, W. S. (1971): The Principles of Gas Extraction. London: Mills & Boon.

Peng, Ding-Yu; Robinson, Donald B. (1976): A New Two-Constant Equation of State. In *Ind. Eng. Chem. Fund.* 15 (1), pp. 59–64. DOI: 10.1021/i160057a011.

Petruzzello, Melissa (2023): xylem. Edited by Encyclopedia Britannica. Available online at https://www.britannica.com/science/xylem, updated on 7/14/2023, checked on 8/14/2023.

Pittia, Paola; Sacchetti, Giampiero; Mancini, Lucia; Voltolini, Marco; Sodini, Nicola; Tromba, Giuliana; Zanini, Franco (2011): Evaluation of microstructural properties of coffee beans by synchrotron X-ray microtomography: a methodological approach. In *Journal of food science* 76 (2), E222-31. DOI: 10.1111/j.1750-3841.2010.02009.x.

Poling, Bruce E.; O'Connell, John P.; Prausnitz, John M. (2001): The properties of gases and liquids. 5. rev. ed. New York [u.a.]: McGraw-Hill.

Pronyk, C.; Mazza, G. (2009): Design and scale-up of pressurized fluid extractors for food and bioproducts. In *Journal of Food Engineering* 95 (2), pp. 215–226. DOI: 10.1016/j.jfoodeng.2009.06.002.

Quarteroni, Alfio (2017): Numerical Models for Differential Problems. Cham: Springer International Publishing (16).

Reverchon, E. (1996): Mathematical modeling of supercritical extraction of sage oil. In *AIChE J.* 42 (6), pp. 1765–1771. DOI: 10.1002/aic.690420627.

Saffarionpour, Shima; Ottens, Marcel (2018): Recent Advances in Techniques for Flavor Recovery in Liquid Food Processing. In *Food Eng Rev* 10 (2), pp. 81–94. DOI: 10.1007/s12393-017-9172-8.

Salamanca, C. Alejandra; Fiol, Núria; González, Carlos; Saez, Marc; Villaescusa, Isabel (2017): Extraction of espresso coffee by using gradient of temperature. Effect on physicochemical and sensorial characteristics of espresso. In *Food chemistry* 214, pp. 622–630. DOI: 10.1016/j.foodchem.2016.07.120.

Sano, Yoshihiko; Kubota, Shun; Kawarazaki, Akito; Kawamura, Kazuhiko; Kashiwai, Hajime; Kuwahara, Fujio (2019): Mathematical model for coffee extraction based on the volume averaging theory. In *Journal of Food Engineering* 263 (3), pp. 1–12. DOI: 10.1016/j.jfoodeng.2019.05.025.

Schmieder, Benedikt K. L.; Pannusch, Verena B.; Vannieuwenhuyse, Lara; Briesen, Heiko; Minceva, Mirjana (2023): Influence of Flow Rate, Particle Size, and Temperature on Espresso Extraction Kinetics. In *Foods* 12 (15). DOI: 10.3390/foods12152871.

Schneider, Gerhard M. (1980): Extraction with Supercritical Gases. Weinheim: Verl. Chemie.

SCM (2023): COSMO-RS. Pure Compound property prediction. Available online at https://www.scm.com/doc/COSMO-RS/Property_Prediction.html, checked on 9/7/2023.

Sovová, Helena (1994): Rate of the vegetable oil extraction with supercritical CO2 - I. Modelling of extraction curves. In *Chemical Engineering Science* 49 (3), pp. 409–414. DOI: 10.1016/0009-2509(94)87012-8.

Sovová, Helena (2005): Mathematical model for supercritical fluid extraction of natural products and extraction curve evaluation. In *The Journal of Supercritical Fluids* 33 (1), pp. 35–52. DOI: 10.1016/j.supflu.2004.03.005.

Sovová, Helena; Jez, Jaromír; Bártlová, Milena; St'astová, Jitka (1995): Supercritical carbon dioxide extraction of black pepper. In *The Journal of Supercritical Fluids* 8 (4), pp. 295–301. DOI: 10.1016/0896-8446(95)90004-7.

Span, Roland; Wagner, Wolfgang (1996): A new equation of state for carbon dioxide covering the fluid region from the triple-point temperature to 1100 K at pressures up to 800 MPa. In *Journal of Physical and Chemical Reference Data* 25 (6), pp. 1509–1596. DOI: 10.1063/1.555991.

Spiro, Michael; Selwood, Robert M. (1984): The kinetics and mechanism of caffeine infusion from coffee: The effect of particle size. In *J. Sci. Food Agric.* 35 (8), pp. 915–924. DOI: 10.1002/jsfa.2740350817.

Squire, William; Trapp, George (1998): Using Complex Variables to Estimate Derivatives of Real Functions. In *SIAM Review* (40), Article 1, pp. 110–112. Available online at https://www.jstor.org/stable/2653003.

Stahl, Egon; Quirin, Karl-Werner; Gerard, Dieter (1988): Dense Gases for Extraction and Refining. Berlin, Heidelberg: Springer Berlin Heidelberg.

Stamenic, M.; Zizovic, I.; Eggers, R.; Jaeger, P.; Heinrich, H.; Roj, E. et al. (2010): Swelling of plant material in supercritical carbon dioxide. In *The Journal of Supercritical Fluids* 52 (1), pp. 125–133. DOI: 10.1016/j.supflu.2009.12.004.

Stampanoni Koeferli, Chantal; Piccinali Schwegler, Patrizia; Hong-Chen, Doreen (1998): Application of Classical and Novel Sensory Techniques in Product Optimization. In *LWT - Food Science and Technology* 31 (5), pp. 407–417. DOI: 10.1006/fstl.1998.0379.

Terada, Akihiro; Kitajima, Nahoko; Machmudah, Siti; Tanaka, Masahiro; Sasaki, Mitsuru; Goto, Motonobu (2010): Cold-pressed yuzu oil fractionation using countercurrent supercritical CO2 extraction column. In *Separation and Purification Technology* 71 (1), pp. 107–113. DOI: 10.1016/j.seppur.2009.11.009.

The Good Scents Company: TGSC Information System. alpha-humulene. Available online at http://thegoodscentscompany.com/data/rw1027221.html, checked on 4/5/2023.

The Good Scents Company (1988a): TGSC Information System. dipentene. Available online at http://thegoodscentscompany.com/data/rw1240221.html, checked on 4/5/2023.

The Good Scents Company (1988b): TGSC Information System. myrcene. Available online at http://www.thegoodscentscompany.com/data/rw1016531.html, checked on 8/31/2023.

The Good Scents Company (1999): TGSC Information System. beta-caryophyllene. Available online at http://thegoodscentscompany.com/data/rw1060851.html, checked on 4/5/2023.

The Good Scents Company (2000): TGSC Information System. alpha-pinene. Available online at http://thegoodscentscompany.com/data/rw1006351.html, checked on 4/5/2023.

The Merck index. An encyclopedia for chemicals, drugs, and biologicals (2013). 15th ed. Cambridge: Royal Society of Chemistry.

Tzia, Constantina (Ed.) (2003): Extraction optimization in food engineering. New York: Dekker (Food science and technology, 128). Available online at http://www.loc.gov/catdir/enhancements/fy0647/2003273538-d.html.

U. S. Food and Drug Administration (1979): Select Committee on GRAS Substances (SCOGS). Opinion: Carbon dioxide. Available online at http://wayback.archive-it.org/7993/20171031063924/https://www.fda.gov/Food/IngredientsPackagingLabeling/GRAS/SCOGS/ucm261241.htm, updated on 9/29/2015, checked on 8/31/2023.

Vaca Guerra, Mauricio; Harshe, Yogesh M.; Fries, Lennart; Pietsch-Braune, Swantje; Palzer, Stefan; Heinrich, Stefan (2023a): Tuning the packed bed configuration for selective extraction of espresso non-volatiles based on polarity. In *Journal of Food Engineering* 354, p. 111554. DOI: 10.1016/j.jfoodeng.2023.111554.

Vaca Guerra, Mauricio; Harshe, Yogesh M.; Fries, Lennart; Rothberg, Sophia; Palzer, Stefan; Heinrich, Stefan (2023b): Influence of particle size distribution on espresso extraction via packed bed compression. In *Journal of Food Engineering* 340, p. 111301. DOI: 10.1016/j.jfoodeng.2022.111301.

Valenzuela, Loreto M.; Reveco-Chilla, Andrea G.; del Valle, José M. (2014): Modeling solubility in supercritical carbon dioxide using quantitative structure–property relationships. In *The Journal of Supercritical Fluids* 94, pp. 113–122. DOI: 10.1016/j.supflu.2014.06.022.

van Opstaele, Filip; Goiris, Koen; Rouck, Gert de; Aerts, Guido; Cooman, Luc de (2012a): Production of novel varietal hop aromas by supercritical fluid extraction of hop pellets - Part 1: Preparation of single variety total hop essential oils and polar hop essences. In *The Journal of Supercritical Fluids* 69, pp. 45–56. DOI: 10.1016/j.supflu.2012.05.009.

van Opstaele, Filip; Goiris, Koen; Rouck, Gert de; Aerts, Guido; Cooman, Luc de (2012b): Production of novel varietal hop aromas by supercritical fluid extraction of hop pellets—Part 2: Preparation of single variety floral, citrus, and spicy hop oil essences by density programmed supercritical fluid extraction. In *The Journal of Supercritical Fluids* 71 (2), pp. 147–161. DOI: 10.1016/j.supflu.2012.06.004.

Vande Wouwer, Alain; Saucez, Philippe; Vilas, Carlos (2014): Simulation of ODE/PDE Models with MATLAB®, OCTAVE and SCILAB. Cham: Springer International Publishing.

VDI-Wärmeatlas (2006). Berlin, Heidelberg: Springer Berlin Heidelberg.

Verschuere, Mirana; Sandra, Patrick; David, Frank (1992): Fractionation by SFE and microcolumn analysis of the essential oil and the bitter principles of hops. In *Journal of chromatographic science* 30 (10), pp. 388–391. DOI: 10.1093/chromsci/30.10.388.

Walter, Éric; Pronzato, Luc (1997): Identification of parametric models from experimental data. Berlin, Heidelberg: Springer (Communications and control engineering series).

Wijngaard, Hilde; Hossain, Mohammad B.; Rai, Dilip K.; Brunton, Nigel (2012): Techniques to extract bioactive compounds from food by-products of plant origin. In *Food Research International* 46 (2), pp. 505–513. DOI: 10.1016/j.foodres.2011.09.027.

Williams, John R.; Clifford, Anthony A. (2000): Supercritical Fluid Methods and Protocols. New Jersey: Humana Press (13).

Wong, J. M.; Johnston, K. P. (1986): Solubilization of biomolecules in carbon dioxide based supercritical fluids. In *Biotechnology progress* 2 (1), pp. 29–39. DOI: 10.1002/btpr.5420020107.

Zekovic, Zoran; Pfaf-Sovljanski, Ivana; Grujic, Olgica (2007): Supercritical fluid extraction of hops. In *J Serb Chem Soc* 72 (1), pp. 81–87. DOI: 10.2298/JSC0701081Z.

Zhang, Yang; Yang, Jichu; Yu, Yang-Xin (2005): Dielectric constant and density dependence of the structure of supercritical carbon dioxide using a new modified empirical potential model: a Monte Carlo simulation study. In *The journal of physical chemistry. B* 109 (27), pp. 13375–13382. DOI: 10.1021/jp045741r.

Zhuang, Bilin; Ramanauskaite, Gabriele; Koa, Zhao Yuan; Wang, Zhen-Gang (2021): Like dissolves like: A first-principles theory for predicting liquid miscibility and mixture dielectric constant. In *Science advances* 7 (7). DOI: 10.1126/sciadv.abe7275.

Appendix A. Derivation of Extraction Models

I. Solid-phase mass transport

Molecular diffusion can be described by Fick's second law with the concentration $c_{i,s}$ of a compound i in the particle pore phase of the solid s, time t and the molecular diffusion coefficient D_i:

$$\frac{\partial c_{i,s}}{\partial t} = \nabla \cdot \left(D_i \, \nabla c_{i,s} \right) \qquad \text{Eq. A.1}$$

This law is valid for molecules that are motile in a liquid with unlimited paths and directions of movement. Inside a porous particle, however, molecular diffusion is not "free" but slowed down or hindered due to cell walls and a tortuous pore network. For this purpose, the theory of volume averaging is applied based on the approach of Bear and Bachmat (Bear 2018, pp. 62–70). After specifying a representative elementary volume (REV), the microscale balance equation (Eq. A.1) is averaged over the REV being the total solid phase following some general rules. The macroscopic balance equations for the porous particle are then specified for the intrinsic liquid-phase average concentration of a solute in the particle pore phase s. Note that the index s is used for this phase to distinguish it from the liquid phase l between particles although it specifies the pore phase of the solid particles and not the solid cell network itself. For a comprehensive explanation about the volume averaging procedure and rules, the reader is referred to (Bear 2018, pp. 62–70).

Volume averaging of Eq. A.1 to the particle macroscale leads to (Bear 2018, pp. 223–224):

$$\frac{\partial \phi \, \overline{c_i}^s}{\partial t} = -\nabla \cdot \phi \left(D_i \, \boldsymbol{T}^* \, \nabla \, \overline{c_i}^s \right) \qquad \text{Eq. A.2}$$

$\overline{c_i}^s$ stands for the intrinsic average of the solute concentration in the pore liquid inside the solid phase, ϕ is the porosity of the particle and $\boldsymbol{T}^*$ is the second rank tortuosity tensor of an anisotropic porous particle (Bear 2018, pp. 460–461). In an isotropic case, which is applicable in most cases, the product of porosity, molecular diffusion coefficient and tortuosity can be summarized to the effective diffusion coefficient of the porous medium (Tzia 2003, p. 44; Bear and Bachmat 1991, p. 192):

$$D_{i,eff} = D_i \frac{\phi}{\tau} \qquad \text{Eq. A.3}$$

With τ being the scalar tortuosity of the isotropic porous medium and Eq. A.2 becomes:

$$\frac{\partial \phi \, \overline{c_i}^s}{\partial t} = -\nabla \cdot D_{i,eff} \, \nabla \, \overline{c_i}^s \qquad\qquad \text{Eq. A.4}$$

The nabla operator in Eq. A.2 can be replaced for different shapes of homogeneous isotropic particles considering only one dimension, i.e., the distance from the particle center r. The following general formulation can be used (Tzia 2003, p. 39):

$$\frac{\partial \phi \overline{c_i}^s}{\partial t} = \frac{1}{r^{v-1}} \frac{\partial}{\partial r} \left(r^{v-1} \, D_{i,eff} \, \frac{\partial \overline{c_i}^s}{\partial r} \right) \qquad\qquad \text{Eq. A.5}$$

Assigning different values to the index v gives different shapes: $v = 1$ for an infinite slab (suitable for thin leaves or flakes), $v = 2$ for an infinite cylinder (suitable for rods or fibers), and $v = 3$ for spherical particles (suitable for ground seeds) (Tzia 2003, p. 39). For extraction from crushed or ground seeds, a spherical shape is often appropriate:

$$\frac{\partial \phi \overline{c_i}^s}{\partial t} = \frac{D_{i,eff}}{r^2} \frac{\partial}{\partial r} \left(r^2 \frac{\partial \overline{c_i}^s}{\partial r} \right) \qquad\qquad \text{Eq. A.6}$$

For extractions from thin leaves and flowers, the assumption of infinite slabs is suitable:

$$\frac{\partial \phi \overline{c_i}^s}{\partial t} = D_{i,eff} \, \frac{\partial^2 \overline{c_i}^s}{\partial r^2} \qquad\qquad \text{Eq. A.7}$$

In this thesis, the particles are considered spherical in solid-liquid extraction, thus, the subsequent model derivation is based on Eq. A.6. Eq. A.6 is valid for dispersed particles in stirred immersion processes, where the solute mass in the continuous phase surrounding the particle is assumed to be ideally mixed. In percolation processes, however, the porous fixed bed of particles with bulk porosity ε needs to be considered for the macroscale equation as well. Thus, Eq. A.6 is additionally averaged over the REV of the fixed bed of particles:

$$\frac{\partial (1 - \varepsilon) \phi \overline{c_i}^s}{\partial t} = (1 - \varepsilon) \frac{D_{i,eff}}{r^2} \frac{\partial}{\partial r} \left(r^2 \frac{\partial \overline{c_i}^s}{\partial r} \right) \qquad\qquad \text{Eq. A.8}$$

Additional differential equations for the temporal change of ε and ϕ add to the balance equations if intra-particle and/or bulk porosity change significantly during the extraction process. If the assumption that both ε and ϕ are constant is admissible, e.g., when the total dissolved mass is small in comparison to the mass of the insoluble plant matrix, Eq. A.8 can be simplified to:

$$\phi \frac{\partial \overline{c_i}^s}{\partial t} = \frac{D_{i,eff}}{r^2} \frac{\partial}{\partial r} \left(r^2 \frac{\partial \overline{c_i}^s}{\partial r} \right)$$

Eq. A.9

II.   Liquid-phase mass transport

Besides solid-phase mass transport properties, the flow properties through the porous fixed bed in percolation processes influences mass transport and the concentration of a solute in the final extract. The solvent enters the fixed bed of particles on one side and flows through the pores carrying solutes to the other side, where it passes a filter medium or perforated plate retaining solid particles. As for the solid-phase intra-particle diffusion, one starts with the single-phase microscale balance equation, a convection-diffusion equation assuming that no solute mass is produced or removed by chemical reactions (hence no source or sink term) (Bear 2018, p. 188):

$$\frac{\partial c_{i,l}}{\partial t} = -\nabla \cdot \left(\boldsymbol{V_l} \, c_{i,l} - D_i \nabla c_{i,l} \right)$$

Eq. A.10

The variable $c_{i,l}$ represents the mass concentration of a solute i in the liquid phase l, and $\boldsymbol{V_l}$ is the second rank tensor of the liquid velocity. Averaging over the fixed bed yields the macroscopic mass balance equation (Bear 2018, pp. 223–224):

$$\frac{\partial \varepsilon \overline{c_i}^l}{\partial t} = -\nabla \cdot \varepsilon \left(\boldsymbol{V_l} \, \overline{c_i}^l - \boldsymbol{D_{dis}} \nabla \overline{c_i}^l - D_i \boldsymbol{T}^* \nabla \overline{c_i}^l \right) + \bar{f}_{s \to l}^l$$

Eq. A.11

Through volume averaging, a term for mechanical dispersion appears in the macroscopic balance equation (second term in the parentheses on the right-hand side of Eq. A.11). It describes how the solute is "dispersed (i.e., it spreads out) by longitudinal advection and radial molecular diffusion" (Bear 2018, p. 465). Mechanical dispersion can be described by a variant of Fick's diffusion law with $\boldsymbol{D_{dis}}$ being the dispersion coefficient, a second rank tensor, which, in case of an isotropic medium and uniform flow, reduces to:

$$\boldsymbol{D_{dis}} = \begin{bmatrix} D_L & 0 & 0 \\ 0 & D_T & 0 \\ 0 & 0 & D_T \end{bmatrix}$$

Eq. A.12

D_L is the longitudinal or axial dispersion coefficent and D_T is the transversal or radial dispersion coefficient. In Eq. A.11, the source term $\bar{f}_{s \to l}^l$ describes the average flux from solid to liquid phase. This two-phase mass transfer can be described by the average diffusive flux $\boldsymbol{j_{dif}}$ passing the solid-liquid interface which is derived using Gauss divergence theorem (Bear 2018, p. 185):

$$\bar{f}_{s \to l}^{l} = \frac{1}{V_0} \int_{V_0} \boldsymbol{j_{dif}} \, dV = \frac{1}{V_0} \int_{S_{sl}} \boldsymbol{j_{dif}} \cdot \boldsymbol{n} \, dS \qquad\qquad \text{Eq. A.13}$$

The volume over which averaging is done is the volume of the REV V_0. According to Gauss divergence theorem, the volume integral of the divergence of $\boldsymbol{j_{dif}}$ is equal to the flux across the closed solid-liquid interface S_{sl} in the direction of the outward-pointing normal vector $\boldsymbol{n}$ (orthogonal to the surface). Replacing the integrand in Eq. A.13 by Fick's law for diffusion with the concentration gradient between the solid-phase concentration at the interface $c_{i,l}|_R$ (surface of particle with radius or half slab thickness R) and the liquid-phase bulk concentration $c_{i,l}$ across a distance Δ, we obtain:

$$\bar{f}_{s \to l}^{l} = \frac{1}{V_0} \int_{S_{sl}} -D_i \, \frac{(c_{i,l} - c_{i,l}|_R)}{\Delta} \, dS = \frac{S_{sl}}{V_0} \frac{D_i}{\Delta} \left(\bar{c}_i{}^l|_R - \bar{c}_i{}^l \right) \qquad\qquad \text{Eq. A.14}$$

The fraction S_{sl}/V_0 represents the volume specific surface area of the solid-liquid interface (Bear and Whitaker 1999, p. 14):

$$a_V = \frac{S_{sl}}{V_0} \qquad\qquad \text{Eq. A.15}$$

a_V can be derived from the specific surface area of a representative particle a_p with diameter d_p (Bear and Whitaker 1999, p. 68):

$$a_V = a_p \, (1 - \varepsilon) = \frac{A_p}{V_p} \, (1 - \varepsilon) \qquad\qquad \text{Eq. A.16}$$

In case of a spherical particle, the volume specific surface is:

$$a_p = \frac{\pi \, d_p^2}{\frac{\pi}{6} \, d_p^3} = \frac{6}{d_p} \qquad\qquad \text{Eq. A.17}$$

For an infinite slab with surface A_s and thickness d_s, it is:

$$a_s = \frac{2A_s}{A_s d_s} = \frac{2}{d_s} \qquad\qquad \text{Eq. A.18}$$

The ratio of molecular diffusion coefficient D_i and the length Δ along which diffusion takes place is the solid-liquid mass transfer coefficient k_{sl}:

$$k_{sl} = \frac{D_i}{\Delta} \qquad\qquad \text{Eq. A.19}$$

Sometimes, the mass transfer coefficient is also referred to as the product of a_v and k_{sl} (Bear 2018, p. 675). To distinguish between these two definitions, we define the global mass transfer coefficient K_{sl}:

$$K_{sl} = a_V \, k_{sl}$$

Depending on interest, both definitions are useful. If one is interested in the impact of particle size on the mass transfer rate, Eq. A.19 is recommended. However, if a_V is difficult to estimate or not measurable, the use of K_{sl} is preferable.

Substituting the factors in Eq. A.14 by the definitions of Eq. A.16 and Eq. A.19 and inserting Eq. A.14 into Eq. A.11, we obtain the mass balance equation for a solute i in the liquid phase:

$$\frac{\partial \varepsilon \overline{c}_i^l}{\partial t} = -\nabla \cdot \varepsilon \left(\boldsymbol{V_l} \, \overline{c}_i^l - \boldsymbol{D_{dis}} \nabla \overline{c}_i^l - D_i \, \boldsymbol{T^*} \, \nabla \overline{c}_i^l \right) + a_V \, k_{sl} \, (\overline{c}_i^l|_R - \bar{c}_i^l)$$

Depending on the type of percolation extractor, different assumptions and simplifications of Eq. A.21 are possible. First, the model is reduced from a three-dimensional model to two dimensions by assuming that the porous medium is isotropic and flow is unidirectional and uniform (axial symmetry). Eq. A.21 is accordingly reduced to the z coordinate (parallel to cylindrical axis and flow) and the radial coordinate r_b of a cylindrical packed bed:

$$\frac{\partial \varepsilon \overline{c}_i^l}{\partial t} = -\varepsilon \left(v_{l,z} \, \frac{\partial \overline{c}_i^l}{\partial z} + v_{l,r_b} \, \frac{\partial \overline{c}_i^l}{\partial r_b} - D_L \, \frac{\partial^2 \overline{c}_i^l}{\partial z^2} - \frac{1}{r_b} \frac{\partial}{\partial r_b} \left(D_T \, r_b \, \frac{\partial \overline{c}_i^l}{\partial r_b} \right) \right)$$
$$+ D_{i,eff,b} \, \frac{\partial^2 \overline{c}_i^l}{\partial z^2} + \frac{1}{r_b} \frac{\partial}{\partial r_b} \left(D_{i,eff,b} \, r_b \, \frac{\partial \overline{c}_i^l}{\partial r_b} \right)$$
$$+ a_V \, k_{sl} \, (\overline{c}_i^l|_R - \overline{c}_i^l)$$

Note that index b with regard to $D_{i,eff,b}$ and r_b specifies the effective diffusion coefficient and radial coordinate of the packed bed to distinguish those from the solid-phase properties. Assuming again that the porous medium is isotropic, it can be assumed that D_T is 8 to 24 times smaller than D_L (Bear 2018, p. 470) and hence transversal dispersion can be disregarded in that case. Furthermore, we assume that axial convection dominates over radial diffusion, which reduces Eq. A.22 to the z dimension:

$$\frac{\partial \varepsilon \overline{c}_i^l}{\partial t} = -\varepsilon \left(v_{l,z} \, \frac{\partial \overline{c}_i^l}{\partial z} - D_L \, \frac{\partial^2 \overline{c}_i^l}{\partial z^2} \right) + D_{i,eff,b} \, \frac{\partial^2 \overline{c}_i^l}{\partial z^2} + a_V \, k_{sl} \, (\overline{c}_i^l|_R - \overline{c}_i^l)$$

If ε can be assumed to be constant during extraction as for Eq. A.9 (solid phase), applying the product rule to the left-hand side of Eq. A.23 and setting $\frac{\partial \varepsilon}{\partial t} = 0$ yields:

$$\varepsilon \frac{\partial \overline{c}_i^l}{\partial t} = -\varepsilon \left(v_{l,z} \frac{\partial \overline{c}_i^l}{\partial z} - D_L \frac{\partial^2 \overline{c}_i^l}{\partial z^2} \right) + D_{i,eff,b} \frac{\partial^2 \overline{c}_i^l}{\partial z^2} + a_V \, k_{sl} \, (\overline{c}_i^l|_R - \overline{c}_i^l) \qquad \text{Eq. A.24}$$

In specific cases, longitudinal dispersion and diffusion can be disregarded. Parameters influencing the occurrence of dispersion include: (1) porosity of the packed bed, (2) packed bed length, (3) ratio of the packed bed diameter or length to the particle diameter, (4) PSD and particle shape, (5) viscosity and density of the fluid, (6) fluid velocity, (7) and fluid temperature (Delgado 2006). The dimensionless Peclet number is usually taken into consideration to evaluate if convection dominates over longitudinal dispersion or molecular diffusion. Dominance of convection over longitudinal dispersion can be verified by the condition (Ogata and Banks 1961):

$$Pe_L = \frac{v_{l,z} \, L}{D_L} > 100 \qquad \text{Eq. A.25}$$

With L being the packed bed length. Dominance of convection over molecular diffusion in the packed bed is identified analogously:

$$Pe_{dif} = \frac{v_{l,z} \, L}{D_{i,eff,b}} \qquad \text{Eq. A.26}$$

If $Pe_{dif} \gg 1$, convection dominates and vice versa (Bear 2018, p. 251).

III.   Boundary and initial conditions

The general model of percolation-type solid-liquid extraction, as derived above, consists of two partial differential equations (PDE). Eq. A.9 for the solid phase and Eq. A.24 for the liquid phase. The former is a diffusion equation which is classified as a parabolic PDE (Quarteroni 2017, p. 5). The latter is a convection-diffusion equation that includes hyperbolic and parabolic characteristics as special cases. If convection dominates, it is of hyperbolic type ($\Delta = B^2 - 4AC = 1 > 0$) but if diffusion dominates, it is of parabolic type ($\Delta = B^2 - 4AC = 0$) (Quarteroni 2017, p. 5). Coupling the two PDEs is done by the following boundary condition, which supposes the flux at the interface, i.e., at the particle surface ($r = R$), to be equal for both phases:

$$-D_{i,eff} \frac{\partial \overline{c}_i^s}{\partial r} |_{r=R} = a_v \, k_{sl} \, (\overline{c}_i^l|_R - \overline{c}_i^l) \qquad \text{Eq. A.27}$$

For the center of particles, we apply the Neumann boundary condition:

$$\frac{\partial \bar{c}_i^{\,s}}{\partial r}\Big|_{r=0} = 0$$

Eq. A.28

And the Danckwerts boundary condition for the packed bed inlet:

$$v_{l,z}\,\bar{c}_i^{\,l} - D_L\frac{\partial \bar{c}_i^{\,l}}{\partial z} = 0 \;,\;\; z = 0$$

Eq. A.29

If longitudinal dispersion is disregarded due to dominance of convection as described above, a Dirichlet boundary condition can be applied for $z = 0$, assuming that the concentration at the inlet is constant:

$$\bar{c}_i^{\,l}(z = 0, t) = C_{i,l,z0}$$

Eq. A.30

When fresh solvent is supplied, $C_{i,l,z0} = 0$, whereas for a multistage process, it is the outlet concentration of the previous extraction stage.

The initial conditions are:

$$\bar{c}_i^{\,s}(z, t = 0) = C_{i,s,t0}$$

Eq. A.31

$$\bar{c}_i^{\,l}(z, t = 0) = C_{i,l,t0}$$

Eq. A.32

The concentration $C_{i,s,t0}$ can be set using the maximum extracted mass reached after a long extraction time M_i^{∞} (complete leaching):

$$C_{i,s,t0} = \frac{M_i^{\infty}\,\rho_s}{M_s}$$

Eq. A.33

With M_s being the mass of solid plant material used and ρ_s being its solid density. The initial concentration in the liquid phase $C_{i,l,t0}$ depends on the accessibility of the component, i.e., if a component is located inside closed cells or on the surface of particles. If the extraction of a solute is strongly limited by diffusion and adsorption and the concentration in the extract is low in the beginning of extraction, $C_{i,l,t0}$ can be assumed to be zero. If, on the other hand, a significant solute mass is dissolved and extracted in the beginning, i.e., the concentration in the beginning of extraction is relatively high, an equilibrium concentration can be assumed based on the solubility or solid-liquid phase partitioning of the compound.

IV.   Interphase Mass Transfer

Mass transfer from solid to liquid phase not only depends on the effective diffusion through the solid pore network, but also on physical and chemical interactions between the compound and the solid surface. In solid-liquid extraction, the principle mechanisms are dissolution and ad-/desorption (Bear 2018, p. 519).

Dissolution depends on the solubility of a component in the solvent. The general rule "like dissolves like" applies which states that molecules mix best with similar molecules that exhibit a similar polarity. Accordingly, hydrophilic molecules are soluble at large concentrations in water whereas lipophilic molecules are insoluble in water. The solubility of a chemical species in a liquid is the maximum concentration reachable at a certain temperature. When using a solvent for extraction in which the target molecules are well soluble, the solubility can be assumed to be higher than the concentration of the solutes in the pores (Tzia 2003, pp. 38–39). Thus, molecules are assumed to be dissolved in the liquid inside the pores of the plant matrix during the preliminary wetting step and only diffusion resistance is considered rate limiting for the solid phase mass transport.

Adsorption needs to be considered at the solid-liquid interface. In general, molecules can be adsorbed to the solid by chemisorption through covalent bonds or by physical adsorption through van-der-Waals forces or hydrogen bonds (Bear 2018, p. 520). Only physical adsorption is relevant for solid-liquid extraction. It is commonly described by adsorption isotherms which relate the concentration of adsorbed species, in our case $\overline{c}_i^{\,s}|_R$, to not-adsorbed species $\overline{c}_i^{\,l}|_R$ at equilibrium. The simplest and most common isotherm used in extraction models is the linear isotherm:

$$\overline{c}_i^{\,l}|_R = K_i\, \overline{c}_i^{\,s}|_R \qquad\qquad\qquad \text{Eq. A.34}$$

The constant of proportionality K_i is called distribution constant (or partition coefficient). It is specific for each compound. By replacing $\overline{c}_i^{\,l}|_R$ in the mass balances by Eq. A.34, we obtain the general solid-liquid extraction diffusion model as shown in Eq. 2.1.1 to Eq. 2.1.5.

Appendix B. Published and Peer-Reviewed Articles

B.1 Swelling Properties of Roasted Coffee Particles

Swelling properties of roasted coffee particles

Verena Bernadette Hargarten, ⓘ Michael Kuhn and Heiko Briesen[*]

Abstract

BACKGROUND: In this study, the swelling behavior of roasted coffee particles in water and particularly its impact on particle diameter is examined by applying laser-diffraction analysis and microscopy. Several potential influencing factors are investigated: initial particle size, roasting degree, and temperature. Additionally, the time dependency of swelling and particle shape is evaluated at two different temperatures.

RESULTS: We verify that particle erosion occurs – as observed by an increase of the fine particle fraction after wetting – and it is revealed that this effect is more pronounced with a rise in temperature. The total relative increase in particle size is determined as approximately 15% based on a broad range of different sized coffee grounds. It is demonstrated that the degree of swelling is independent of both the initial particle diameter and the roasting degree. The particle shape is found to be unaffected by swelling. This research reveals that swelling is initially quick, with 60–80% of the final steady-state diameter being reached after 30 s and completed after 4 min of wetting, i.e. within the timescale of conventional coffee brewing methods.

CONCLUSION: This work provides a better understanding of the impact of wetting as part of the coffee brewing process, thus aiding the design, modeling, and optimization of coffee extraction. It clarifies the strong deviation of previous results on coffee-particle swelling by considering particle erosion and degassing and provides a robust method for quantification.
© 2020 The Authors. *Journal of The Science of Food and Agriculture* published by John Wiley & Sons Ltd on behalf of Society of Chemical Industry.

Keywords: erosion; extraction; imbibition; particle size; wetting

INTRODUCTION

In recent decades, researchers have become increasingly interested in coffee extraction. In particular, the highly complex process of percolation conducted for espresso preparation has not been fully explored, a process that combines the mass transport of multiple volatile and non-volatile substances with flow through an inhomogeneous particle packing.

Variations in brewing parameters strongly influence the extraction yield, the composition, and hence the sensory profile of the coffee beverage.[1] Besides water pressure,[2] temperature,[3] coffee/water ratio,[4] extraction method,[5] and water quality,[6] it is known that the particle size distribution of ground roasted coffee beans is an essential variable affecting not only the diffusion of solutes into water but also the flow through the particle bed. Voilley and Simatos[7] showed that a finer coffee ground leads to a higher dissolved solids content. Spiro and Selwood[8] revealed an effect of the particle diameter on the extraction kinetics of caffeine for coffee infusion by demonstrating that with decreasing particle size, the rate constants of caffeine extraction increased by two orders of magnitude. Furthermore, it applies to percolation that the size of coffee particles is positively correlated to the permeability of the particle bed according to the Kozeny–Carman equation; particle size distribution and particle shape also affect permeability by means of the pore size distribution and tortuosity.[9] According to Darcy's law,[9] the flow velocity rises with increased permeability and results in a shorter residence time corresponding to a lower extraction yield, as verified for espresso extraction by Kuhn

et al.;[10] they also discovered that extraction kinetics, and thus, the ratio of compounds in the final beverage, are influenced by the particle size distribution.

It has often been stated in the literature that swelling of coffee particles has a considerable impact on coffee extraction. This swelling process is described as an effect occurring with colloidal imbibition, which means the uptake of water by plant tissue followed by chemical hydration of the biocolloids present in the cell and an expansion of the insoluble cell wall structure.[11,12] Compounds that are abundant in roasted coffee and are assumed to contribute to swelling due to their hydrophilicity[13] are water-insoluble polysaccharides, referred to as holocellulose.

Three principal polysaccharides have been identified in green coffee: arabinogalactan,[14] mannan,[15] and cellulose.[16] Their structure and contents were analyzed by Bradbury and Halliday,[17] who found similar contents of mannan and cellulose in arabica and robusta beans: 2.2 g kg^{-1} mannan and 0.8 g kg^{-1} cellulose. The arabinogalactan content is slightly higher in robusta beans at 1.7 g kg^{-1}, with 1.4 g kg^{-1} in arabica beans. During roasting, holocellulose polysaccharides are thermally degraded.[18] The total

---

[*] Correspondence to: H Briesen, Chair of Process Systems Engineering, TUM School of Life Sciences, Technical University of Munich, Gregor-Mendel-Straße 4, D-85354 Freising, Germany. E-mail: heiko.briesen@tum.de

Chair of Process Systems Engineering, TUM School of Life Sciences, Technical University of Munich, Munich, Germany

content decreases from approximately 3.2 g kg^{-1} on a dry basis to 2.5 g kg^{-1} when light roasted, 1.9 g kg^{-1} when medium roasted, and 1.7 g kg^{-1} when dark roasted, whereby cellulose remains the most stable throughout the roasting process.[18] Asante and Thaler[19] demonstrated that the water solubility of mannan increases during the roasting process, leading to a decrease in the insoluble fraction of the bean and an increase in the viscosity of the beverage.[20] Due to this change in the amount of insoluble polysaccharides, it can be assumed that the roasting degree influences swelling. Furthermore, it is understood that the swelling of pulp fibers composed of cellulose, lignin, and hemicellulose is influenced by pH and salt content,[21] lignin content,[22] temperature,[23] hemicellulose,[23] and fibrillar content.[24] Cuissinat and Navard[25] revealed that plant fibers mainly composed of cellulose and hemicellulose and small contents of lignin and pectin exhibited homogeneous swelling without dissolution in 0.76 g kg^{-1} sodium hydroxide (NaOH) and in most aqueous N-methylmorpholine-N-oxide (NMMO) solutions. The ratio of swelling decreased with lower concentrations of the solvent. According to Wolfrom et al.,[15] mannan is partially soluble in a 1.8 g kg^{-1} aqueous NaOH solution. Based on these findings on the individual insoluble polysaccharides comprising the coffee matrix, the occurrence of swelling in water is basically presumable but possibly depends on the composition of coffee ground and solvent.

Rivetti et al.[26] concluded that swelling is influenced by water alkalinity resulting in an increase in percolation time. They demonstrated by means of discriminant analysis that alkalinity has a significant effect on the swelling of coffee particles using particle-size-distribution measurements; however, they did not present data concerning the quantitative size increase of particles. Measurements of particle size and particle size distribution have been applied by several other authors during recent decades, but their results differ widely. Sivetz and Desrosier[27] reported a size increase of 7% based on microscopy measurements without presenting any information about the applied method and the initial particle size. Spiro et al.[28] determined an increase in size of 20 ± 4% for green coffee and an increase of 17 ± 5% for roasted coffee with an initial mean diameter of 1.072 and 0.994 mm respectively. Measurements were limited to relatively large particles and visual inspection, which does not enable a conclusion to be drawn for smaller particles applied for espresso and drip coffee brewing. The swelling of single particles was questioned by Hinz et al.[29] and Steer[30] as they reported a volume increase for whole coffee beans and pressed tablets of coffee particles but no increase regarding individual particles under the microscope. Furthermore, Hinz[31] determined the particle size distribution by laser-diffraction analysis of coffee particles after different periods of extraction. An increase in the fine fraction of particles < 250 μm was detected along with a slight shift of coarser particles toward larger particle sizes. In that work, no dispersing unit was mentioned, but Hinz states that the moisture contents of the measured particles were between 0.047 × 10^{-3} g kg^{-1} and 1.847 × 10^{-3} g kg^{-1}, indicating that moist particles were measured in an air stream. As the particle size differs with varying moisture content, there are advantages to measuring particle size distribution in an aqueous medium to eliminate this degree of freedom. Such measurements in a wet state were applied by Mateus et al.,[13] who found an increase of the $d_{4,3}$ by 20–23% 10 to 15 min after wetting. They measured particles with an initial size of 750 and 1050 μm and they also demonstrated (by using scanning electron microscopy) that water

penetrated into the cell lumen, which supports the hypothesis that imbibition occurs.

Finer particles were analyzed by Corrochano,[32] who compared laser-diffraction measurements of dry and wet particles by dispersing them in an air stream and in tap water at 15 °C. He revealed that the fine particle fraction is higher when using the wet method compared with the dry and that the wet method detects finer particles. These fine particles are assumed to be fine cell fragments that are either detached from the coffee-particle's pores or are lumps of substances that are insoluble at the measuring temperature, but which are possibly soluble at higher temperatures. Comparing the $d_{4,3}$ of two roasted coffee grounds, Corrochano found a volume increase in the $d_{4,3}$ of 12% for medium-coarse particles with an initial $d_{4,3}$ of 363.6 ± 3.8 μm, but no significant increase in the $d_{4,3}$ for fine particles with an initial $d_{4,3}$ of 198.8 ± 0.9 μm. According to Corrochano, the strong deviation from Mateus et al.'s[13] results might be attributed to a different dispersant or the roasting degree. The absence of significant swelling of fine particles in Corrochano's work may lead to the assumption that the degree of swelling depends on the initial size of coffee particles. Accordingly, this aspect is addressed in this study.

It is clear from the widely differing values and contradictory statements mentioned earlier that no consensus exists about the occurrence and degree of coffee-particle swelling. Additionally, relevant factors – such as the initial particle size, the roasting degree, and temperature – have not been investigated sufficiently. This work aims to clarify the effect of water on the particle dimensions of ground roasted coffee in a statistically significant and reproducible way; it considers the entire range of grinding degrees applied in common brewing methods as well as the influences of temperature and the degree of roasting. The effect of water quality, i.e. alkalinity/acidity and mineral content is not considered in this article. In addition to laser-diffraction measurements of sieved samples, microscopy is applied to assess the time evolution of swelling and its relevance for different extraction techniques.

With regard to the influence of temperature on swelling, Spiro and Chong[33] state that swelling is more pronounced at elevated temperatures but indicate that obtaining quantitative measurements was challenging. Through microscopy measurements of single particles at two different temperatures (25 and 80 °C), this study investigates the effect of temperature on both the rate and the degree of swelling.

MATERIALS AND METHODS

Roasted coffee

The medium-roast coffee (of a single origin from Marcala, Honduras, 100% arabica, organic certified DE-ÖKO-039) was supplied in 250 g packages (of a synthetic polymer with an aluminum barrier and a one-way degassing valve) by a local roaster (Fausto Kaffeerösterei GmbH, Munich, Germany). The light-roast coffee (of mixed origin from Colombia, South America and Tanzania, Africa, 100% arabica, rainforest alliance certified) was a product called Blonde Roast (produced by Tchibo GmbH, Bremen, Germany), which was packed in 250 g packages (of low-density polyethylene with aluminum barrier and no degassing valve). Both raw materials are depicted in Fig. 1. From visual comparison with images presented by Wang and Lim,[34] the roasting degree of both products is estimated to be between the first and second crack, i.e. within a conventional range for customary roast coffee.

2

Figure 1 Light roast (left) and medium roast (right) coffee beans.

Grinding and sieving

The coffee was ground using a professional grinder (Mahlkönig EK 43, Hemro Manufacturing Germany GmbH, Hamburg, Germany) equipped with cast steel grinding disks and a continuous dial for grind adjustment (scaled between 1–11 in increments of 0.1). Good reproducibility of grinding was confirmed in preliminary experiments. To prevent contamination of the grinder with residual particles, a small amount of coffee was ground and discarded before collecting the samples. The coffee was ground at settings of 2.0 (fine), 5.0 (medium), and 8.0 (coarse), which are subsequently referred to as grinding degree. Directly after grinding, the coffee was partially sieved in a vibrational sieving tower (AS 200, RETSCH GmbH, Haan, Germany). Approximately 50 g of ground coffee was sieved continuously for 10 min at an amplitude of 1.2 mm. Using a soft brush, agglomerates were separated and fine particles adhering to the sieves were detached. Subsequently, the sieving procedure was repeated as described earlier. In the case of grinding degree 2.0, vibrational sieving was conducted three times for 2 min at 10 s intervals, and between each sieving step the adhesion and cohesion of the particles was counteracted using the brush. The sieves used and the corresponding grinding settings and fractions, described as F (fine), S (small), M (medium), and L (large), are listed in Table 1. Air jet screening (LPS 200 MC, RHEWUM GmbH, Remscheid, Germany) was applied to remove adhering fines from the particles and to further separate agglomerates. This was conducted for 5 min at an air flow of 70 $m^3\ h^{-1}$ and a rotation speed of 50 rpm.

Laser-diffraction analysis

Particle-size-distribution measurements were conducted with a laser-diffraction system (HELOS/BR, Sympatec GmbH, Clausthal-Zellerfeld, Germany). Particles were supplied and dispersed

either in a dry state by air pressure (VIBRI and RODOS, Sympatec GmbH) or in circulated, demineralized water (QUIXEL, Sympatec GmbH). Data from the detector were collected and evaluated (based on the Fraunhofer diffraction theory) by a compatible software (WINDOX Software, Sympatec GmbH). The measuring ranges of the lenses used for different fractions are shown in Table 1. Interval classification differs between the measuring ranges and along the scale of particle sizes with increasing interval sizes for larger particle fractions. Volume distributions were determined, i.e. the cumulative and density distribution of the volume of spheres with a diffraction-equivalent diameter. The volume density describes the difference quotient of the cumulative distribution for a specific particle size interval given by the measuring range.

For dry measurements, the sieved samples were split (DR 1000, RETSCH GmbH, Haan, Germany; Laborette Type 10.102, FRITSCH GmbH, Idar-Oberstein, Germany) to achieve homogeneous samples and weighed to ensure an equal sample weight of 10.00 g (FB6CCE-H, Sartorius AG, Göttingen, Germany). Three samples per sieving fraction were measured at a conveying speed of 80% relative to maximum speed and a primary pressure of 2.5 bar.

Wet measurements were conducted after particle-water contact of 20 min, after which the steady state of swelling was assumed.[13] Briefly, 10 g of particles were immersed in 300 mL of boiled, demineralized water at a temperature of 90 °C on a heated magnetic stirrer and were stirred for 20 min. During this period, the temperature decreased to approximately 60 °C due to heat loss. To investigate the effect of extraction temperature, stirring was also performed at a temperature of 25 °C, following the same procedure. Subsequently, non-sieved samples from the stirred suspension were inserted directly into the dispersion unit of the laser-diffraction instrument with a Pasteur pipette. Before the analysis commenced, ultrasound was applied for 60 s to separate agglomerates; after a pause of 10 s, laser-diffraction measurements were conducted four times for 10 s with 5 s pauses in between. The pumping velocity in the system was 30% (relative to maximum velocity) for all experiments. In the case of the sieved particle fractions S, M, and L, the extracted coffee ground was separated from water in a 200 μm sieve and washed for 5 min with demineralized water to remove the fine particles. This step was essential to approximate monomodal particle size distributions, which are necessary for accurate quantification of differences and to exclude the effects of particle erosion and fluctuations in optical density throughout the measurements. After adding the coffee particles to the dispersant and waiting 5 min to reach a constant optical density, measurement commenced. For a period of 120 s, diffraction was analyzed; the measurement was repeated

Table 1. Specification of grinding and sieving settings and corresponding measuring range of laser diffraction analysis

Sieving	Grinding degree	Sieving range (μm)	Measuring range (μm)
None	2	—	0.5–1750
F[a]	2	< 200	0.5–875
S[b]	2	200–300	0.5–1750
M[c]	5	400–500	0.5–1750
L[d]	8	710–800	0.5 – 3500

[a] F (fine).
[b] S (small).
[c] M (medium).
[d] L (large).

four times with 5 s pauses. No ultrasound was used to avoid an undesired degradation of particles. Four to five samples were analyzed per sieved fraction, and three to five samples were analyzed from three ground batches with reference to the non-sieved samples. Weighted mean values and variances, outliers, and 95% confidence intervals (assumption of t-distribution) were calculated in Microsoft Excel 2016. Statistical analysis was conducted in MATLAB R2018a software using the functions *ttest2* and *ranksum* to identify significant differences between particle size classes. Additionally, the functions *fitlm* combined with *anova* were used to check for linear correlation. The relative diameter increase was calculated as:

$$\Delta d_{rel} = \frac{(d_f - d_0)}{d_0} \cdot 100\%. \tag{1}$$

where d_f defines the final diameter of the swollen particle and d_0 the initial diameter. The relative diameter increase was determined for the diameters $d_{10,3}$, $d_{16,3}$, $d_{50,3}$, $d_{84,3}$, $d_{90,3}$, and $d_{99,3}$ which correspond to a specific quantile of the volume distribution, where the first index represents the respective quantile expressed in a percentage. This description must be distinguished from the De Brouckere mean diameter $d_{4,3}$ which defines the volume moment mean of the particle size distribution. Based on the calculations using Eqn (1) for the previously mentioned quantiles, the mean diameter increase and the respective standard deviation was calculated for different sized particles. Outliers, (occurring mostly for fine particles where the standard deviation was large) were excluded, but through comparison with the result for a complete data set, it was revealed that this did not change the mean value (see Results section).

Microscopy

A light microscope (BX51, OLYMPUS Corporation, Tokyo, Japan) was used for single-particle measurements. The microscope was equipped with a motorized revolving nosepiece (BX-REMCB & U-HS, OLYMPUS Corporation), a scanning stage (SCAN, 130 × 85 travel range, 4 mm ball screw pitch, Märzhäuser Wetzlar GmbH & Co. KG, Wetzlar, Germany), a motorized focus drive (MFD-2, Märzhäuser Wetzlar GmbH & Co. KG), and a stepper motor controller connected to a joystick (TANGO 3 Desktop & 3-Axes Joystick, Märzhäuser Wetzlar GmbH & Co. KG). This enabled the fine adjustment of focus and table position. Images and videos were recorded using a high-resolution camera (XC50, OLYMPUS Corporation) and analyzed in a compatible software (analySIS, OLYMPUS Corporation).

To remove gas bubbles from the surface of coffee particles that appeared with degassing, a sealed flow cell was constructed from acrylic glass, which enabled the analysis of particles surrounded by water flow. Without removal, these gas bubbles would have disturbed the measurement of the projection area as they obscure the outline of particles. The coffee particles were affixed on a cover glass using a water-resistant, transparent, two-component adhesive (epoxy resins and amines, UHU GmbH & Co. KG, Bühl, Germany) and fixed inside the flow cell with transparent tape (tesafilm transparent, tesa SE, Norderstedt, Germany). The adhesive layer was spread as thin as possible to prevent immobilization of the particles in the direction of the projection plane. All particles analyzed were within the size range of 400 to 1000 μm, which reflects the coarse fraction of coffee grounds applied for drip and infusion brewing. Smaller particles were not measurable due to handling difficulties. Demineralized water

was pumped through at temperatures of approximately 80 and 25 °C at a flow rate of 50 to 80 mL min^{-1} respectively using a peristaltic pump (TU/200, medorex e. K., Nörten-Hardenberg, Germany). Prior to each experiment, a beaker on a magnetic stirrer (serving as a water reservoir for the pump) was filled with fresh demineralized water; in the case of the measurements at 80 °C it was preheated with boiling demineralized water. The flow cell, hoses, and beaker were isolated with rubber foam (adhesive rubber tape 5 m x 50 mm x 3 mm, HORNBACH Baumarkt AG, Bornheim, Germany; insulating tube and insulating mat: 9 mm insulating thickness, 6 mm tube diameter, Koste/Weitzel GbR, Wiesloch, Germany) to reduce heat loss. The temperature inside the flow cell (after passing through the beaker, pump, and hose) was 80 °C (temperature sensor: HI 98509, Hanna Instruments Inc., Woonsocket, RI, USA). A characteristic extraction temperature of 90 °C was not achieved due to heat loss despite insulation measures and preheating. Shortly before the water boundary surface had reached the particles, video recording commenced and then stopped after 150 s. Images were taken from this video for analysis after the beginning of wetting at 10, 20, 30, 40, 50, 60, 90, and 120 s, after which single images were regularly taken at defined time intervals. The water temperature in the beaker reached approximately 60 °C at the end of the experiment due to inevitable heat loss, yielding a temperature profile close to the extraction conditions described for laser-diffraction analysis (see earlier).

All photographs were transformed into binary images and the particles' projection area A_{proj} as well as the maximum and minimum Feret diameter $d_{F, max}$ and $d_{F, min}$ were determined. Any bubbles not removed by flow were separated from the particle outline using image processing. Based on the collected data, the projection-area-equivalent diameter of a circle d_{proj} was calculated as

$$d_{proj} = \sqrt{\frac{4}{\pi} A_{proj}} \tag{2}$$

and the aspect ratio AR was computed as the ratio of the minimum to the maximum Feret diameter, as follows:

$$AR = \frac{d_{F,min}}{d_{F,max}}. \tag{3}$$

The relative diameter increase was determined according to Eqn (1) using d_{proj} at time t as diameter of the swollen particle and d_{proj} in the dry state ($t = 0$) as initial diameter. The progress of swelling was determined as

$$\text{Progress of swelling} = \frac{(d(t) - d_0)}{(d_f - d_0)} \cdot 100\%, \tag{4}$$

where $d(t)$ is d_{proj} at time t and d_f is the final projection area equivalent diameter 20 min after the beginning of wetting.

RESULTS
Impact of swelling on the particle size distribution
As described, non-sieved medium-roast coffee grounds were analyzed at two different extraction temperatures: 25 and 90 °C. The volume distributions of these samples are presented in Fig. 2. The presented error bars represent 95% confidence intervals, which applies to all particle size distributions subsequently presented.
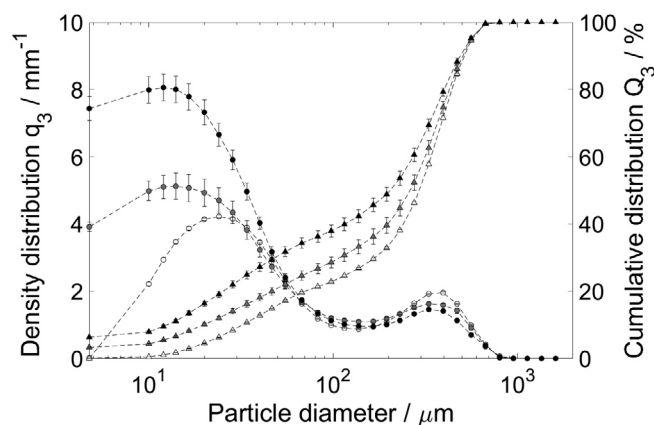
Figure 2 Density (○) and cumulative (△) distributions of non-sieved medium-roast coffee particles in dry state (white), wetted at 25 °C (gray) and wetted at 90 °C (black).

For better visibility of the fine fraction, the scaling of the abscissa is logarithmic. For clarity, it should be noted that the area of the density distribution does not represent the actual volume proportion due to its logarithmic transformation, i.e. the fine fraction is distinctly smaller than it appears from this plot. Each data point represents the middle of the respective particle size interval. For the dry coffee grounds, a bimodal distribution typical for coffee is recognizable with the first mode between 20 and 30 µm and the second at approximately 400 µm. Comparing the coffee grounds' distribution in dry and wet state, it is evident that the volume density for particles < 40 µm is significantly higher after wetting. For the coarse fraction, the volume density for particles > 250 µm is reduced for wet particles. This result is confirmed by a two-sample t-test and a Mann–Whitney U-test at the 1% significance level, summarized in Table A1 in the Appendix. In a wet state, both modes are shifted to smaller particle sizes; the first one is located at 12 µm and the second at 330 µm. Additionally, it is evident that very fine particles appear with the wet samples, which are small enough to exceed the lower threshold of the measuring range (< 10 µm). A further increase in the fine particle fraction can be seen with increased extraction temperature. With reference to the distribution of hot, extracted coffee grounds, the volume density of particles < 50 µm is significantly increased compared to the wet measurements at an extraction temperature of 25 °C and is simultaneously decreased in the range 90–500 µm (see Table A1, Appendix).

Figure 3 shows the particle size distributions of the sieving fractions F, S, M, and L (for specifications see Table 1) derived from medium-roast coffee grounds. The lines between values enable accurate readability of the individual distributions. A shift of the entire density and cumulative distribution toward larger particle sizes after wetting can be seen in the coarse fractions S, M, and L. This shift indicates a size increase of the particles. A small peak at the density distribution's left end is still visible for the wet dispersion. However, the proportion of these fine particles is small due to the washing action described earlier; therefore, their influence on the cumulative distribution can be neglected. This is not the case for the fine fraction F, where a strong increase in the volume density is still visible at the distribution's left end. A significant shift of the cumulative distribution on the right side of the mode is detected, and the mode itself shifts slightly from around 28 µm to 34 µm. Nonetheless, results in this size range must be

treated with caution as separation by means of sieving is not achieved with sufficient precision.

The relative diameter increase is plotted against the initial particle diameter in Fig. 4. Data from all particle fractions F, S, M, and L after the exclusion of three outliers ($d_{10,3}$ and $d_{50,3}$ of fraction F and $d_{99,3}$ of fraction S) is shown. The presented values result in a mean relative diameter increase of 15 ± 4%. Including the complete dataset in the calculation yields a relative diameter increase of 15 ± 7%. A linear regression coupled with an analysis of variance for the linear model's slope reveals no significant correlation between relative diameter increase and initial particle diameter (see Table A2, Appendix). Thus, it is concluded that the diameter increase is independent of the initial particle size when referring to the size range presented in Fig. 4.

To investigate possible effects from the type of roasting, measurements were repeated with a light-roast coffee, as described earlier. The dry and wet particle size distributions for sieving fractions F, S, and M are shown in Fig. 5. The same shift of the modes and cumulative distribution curves toward larger particle sizes is visible as for medium-roast coffee (see Fig. 3) with respect to sieving fractions S and M. Sieving fraction F does not exhibit a shift of the mode located at around 40 µm, but the cumulative distribution is shifted to the right for particles > 100 µm. It is assumed that the very fine particles located at the distribution's left end (which are not measured in a dry state due to their adherence on the larger particle's surface) are responsible for this difference compared to larger fractions where separation is feasible. The separation of agglomerates in a wet state might also be influential.

It is evident from Fig. 6 that the mean relative diameter increase for the sieved light-roast coffee ground is identical to that for medium-roast coffee at 15 ± 3% when the three extreme outliers $d_{10,3}$ and $d_{16,3}$ of fraction F and $d_{99,3}$ of fraction M are excluded. Including outliers slightly shifts the mean value to 13 ± 10%. Additionally, no significant correlation is found between relative size increase and initial particle diameter, as shown in Table A2 in the Appendix. These results imply that the roasting degree does not significantly influence the degree of swelling if the water quality and temperature is kept constant.

Time dependency

Time courses of the relative diameter increase Δd_{rel} for individual particles, which were determined by microscopy according to Eqn (1), are presented in Fig. 7(a) for the medium-roast coffee and in Fig. 7(b) for the light-roast coffee. As the final relative diameter increase differs strongly for particles measured at the same conditions and exhibiting similar initial particle sizes, image analysis by microscopy is found to be an inappropriate method for the quantification of total swelling. In Table A3 (Appendix), statistical results are listed for the comparison of total swelling for different temperatures and roasts. No significant difference in the total size increase is found for different roasting degrees due to the strong deviation of measurements confirming the result from laser-diffraction analysis. Comparing the results determined at different water temperatures (80 versus 25 °C), no significant difference between the medium-roast and the light-roast coffee is evident, which is also based on the large scattering within both series of experiments. At 25 °C single, markedly higher diameter increases are measured for both roasts. However, this is possibly caused by the growth and adhesion of gas bubbles that could not be completely removed by water flow at lower temperatures and that had to be distinguished and subtracted from the particles
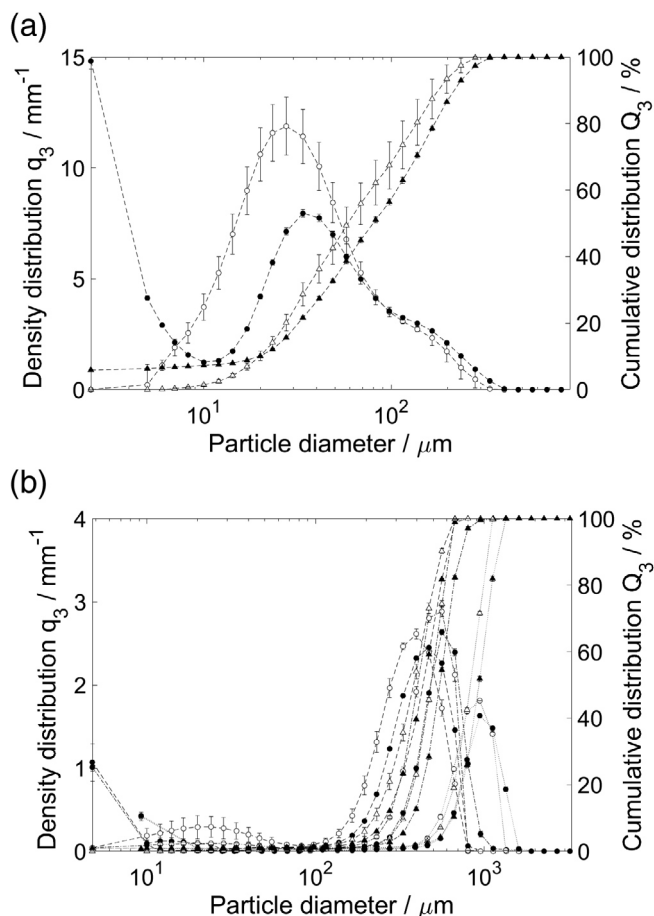
Figure 3 Density (○) and cumulative (△) distributions of sieved medium-roast coffee particles in dry state (white) and wetted at 90 °C (black). (a) Sieving fraction F (fine). (b) From left to right: sieving fractions S (small), M (medium), and L (large).
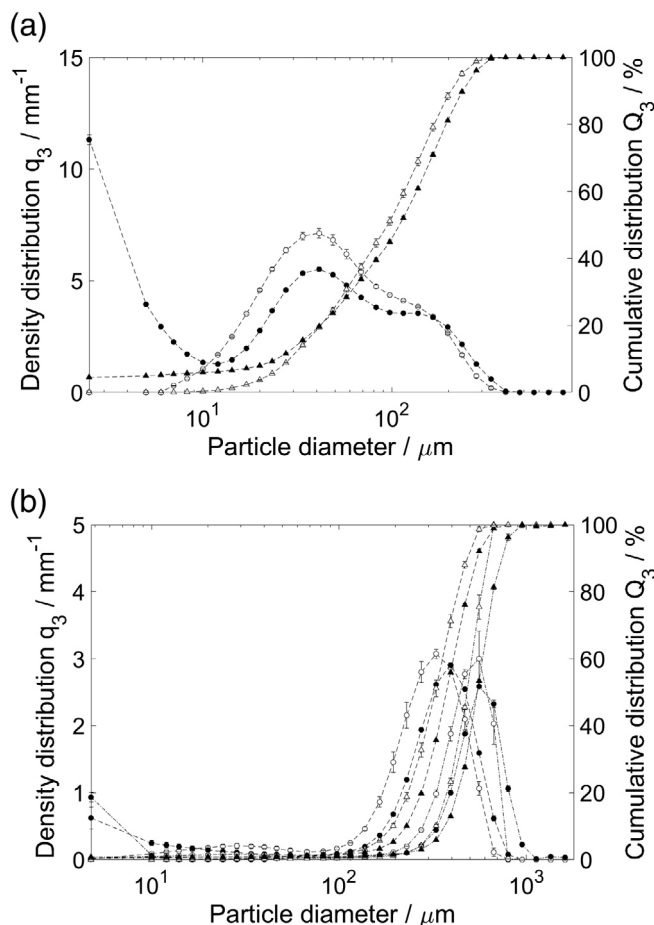

Figure 5 Density (○) and cumulative (△) distributions of sieved light-roast coffee particles in dry state (white) and wetted at 90 °C (black). (a) Sieving fraction F (fine). (b) From left to right: sieving fractions S (small), M (medium), and L (large).
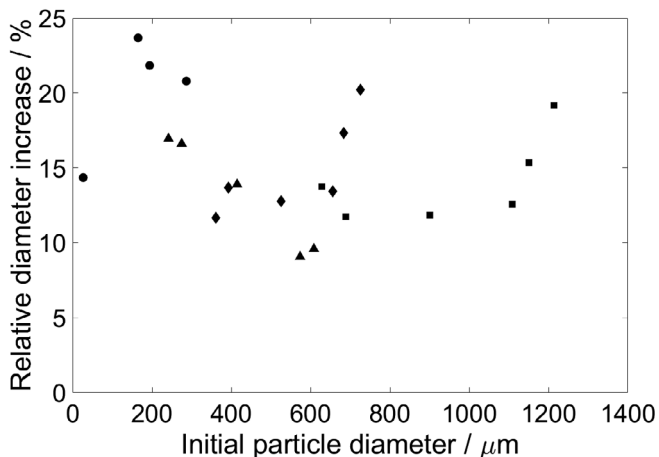
Figure 4 Relative diameter increase for medium-roast coffee *versus* initial particle diameters of sieving fractions F (fine) (●), S (small) (▲), M (medium) (◆), and L (large) (■).

during image processing. However, this could not guarantee the complete exclusion of undetected bubbles from the measured projection area. Two exemplary images showing light-roast particles before and after a wetting period of 20 min are presented in

Fig. 8. Large and small gas bubbles as well as cell fragments adhering to the particle surfaces are visible. Additionally, a detachment of small particles and color pigments carried away with the fluid flow was observed, complying with the increase in fines detected by laser diffraction analysis.

In addition to the particles' projection area, the minimal and maximal Feret diameter was determined and used for calculating the aspect ratio as a characteristic descriptor of particle shape (Eqn (3)). Figure 9 shows the aspect ratio of the same particles as depicted in Fig. 7, plotted over time. Most particles exhibit an aspect ratio between 0.6 and 0.8, visible for both roasts. This confirms that coffee particles within the measured size range are not spherical in shape but instead are flat and elongated. It is revealed by applying linear regression and analysis of variance (ANOVA) that no significant change occurs during swelling, as presented in Table A4 in the Appendix.

Figure 7 reveals that the final degree of swelling is reached within the first couple of minutes. Small decreases and fluctuations of the relative diameter increase are visible, but these are based on the experimental error from detaching fragments and gas bubbles. To investigate the time dependency of swelling, the progress of swelling described by Eqn (4) is shown for the first 5 min in Fig. 10. No clear distinction in terms of time dependency is possible when comparing different roasts and water temperatures due to the large differences between individual particles.
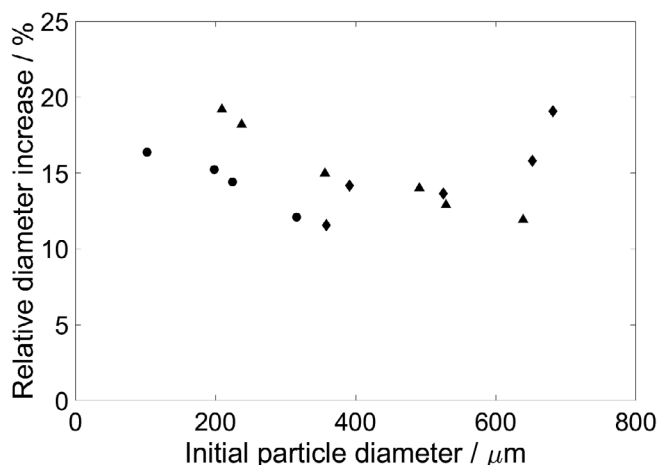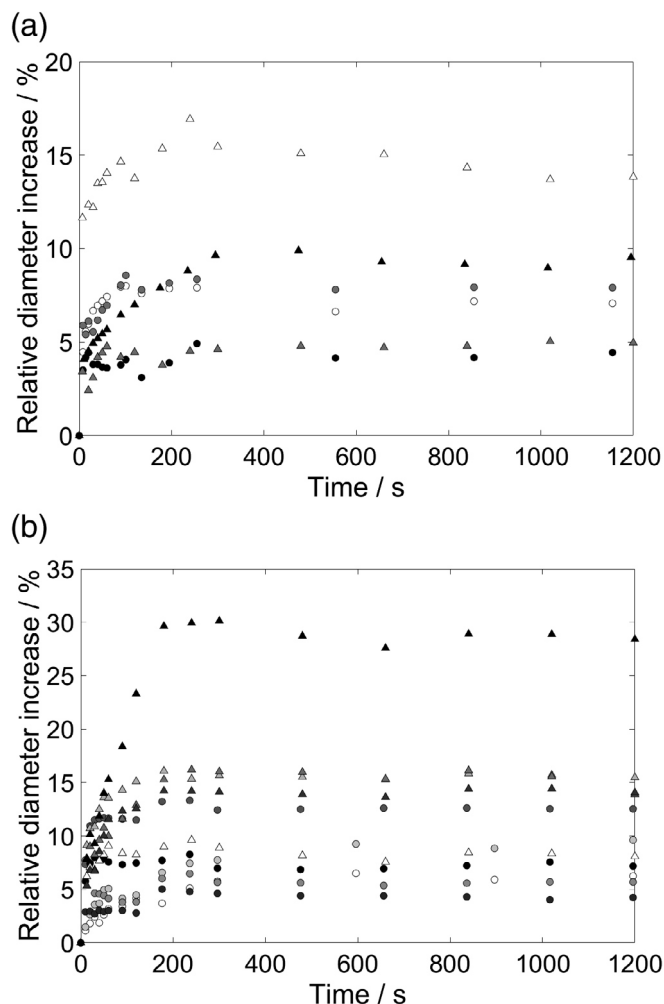
Figure 6 Relative diameter increase for light-roast coffee *versus* initial particle diameters of sieving fractions F (fine) (●), S (small) (▲), and M (medium) (♦).

The results for light-roast coffee show a broader scattering of the values for the first 100 s, which can be attributed to the slightly larger sample size. However, estimations about the status of swelling in the scope of characteristic brewing times are possible. Table 2 lists the average values for two conventional brewing times: 30 s as a typical residence time for espresso and 4 min as a usual contact time for infusion methods. After 30 s, around 83% of the final diameter is reached (on average) both at 80 and 25 °C for medium-roast coffee; the average for light-roast coffee is 71% and 59%, respectively. After 4 min of wetting, a steady state is reached. Values > 100% arise from relating the diameter increase to the diameter increase after 20 min (see Eqn (4)), which is subject to experimental error; therefore, it is partially lower than previous measures.

DISCUSSION

Particle erosion
Using laser-diffraction analysis and microscopy, it can be confirmed that during dispersion in water, fine particles < 40 μm adhering to the surface of coffee particles are detached by the surrounding water flow. Regarding the total particle size distribution, a significant increase of the fine fraction is discernible. This effect of particle erosion was previously observed by Corrochano[32] and stated to be relevant for extraction modeling by Ellero and Navarini.[35] A contribution by lipid droplets to the fine fraction can be neglected as the lipid content in coffee extracts is low compared to the volume of fine particles.[36] Moreover, this study revealed a remarkable increase in the fine fraction with an increase in extraction temperature. This positive correlation of the fine fraction with temperature refutes Corrochano's second hypothesis that the detected particles were lumps of solutes, which are soluble at higher temperatures. Instead, this research proposes that these fines are caused by particle erosion. It is assumed that the increase of solubility with increasing temperature,[3] (e.g. valid for bitter components such as caffeine), leads to a higher pore accessibility and thus enables the release of more fine fragments into the liquid phase. Moreover, a reduction of the liquid's surface tension with extraction and temperature (according to the work of Navarini *et al.*[37]) as well as the drop in water viscosity with rising temperature facilitates wetting


(a)

(b)

Figure 7 Relative diameter increase after different times of wetting at 80 °C (○) and at 25 °C (△). (a) Medium-roast coffee particles with initial diameters (in μm) of 608 (○), 519 (◉), 675 (●), 585 (△), 543 (▲), and 914 (▲). (b) Light-roast coffee particles with initial diameters (in μm) of 652 (○), 626 (◉), 462 (◉), 665 (●), 653 (●), 547 (●), 472 (△), 589 (△), 520 (▲), 568 (▲), and 592 (▲).

and water ingress and probably enables more fragments to be washed from pores and capillaries. Accordingly, the effect of temperature on particle erosion must be taken into account – especially for filtration methods where fine particles have a strong influence on the specific cake filtration resistance.[35,38]

Degree of swelling
Particle size distribution analysis yielded a total increase of the particle diameter by approximately 15%. This value is close to the results obtained by Spiro *et al.*[28] but is higher than the results from laser-diffraction analysis subsequently produced by other authors.[13,31,32] This difference can be explained by the effect of particle erosion. The increase of the volume density for fine particle size classes connected with the simultaneous decrease for larger particle size classes leads to a change in the bimodal distribution, thereby affecting the value of the $d_{4,3}$. Thus, the $d_{4,3}$ (including all particle size classes) is underestimated along with the total increase calculated from the difference to the dry state. By previous sieving, air jet screening, and washing, the effect of particle erosion can be excluded – except for fine particles
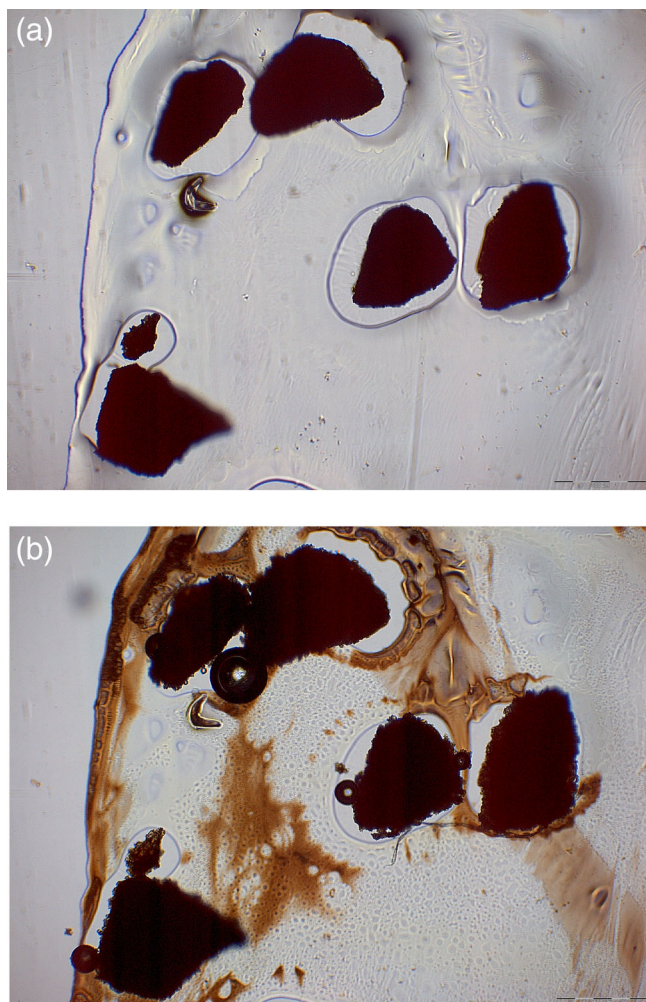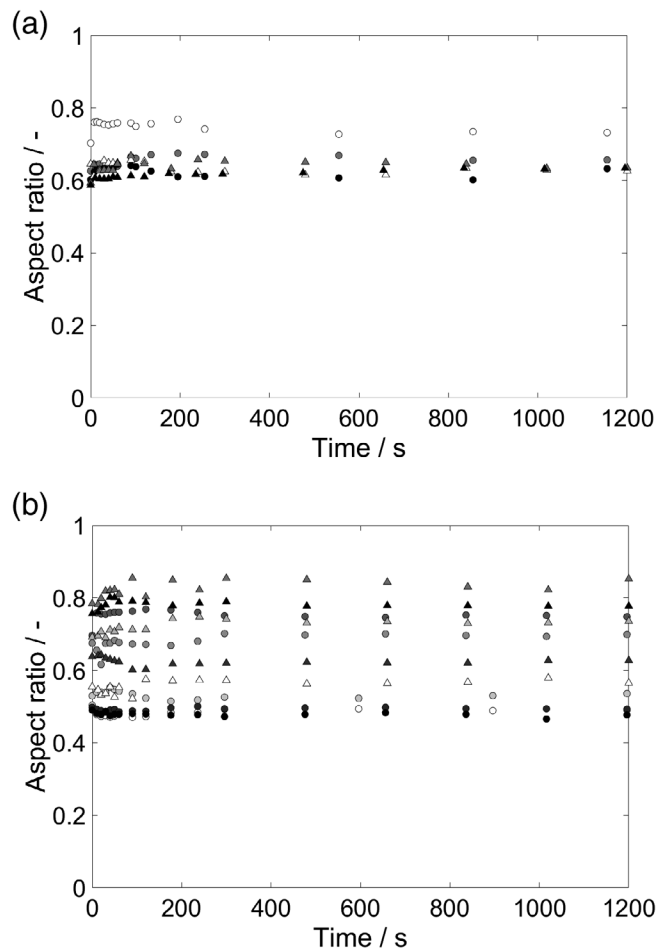
Figure 8 Light-roast particles in a dry and swollen state at 25 °C; gas bubbles and loosening fragments are visible at the surface of particles. (a) Before wetting. (b) After 20 min of wetting.

Figure 9 Aspect ratio after different times of wetting at 80 °C (○) and at 25 °C (△). (a) Medium-roast coffee particles with initial diameters (in μm) of 608 (○), 519 (◒), 675 (●), 585 (△), 543 (▲), and 914 (▲). (b) Light-roast coffee particles with initial diameters (in μm) of 652 (○), 626 (◒), 462 (◉), 665 (◒), 653 (●), 547 (●), 472 (△), 589 (△), 520 (▲), 568 (▲), and 592 (▲).

< 100 μm where separation efficiency was insufficient. This explains why this study's results for the total increase of the particle diameter are higher. Moreover, the analysis of cumulative distributions instead of the $d_{4,3}$ allowed an investigation of individual regions of the distributions and to exclude outliers at the distributions' left end, (which occurred due to residual fines and experimental error).

Influence of initial particle diameter and roasting degree

Neither by analysis of the particle size distribution nor by investigating individual particles under the microscope could a difference in swelling be seen with different initial particle diameters. An impact of the initial diameter (as might be assumed from Corrochano's[32] results) does not seem to exist, which implies that the relative degree of swelling is not affected by grinding variations. The same applies to the roasting degree, as no significant difference was observed for light-roast coffee compared to medium roast. With regard to the content of insoluble polysaccharides, only the cellulose content remains virtually constant throughout roasting.[18] Thus, it is hypothesized that cellulose has the highest influence on swelling according to the fact that no difference in swelling was observed for different roasting degrees at identical water quality and temperature.

Time dependency of swelling

Image analysis revealed that the rate and final degree of swelling varies widely when comparing individual particles, which makes a verification of laser-diffraction measurements difficult. Additionally, the wide scattering of values and the appearance of gas bubbles complicated the investigation of influencing factors on swelling kinetics such as temperature and roasting degree. The large differences between single particles can be attributed to their individual physical structure, e.g. of pores and fibers, as well as their composition (depending on where the respective cells were located in the bean before grinding) and on the whole growth and processing history of the beans. To enable statistically significant results, vastly larger sample sizes would be needed, along with an automated method of analysis. However, it can be stated that swelling is quick and not negligible for the regular time of espresso brewing, as approximately 60–80% of the final diameter is reached after only 30 s. Regarding espresso extraction, however, it has to be considered that the effect of an elevated pressure on the swelling dynamics is not covered by this study and potential effects from this parameter require further investigations. With a typical duration of infusion brewing of around 4 min, it can be expected that swelling is completed according to the measurements in this research. Therefore, the

(a)

(b)
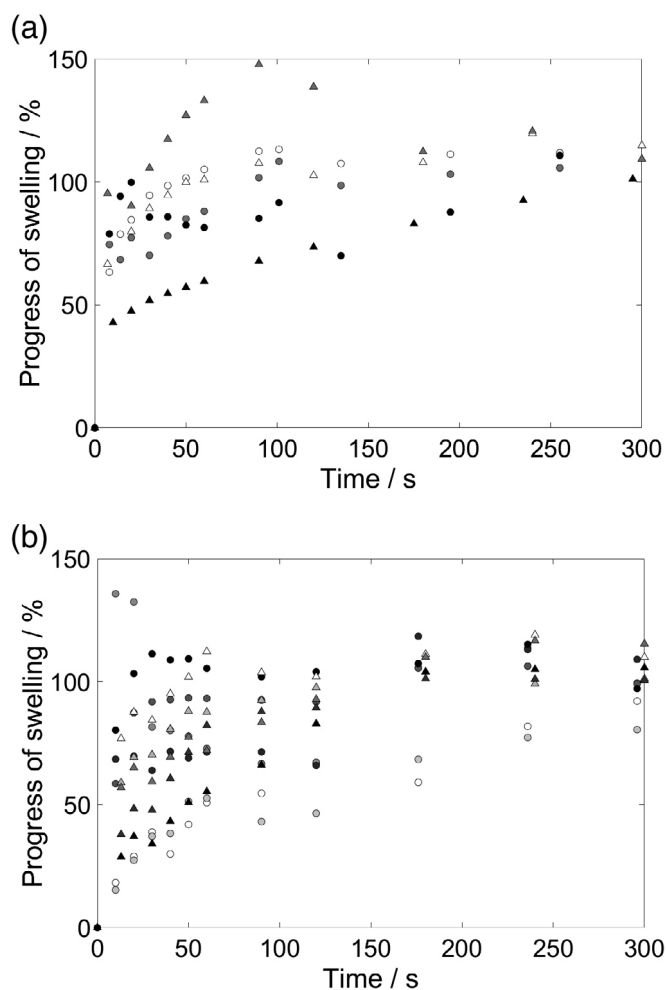
Figure 10 Progress of swelling after different times of wetting at 80 °C (○) and 25 °C (△). (a) Medium-roast coffee particles with initial diameters (in μm) of 608 (○), 519 (◉), 675 (●), 585 (△), and 543 (△), and 914 (▲). (b) Light-roast coffee particles with initial diameters (in μm) of 652 (○), 626 (◎), 462 (◉), 665 (◉), 653 (●), 547 (●), 472 (△), 589 (△), 520 (△), 568 (▲), and 592 (▲).

Table 2. Average progress of swelling after conventional brewing times

Water temperature	Progress of swelling	
	Medium roast	Light roast
30 s of wetting		
80 °C	83%	71%
25 °C	82%	59%
4 min of wetting		
80 °C	109%	101%
25 °C	111%	108%

grounds used for different brewing techniques. Two different conventional roasts have been compared with regard to their total degree of swelling. Both roasts exhibit the same size increase, leading to the conclusion that swelling is not influenced significantly by the roasting degree.

We furthermore reveal by measurements at different times after wetting that swelling is homogeneous in all directions and that it is completed within the first 4 min. A remarkable size increase already appears within the first 30 s. These findings emphasize the requirement of further research on potential effects from swelling on the extraction kinetics at specific extraction conditions.

swelling duration is expected to be distinctly shorter than that stated by Mateus et al.[13]

Furthermore, it can be concluded from the unchanged aspect ratio of particles and from visual observation (see Fig. 8) that coffee particles swell rather homogeneously, i.e. volume increase is isotropic and particle shape is barely influenced by swelling. This perception is consistent with the swelling behavior of cellulose being homogeneous in aqueous media.[25]

CONCLUSIONS

Using laser diffraction analysis and microscopy, we have demonstrated that single particles of ground coffee swell distinctly as a consequence of wetting. The total size increase amounts to approximately 15%. The strong discrepancies in values measured by different authors in the past is traced back to the phenomenon of particle erosion which is increased with a rise in extraction temperature from 25 to 90 °C. A sieving method is proposed in this article to circumvent this distortion of the volume distribution.

The final degree of swelling is shown to be independent of the initial particle size. Our results are hence transferable to different

REFERENCES

1 Voilley A, Sauvageot F, Simatos D and Wojcik G, Influence of some processing conditions on the quality of coffee brew. *J Food Process Pres* **5**:135–143 (1981).
2 Andueza S, Maeztu L, Dean B, de Peña MP, Bello J and Cid C, Influence of water pressure on the final quality of arabica espresso coffee. Application of multivariate analysis. *J Agric Food Chem* **50**:7426–7431 (2002).
3 Andueza S, Maeztu L, Pascual L, Ibáñez C, de Peña MP and Cid C, Influence of extraction temperature on the final quality of espresso coffee. *J Sci Food Agric* **83**:240–248 (2003).
4 Andueza S, Vila MA, Paz de Peña M and Cid C, Influence of coffee/water ratio on the final quality of espresso coffee. *J Sci Food Agric* **87**:586–592 (2007).
5 Gloess AN, Schönbächler B, Klopprogge B, D`Ambrosio L, Chatelain K, Bongartz A et al., Comparison of nine common coffee extraction methods: instrumental and sensory analysis. *Eur Food Res Technol* **236**:607–627 (2013).
6 Navarini L and Rivetti D, Water quality for espresso coffee. *Food Chem* **122**:424–428 (2010).
7 Voilley A and Simatos D, Modeling the solubilization process during coffee brewing. *J Food Process Eng* **3**:185–198 (1979).
8 Spiro M and Selwood RM, The kinetics and mechanism of caffeine infusion from coffee: the effect of particle size. *J Sci Food Agric* **35**:915–924 (1984).
9 Bear J, *Modeling Phenomena of Flow and Transport in Porous Media*. Springer International Publishing, Cham (2018).
10 Kuhn M, Lang S, Bezold F, Minceva M and Briesen H, Time-resolved extraction of caffeine and trigonelline from finely-ground espresso

coffee with varying particle sizes and tamping pressures. *J Food Eng* **206**:37–47 (2017).

11 Illy A and Viani R, *Espresso Coffee. The Science of Quality*, 2nd edn. Elsevier Academic, Amsterdam (2005).

12 MacDougal DT and Spoehr HA, Growth and imbibition. *Proc Am Philos Soc* **56**:289–352 (1917).

13 Mateus M-L, Rouvet M, Gumy J-C and Liardon R, Interactions of water with roasted and ground coffee in the wetting process investigated by a combination of physical determinations. *J Agric Food Chem* **55**: 2979–2984 (2007).

14 Wolfrom ML and Patin DL, Carbohydrates of the coffee bean. IV. An arabinogalactan 1. *J Org Chem* **30**:4060–4063 (1965).

15 Wolfrom ML, Laver ML and Patin DL, Carbohydrates of the coffee bean. II. Isolation and characterization of a mannan 1. *J Org Chem* **26**: 4533–4535 (1961).

16 Wolfrom ML and Patin DL, Coffee constituents, isolation and characterization of cellulose in coffee bean. *J Agric Food Chem* **12**:376–377 (1964).

17 Bradbury AG and Halliday DJ, Chemical structures of green coffee bean polysaccharides. *J Agric Food Chem* **38**:389–392 (1990).

18 Thaler H and Arneth W, Untersuchungen an Kaffee und Kaffee-Ersatz. XIII Mitteilung Verhalten der Polysaccharid-Komplexe des rohen Arabica-Kaffees beim Rösten. *Zeitschrift für Lebensmittel-Untersuchung und Forschung* **140**:101–109 (1969).

19 Asante M and Thaler H, Untersuchungen an Kaffee und Kaffee-Ersatz. XVII Verhalten der Polysaccharid-Komplexe von Robusta-Kaffee beim Rösten. *Zeitschrift für Lebensmittel-Untersuchung und Forschung* **159**:93–96 (1975).

20 Sachslehner A, Foidl G, Foidl N, Gübitz G and Haltrich D, Hydrolysis of isolated coffee mannan and coffee extract by mannanases of *Sclerotium rolfsii. J Biotechnol* **80**:127–134 (2000).

21 Grignon J and Scallan AM, Effect of pH and neutral salts upon the swelling of cellulose gels. *J Appl Polym Sci* **25**:2829–2843 (1980).

22 Carlsson G, Kolseth P and Lindström T, Polyelectrolyte swelling behavior of chlorite delignified spruce wood fibers. *Wood Sci Technol* **17**: 69–73 (1983).

23 Eriksson I, Haglind I, Lidbrandt O and Sahnén L, Fiber swelling favoured by lignin softening. *Wood Sci Technol* **25**:135–144 (1991).

24 Luukko K and Maloney TC, Swelling of mechanical pulp fines. *Cellulose* **6**:123–135 (1999).

25 Cuissinat C and Navard P, Swelling and dissolution of cellulose, part III: plant fibres in aqueous systems. *Cellulose* **15**:67–74 (2008).

26 Rivetti D, Navarini L, Cappuccio R, Abatangelo A, Petracco M and Suggi-Liverani F, Effect of water composition and water treatment on espresso coffee percolation. In ASIC Proceedings, 19th International Scientific Colloquium on Coffee, Trieste, Italy (2001).

27 Sivetz M and Desrosier NW, *Coffee Technology*. AVI Publishing Company, Westport, CT (1979).

28 Spiro M, Toumi R and Kandiah M, The kinetics and mechanism of caffeine infusion from coffee: the hindrance factor in intra-bean diffusion. *J Sci Food Agric* **46**:349–356 (1989).

29 Hinz T, Steer A, Waldmann C, Cammenga HK and Eggers R, Röstkaffee-Extraktion: Einflußparameter und Modellierung. *Chem Ing Tech* **69**: 685–690 (1997).

30 Steer AG, *Physikalisch-chemische Parameter des Kaffeegetränkes und Untersuchungen zur Röstkaffee-Extraktion*, 1st edn. Cuvillier Verlag, Göttingen (2003).

31 Hinz, T. Strukturbeschreibung disperser Naturstoffe als Grundlage für Modellentwicklungen. Doctoral Thesis, Technical University Hamburg, Hamburg (1997).

32 Corrochano, B. R. Advancing the Engineering Understanding of Coffee Extraction. Doctoral Thesis, The University of Birmingham, Birmingham (2015).

33 Spiro M and Chong YY, The kinetics and mechanism of caffeine infusion from coffee: the temperature variation of the hindrance factor. *J Sci Food Agric* **74**:416–420 (1997).

34 Wang X and Lim L-T, A kinetics and modeling study of coffee roasting under isothermal conditions. *Food Bioproc Tech* **7**:621–632 (2014).

35 Ellero M and Navarini L, Mesoscopic modelling and simulation of espresso coffee extraction. *J Food Eng* **263**:181–194 (2019).

36 Ratnayake WMN, Hollywood R, O'Grady E and Stavric B, Lipid content and composition of coffee brews prepared by different methods. *Food Chem Toxicol* **31**:263–269 (1993).

37 Navarini L, Ferrari M, Liverani FS, Liggieri L and Ravera F, Dynamic tensiometric characterization of espresso coffee beverage. *Food Hydrocoll* **18**:387–393 (2004).

38 Hwang K-J and Lin I-L, Effects of mixing ratio of binary fine particles on the packing density and filtration characteristics. *KONA Powder Part J* **33**:296–303 (2016).

APPENDIX
STATISTICAL ANALYSIS RESULTS

In this appendix, the results from statistical tests are presented supporting our statements in the Results section. The P-values of the two-sample t-tests, Mann–Whitney U-tests, and ANOVA are listed as well as the slopes from linear regressions.

Table A1 Statistical comparison of volume density for dry *versus* wet measurements and 25 *versus* 90 °C

Compared parameters	Range of size classes (µm)	Difference of means[a]	P-Value t-Test	Range of size classes (µm)	P-Value Mann–Whitney
Dry *versus* wet	0.5–31	< 0	< 0.01	0.5–22	< 0.01
	31–60	> 0	> 0.01[b]	22–75	> 0.01
	60–250	< 0	< 0.01[c]	75–250	< 0.01
	250–730	> 0	< 0.01	250–730	< 0.01
	730–1750	≤ 0	> 0.01[d]	730–1750	> 0.01
25 °C *versus* 90 °C	0.5–50	< 0	< 0.01	0.5–50	< 0.01
	50–90	< 0 or > 0	> 0.01	90–510	> 0.01
	90–510	> 0	< 0.01	90–510	< 0.01
	510–1750	≤ 0 or > 0	> 0.01	510–1750	> 0.01

[a] Difference is calculated as mean of first parameter minus mean of second parameter, i.e. dry minus wet and 90–25 °C.
[b] Except for 31–37 µm: $P < 0.01$.
[c] Except for 210–250 µm: $P > 0.01$.
[d] Except for 730–870 µm: $P < 0.01$.

Table A2 Statistical results for the correlation analysis of relative diameter increase and initial particle diameter

	Slope $\times 10^{-3}$ (% µm^{-1})	P-Value
Medium roast	−2.95	0.291
Light roast	−2.54	0.498

Table A3 Statistical comparison of total swelling for different temperatures and roasts based on microscopy measurements

Compared parameters	Identical parameters	P-Value t-Test	Mann–Whitney
25 °C	Medium roast	0.372	0.400
versus	Light roast	0.065	0.017
80 °C			
Medium roast *versus*	80 °C	0.517	0.905
light roast	25 °C	0.173	0.143

Table A4 Statistical results for the correlation analysis of aspect ratio and time for single particles

	80 °C			25 °C		
	d_0 (µm)	Slope $\times 10^{-5}$ (s^{-1})	P-Value	d_0 (µm)	Slope $\times 10^{-5}$ (s^{-1})	P-Value
Medium roast	608	−2.11	0.100	585	−1.63	0.095
	519	1.62	0.171	543	0.660	0.559
	675	−1.24	0.250	914	2.84	4.35×10^{-6}
Light roast	652	1.26	0.088	472	2.51	0.025
	626	−0.723	0.392	589	2.78	0.013
	462	3.37	0.008	520	2.97	0.051
	665	−0.292	0.788	568	−0.291	0.706
	653	0.368	0.206	592	−0.344	0.667
	547	−0.621	0.075			

B.2 Influence of Flow Rate, Particle Size, and Temperature on Espresso Extraction Kinetics

Influence of Flow Rate, Particle Size, and Temperature on Espresso Extraction Kinetics

Benedikt K. L. Schmieder [1] [ID], Verena B. Pannusch [2], Lara Vannieuwenhuyse [1], Heiko Briesen [2] and Mirjana Minceva [1,*] [ID]

1   Biothermodynamics, TUM School of Life Sciences, Technical University of Munich, 85354 Freising, Germany
2   Process Systems Engineering, TUM School of Life Sciences, Technical University of Munich, 85354 Freising, Germany
*   Correspondence: mirjana.minceva@tum.de

Abstract: Brewing espresso coffee (EC) is considered a craft and, by some, even an art. Therefore, in this study, we systematically investigated the influence of coffee grinding, water flow rate, and temperature on the extraction kinetics of representative EC components, employing a central composite experimental design. The extraction kinetics of trigonelline, caffeine, 5-caffeoylquinic acid (5-CQA), and Total Dissolved Solids (TDS) were determined by collecting and analyzing ten consecutive fractions during the EC brewing process. From the extraction kinetics, the component masses in the cup were calculated for Ristretto, Espresso, and Espresso Lungo. The analysis of the studied parameters revealed that flow rate had the strongest effect on the component mass in the cup. The intensity of the flow rate influence was more pronounced at finer grindings and higher water temperatures. Overall, the observed influences were minor compared to changes resulting from differences in total extracted EC mass.

Keywords: espresso; coffee; extraction kinetics; non-volatiles; caffeine; trigonelline; caffeoylquinic acid; brew ratio

1. Introduction

Espresso coffee (EC) brewing is a solid–liquid extraction process from a packed (coffee) bed—the coffee puck [1]. A commonly recommended extraction method for the preparation of EC utilizes a pump (9 ± 2 bar) to infuse 6 ± 1.5 g fine ground and tamped coffee in a portafilter with heated water ($90 \pm 5\,^\circ$C). The typical extraction for a single espresso (25 ± 5 mL) takes approximately 30 ± 5 s. The ranges of these recommendations for EC extraction leave much leeway to the barista, as the complex influence of the operating parameters on the final product is not fully understood. Hence, brewing espresso coffee is a craft, even considered an art by some.

EC is obtained from only two main ingredients: water and ground, roasted coffee beans. The type and quality of the used coffee beans and water set the quality window attainable by the EC extraction. The most common coffee bean species *Coffea arabica* (Arabica) and *Coffea canephora* (Robusta) differ significantly in their chemical, physical, and sensory properties [2]. Additionally, the post-harvest processes [3], storage [4] and the degree of roasting [5,6] change the chemical compositions of the beans through thermal degradation or neogenesis of new compounds, e.g., by the Maillard reaction [7]. The water mineral content and composition also influence the EC extraction [8,9].

Most scientific studies on EC extraction focus on analyzing sensory attributes, volatile and non-volatile EC components. Over 1000 components are present in an EC cup, of which around 30–50 are considered key odorants [10,11]. For non-volatile components, typically, trigonelline, caffeine, caffeoylquinic acids, caffeoylquinic acid lactones, organic acids, fatty acids, and lipids, are analyzed [12]. The main aspects considered for an EC extraction are grinding and tamping the coffee in the portafilter, the water flow rate, pressure, and

temperature, as well as the extraction time that determines the EC mass in the cup [12]. The ratio between the ground coffee mass in the puck and the extracted EC mass in the cup is called the brew ratio (BR).

The grinding process defines the particle size distribution and the amount of coffee mass in the portafilter. Finer grinding levels (GL) increase the particle surface area in contact with water, enabling a higher extraction yield for trigonelline, caffeine, and 5-caffeoylquinic acid (5-CQA) [13–17]. Increasing the ground coffee mass at a similar extracted EC volume increases the masses of trigonelline, caffeine, and 5-CQA in the cup [18,19]. Particle size distribution, coffee mass, and tamping define the puck's mechanical structure and hydraulic resistance, which, in turn, sets the relation of water flow rate and pressure [20]. The relation between water pressure and flow rate can be described by Darcy's law [21].

In previous studies, increasing the applied pressure from 7 to 11 bar has shown a decreasing trend in extracted component mass in the coffee cup [22–24]. The corresponding flow rates (F) for the pressure-controlled experiments were not reported. Though, Lee et al. pointed out that the flow through a coffee puck is non-uniform and could lead to irregular EC extractions [25].

Higher water temperatures (T) increase the components' solubility and reduce water viscosity [26]. However, the influence of water temperature on EC component mass in the cup has been inconclusive for experiments with otherwise constant conditions [13]. Albanese et al. [27] analyzed coffee pods and reported increased caffeine concentration with rising temperatures from 90 °C to 110 °C. Masella et al. [28] found no significant difference in trigonelline, caffeine, and chlorogenic acid concentrations in the EC cup for 75 °C, 80 °C, or 85 °C. For similar EC components, Andueza et al. [29] reported several ambiguous temperature correlations for significant differences between EC brewed at 88 °C, 92 °C, 96 °C, and 98 °C. Also, Salamanca et al. [30] described different influences on the caffeine and 5-CQA concentrations in the cup for upward and downward temperature gradients between 88 °C and 93 °C without identifying a conclusive correlation.

While most studies analyze full EC cups, some authors have highlighted the importance of understanding extraction kinetics, as the concentration of extracted components strongly changes over time. Generally, the majority of EC components are extracted at the beginning of the brew [24,31,32]. Only a few studies compared extraction kinetics for varying preparation and processing conditions. Kuhn et al. [14] and Severini et al. [33] compared the extraction kinetics for different particle size distributions. They observed that trigonelline and caffeine were extracted faster from smaller rather than larger particles.

Overall, there is a highly complex interplay of several preparation and processing parameters on the EC component masses in the cup. Though known to be decisive, only very few data on extraction kinetics for controlled varying conditions are available. This study combines a rigorous statistical experimental design (central composite) with a detailed analysis of time-dependent extraction behaviors (extraction kinetics). This work aims to investigate the individual and combined influences of the extraction process parameters flow rate (F), coffee grinding level (GL), and water temperature (T) on trigonelline, caffeine, 5-caffeoylquinic acid (5-CQA), and Total Dissolved Solids (TDS) masses in the EC cup for Ristretto (BR 1/1), Espresso (BR 1/2), and Espresso Lungo (BR 1/3).

2. Materials and Methods

2.1. Chemicals

Trigonelline hydrochloride (≥97.5% purity), caffeine (≥99.0%), and 5-caffeoylquinic acid (≥96%) analytical standards were purchased from Sigma-Aldrich Chemie GmbH (Taufkirchen, Germany). HPLC-water (≥99.9%, HiPerSolv Chromanorm), methanol (≥99.9%, HiPerSolv Chromanorm Reag. Ph. Eur.), and formic acid (≥98%, AnalaR Normapur) for the high-performance liquid chromatography (HPLC) analysis were acquired from VWR Chemicals GmbH (Darmstadt, Germany).

2.2. Coffee Beans and Roasting

The coffee beans were obtained from List + Beisler GmbH (Hamburg, Germany). The brand *Colombia Suprema Huila* consisted of 100% Arabica and was washed in a post-harvest process. For the experiment, 5 kg was roasted by BB Coffee Company GmbH (Unterhaching, Germany). The coffee beans were roasted in a CRS-30 roaster (Joper SA, Canelas, Portugal) with an increasing temperature profile from 180 °C to 212 °C (190 °C at first crack) for approximately 10 min. Two roasting batches of the same coffee beans were used for the experiments. Both roasting batches were tested in triplicate under the same extraction conditions (20 g puck, flow rate F 2.0 mL s^{-1}, grinding level GL 1.7, temperature T 89 °C, 40 g EC) and showed no significant differences for trigonelline, caffeine, 5-CQA, and TDS concentrations in the espresso coffee (EC) cup. After roasting, the coffee beans were stored in 250 g packages for two weeks. The evening before each experiment, the required 250 g packages were opened and divided into air–sealed 50 g packs per EC extraction to prevent aroma loss over the course of the day.

2.3. Brewing Water

Bottled 750 mL water *Acqua Panna* (Sanpellegrino S.p.A., Pellegrino Terme, Italy) with the following composition was used to prepare the coffee samples: 106 mg L^{-1} HCO$_3^-$, 32.2 mg L^{-1} Ca^{2+}, 22.0 mg L^{-1} SO$_4^{2-}$, 7.8 mg L^{-1} Cl$^-$, 6.9 mg L^{-1} SiO$_2$, 6.6 mg L^{-1} Na$^+$, and 6.5 mg L^{-1} Mg^{2+}.

2.4. Coffee Puck Preparation

The coffee beans were ground on the Mahlkönig E65S (Hemro International AG, Zurich, Switzerland). As EC is typically brewed using fine ground coffee, the grinder was set to the EC grinding levels GL 1.4, GL 1.7, and GL 2.0. The chosen interval corresponded to 7.5% of the available scale, for which the manufacturer declared a volume mean diameter bandwidth of 180–580 μm [34]. The particle size distributions for the used grinding levels were measured dry and wet by laser diffractometer (Helos/BR + Rodos/Quixel, Sympatec GmbH, Clausthal-Zellerfeld, Germany) and showed high similarity (Appendix A Figure A1). The wet-measured, volume-based De Broucker mean particle diameter (standard deviation SD) for the GL 1.4, GL 1.7, and GL 2.0 increased from 273 μm (SD 7.6) to 277 μm (SD 17.0) and 295 μm (SD 18). The respective surface-area-based Sauter mean diameters were 28.3 μm (SD 1.6), 26.9 μm (SD 3.2), and 29.2 μm (SD 1.4) for GL 1.4, GL 1.7, and GL 2.0.

The mass of ground coffee for all experiments was 20 ± 0.01 g. The ground coffee was distributed and levelled with the distribution tool Grande TRE (Sahdia Enterprises GmbH, Frankfurt, Germany). The levelled puck was then tamped parallel to the basket bottom with a force equal to 25 kg on the tamping station CPS Tamper (Macap SRL, Maerne, Italy).

2.5. Espresso Coffee Preparation

The extraction was performed with a Decent DE1 Pro (Decent Espresso Intl. Ltd., Hong Kong, China). The machine was equipped with an IMS Cl 200 IM shower screen attached to the original Decent shower head and an IMS BT702Th26.5M precision portafilter basket (I.M.S. spa, Torre D'isola, Italy). During the coffee extraction, ten fractions were collected with a time-controlled sampling wheel developed by Kuhn et al. [14]. The velocity of the sampling wheel was chosen so that ten fractions of similar mass were collected for an average total EC mass of 58.1 g (SD 4.1) for each of the studied flow rates. The average mass of a single fraction was 6.0 g (SD 0.9). Fraction 1 exhibited the highest mass variation because of inaccuracies in starting the sample wheel on the first EC drop. The sampling wheel was positioned on a KB 2400-2N digital scale (Kern & Sohn GmbH, Balingen, Germany) to record the extracted EC mass continuously.

Water temperature, flow rate, or pressure profiles could be set on the Decent DE1 Pro. The machine measured the brew temperature just above the coffee puck and the brew pressure between the boiler and portafilter. In the experiments performed in this work, the

extraction was flow rate controlled in order to keep a constant residence time and to be able to collect fractions of constant mass. In the preinfusion phase, the coffee machine was set to 7 mL s^{-1} and to a preselected temperature (80 °C, 89 °C, or 98 °C), which matched the one used in the extraction phase. The machine changed to the extraction phase setting when the portafilter basket was filled, and the pressure rose above 2.5 bar. For the set water flow rates 1.0 mL s^{-1}, 2.0 mL s^{-1}, and 3.0 mL s^{-1}, the achieved average flow rates of 0.96 mL s^{-1} (SD 0.1), 1.9 mL s^{-1} (SD 0.0), and 2.8 mL s^{-1} (SD 0.1) were determined based on the scale's time-stamped measurements of the extracted EC mass. The set water temperatures of 80 °C, 89 °C, and 98 °C resulted in average brew temperatures of 79.1 °C (SD 0.5), 88.2 °C (SD 0.5), and 96.5 °C (SD 0.5), as continuously measured by the Decent DE1 Pro. An example of water flow and temperature course during the EC preparation is shown in Appendix A Figure A2. Before each EC extraction experiment, one test EC was brewed with identical settings to pre-heat the machine.

Fractions 1, 2, 3, 5, 7, and 10 were cooled immediately after the extraction in an ice bath. For HPLC analysis, fractions 1 and 2 were diluted with HPLC-water by mass ratios of 1:50, fractions 3 and 5 were diluted by 1:20, and fractions 7 and 10 were diluted by 1:5. The diluted samples were filtered with 0.2 μm Chromafil PET-20/15 MS syringe filters (Macherey-Nagel GmbH & Co., KG, Düren, Germany), and an aliquot of 1.5 mL was stored in a refrigerator at 9 °C until the analysis. For the TDS analysis, 2 mL per fraction was centrifuged at 4700 rpm for 10 min in the Centrifuge 5804 R (Eppendorf AG, Hamburg, Germany), and 0.1 mL of the supernatant was stored in a freezer at −20 °C.

2.6. HPLC Analysis

Trigonelline, caffeine, and 5-CQA were analyzed by high performance liquid chromatography (HPLC) on an Agilent 1290 Infinity LC System (Agilent Technologies Inc., Santa Clara, CA, USA) equipped with a UV/VIS detector. The analysis was performed with the reverse phase column VDSpher PUR C18-E (150 mm × 4.6 mm, 5 μm; VDS optilab Chromatographie Technik GmbH, Berlin, Germany). The method described by Farah et al. [5] was modified for the analysis. Eluent A consisted of HPLC-water with 0.5% formic acid and eluent B of methanol with 0.5% formic acid. At the constant flow rate of 1.2 mL min^{-1}, the following gradient method was used for 10 μL injected sample volume: 2% B (0–1.2 min), 20% B (2.5 min), 40% B (13 min), 95% B (14.5–15 min), 2% B (15.5–21 min). Trigonelline and caffeine were detected at λ = 272 nm, whereas 5-CQA was detected at λ = 324 nm. The component concentrations were calculated by preparing calibration curves from two stock solutions of the corresponding standards with five calibration points each.

2.7. Determination of TDS

The centrifuged (4700 rpm, 10 min) and frozen samples of 0.1 mL were thawed at room temperature and diluted by volume ratio 1:3 with demineralized water from a Milli-Q Direct 8 (Merck KGaA, Darmstadt, Germany). To determine the Total Dissolved Solids (TDS) mass, the limit angle and refractive index at λ = 589 nm and 20 °C were measured in the refractometer DR6000-T (A. Kruess Optronic GmbH, Hamburg, Germany). The calibration was performed according to the German norm DIN 10775 [35] by correlating the refractive index with the mass of dried samples.

2.8. Data Processing and Statistical Analysis

2.8.1. Extraction Kinetics Fitting

To characterize the extraction kinetics, the extract's component concentration at the portafilter outlet was considered as a function of the cumulative extracted EC mass. As no continuous measure of the concentration at the outlet was available, such a function was derived from six analyzed EC fractions (1, 2, 3, 5, 7, and 10). For the discrete samples, the accumulated extracted EC mass until fraction *n* was calculated according to:

$$m_{\Sigma}^{n} = 0.5 * m_n + \sum_{1}^{n-1} m_n \tag{1}$$

The extraction kinetic $c(m_{\Sigma})$ for continuous accumulated EC mass m_{Σ} was obtained by least-square fitting the discrete concentrations of the analyzed components using the following exponential function:

$$c(m_{\Sigma}) = c_0 \cdot e^{-\frac{m_{\Sigma}}{\lambda}} \tag{2}$$

The accumulated extraction mass m_{Σ} was utilized to describe the EC extraction progress and highly correlated with the extraction time for flow-controlled EC brewing. Therefore, λ could be interpreted as a time constant. The theoretical start concentration was represented by c_0. Extraction kinetics were determined individually for every single experimental run. Additionally, for each of the 15 experiment settings presented in Section 2.8.3, the average extraction kinetics were determined by fitting Equation (2) to data obtained in triplicate (6 replicates at DoE central point).

2.8.2. Calculation of Component Mass in EC Cup

From the extraction kinetics, it is possible to calculate the component mass in the EC cup for different beverage sizes at their respective brew ratios (BR). In this study, the influence of flow rate, coffee grinding level, and water temperature on the component mass in the cup for Ristretto (~BR 1/1), Espresso (~BR 1/2), and Espresso Lungo (~BR 1/3) are discussed. Thus, beverage masses of 20 g, 40 g, and 60 g were chosen for the calculation to match the coffee puck mass of 20 ± 0.01 g and achieve the brew ratios of BR 1/1, BR 1/2, and BR 1/3.

The exact extraction kinetic at the beginning of the brew ($m_{cup} \ll m_{Frak.1}$) was unknown and suspected to deviate from the exponential decay described by Equation (2) [36]. Therefore, to calculate the component mass in the cup, the discrete component mass in the first fraction was combined with the mass obtained by integration of the extraction kinetics curve:
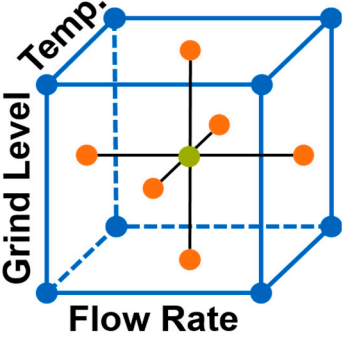
$$m_{cup}^{BR} = m_{Frak.1} \cdot c_{Frak.1} + \int_{m_{Frak.1}}^{20\ g/BR} c(m_{\Sigma})\ dm_{\Sigma} \text{ with } BR \in \{1/1,\ 1/2,\ 1/3\} \tag{3}$$

The component mass of the first fraction was determined by multiplying the measured fraction mass $m_{Frak.1}$ and component concentration in this fraction $c_{Frak.1}$. For the remaining duration of the extraction process, the component mass was determined by integrating the extraction kinetic curve $c(m_{\Sigma})$, correlated with Equation (2), from the first fraction mass $m_{Frak.1}$ to the desired end mass of the EC beverage.

2.8.3. Statistical Analysis

The influence of flow rate, grinding level, and temperature on the extraction kinetics of trigonelline, caffeine, 5-CQA, and TDS was studied. The experiment set was defined using a face-centered Central Composite Design [37]. Table 1 provides the design of experiment (DoE) operating conditions for the 15 experiments (each with 3 repetitions, 6 repetitions for the central point).

Table 1. Face-centered Central Composite Design including axis, central (CP) and corner points with the parameter settings for flow rate (mL s^{-1}), grinding level ($-$), and temperature (°C).

		Experiment	Replicates	Flow Rate (mL s^{-1})	Grinding Level ($-$)	Temp. (°C)
DoE Axis Points		1	3	1.0	1.7	89
		2	3	3.0	1.7	89
		3	3	2.0	1.4	89
		4	3	2.0	2.0	89
		5	3	2.0	1.7	80
		6	3	2.0	1.7	98
DoE CP		7	6	2.0	1.7	89
DoE Corner Points		8	3	1.0	1.4	80
		9	3	1.0	1.4	98
		10	3	1.0	2.0	80
		11	3	1.0	2.0	98
		12	3	3.0	1.4	80
		13	3	3.0	1.4	98
		14	3	3.0	2.0	80
		15	3	3.0	2.0	98

The masses of trigonelline, caffeine, 5-CQA, and TDS in the EC cup (m_{cup}) for three different brew ratios (BR 1/1, BR 1/2, and BR 1/3) were used as response variables to evaluate the influence of the studied process parameters flow rate, grinding level, and temperature on the EC extraction. The necessary 12 response sets were calculated with Equation (3) and evaluated by response surface methodology in OriginPro 2021b (OriginLab Corporation, Northampton, MA, USA). The response surface method was based on the following full-quadratic model function:

$$m_{cup} = \beta_0 + \beta_1 x_{flow} + \beta_2 x_{grind} + \beta_3 x_{temp} + \beta_4 x_{flow}^2 + \beta_5 x_{grind}^2 + \beta_6 x_{temp}^2 + \beta_7 x_{flow} x_{grind} + \beta_8 x_{flow} x_{temp} + \beta_9 x_{grind} x_{temp} \quad (4)$$

For the evaluation, the set grinding levels x_{grind} as well as the experimental values for the flow rate x_{flow} and the temperature x_{temp} were used. The coefficient β_0 is the intercept, β_1–β_3 are the linear coefficients, β_4–β_6 are the quadratic coefficients, and β_7–β_9 are the interactive coefficients. The significance of each effect was determined by ANOVA. Based on the ANOVA and the standardized effects, backward elimination was used to reduce the full-quadratic fitting to the significant effect parameters for higher-order factors (significance level $\alpha = 0.05$) [38].

3. Results & Discussion

3.1. Extraction Kinetics

The extraction kinetics describe the components' concentration change in the espresso coffee (EC) extract as a function of the cumulative extracted EC mass in the cup. The extract concentration of all compounds was highest at the beginning of the brewing process (i.e., in the first collected fraction) and decreased exponentially the more EC was extracted. The fastest decrease was observed for trigonelline and Total Dissolved Solids (TDS), followed by 5-caffeoylquinic acid (5-CQA) and caffeine. This behavior was also described in the literature and correlated with the components' polarity for trigonelline, caffeine, and 5-CQA [39,40]. For comparison, Figure 1 shows the extraction kinetic curves normalized with respect to the corresponding initial concentration c_0 for different components obtained

by fitting Equation (2) to the experimental data of the design of experiment's (DoE) central point.
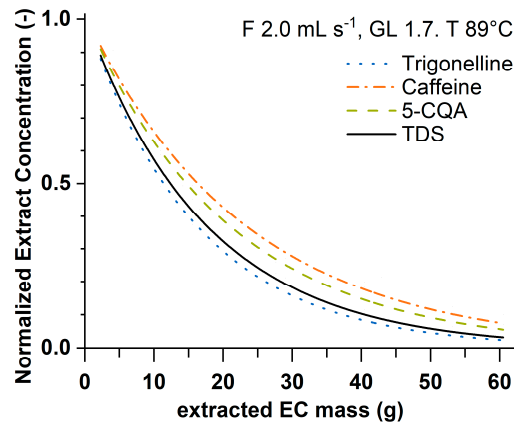

Figure 1. Normalized (with respect to corresponding initial concentration c_0 from Equation (2)) extraction kinetics for trigonelline, caffeine, 5-CQA, and TDS for the DoE central point (F 2.0 mL s^{-1}, GL 1.7, and T 89 °C).

For all 15 performed experiments, the fit parameters of the average extraction kinetic curves can be found in Appendix A Table A1. In addition, the raw concentration data for the fractions 1, 2, 3, 5, 7, and 10 for all experiments' replicates are available in Supplementary Materials Table S1. For the experiments at the DoE axis points (Exp. 1–6 in Table 1), the average extraction kinetics for the concentration of trigonelline, caffeine, 5-CQA, and TDS in the EC extract are shown in Figure 2. At the DoE axis points, only one process parameter is changed at a time compared to the DoE central point settings (F 2.0 mL s^{-1}, GL 1.7, and T 89 °C). The process parameters are set to the lower and upper boundaries of the DoE space (see Table 1). In general, the studied components show similar behaviors toward the different influences of the process parameters flow rate (F), grinding level (GL), and temperature (T).
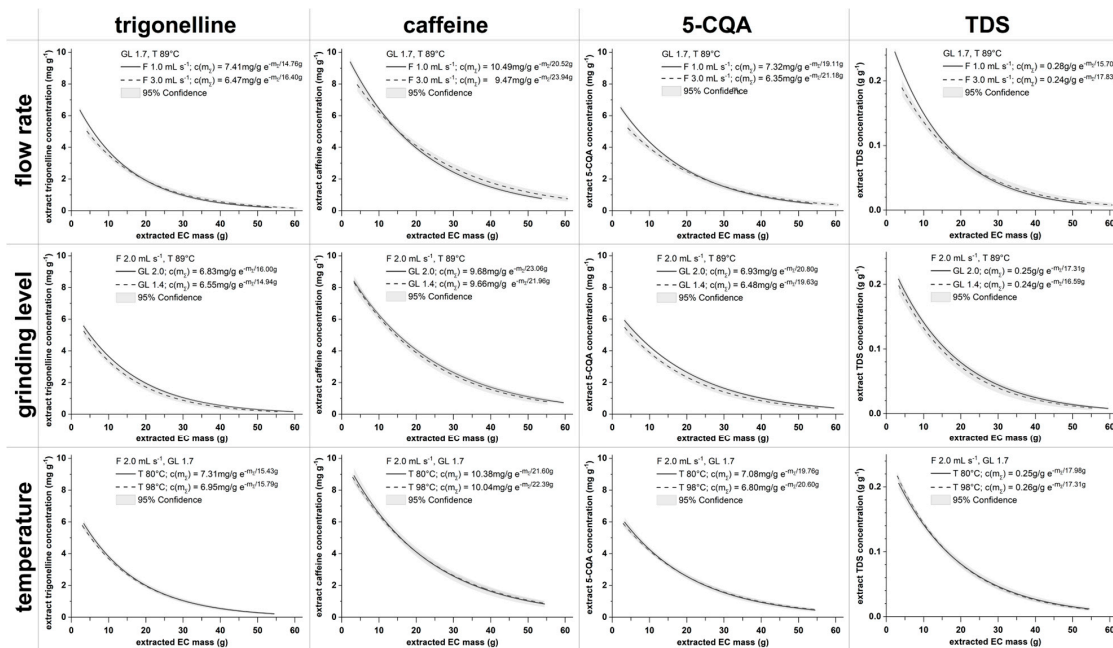

Figure 2. Trigonelline, caffeine, 5-CQA, and TDS extraction kinetics $c(m_\Sigma)$ for lower and upper DoE boundary settings of water flow rate (F), grinding level (GL), and temperature (T), whereas the remaining process parameters were kept at DoE central point settings (F 2.0 mL s^{-1}, GL 1.7, and T 89 °C).

The component extraction kinetics for the flow rates at the lower and upper boundaries (Figure 2, top row) differ at the beginning of the extraction and in their extraction dynamics. The extract's component concentrations at the beginning are higher for the slower flow rate of 1.0 mL s^{-1} but decrease faster during the brew than for the faster flow rate of 3.0 mL s^{-1}. The difference in the extract's component concentrations between the slow and fast flow rates decreases as the extraction progresses. A slower flow rate allows for a longer contact time between water and ground coffee. As the extraction process is time dependent, the longer contact time explains the higher concentrations of the EC extract at the beginning of the brew [1].

The extraction kinetics obtained for the lower and upper boundaries of the grinding level (Figure 2, middle row) behave similarly considering their extraction rates. However, the lower grinding level GL 1.4 extract's component concentration is slightly smaller than GL 2.0. Their 95% confidence bands overlap for most of the brewing process.

The obtained extraction kinetics are nearly identical for the temperature lower and upper boundary settings (Figure 2, bottom row), and their 95% confidence bands overlap for the whole analyzed brewing process. Consequently, in contrast to the literature [23,30], no measurable influence on the trigonelline, caffeine, 5-CQA, and TDS masses in the cup would be expected by individually changing the water temperatures from 80 °C to 98 °C.

3.2. Extracted Component Mass in the Cup for Brew Ratios 1/1, 1/2, and 1/3
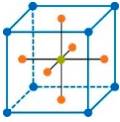
The average trigonelline, caffeine, 5-CQA, and TDS masses in the EC cup for brew ratios BR 1/1, BR1/2, and BR1/3 are presented in Table 2, together with the set grinding levels and the measured process parameters flow rates, temperatures, and pressures. The presented component masses in the cup are average values for each of the 15 experiments based on integrating each replicate's extraction kinetics individually with Equation (3) for extracted EC mass of 20 g (BR 1/1), 40 g (BR 1/2), and 60 g (BR 1/3). The parameters for the extraction kinetic curves for the individual replicates can be found in Supplementary Materials Table S3.

The overall average concentrations for all experiments for a 40 g EC cup (BR 1/2) were 2.45 mg g^{-1} for trigonelline, 4.57 mg g^{-1} for caffeine, 2.96 mg g^{-1} for 5-CQA, and 9.68 g (100 g)$^{-1}$ for TDS. The use of different coffee and water types, roasting levels, coffee puck masses, beverage sizes, and extraction machines impeded quantitative comparisons to other studies. Angeloni et al., who also used a 20 g Arabica coffee puck and a ~BR 1/2, extracted, on average, 3.39 mg g^{-1} trigonelline, 5.18 mg g^{-1} caffeine, 5.27 mg g^{-1} 5-CQA, and 10.02 g (100 g)$^{-1}$ TDS [13]. Taking into consideration that Caprioli et al. reported trigonelline masses in the cup ranging from 28.20 mg to 65.08 mg and caffeine masses from 116.87 mg to 199.68 mg for the same extraction settings (7.5 g ground coffee, 25 mL EC, 25 s) for 20 different EC coffee brands, the experimental results were within the expected range [24]. Additionally, 5-CQA is known to be affected strongly by different roasting processes [41,42], which could further explain the concentration differences between the two studies. For TDS, the measured values were in accordance with Angeloni et al. [13].

In the literature, relative standard deviations (RSD) of <5–10% [19,23,24] for either component concentration or mass in the cup are generally reported but can reach up to 20% [13]. The average relative standard deviation for the studied experimental set was 2.5%, with the highest RSD of 8.5%. In this work, the component masses in the cup were calculated by integration of the extraction kinetics curves with Equation (3). Hence, the error caused by the variation in the final EC mass in the cup was minimized.

Table 2. Trigonelline, caffeine, 5-CQA, and TDS masses in the EC cup for brew ratios BR 1/1, BR 1/2, and BR 1/3, set grinding levels, and the measured flow rates, temperatures, and pressures. The reported masses are averaged values with relative standard deviations in % provided in brackets.

	Experiment	Flow Rate (mL s^{-1})	Grinding Level (–)	Temp. (°C)	Replicates	Trigonelline (mg) Brew Ratio 1/1	1/2	1/3	Caffeine (mg) Brew Ratio 1/1	1/2	1/3	5-CQA (mg) Brew Ratio 1/1	1/2	1/3	TDS (g) Brew Ratio 1/1	1/2	1/3	Pressure (Bar)
DOE Axis Points	1	1.0 (7.5)	1.7	87.3 (0.2)	3	81.2 (1.1)	102.1 (1.1)	107.5 (1.2)	134.0 (1.9)	184.6 (2.4)	203.7 (2.7)	90.8 (1.7)	122.7 (2.1)	133.9 (2.3)	3.20 (0.7)	4.10 (0.6)	4.35 (0.6)	2.7 (4.0)
	2	2.8 (1.0)	1.7	88.2 (0.3)	3	74.9 (1.9)	97.1 (2.4)	103.7 (2.8)	129.4 (3.6)	183.9 (2.9)	208.2 (2.8)	82.3 (3.3)	114.4 (3.3)	126.9 (3.3)	2.87 (1.7)	3.81 (1.5)	4.12 (1.3)	5.3 (35.3)
	3	1.9 (0.3)	1.4	88.5 (0.1)	3	72.2 (2.8)	91.1 (2.9)	96.0 (3.4)	126.9 (1.6)	177.9 (2.7)	198.4 (3.6)	81.3 (3.7)	110.5 (4.1)	121.1 (4.6)	2.81 (2.4)	3.65 (3.0)	3.91 (3.9)	3.9 (5.1)
	4	2.0 (0.2)	2.0	88.6 (0.1)	3	78.0 (2.0)	100.3 (1.9)	106.7 (1.9)	129.4 (0.7)	183.7 (1.0)	206.7 (1.1)	89.0 (0.5)	123.0 (0.3)	136.1 (0.4)	2.98 (0.5)	3.92 (0.4)	4.22 (0.3)	3.3 (3.4)
	5	1.9 (0.7)	1.7	79.2 (0.1)	3	81.9 (1.8)	104.3 (2.1)	110.4 (2.6)	134.8 (5.3)	188.2 (3.3)	209.3 (2.0)	88.9 (3.1)	121.2 (1.3)	132.9 (0.6)	2.99 (1.7)	3.96 (3.1)	4.29 (4.0)	3.6 (7.7)
	6	1.9 (1.0)	1.7	96.7 (0.2)	3	78.9 (1.9)	101.1 (1.6)	107.3 (1.9)	133.0 (3.5)	187.2 (3.5)	209.3 (3.6)	87.2 (4.4)	120.0 (4.0)	132.4 (3.8)	3.05 (2.4)	4.01 (1.8)	4.31 (1.8)	3.0 (4.6)
DoE Central Point	7	1.9 (2.3)	1.7	88.3 (0.5)	6	75.9 (2.2)	98.3 (1.9)	104.9 (1.8)	129.0 (1.1)	183.8 (1.1)	207.1 (1.3)	86.5 (3.3)	120.0 (3.2)	133.1 (3.3)	2.92 (1.9)	3.88 (0.8)	4.19 (0.8)	3.4 (15.6)
DOE Corner Points	8	1.0 (0.1)	1.4	78.8 (0.1)	3	78.2 (0.7)	95.3 (1.5)	99.0 (1.9)	132.1 (2.2)	177.8 (2.0)	193.6 (2.0)	86.7 (0.5)	114.0 (0.5)	122.6 (0.9)	3.15 (4.6)	3.84 (1.1)	3.99 (0.7)	2.9 (3.6)
	9	0.9 (2.3)	1.4	96.2 (0.2)	3	80.1 (5.0)	102.2 (5.6)	108.4 (6.0)	139.8 (4.2)	195.2 (5.1)	217.2 (5.8)	92.6 (3.5)	126.4 (4.4)	138.8 (5.0)	3.22 (3.9)	4.18 (4.7)	4.46 (5.1)	2.8 (4.3)
	10	1.0 (0.9)	2.0	78.7 (0.1)	3	78.0 (4.1)	96.6 (7.3)	101.1 (8.5)	127.0 (3.6)	172.9 (6.0)	189.6 (7.4)	87.5 (3.9)	117.0 (6.2)	126.9 (7.4)	2.92 (3.7)	3.72 (6.5)	3.94 (7.7)	2.9 (3.8)
	11	0.9 (5.9)	2.0	96.1 (0.3)	3	83.9 (0.8)	106.1 (1.4)	111.9 (1.6)	135.3 (0.6)	187.8 (1.0)	208.2 (1.3)	94.9 (1.6)	129.0 (2.2)	141.3 (2.5)	3.19 (1.0)	4.11 (0.6)	4.38 (1.0)	2.6 (2.3)
	12	2.7 (3.7)	1.4	79.8 (1.0)	3	69.0 (4.3)	88.3 (2.9)	93.8 (2.2)	120.4 (5.7)	172.4 (4.3)	195.0 (3.4)	77.1 (4.3)	106.9 (3.1)	118.4 (2.4)	2.67 (4.3)	3.53 (2.0)	3.81 (0.9)	8.4 (16.7)
	13	2.7 (2.3)	1.4	97.1 (0.4)	3	72.8 (2.2)	93.2 (2.0)	99.0 (2.5)	129.2 (1.8)	184.0 (1.5)	207.2 (2.0)	83.0 (2.7)	114.4 (2.3)	126.3 (2.4)	2.89 (2.3)	3.83 (1.9)	4.13 (2.5)	7.6 (9.3)
	14	2.9 (0.8)	2.0	79.1 (0.1)	3	75.1 (2.9)	97.8 (1.9)	104.7 (1.5)	122.6 (3.4)	176.3 (2.8)	199.8 (2.5)	81.8 (0.5)	115.5 (0.7)	128.7 (0.2)	2.75 (1.3)	3.68 (0.9)	3.99 (1.0)	3.6 (7.4)
	15	2.8 (8.0)	2.0	96.4 (0.5)	3	76.2 (1.7)	98.9 (1.0)	105.7 (0.8)	127.5 (1.7)	182.7 (1.9)	206.6 (2.1)	86.9 (1.9)	120.7 (1.5)	131.4 (1.6)	2.93 (0.8)	3.88 (0.9)	4.19 (1.0)	3.5 (7.9)
	Average mass in cup:					77.1	98.2	104.0	130.0	182.6	204.0	86.4	118.4	130.1	2.97	3.87	4.15	

3.3. Influencing the EC Component Mass in the Cup

3.3.1. Linear Response Surfaces

The results from the experiments of the central composite design were evaluated using the response surface methodology (Section 2.8.3). The resulting linear regression parameters for the analyzed components and brew ratios are available in Table 3. The OriginPro file, including the utilized ANOVA tables, F-tests, and Pareto charts of standardized effects, can be found in Supplementary Materials S4.1 and S4.2.

Table 3. Linear regressions and respective adjusted R^2, derived by response surface methodology for flow rates [1.0 mL s^{-1}, 3.0 mL s^{-1}], grinding levels [1.4, 2.0], and temperatures [80 °C, 98 °C] to calculate the component masses in the EC cup for trigonelline, caffeine, 5-CQA, and TDS at brew ratios BR 1/1, BR 1/2, and BR 1/3.

$$m_{cup} = \beta_0 + \beta_1 x_{flow} + \beta_2 x_{grind} + \beta_3 x_{temp} + \beta_4 x_{flow}^2 + \beta_5 x_{grind}^2 + \beta_6 x_{temp}^2 + \beta_7 x_{flow} x_{grind} + \beta_8 x_{flow} x_{temp} + \beta_9 x_{grind} x_{temp}$$

Components	Brew Ratio	β_0 (mg)	β_1 (mg s mL^{-1})	β_2 (mg)	β_3 (mg °C^{-1})	β_4 (mg s^2 mL^{-2})	β_5 (mg)	β_6 (mg °C^{-2})	β_7 (mg s mL^{-1})	β_8 (mg °C^{-1} s mL^{-1})	β_9 (mg °C^{-1})	R^2 (adj.)
Trigonelline	1/1	185.8	−9.17	105.90	−4.48	0	−30.96	0.03	3.24	0	0	0.66
	1/2	134.6	4.28	163.33	−4.40	0	−47.80	0.03	4.92	−0.18	0	0.60
	1/3	99.9	8.54	184.84	−4.06	0	−54.17	0.03	5.71	−0.24	0	0.58
Caffeine	1/1	192.0	−13.85	118.83	−3.59	0	−38.45	0.02	5.52	0	0	0.50
	1/2	−9.2	2.92	149.27	0.97	0	−48.37	0	7.57	−0.21	0	0.41
	1/3	−57.7	15.87	186.29	1.37	0	−59.53	0	8.42	−0.34	0	0.42
5-CQA	1/1	112.2	−10.32	56.75	−1.74	0	−16.42	0.01	3.33	0	0	0.69
	1/2	−10.4	2.96	83.84	0.74	0	−24.01	0	4.97	−0.18	0	0.62
	1/3	−54.7	13.94	119.15	1.02	0	−34.02	0	4.93	−0.30	0	0.57
		(g)	(g s mL^{-1})	(g)	(g °C^{-1})	(g s^2 mL^{-2})	(g)	(g °C^{-2})	(g s mL^{-1})	(g °C^{-1} s mL^{-1})	(g °C^{-1})	
TDS	1/1	3.65	−0.70	2.78	−0.06	0.05	−0.91	0.001	0.19	0	0	0.75
	1/2	4.19	−0.50	4.75	−0.10	0	−1.48	0.001	0.21	0	0	0.64
	1/3	2.91	0.12	6.16	−0.11	0	−1.87	0.001	0.20	−0.01	0	0.57

Additionally, in Table 3, the adjusted coefficient of determination (adjusted R^2) is included as an indicator of how well the fitted parameters describe the experimental data. The comparatively low coefficients of determination show that the response surface methodology can only partially explain the observed data variations. The adjusted coefficients of determination are particularly low for caffeine.

A quantitative interpretation, therefore, should be treated with care. Nevertheless, this study is the most comprehensive experimental study for extraction kinetics to date and yields important trends for trigonelline, caffeine, 5-CQA, and TSD mass in the EC cup. For quantitative analysis, mechanistic modelling should be considered. The trends for the analyzed parameters are discussed in the following Sections 3.3.2–3.3.5 based on cross-sections of the response surface generated by Equation (4) with the coefficients β_m (Table 3).

3.3.2. Flow Rate Influence

As can be observed in Figure 3, increasing the flow rate reduced the mass in the cup for all components. The influence of the flow rate on the component mass in the cup was smallest for caffeine. While most components showed a similar trend (with respect to the slope) for the different brew ratios, the effect of flow rate on the caffeine concentration decreased from BR 1/1 to BR 1/3. In the literature, pressure control was preferred for the EC brewing process. Hence, no systematic study was found to compare the flow rate influence on the component mass in the cup. However, as postulated by Darcy's Law, an increasing flow rate corresponded directly to an increasing brew pressure at otherwise constant conditions. As reported in the literature [22–24], increasing pressure reduces component masses in the cup, which correlates well with the observed reduction in trigonelline, caffeine, 5-CQA, and TDS masses in the cup by increasing flow rates. As observed in Section 3.1 for the beginning of the brew, a faster flow rate reduces the extract's component concentration, which the time-dependent mass transport process can achieve.
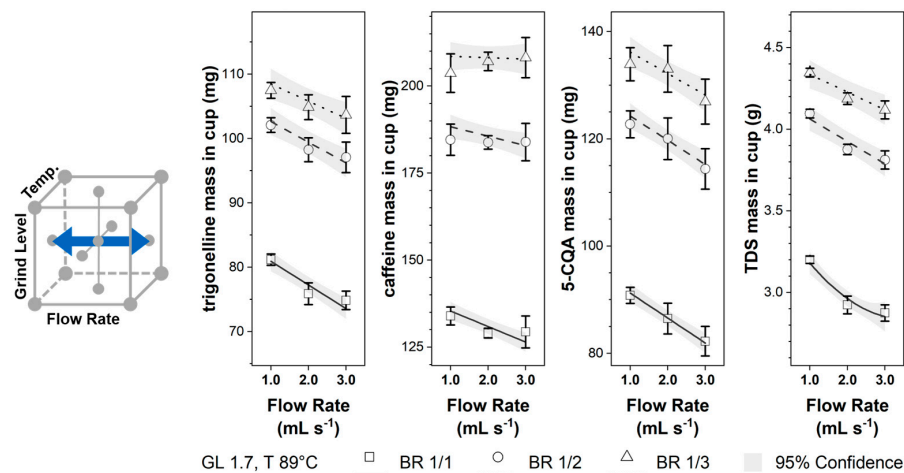
Figure 3. Trigonelline, caffeine, 5-CQA, and TDS masses in the EC cup for flow rates 1.0–3.0 mL s^{-1} and brew ratios BR 1/1, BR 1/2, and BR 1/3 at constant grinding level GL 1.7 and temperature T 89 °C; Lines: calculated data (Table 3) with 95% confidence band; □, o, △: experimental data (Table 2) with standard deviation.

3.3.3. Grinding Level Influence

For the analyzed grinding levels, the component masses in the cup for trigonelline, caffeine, 5-CQA, and TDS in Figure 4 show a parabolic behavior, as indicated by the significance of the coefficient β_5 (see Table 3). Changing the grinding level from GL 1.4 to GL 1.7 increases the component mass in the cup. Further increasing the grinding level to GL 2.0 results in a near-constant 5-CQA mass in the cup and decreases the component mass in the cup for trigonelline, caffeine, and TDS. Again, the caffeine mass in the cup is only slightly influenced.
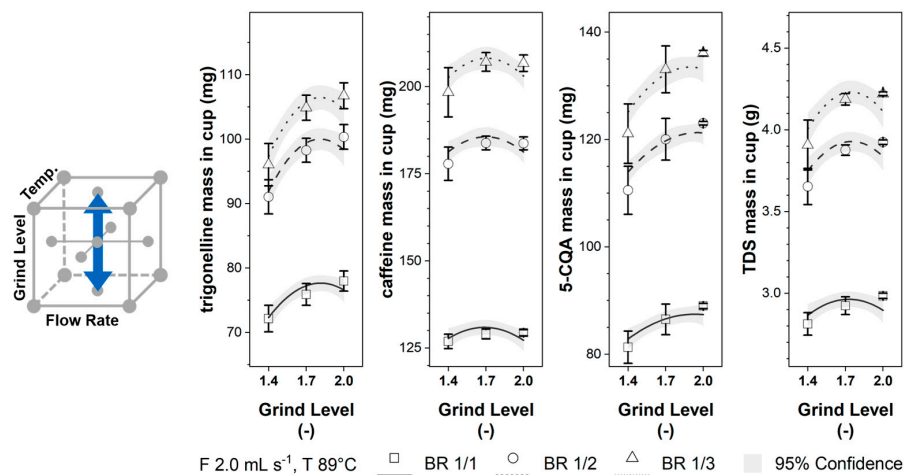
Figure 4. Trigonelline, caffeine, 5-CQA, and TDS masses in the EC cup for grinding levels 1.4–2.0 and brew ratios BR 1/1, BR 1/2, and BR 1/3 at constant flow rate F 2.0 mL s^{-1} and temperature T 89 °C; Lines: calculated data (Table 3) with 95% confidence band; □, o, △: experimental data (Table 2) with standard deviation.

In the literature, an increase in the extracted component mass in the cup is reported for smaller particles and commonly explained by the larger particle surface area [14–17]. The influence was described for ground coffee with significantly different particle sizes, often generated by sieving the coffee particles into fine and coarse fractions after grinding. The grinder settings used in this study resulted in more realistic, however, rather similar particle size distributions (see Appendix A Figure A1). The characteristic Sauter diameters for the particle size distributions were not significantly different for GL 1.4, GL 1.7, and

GL 2.0; $d_{32}^{GL1.4}$ = 28.3 (SD 1.6), $d_{32}^{GL1.7}$ = 26.9 (SD 3.2) and $d_{32}^{GL2.0}$ = 29.2 (SD 1.4). The Sauter diameter is an integral measure of the particle size distribution, representing its specific surface area. Thus, the insignificance of difference in Sauter diameters indicates similar specific surface areas. Therefore, the explanation found in the literature, based on the particle surface area, cannot explain the observed influence of the grinding levels on the component masses in the cup in this study. It should, however, be noted that the minor differences in the particle size distributions for GL 1.4, GL 1.7, and GL 2.0 are already sufficient to influence the maximal brew pressure.

For similar EC grinding levels, Cameron et al. observed a reassembling influence on the extraction yield [43]. They attribute the decrease in the extraction yield for finer grinding levels to a possible partial clogging inside the coffee puck, which might decrease its permeability and increase the pressures needed to keep a set flow rate. The pressure measured during our experiments agrees with the hypothesis of possible clogging. Namely, the pressure was 3.8 bar, 7.4 bar, and 9.3 bar for the respective grinding levels GL 2.0, GL 1.7, and GL 1.4 and hence was higher for finer grinding.

3.3.4. Temperature Influence

The influence of the temperature variation from 80 °C to 98 °C is shown in Figure 5. As can be seen in Table 3, the quadratic coefficient β_6 is only significant for selected components and brew ratios yielding parabolic shapes. Generally, increasing temperature increases the component mass in the EC cup, which was not expected from the extraction kinetics presented in Section 3.1 for individually changing the temperature at the DoE central point.
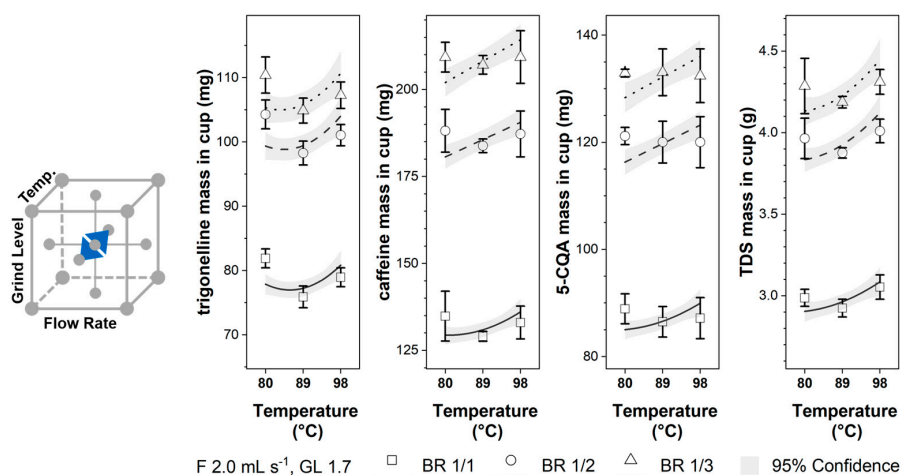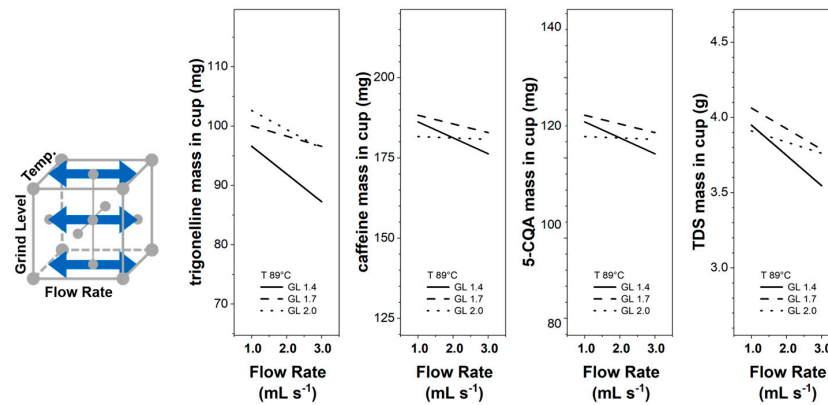

Figure 5. Trigonelline, caffeine, 5-CQA, and TDS masses in the EC cup for temperatures 80–98 °C and brew ratios BR 1/1, BR 1/2, and BR 1/3 at constant flow rate F 2.0 mL s^{-1} and grinding level GL 1.7; Lines: calculated data (Table 3) with 95% confidence band; □, o, Δ: experimental data (Table 2) with standard deviation.

As discussed in the introduction, literature knowledge on the effect of temperature is inconclusive. The literature reports different trends and only minor information to track potentially overlapping effects, which this study has attempted to avoid. However, note that the differences found in this study are significantly smaller than the values reported in the literature [13,29,30].

3.3.5. Interactive Influences

The combined effects of the operating parameters are reflected in the parameters β_7–β_9 in Table 3. The combined effect of the grinding level and temperature is not significant for the investigated parameter space ($\beta_9 = 0$). However, there are combined effects of the flow rate with the grinding level (β_7) and the flow rate with the temperature (β_8).

Figure 6 presents the influence of the flow rate on the component mass in the cup for three different grinding levels at BR 1/2 and T 89 °C. The flow rate increase has a higher effect on decreasing the component mass in the cup for the finer grinding level (GL 1.4) than for the coarser grinding levels. For different grinding levels, even though the particle size distribution was similar, the flow rate change resulted in different brew pressures.

Figure 6. Trigonelline, caffeine, 5-CQA, and TDS masses in the EC cup for flow rates F 1.0–3.0 mL s^{-1} and grinding levels GL 1.4, GL 1.7, and GL 2.0 at temperatures 89 °C and brew ratio BR 1/2; 95% confidence bands omitted for clarity.

For GL 1.4, the brew pressure increases from 2.9 bar for flow rate 1.0 mL s^{-1} (average pressure of Exp. 8 and Exp. 9 in Table 2) to 8.0 bar for flow rate 3.0 mL s^{-1} (Exp. 12, Exp. 13). For the same flow rate settings at GL 2.0, the pressure increases from 2.8 bar for flow rate 1.0 mL s^{-1} (Exp. 10, Exp. 11) to 3.6 bar for flow rate 3.0 mL s^{-1} (Exp. 14, Exp. 15). Higher pressures are known to decrease the component mass in the cup [22–24], which is in agreement with the experimental data in Table 2 and could explain the interaction between the influence of the flow rate and grinding level.

In Figure 7, the flow rate influence on the component mass in the cup is presented for three different temperatures at BR 1/2 and GL 1.7. The component mass in the cup decreases with an increase in the flow rate, whereas the influence is stronger at higher temperatures. This interaction could possibly explain the different temperature influences seen in Section 3.1 for the extraction kinetic curves and Section 3.3.4 resulting from the response surfaces. Temperature influences water viscosity and density [26], which might change uneven pressure and flow distributions in the coffee puck [25] and, in turn, influence the component mass transfer rate.
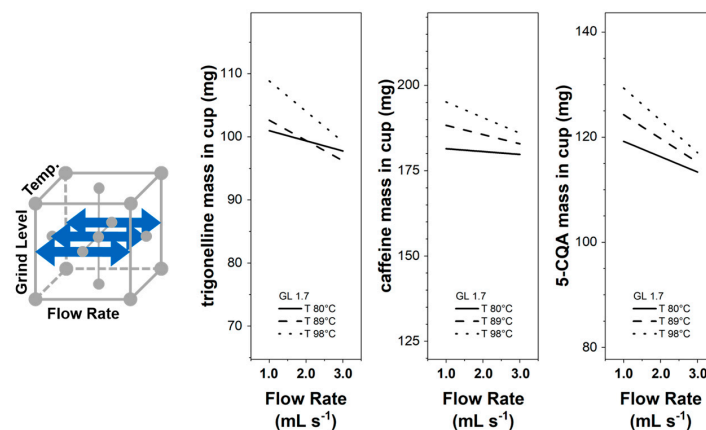
Figure 7. Trigonelline, caffeine, and 5-CQA masses in the EC cup for flow rates F 1.0–3.0 mL s^{-1} and temperatures 80 °C, 89 °C and 98 °C at grinding level GL 1.7 and brew ratio BR 1/2; 95% confidence bands omitted for clarity.

3.3.6. Brew Ratio Influence

Overall, the effect of the parameters flow rate, grinding level, and temperature are small compared to the influences of different brew ratios. For example, decreasing the flow rate at the DoE central point (GL 1.7, T 89 °C) from 2.0 mL s^{-1} to 1.0 mL s^{-1} for the BR 1/2 changes the cup concentration of 5-CQA according to the response surface (see Table 3) from 2.99 mg g^{-1} to 3.11 mg g^{-1}.

Using the extraction kinetics Equation (2), one can estimate the concentration in an EC cup if the specified brew ratio is experimentally not perfectly met. E.g. extracting 38 g instead of the intended 40 g (BR 1/2) already results in a concentration difference comparable to the one obtained by the above flow rate decrease from 2.0 mL s^{-1} to 1.0 mL s^{-1}. While a 5% decrease in extracted mass appears to be larger, it corresponds to a decrease in extraction time of ~1 s. Hence, for practical applications to extract a consistent EC, the brew ratio is the first parameter to control with high accuracy before optimizing the process parameters flow rate, grinding level and water temperature.

4. Conclusions

The extraction kinetics for the espresso coffee (EC) components trigonelline, caffeine, 5-caffeoylquinic acid (5-CQA), and Total Dissolved Solids (TDS) were studied for water flow rates 1.0–3.0 mL s^{-1}, grinding levels 1.4–2.0 (Mahlkoenig E65S), and water temperatures 80–98 °C. Through integration of the extraction kinetics, the component masses in the EC cup were determined for different brew rations. Based on a central composite design of experiment (DoE), the influence of the process parameters on the component masses in the cup for brew ratios BR 1/1, BR 1/2, and BR 1/3 were analyzed by response surface methodology. Comparably, low coefficients of variation allowed for qualitative rather than quantitative statements. For a quantitative assessment, the data-driven approach seems not to be entirely sufficient to capture the inherent complexity and irregularity of the coffee extraction process. Nevertheless, the following qualitative trends could be identified:

Trigonelline, 5-CQA, and TDS showed similar behaviors with respect to flow rate, grinding level, and temperature. Caffeine mass in the EC cup was only slightly influenced by different flow rates and grinding levels. Increasing the flow rate from 1.0 to 3.0 mL s^{-1} decreased the component masses in the cup. Despite the grinding level range of GL 1.4 to GL 2.0 leading to nearly identical particle size distributions, it still affected the brew pressure and component masses in the cup. In addition, finer grinding levels and higher temperatures increased the intensity of the flow rate influence on the component mass in the cup.

Overall, the experimental data showed good reproducibility and allowed interpretation of the extraction kinetics instead of only final concentrations in the EC cup. Especially, such kinetic data provide excellent grounds for further mechanistic modelling of the extraction process, potentially yielding a quantitative interpretation.

Appendix A

(**a**)   (**b**)

Figure A1. Density volume distribution q3 and cumulative volume distributions Q3 for Mahlkoenig EK65S grinding levels GL 1.4, GL 1.7, and GL 2.0, measured (**a**) dry and (**b**) wet.

(**a**)   (**b**)
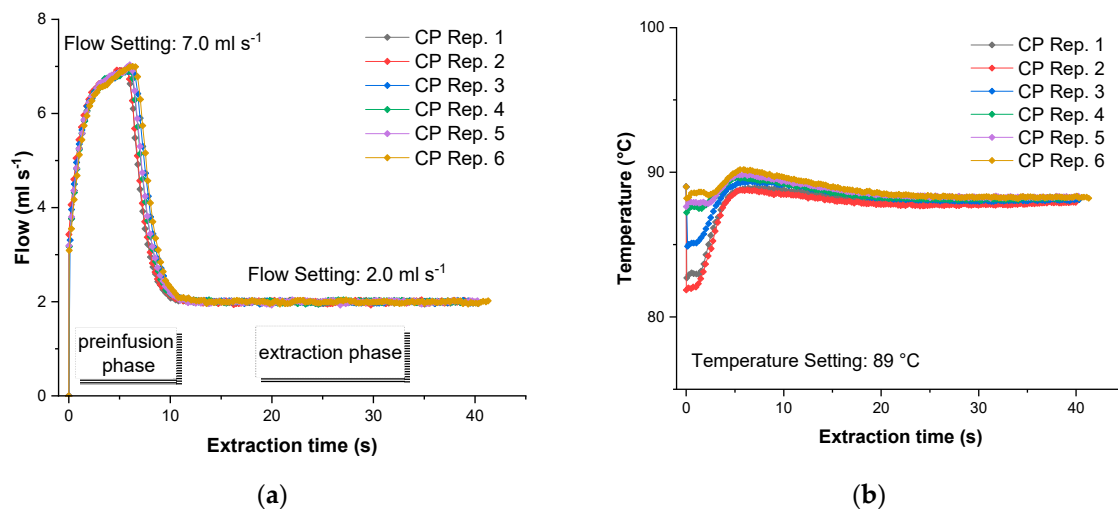
Figure A2. Representative (**a**) flow and (**b**) temperature courses during the espresso coffee preparation with the Decent DE1 Pro for a set preinfusion flow rate of 7.0 mL s^{-1} and for the extraction flow rate of 2.0 mL s^{-1} as well as a temperature of 89 °C.

Table A1. Parameter values with standard error (SE) for the experiments' average extraction kinetics $c(m_\Sigma)$ for trigonelline, caffeine, 5-CQA, and TDS, based on Equation (2).

Experiment	$c(m_\Sigma) = c_0 \exp(-m_\Sigma/\lambda)$											
	Trigonelline						Caffeine					
	c_0 (mg g^{-1})		λ (g)		Statistics		c_0 (mg g^{-1})		λ (g)		Statistics	
	Value	SE	Value	SE	Red. Chi-Sqr	Adj. R^2	Value	SE	Value	SE	Red. Chi-Sqr	Adj. R^2
1	7.40899	0.12316	14.76344	0.42552	0.02561	0.99481	10.4887	0.14327	20.52467	0.5199	0.04752	0.99493
2	6.46932	0.23064	16.40303	0.86193	0.05312	0.9806	9.46765	0.28924	23.93518	1.18507	0.13117	0.97824
3	6.54716	0.23705	14.93682	0.84702	0.06872	0.97702	9.66427	0.27442	21.96458	1.0845	0.14334	0.97831
4	6.83473	0.11231	15.99516	0.42845	0.01714	0.99521	9.67546	0.15595	23.05736	0.66335	0.04944	0.99303
5	7.30706	0.16914	15.42548	0.57294	0.03804	0.9907	10.38155	0.30436	21.59864	1.08663	0.174	0.97851
6	6.95468	0.10214	15.7859	0.3698	0.01422	0.99616	10.04235	0.15921	22.39093	0.62077	0.05039	0.99327
7	6.69949	0.09587	16.08737	0.36681	2.47×10^{-2}	0.99227	9.70981	0.13064	23.09434	0.5462	0.06781	0.9897
8	7.62541	0.09065	13.12089	0.27877	0.01422	0.9973	10.69172	0.15672	18.92703	0.52514	0.0595	0.99409
9	7.08449	0.1493	15.63306	0.56872	0.03722	0.99154	10.69195	0.19535	21.67685	0.73662	0.08821	0.99072
10	7.34872	0.18011	14.07208	0.54291	0.03783	0.99095	10.13843	0.25125	19.75409	0.82583	0.10739	0.98646
11	7.57984	0.13439	15.04329	0.43899	0.02663	0.99434	10.45723	0.1349	21.14279	0.4897	0.03828	0.99552
12	6.17348	0.332	15.48473	1.32764	0.13618	0.94866	8.97304	0.39549	23.57685	1.85949	0.3117	0.94656
13	6.50908	0.26715	15.53493	1.03374	0.09268	0.97024	9.67713	0.31126	23.15069	1.31948	0.19488	0.97264
14	6.47069	0.1751	16.63498	0.70499	0.03894	0.98677	9.03485	0.21274	24.1222	0.98821	0.08722	0.98465
15	6.62197	0.14144	16.37875	0.56426	0.02867	0.9911	9.45174	0.17933	23.78621	0.80464	0.06779	0.98933

Experiment	5-CQA						TDS					
	c_0 (mg g^{-1})		λ (g)		Statistics		c_0 (g g^{-1})		λ (g)		Statistics	
	Value	SE	Value	SE	Red. Chi-Sqr	Adj. R^2	Value	SE	Value	SE	Red. Chi-Sqr	Adj. R^2
1	7.32493	0.1108	19.11304	0.52774	0.02668	0.99429	0.28305	0.00386	15.70033	0.37567	2.68×10^{-5}	0.9962
2	6.35357	0.22661	21.1787	1.18384	0.07051	0.97413	0.23924	0.00955	17.83024	1.06401	1.02×10^{-4}	0.97201
3	6.47778	0.22434	19.62703	1.14453	0.08511	0.97164	0.24196	0.00933	16.59384	1.03039	1.21×10^{-4}	0.97078
4	6.92748	0.11967	20.80018	0.62438	0.02622	0.99288	0.25164	0.00514	17.31233	0.58753	3.94×10^{-5}	0.99185
5	7.08289	0.1861	19.75796	0.87311	0.05984	0.98429	0.2474	0.00636	17.98499	0.75292	6.37×10^{-5}	0.98585
6	6.80018	0.12522	20.60333	0.6479	0.02871	0.9918	0.25713	0.00367	17.3144	0.40346	2.05×10^{-5}	0.99593

Table A1. *Cont.*

Experiment	5-CQA						TDS					
7	6.79246	0.10682	20.77137	0.55683	4.08×10^{-2}	0.98752	0.24827	0.00419	17.47261	0.48029	5.20×10^{-5}	0.98811
8	7.31745	0.09572	17.29798	0.4219	0.02055	0.99572	0.30725	0.00999	13.16232	0.76497	1.73×10^{-4}	0.97956
9	7.32619	0.12423	19.92738	0.61563	0.03302	0.99274	0.27778	0.00462	16.50264	0.47902	3.77×10^{-5}	0.99428
10	7.18869	0.17832	18.48345	0.76212	0.05056	0.98742	0.2599	0.00608	15.62012	0.58694	4.89×10^{-5}	0.99069
11	7.57346	0.10943	19.56499	0.49683	0.02338	0.99488	0.27975	0.00446	16.03038	0.42671	3.15×10^{-5}	0.99499
12	6.02455	0.29418	20.79431	1.75317	0.15129	0.94255	0.22578	0.01287	17.38228	1.62994	2.36×10^{-4}	0.93514
13	6.53399	0.25585	20.40671	1.37513	0.11588	0.96435	0.24308	0.01083	17.58935	1.30555	1.76×10^{-4}	0.96041
14	6.35075	0.15431	21.56882	0.88151	0.04089	0.98564	0.22567	0.00635	18.4123	0.83369	5.79×10^{-5}	0.98403
15	6.76424	0.14962	21.01016	0.79908	0.04192	0.98738	0.24533	0.00629	17.69504	0.74554	6.18×10^{-5}	0.98599

References

1. Petracco, M. Technology IV: Beverage Preparation: Brewing Trends for the New Millennium. In *Coffee*; Clarke, R.J., Vitzthum, O.G., Eds.; Blackwell Science Ltd.: Oxford, UK, 2001; pp. 140–164; ISBN 9780470690499.
2. Bee, S.; Brando, C.; Brumen, G.; Carvalhaes, N.; Kölling-Speer, I.; Speer, K.; Suggi Liverani, F.; Teixeira, A.A.; Teixeira, R.; Thomaziello, R.A.; et al. The raw bean. In *Espresso Coffee: The Science of Quality*, 2nd ed.; Illy, A., Viani, R., Eds.; Elsevier Academic Press: Amsterdam, The Netherlands, 2005; pp. 87–178.

3. Sanz-Uribe, J.R.; Sunalini, N.M.; Penuela, A.; Oliveros, C.; Husson, J.; Brando, C.; Rodriguez, A. Post-harvest Processing—Revealing the Green Bean. In *The Craft and Science of Coffee*; Folmer, B., Ed.; Elsevier: Amsterdam, The Netherlands, 2017; pp. 51–75; ISBN 978-0-12-803520-7.

4. Nicoli, M.C.; Savonitti, O. Storage and packaging. In *Espresso Coffee: The Science of Quality*, 2nd ed.; Illy, A., Viani, R., Eds.; Elsevier Academic Press: Amsterdam, The Netherlands, 2005; pp. 230–258.

5. Farah, A.; de Paulis, T.; Trugo, L.C.; Martin, P.R. Effect of roasting on the formation of chlorogenic acid lactones in coffee. *J. Agric. Food Chem.* **2005**, *53*, 1505–1513. [CrossRef]

6. Spiro, M.; Hunter, J.E. The kinetics and mechanism of caffeine infusion from coffee: The effect of roasting. *J. Sci. Food Agric.* **1985**, *36*, 871–876. [CrossRef]

7. Martins, S.I.; Jongen, W.M.; van Boekel, M.A. A review of Maillard reaction in food and implications to kinetic modelling. *Trends Food Sci. Technol.* **2000**, *11*, 364–373. [CrossRef]

8. Navarini, L.; Rivetti, D. Water quality for Espresso coffee. *Food Chem.* **2010**, *122*, 424–428. [CrossRef]

9. Hendon, C.H.; Colonna-Dashwood, L.; Colonna-Dashwood, M. The role of dissolved cations in coffee extraction. *J. Agric. Food Chem.* **2014**, *62*, 4947–4950. [CrossRef]

10. Angeloni, S.; Mustafa, A.M.; Abouelenein, D.; Alessandroni, L.; Acquaticci, L.; Nzekoue, F.K.; Petrelli, R.; Sagratini, G.; Vittori, S.; Torregiani, E.; et al. Characterization of the Aroma Profile and Main Key Odorants of Espresso Coffee. *Molecules* **2021**, *26*, 3856. [CrossRef]

11. Stadler, R.H.; Varga, N.; Hau, J.; Vera, F.A.; Welti, D.H. Alkylpyridiniums. 1. Formation in model systems via thermal degradation of trigonelline. *J. Agric. Food Chem.* **2002**, *50*, 1192–1199. [CrossRef]

12. Cordoba, N.; Fernandez-Alduenda, M.; Moreno, F.L.; Ruiz, Y. Coffee extraction: A review of parameters and their influence on the physicochemical characteristics and flavour of coffee brews. *Trends Food Sci. Technol.* **2020**, *96*, 45–60. [CrossRef]

13. Angeloni, S.; Giacomini, J.; Maponi, P.; Perticarini, A.; Vittori, S.; Cognigni, L.; Fioretti, L. Computer Percolation Models for Espresso Coffee: State of the Art, Results and Future Perspectives. *Appl. Sci.* **2023**, *13*, 2688. [CrossRef]

14. Kuhn, M.; Lang, S.; Bezold, F.; Minceva, M.; Briesen, H. Time-resolved extraction of caffeine and trigonelline from finely-ground espresso coffee with varying particle sizes and tamping pressures. *J. Food Eng.* **2017**, *206*, 37–47. [CrossRef]

15. Andueza, S.; de Peña, M.P.; Cid, C. Chemical and sensorial characteristics of espresso coffee as affected by grinding and torrefacto roast. *J. Agric. Food Chem.* **2003**, *51*, 7034–7039. [CrossRef] [PubMed]

16. Bell, L.N.; Wetzel, C.R.; Grand, A.N. Caffeine content in coffee as influenced by grinding and brewing techniques. *Food Res. Int.* **1996**, *29*, 785–789. [CrossRef]

17. Spiro, M.; Selwood, R.M. The kinetics and mechanism of caffeine infusion from coffee: The effect of particle size. *J. Sci. Food Agric.* **1984**, *35*, 915–924. [CrossRef]

18. Andueza, S.; Vila, M.A.; Paz de Peña, M.; Cid, C. Influence of coffee/water ratio on the final quality of espresso coffee. *J. Sci. Food Agric.* **2007**, *87*, 586–592. [CrossRef]

19. Khamitova, G.; Angeloni, S.; Borsetta, G.; Xiao, J.; Maggi, F.; Sagratini, G.; Vittori, S.; Caprioli, G. Optimization of espresso coffee extraction through variation of particle sizes, perforated disk height and filter basket aimed at lowering the amount of ground coffee used. *Food Chem.* **2020**, *314*, 126220. [CrossRef]

20. Fasano, A.; Talamucci, F.; Petracco, M. The Espresso Coffee Problem. In *Complex Flows in Industrial Processes*; Birkhäuser: Boston, MA, USA, 2000; pp. 241–280.

21. Bear, J. *Modeling Phenomena of Flow and Transport in Porous Media*; Springer: Cham, Switzerland, 2018; pp. 263–282; ISBN 9783319728254.

22. Giacomini, J.; Khamitova, G.; Maponi, P.; Vittori, S.; Fioretti, L. Water flow and transport in porous media for in-silico espresso coffee. *Int. J. Multiph. Flow* **2020**, *126*, 103252. [CrossRef]

23. Andueza, S.; Maeztu, L.; Dean, B.; de Peña, M.P.; Bello, J.; Cid, C. Influence of water pressure on the final quality of arabica espresso coffee. Application of multivariate analysis. *J. Agric. Food Chem.* **2002**, *50*, 7426–7431. [CrossRef]

24. Caprioli, G.; Cortese, M.; Maggi, F.; Minnetti, C.; Odello, L.; Sagratini, G.; Vittori, S. Quantification of caffeine, trigonelline and nicotinic acid in espresso coffee: The influence of espresso machines and coffee cultivars. *Int. J. Food Sci. Nutr.* **2014**, *65*, 465–469. [CrossRef]

25. Lee, W.T.; Smith, A.; Arshad, A. Uneven extraction in coffee brewing. *Phys. Fluids* **2023**, *35*, 054110. [CrossRef]

26. Mestdagh, F.; Glabasnia, A.; Giuliano, P. The Brew—Extracting for Excellence. In *The Craft and Science of Coffee*; Elsevier: Amsterdam, The Netherlands, 2017; pp. 355–380; ISBN 9780128035207.

27. Albanese, D.; Di Matteo, M.; Poiana, M.; Spagnamusso, S. Espresso coffee (EC) by POD: Study of thermal profile during extraction process and influence of water temperature on chemical–physical and sensorial properties. *Food Res. Int.* **2009**, *42*, 727–732. [CrossRef]

28. Masella, P.; Guerrini, L.; Spinelli, S.; Calamai, L.; Spugnoli, P.; Illy, F.; Parenti, A. A new espresso brewing method. *J. Food Eng.* **2015**, *146*, 204–208. [CrossRef]

29. Andueza, S.; Maeztu, L.; Pascual, L.; Ibáñez, C.; de Peña, M.P.; Cid, C. Influence of extraction temperature on the final quality of espresso coffee. *J. Sci. Food Agric.* **2003**, *83*, 240–248. [CrossRef]

30. Salamanca, C.A.; Fiol, N.; González, C.; Saez, M.; Villaescusa, I. Extraction of espresso coffee by using gradient of temperature. Effect on physicochemical and sensorial characteristics of espresso. *Food Chem.* **2017**, *214*, 622–630. [CrossRef]

31. Ludwig, I.A.; Sanchez, L.; Caemmerer, B.; Kroh, L.W.; de Peña, M.P.; Cid, C. Extraction of coffee antioxidants: Impact of brewing time and method. *Food Res. Int.* **2012**, *48*, 57–64. [CrossRef]

32. Matias, A.F.V.; Valente-Matias, D.F.; Neng, N.R.; Nogueira, J.M.F.; Andrade, J.S.; Coelho, R.C.V.; Araújo, N.A.M. Continuum model for extraction and retention in porous media. *arXiv* **2023**, arXiv:2304.03161.

33. Severini, C.; Derossi, A.; Fiore, A.G.; de Pilli, T.; Alessandrino, O.; Del Mastro, A. How the variance of some extraction variables may affect the quality of espresso coffees served in coffee shops. *J. Sci. Food Agric.* **2016**, *96*, 3023–3031. [CrossRef] [PubMed]

34. Hemro International AG. Mahlkoenig_E65S_Espresso_Grinder_Product_Brochure_DE. Available online: https://downloads.mahlkoenig.de/Products/Mahlkoenig_E65S_Espresso_Grinder_Product_Brochure_DE.pdf (accessed on 4 April 2023).

35. Deutsches Institut für Normung e.V. *Analysis of Coffee and Coffee Products—Determination of Water-Soluble Extract—Method for Roasted Coffee*; Beuth: Berlin, Germany, 2016.

36. Moroney, K.M.; Lee, W.T.; O'Brien, S.; Suijver, F.; Marra, J. Modelling of coffee extraction during brewing using multiscale methods: An experimentally validated model. *Chem. Eng. Sci.* **2015**, *137*, 216–234. [CrossRef]

37. Box, G.E.P.; Wilson, K.B. On the Experimental Attainment of Optimum Conditions. In *Breakthroughs in Statistics*; Springer: New York, NY, USA, 1992; pp. 270–310.

38. Fahrmeir, L.; Kneib, T.; Lang, S.; Marx, B.D. *Regression: Models, Methods and Applications*, 2nd ed.; Springer: Berlin/Heidelberg, Germany, 2021; pp. 165–167.

39. Vaca Guerra, M.; Harshe, Y.M.; Fries, L.; Pietsch-Braune, S.; Palzer, S.; Heinrich, S. Tuning the packed bed configuration for selective extraction of espresso non-volatiles based on polarity. *J. Food Eng.* **2023**, *354*. [CrossRef]

40. Sánchez López, J.A.; Wellinger, M.; Gloess, A.N.; Zimmermann, R.; Yeretzian, C. Extraction kinetics of coffee aroma compounds using a semi-automatic machine: On-line analysis by PTR-ToF-MS. *Int. J. Mass Spectrom.* **2016**, *401*, 22–30. [CrossRef]

41. Frank, O.; Blumberg, S.; Kunert, C.; Zehentbauer, G.; Hofmann, T. Structure determination and sensory analysis of bitter-tasting 4-vinylcatechol oligomers and their identification in roasted coffee by means of LC-MS/MS. *J. Agric. Food Chem.* **2007**, *55*, 1945–1954. [CrossRef]

42. Trugo, L.C.; Macrae, R. A study of the effect of roasting on the chlorogenic acid composition of coffee using HPLC. *Food Chem.* **1984**, *15*, 219–227. [CrossRef]

43. Cameron, M.I.; Morisco, D.; Hofstetter, D.; Uman, E.; Wilkinson, J.; Kennedy, Z.C.; Fontenot, S.A.; Lee, W.T.; Hendon, C.H.; Foster, J.M. Systematically improving Espresso: Insights from mathematical modeling and experiment. *Matter* **2020**, *2*, 631–648. [CrossRef]

B.3 Model-Based Kinetic Espresso Brewing Control Chart for Representative Taste Components

Model-based kinetic espresso brewing control chart for representative taste components

Verena B. Pannusch [a], Benedikt K.L. Schmieder [b], Lara Vannieuwenhuyse [b], Mirjana Minceva [b], Heiko Briesen [a,*]

[a] *Process Systems Engineering, Technical University of Munich, Germany*
[b] *Biothermodynamics, Technical University of Munich, Germany*

ABSTRACT

Influencing espresso coffee quality by adjusting the extraction process parameters is a current issue in coffee research. In previous literature, significant effects of the brewing parameters on taste have been demonstrated for espresso, and mathematical models were developed describing extraction kinetics. However, an attempt to include the effects of process parameters in a model for predicting the extraction kinetics of taste-relevant solutes had been lacking.

In this study, the *two-grain model,* originating from the work of Melrose and Corrochano et al. (2012, 2015, 2018), and adopted by Moroney et al. (2019), was extended by equations describing the influence of water flow rate and temperature on mass transfer. The model parameters were estimated using experimental extraction kinetics data for total dissolved solids, caffeine, trigonelline, and chlorogenic acid from our previous study. Model predictions were compared with experimental data, including time-varying temperature and flow rate. The results are summarized in a control chart and a publicly available app visualizing the importance of extraction kinetics on espresso composition.

1. Introduction

Systematically improving espresso extraction requires adjusting the grind level, the water temperature, and the applied water pressure or flow rate. Total dissolved solids (TDS) are a standard measure regarding quality and yield. Other characteristic components, whose concentrations are usually determined, include caffeine, trigonelline, and chlorogenic acid. Caffeine is a compound representative of bitter taste (Klade, 2019), and chlorogenic acid can serve as a proxy compound for sour taste. Although chlorogenic acid only marginally contributes to the sour taste of coffee (Engelhardt and Maier, 1985), its advantage over other organic acids is that it can be measured using the same high performance liquid chromatography (HPLC) method as caffeine and trigonelline (Schmieder et al., 2023).

TDS, caffeine, and trigonelline concentrations in espresso were found to increase significantly with water temperature (Andueza et al., 2003). Salamanca et al. (2017) proposed an approach for tuning the taste and aroma profile of espresso coffee by using temperature gradients.

Flow rate and pressure are correlated through the permeability of the coffee puck (packed bed of ground coffee) (Corrochano et al., 2015). Explained briefly, the higher the applied pressure, the higher the water flow rate. The water flow rate is hypothesized to influence the extraction of solutes because it determines the contact time between solids and water and influences solid-liquid mass transfer (Wilson and Geankoplis, 1966).

The bimodal particle size distribution (PSD) of ground coffee is crucial to achieving a target pressure and flow rate. Vaca Guerra et al. (2023a) recently showed that particle size uniformity and mean size contribute to bed permeability at constant axial compression. The particle size distribution furthermore defines the specific surface area as higher concentrations of solutes are obtained when increasing the fine particle fraction (Kuhn et al., 2017) or when decreasing the ratio of coarse vs. fine particle mean diameters (Vaca Guerra et al., 2023b).

Mathematical modeling is gaining popularity in coffee research, with several recent studies focusing on modeling espresso extraction in dependence on the grind level, water temperature, and pressure (Kuhn et al., 2017; Cameron et al., 2020; Giacomini et al., 2020; Angeloni et al., 2023; Lee et al., 2023). The first multiscale model, which describes the

---

diffusive and convective mass transport in percolation coffee brewing, was introduced by Melrose et al. (2012). Three years later, Moroney et al. (2015) presented a multiscale model similar to the broken plus intact cells models widely used in modeling supercritical fluid extraction. Subsequently, models have been presented for the purpose of understanding and optimizing espresso coffee extraction focusing on the grind level and coffee dosage (Cameron et al., 2020; Lee et al., 2023) as well as considering varying water temperature, pressure, and tamping force (Giacomini et al., 2020; Angeloni et al., 2023). Although Giacomini et al. (2020) and Angeloni et al. (2023) modeled the effects of temperature, pressure, and grinding on the final concentrations in the cup, they did not validate their model concerning extraction kinetics data (concentrations vs. time or beverage volume). One difficulty in modeling espresso extraction is how the bimodal particle size distribution determining the surface area is incorporated into the model. While (Cameron et al., 2020), (Giacomini et al., 2020), and (Angeloni et al., 2023) did not include a relation between PSD and specific surface area (Lee et al. (2023) related the surface area to the grind level directly) in their recently published models, a promising *two-grain model*, which considers separate mass transfer rates for fine and coarse particles, was presented by Melrose et al., (2012, 2018) and Corrochano (2015) and adopted by Moroney et al. (2019), who described mass transfer from the particles by first order rate equations (averaging over the particle volume) instead of modeling diffusion across the particle radius, as done in (Melrose et al., 2018). The *two-grain model* describes the coffee puck as a packed bed composed of a mixture of two characteristic particles: fine and coarse particles. Moroney et al. (2019) modeled and analyzed TDS data at different extraction times and demonstrated that the goodness of fit with respect to TDS extraction kinetics was substantially improved over a *single-grain model*. The *two-grain model's* superiority stems from its ability to capture both stages of espresso extraction: quick initial extraction from mostly fine particles and slower extraction from coarse particles during the final seconds of espresso coffee preparation. Accordingly, the *two-grain model* as adopted by Moroney et al. (2019) was the model of choice in this study.

Although the development of mechanistic espresso extraction models has progressed quickly during the last decade, the models were not ready for practical use. First, there needed to be more extraction kinetics data for representative compounds. Either only TDS was measured during the extraction process (Cameron et al., 2020; Moroney et al., 2015, 2019; Melrose et al., 2018), or component concentrations were only measured for the final beverage (Giacomini et al., 2020; Angeloni et al., 2023). In contrast, our study considers TDS and the extraction kinetics of representative components: caffeine (bitter taste), trigonelline, and chlorogenic acid (sour taste). This study aims to achieve greater practical usefulness of mechanistic modeling by extending existing models towards the dependence on temperature and flow rate and estimating parameters based on kinetic experimental data of various components presented in (Schmieder et al., 2023). Predictions by the parameterized model at water temperatures and flow rates (constant and dynamic profiles), different from the ones in (Schmieder et al., 2023), were validated by a second set of experiments conducted in this study.

In practice, the coffee brewing control chart (Lockhart, 1957) is a standard tool used to classify the sensory quality of drip coffee and is based on the yield (Eq. (18)) and the TDS. Alternative model-based charts were proposed by Melrose et al. (2018) and Moroney et al. (2019) for espresso coffee. However, these control charts neither consider the ratio of different bitter- and sour-tasting compounds (balance) nor the effect of water temperature. The present study proposes a new model-based espresso brewing control chart to compare the influence of flow rate, temperature, and brew ratio on the yields and concentrations of taste-relevant compounds.

2. Experimental methods

Part of the experimental data in this article is already reported in our recent publication (Schmieder et al., 2023). Instead of a purely statistical evaluation of the effects of the brewing parameters on the solute concentrations as done in (Schmieder et al., 2023), we here use the data as a basis for mechanistic modeling. Although the statistical evaluation provided insight into the various parameter dependencies, the statistical quadratic models could not correlate the data with high fidelity. Mechanistic modeling has the potential to uncover the full complexity of the interdependence of control parameters. The experimental design from (Schmieder et al., 2023) is included in Supplementary Material (SM) Table S1. Additional experimental conditions for model validation are listed in Table 1. Details on the materials and methods are described in (Schmieder et al., 2023). For data reproducibility, a description of the temperature and flow rate gradient data, sampling procedure, and data processing conducted in the scope of this study is provided in SM Section 3.1-3.3.

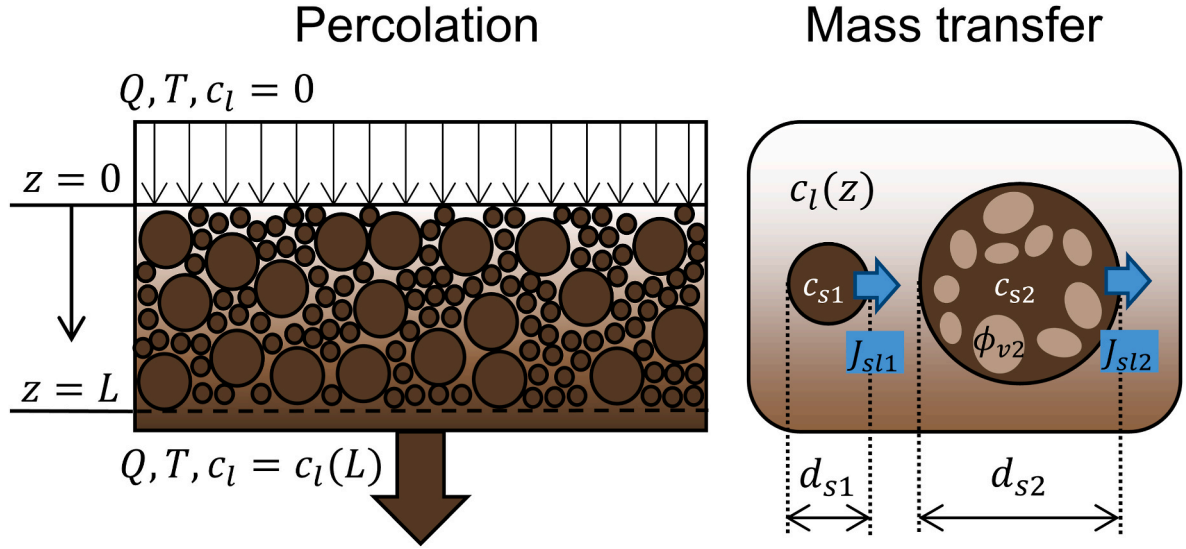## 3. Theory and calculation

3.1. Mathematical modeling

The mechanistic *two-grain model* to model the mass transport of solutes during espresso coffee extraction is based on the model proposed by Moroney et al. (2019). The model is conceptually illustrated in Fig. 1 and consists of convective mass transport by percolation (Fig. 1, left) and diffusive mass transfer from the solid particles to the liquid (Fig. 1, right). The packed bed of coffee particles was modeled as a bi-disperse system, i.e., only particles of two different sizes are assumed to be present. The model is one-dimensional, with the spatial coordinate z assuming uni-directional flow, demonstrated to be an admissible simplification for the case of a cylindrical geometry (Moroney et al., 2019). The volume fractions of liquid and solid phases, fine and coarse solid particles, and intragranular pores were assumed to be constant during extraction following (Moroney et al., 2019). In the absence of data and considering the yet high goodness of fit in (Moroney et al., 2019), the assumption of constant porosity was acceptable. Initial wetting was assumed to be completed at $t = 0$, i.e., the inter- and intragranular pores were assumed to be completely filled with water, which was ensured in experiments by applying an initial preinfusion (wetting) step (Schmieder et al., 2023). TDS was treated as a single component with the same molecular properties as caffeine (same as in (Moroney et al., 2015)). The temperature was assumed to be equal in the solid and liquid phases and equal along the height and diameter of the packed bed since heat transfer can be considered much faster than mass transfer. For this study, three modifications to the original model in (Moroney et al., 2019) were necessary. (I) The distribution constant K_i describes the partitioning between the solid phase, disregarding intragranular porosity, and the water phase at the solid-liquid interface. The distribution constant was introduced to account for changes of this parameter

Table 1

Design of experiments for validating the model predictions; coffee machine settings for the start point (t_0) and the end point of extraction (t_E).

Experiment no.	Flow rate (t_0) (mL s^{-1})	Flow rate (t_E) (mL s^{-1})	Temperature (t_0) (°C)	Temperature (t_E) (°C)
1	2.0	2.0	86.0	86.0
2	2.0	2.0	92.0	92.0
3	2.0	2.0	88.0	93.0
4	2.0	2.0	93.0	88.0
5	1.7	1.7	90.0	90.0
6	2.3	2.3	90.0	90.0
7	1.7	2.3	90.0	90.0
8	2.3	1.7	90.0	90.0

Percolation

Mass transfer

Fig. 1. Illustration of modified *two-grain model* by Moroney et al. (2019). z: spatial coordinate, c_l: average concentration in liquid phase, c_{s1}: average concentration in solid fine particles, c_{s2}: average concentration in solid coarse particles, Q: water flow rate, T: water temperature, J_{sl1}: solute flux from fine particles, J_{sl2}: solute flux from coarse particles, d_{s1}: particle size of fine particles, d_{s2}: particle size of coarse particles.

via temperature variation. In (Moroney et al., 2019), K_i was assumed to be equal to 1, which is only reasonable if temperature effects on phase distribution are not supposed to be studied. (II) The fine particles were considered to not have an intragranular porosity φ_{v1} (volume fraction of pores) because the fine particles are cell fragments without intact intragranular pores. (III) A relation between mass transfer and fluid velocity is introduced using dimensionless groups (details below).

The solute mass balance equations are shown in Eqs. (1)–(3). Eq. (1) represents the mass balance of a solute i in the liquid phase ($c_{l,i}$). Eqs. (2) and (3) describe the mass balances of a solute i in the solid phase ($c_{s,i}$) of fine particles (subscript 1) and coarse particles (subscript 2), respectively:

$$\frac{\partial c_{l,i}}{\partial t} + v_l \frac{\partial c_{l,i}}{\partial z} = \frac{6 h_{sl1,i} \alpha_{s1,k}}{\alpha_l d_{s1}} \left(K_i c_{s1,i} - c_{l,i} \right) + \frac{6 h_{sl2,i} \alpha_{s2,k}}{\alpha_l d_{s2,k}} \left(K_i c_{s2,i} - c_{l,i} \right) \tag{1}$$

$$\frac{\partial c_{s1,i}}{\partial t} = -\frac{6 h_{sl1,i}}{d_{s1}} \left(K_i c_{s1,i} - c_{l,i} \right) \tag{2}$$

$$\frac{\partial c_{s2,i}}{\partial t} = -\frac{6 h_{sl2,i}}{\varphi_{v2} d_{s2,k}} \left(K_i c_{s2,i} - c_{l,i} \right) \tag{3}$$

The meaning of symbols and their respective units are listed in Table B.1 (Appendix B). The relation between flow rate Q and average interstitial velocity v_l is:

$$v_l = \frac{Q}{A_{cs} \, \alpha_l} \tag{4}$$

A reasonable selection of the parameters $\alpha_{s1,k}$, $\alpha_{s2,k}$, and $d_{s2,k}$ which are specific to the grind level (d_{s1} is expected to be not affected by the grind level) is critical to achieving an accurate description of the extraction kinetics. The original bimodal PSD spanning a wide range of particle diameters is reduced to a bi-disperse distribution having only two characteristic particle sizes. Moroney et al. (2019) decided upon a threshold diameter of 100 μm in a somewhat arbitrary manner based on PSD measurements from laser diffractometry. They specified the particle sizes by the peak values of the bimodal distribution and defined the volume fraction of fine particles by the cumulative volume distribution value for a diameter of ≤100 μm. A reduction based on any measured PSD is proposed here to make the distinction less arbitrary. One reference value used for characterizing a PSD is the Sauter mean diameter d_{32}, which is characteristic of the volume-specific surface area of a

granular material. In the present study, the volume fraction of fine particles ψ_k of a grind level k was determined from:

$$\psi_k = \frac{\left(\frac{6}{d_{32,k}} - \frac{6}{d_{s2,k}} \right)}{\left(\frac{6}{d_{s1}} - \frac{6}{d_{s2,k}} \right)} \tag{5}$$

Setting the particle diameters d_{s1} and $d_{s2,k}$ to the peak values of the measured PSD, ψ_k was calculated according to Eq. (5). The volume fractions of the respective particle classes, $\alpha_{s1,k}$ and $\alpha_{s2,k}$, can then be calculated using the fines volume fraction ψ_k:

$$\alpha_{s1,k} = (1 - \alpha_l) \, \psi_k \; ; \; \alpha_{s2,k} = (1 - \alpha_l)(1 - \psi_k) \tag{6}$$

As a simplifying assumption, the bulk porosity α_l was in this study assumed not to be affected by the grind level due to minor porosity differences between grinds of ≤0.02 obtained from solid density measurements (see SM Section 3.4). The *two-grain model* presented in (Moroney et al., 2019) did not include the influence of operating parameters such as the water temperature and flow rate/pressure on mass transfer. Therefore, the model was extended by constitutive equations describing the influence of temperature T and flow rate Q on the model parameters regarding mass transfer ($h_{sl1,i}$; $h_{sl2,i}$), and equilibrium (K_i).

One classical means of relating mass transfer properties to flow properties is via dimensionless groups. This approach has been applied for solid-liquid mass transfer in fixed beds at low Reynolds numbers (Wilson and Geankoplis, 1966). The commonly employed empirical relation for particle class x and solute i with coefficients $A_{x,i}$ and $B_{x,i}$ is:

$$Sh_{x,i}(v_l, T) = A_{x,i} \, Re^{B_{x,i}} \, Sc_i^{\frac{1}{3}} \tag{7}$$

The Sherwood number $Sh_{x,i}$, the Reynolds number Re, and the Schmidt number Sc_i in Eq. (7) are defined as follows:

$$Sh_{x,i} = \frac{h_{slx,i} \, d_{32}}{D_i(T)} \tag{8}$$

$$Re = \frac{d_{32} \, v_l \, \rho(T)}{\alpha_l \, \eta(T)} \tag{9}$$

$$Sc_i = \frac{\eta(T)}{\rho(T) \, D_i(T)} \tag{10}$$

The Sauter mean diameter ($d_{32} = 84 \, \mu m$) of the measured PSD was

used as an alternative length for the characteristic cross-section width of a flow channel. It is observable from Eqs. (8)–(10) that the molecular diffusion coefficient D_i of solute i, the liquid density ρ, and the dynamic viscosity η required to calculate the dimensionless variables depend on temperature. The diffusion coefficient as a function of molar volume, molar weight, and temperature was approximated for each molecule using the following correlation by Wilke and Chang (1955):

$$D_i(T) = 7.4 \bullet 10^{-15} \frac{(2.6\,M_i)^{\frac{1}{2}}\,T}{\eta(T)\,V_i^{0.6}} \tag{11}$$

with M_i being the molar mass and V_i being the molar volume defined by the Le Bas group contribution method. The same diffusion coefficient as caffeine was assumed in the case of TDS.

Since the density and viscosity of the liquid phase are expected to comply with the physical properties of pure water, they were approximated by the temperature correlations for water (Stephan et al., 2019). According to the literature, the parameters $A_{x,i}$ and $B_{x,i}$ in Eq. (7) are usually positive, meaning that the mass transfer rate increases with the flow rate (provided external mass transfer is rate limiting). The value of $B_{x,i}$ also reflects the balance between internal and external transport limitation. This balance depends on the particle class x due to different diffusion hindrances of fine and coarse particles and on the component i due to molecule-specific diffusion behavior. If the mass transfer rate of a molecule is, e.g., completely limited by intragranular diffusion, changing the flow rate would not lead to a change in the mass transfer rate and the value of $B_{x,i}$ of that molecule would be zero, i.e., Sh would be independent of Re. The mass transfer coefficients $h_{sl1,i}$ and $h_{sl2,i}$ were treated as lumped parameters describing the effective mass transfer from the particle surface, including limitations by intragranular diffusion (in the case of coarse particles), desorption, and molecular diffusion in the laminar boundary layer (external mass transfer). Each of the two particle size classes and each component was assigned a separate Sherwood number and correlation (Eq. (8)) as the rate-controlling phenomena and the diffusion resistances were assumed to be different in the fine particles consisting of broken cells and the coarse particles consisting of intact cells with broken cells at the surface.

Regarding the distribution constant K_i, a van't-Hoff-type equation was proposed:

$$K_i(T) = K_{ref,i} \exp\left(\gamma_i \left(\frac{1}{T_{ref}} - \frac{1}{T} \right) \right) \tag{12}$$

The value of K_i at a certain temperature T was related to a reference value $K_{ref,i}$ at a reference temperature T_{ref} within the experimental range. The exponential change of K_i with temperature was defined by the correlation parameter γ_i.

The initial conditions applied in this study were:

$$c_{l,i}(t=0,z) = K_i\,c_{s0,i}\ ;\ c_{s1,i}(t=0,z) = c_{s2,i}(t=0,z) = c_{s0,i} \tag{13}$$

The boundary condition at the top of the coffee puck was:

$$c_{l,i}(t,z=0) = 0 \tag{14}$$

Equilibrium between solid phase and liquid phase was assumed at the beginning of extraction due to the preinfusion step applied in the experiments (Schmieder et al., 2023). The concentration in the liquid of a fraction f to be compared to an experiment/extraction j was determined by the integral of $c_{l,i}(z=L)$ from the start time t_{0f} to the end time t_{Ef} of a fraction:

$$C_{fij} = \frac{1}{V_{fj}} \int_{t_{0f}}^{t_{Ef}} c_{l,ij}(z=L,t)\,Q_j(t)\,dt \tag{15}$$

The cup concentration $C_{cup,ij}$, i.e., in an accumulated volume V_{cup} was obtained in the same manner using respective integration limits ($t_0 = 0$ and $t_E \leftrightarrow V(Q_j(t)) = V_{cup}$) and dividing by V_{cup}.

3.2. Numerical solution and parameter estimation

The model and objective function used for parameter estimation were rescaled as shown in Eq. (C.1)-(C.5) in Appendix C. All simulations and least-squares parameter estimations were performed using the rescaled variables. The unknown model parameters to be estimated included the component-specific parameters $A_{1,i}$, $B_{1,i}$, $A_{2,i}$, $B_{2,i}$, $K_{ref,i}$, γ_i, and $c_{s0,i}$, yielding 7 parameters per component (minimization problem in Eq. (D.1) in Appendix D) as well as the non-component specific parameters ψ_k and $d_{s2,k}$ (minimization problem in Eq. (D.2) in Appendix D), which were characteristic of each of the 3 grind levels (k indexing the number of the grind levels investigated). Given the large number of parameters to be estimated, we opted for a sequential parameter estimation strategy. For the sake of brevity, the reader is referred to Appendix D for details on the numerical solution and parameter estimation.

To compare model results with experimental data, the mean absolute percentage error (MAPE) was evaluated using the average concentrations in the fractions from triplicate simulations $\overline{\widehat{C}_{fij}}(Q_j, T_j, k)$ and experiments $\overline{C_{fij}}$:

$$MAPE = \frac{1}{6} \sum_{f=1}^{6} abs\left(\frac{\left(\overline{\widehat{C}_{fij}}(Q_j, T_j, k) - \overline{C_{fij}} \right)}{\overline{C_{fij}}} \right) \times 100 \tag{16}$$

3.3. Statistical analyses

The statistical analyses applied in this study to evaluate if differences in the cup concentrations at different temperatures, flow rates, and grind levels were statistically significant comprised of Analyses of Variance (ANOVA) and Tukey's Honestly Significant Difference (HSD) tests. Details on the analyses are presented in Appendix E.

4. Results and discussion

The model simulations and experimental data were compared with respect to (I), the extraction kinetics of TDS, caffeine, trigonelline, and chlorogenic acid, and (II), the cup concentration, i.e., in an accumulated volume of 60 mL. Extraction kinetics are hereafter represented by the concentrations in the fractions experimentally obtained for fractions 1, 2, 3, 5, 7, and 10 (see SM Section 3.2). The model simulations are presented as stepwise continuous line plots. Each step of the line plot represents the mean simulated concentration C_{fij} (step value) related to the volume of the respective fraction V_{fj} (step width) (Eq. (15)). The experimental data (each in triplicate) are plotted as dots (single experiments) located in the center of the respective fraction interval.

4.1. Parameter estimation

The extraction kinetics obtained by the *two-grain model* matched the experimental data well in all experimental conditions (SM Table S2). The average MAPEs of all experiments (Eq. (16)) were 6.07 % for TDS, 4.59 % for caffeine, 7.85 % for trigonelline, and 4.98 % for chlorogenic acid. For comparison, the average MAPE values were calculated for the exponential fits in (Schmieder et al., 2023) as 16.12 % for TDS, 11.03 % for caffeine, 16.51 % for trigonelline, and 13.01 % for chlorogenic acid, which are more than twice as high as the MAPE values of the model predictions. The higher accuracy of the mechanistic model highlights the importance of modeling for determining and understanding changes and interdependences in espresso extraction. Plots of the extraction kinetics predicted by the model versus experimental data by Schmieder et al. (2023) are provided in SM Figs. S1–S12. The concentration changes in the cup $C_{cup,ij}$ were neither statistically significant concerning temperature changes nor in flow rate or grind level (see SM Table S5) according to an ANOVA. This lack of significance is reasonable considering the minor concentration differences at different experimental conditions and comparing them to the estimated standard deviation,

both listed in SM Table S4 and calculated by Eqs. (E.1) and (E.2) (Appendix E). Low values of adjusted R^2 reported in (Schmieder et al., 2023) confirm this weak correlation. However, qualitative concentration changes with flow rate changes were consistent for all grinds and temperatures in our previous study, and most correlation parameters were significant in that study (Schmieder et al., 2023). Given moreover the limited number of compounds, replicates, and experimental conditions, effects may be more significant for compounds of different polarity that were not investigated in this study or for different grinds or coffees. Despite the lack of significant differences in experimental data, we thus focused on the model's ability to capture qualitative changes in the cup concentration and to correctly predict the extraction kinetics of different molecules at varying flow rates. The effects of temperature, flow rate, and grind level indicated by the model were the same as the ones obtained from multilinear regression in (Schmieder et al., 2023) at brew ratio 1/3: An increase in temperature led to a slight increase in cup concentration $C_{cup,ij}$ for caffeine and TDS. An increase in flow rate led to a decrease in $C_{cup,ij}$ for all components and TDS apart from caffeine, whose concentration slightly increased with flow rate. Regarding the grind level, $C_{cup,ij}$ was lowest at grind level 1.4. As explained in (Schmieder et al., 2023), the obtained PSDs plotted in (Schmieder et al., 2023) did not differ significantly despite large pressure differences. The slight decrease in concentrations at grind level 1.4 could be attributed to flow inhomogeneity (Cameron et al., 2020) which resulted in higher pressures (Schmieder et al., 2023). Due to this lack of influence, the grind level was not considered for the subsequent model validation and the brewing control chart.

All estimated parameters are listed in Table 2. In general, the parameters $A_{1,i}$ and $A_{2,i}$ were two to three orders of magnitude lower than the external mass transfer values reported when using packed beds of inert spheres in the laminar range without intragranular diffusion limitation (Wilson and Geankoplis, 1966). The corresponding mass transfer coefficients $h_{sl1,i}$ and $h_{sl2,i}$ were in the order of magnitude of 10^{-6} (for example: $h_{sl2,caffeine} \approx 1.7 \times 10^{-6}$). Using the molecular diffusion coefficient of caffeine at 90 °C ($D_{caffeine} \approx 8 \times 10^{-9}$, based on (Wilke and Chang, 1955)), a hindrance factor of approximately 10 according to previous literature on caffeine (Spiro et al., 1989), and a characteristic diffusion length of 55 µm (length scale defined from volume-to-surface-area ratio as in (Moroney et al., 2015) for the coarse particles: $\Delta_{s2} = \frac{V_{particle}}{A_{particle}} = \frac{d_{s2}}{6} = \frac{330\ \mu m}{6}$) yields a theoretical estimate of the mass transfer coefficient:

$$h_{sl2,caffeine,theo} = \frac{D_{caffeine}}{10\ \Delta_{s2}} = \frac{8 \times 10^{-9}}{10 \times 5.5 \times 10^{-5}} \approx 1.5 \times 10^{-5} \qquad (17)$$

Comparing the mass transfer coefficient obtained in this study with the theoretically estimated value above, it is about one order of magnitude lower. The comparatively low mass transfer coefficients indicate that intragranular diffusion is rate limiting in espresso extraction. However, the deviations from theoretical calculations based on the

molecular diffusion coefficient may also be attributed to a compensation of overestimating the particles' surface area. Such a discrepancy between the real and estimated specific surface area may be caused by flow inhomogeneity or by disregarded PSD properties that were not captured by the *two-grain model* assumption. Accordingly, the reader is advised that the lack of knowledge regarding the porous medium and flow properties during extraction limits the physical meaning of the mass transfer coefficient values. Experimental investigations of the molecules' hindrance factor at slurry conditions (Spiro et al., 1989) and analyses of the porous medium and flow homogeneity, e.g., by micro-computed tomography (µ-CT) (Mo et al., 2023), may be suitable strategies to get closer to physically meaningful parameters. The values of $B_{1,i}$ and $B_{2,i}$ ranging from 0.06 to 1.13 for the single components were in the same order of magnitude as reported in (Wilson and Geankoplis, 1966). With regard to the distribution constant $K_{ref,i}$ (see Eq. (12)) at reference temperature $T_{ref} = 360.15\ K$, a value close to 1 was confirmed, as assumed by Moroney et al. (2019). However, the values expectedly showed some component-specific variations. The highest value was obtained for trigonelline ($K_{ref,2} = 1.36$), whereas distinctly lower values were estimated for chlorogenic acid ($K_{ref,3} = 0.94$) and caffeine ($K_{ref,1} = 0.81$). One possible explanation might be the polarity of these molecules. Based on the n-octanol-water partition coefficients, trigonelline exhibits a distinctly higher polarity, with a log K_{OW} of -2.53 (National Center for Biotechnology Information, 2023a), than caffeine and chlorogenic acid (log K_{OW} of -0.07 (National Center for Biotechnology Information, 2023b) and -0.356 (National Center for Biotechnology Information, 2023c), respectively). The difference in distribution constants reflects the extraction kinetics of the different compounds, with trigonelline extracted fastest and caffeine extracted slowest, as shown in (Schmieder et al., 2023). Accordingly, the distribution constant could capture the polarity-dependent differences in extraction kinetics of the analyzed molecules, emphasizing the model's applicability to various components. However, the values and temperature dependence of K_i estimated from experiments should not be interpreted as general physical constants because determining those from espresso extraction experiments (no equilibrium conditions) makes them sensitive to experimental error and model assumptions. Alternatively, K_i may be determined from slurry experiments at different temperatures, as done in (Corrochano, 2015).

The estimated parameters ψ_k and $d_{s2,k}$ differed slightly at varying grind levels: a smaller fine particle fraction $\psi_2 = 0.19$ at grind level 1.4 and a smaller coarse-particle diameter $d_{s2,3} = 301\ \mu m$ at grind level 2.0 were estimated, as compared to grind level 1.7. The reduction of ψ at grind level 1.4 could be explained by the occurrence of flow inhomogeneity with a shift to smaller grind levels causing higher pressure losses and a reduced contact surface area.

4.2. Model predictions and validation

The ability of the model to predict solute concentrations in the

Table 2
Model parameters for caffeine, trigonelline, chlorogenic acid, and total dissolved solids obtained by parameter estimation.

Component	A_1 (1)	B_1 (1)	A_2 (1)	B_2 (1)	K_{ref} (1)	γ (K)	c_{s0} (mg mL^{-1})	Grind 1.4[b]		Grind 1.7[a]		Grind 2.0[b]	
								ψ (1)	d_{s2} (µm)	ψ (1)	d_{s2} (µm)	ψ (1)	d_{s2} (µm)
Caffeine	7.92×10^{-3}	0.36	3.11×10^{-2}	1.13	0.81	-371	10.80	0.19	332	0.23	330	0.22	301
Trigonelline	3.33×10^{-3}	0.06	2.06×10^{-2}	0.77	1.36	-431	4.19						
Chlorogenic acid	4.17×10^{-3}	0.06	2.07×10^{-2}	0.82	0.94	-379	6.23						
Total dissolved solids	3.04×10^{-3}	1.08×10^{-7}	2.16×10^{-2}	0.86	1.18	68.3	182						

[a] obtained by parameter estimation to extraction kinetics data of components.
[b] estimated from particle size distribution and Eq. (5).

espresso coffee beverage at different temperatures and flow rates was investigated by performing the experiments shown in Table 1, all of which were within the experimental range used for parameter estimation (SM Table S1). Note that these experimental conditions were selected to avoid extrapolation of the model, mimic the conditions of earlier studies for comparison (Andueza et al., 2003; Salamanca et al., 2017), and investigate the effects of gradient control compared to constant control in a practically feasible manner. Two constant temperatures and two temperature gradients (see Table 1) were selected for comparison with the temperatures used in (Andueza et al., 2003) and the gradients used in (Salamanca et al., 2017). The measured curves $T(t)$ and $Q(t)$ were used for simulations (data provided in SM Figs. S29–S36 and machine programs in SM Figs. S25–S28). Still, the experiments were labeled in Fig. 2-Fig. 5 according to the machine settings (start value-end value) for simplicity. The respective extraction kinetics data and the experimentally obtained cup concentrations were compared with model predictions (experimental data was not used to estimate the model parameters in this case). The cup concentration was experimentally obtained as described in SM Section 3.1.

The predicted and experimental extraction kinetics of caffeine at different temperature settings are shown in Fig. 2 (equal flow rate and grind level). Only caffeine is shown for brevity, but plots of the other components and TDS are available in SM Figs. S13–S18.

The predicted caffeine concentrations at different accumulated volumes of coffee matched the experimental data, with an average MAPE of 4.71 %. (average of temperature experiments). Predictions of trigonelline and TDS exhibited slightly higher MAPEs, but the highest MAPEs were observed for chlorogenic acid (average of 16.86 %), indicating a lack of accuracy (see SM Table S3). We hypothesize that a difference in roasting caused this discrepancy between predictions and experiments because another batch of roasted coffee (same green coffee batch and roasting conditions but different roasting batch) was used for the validation experiments. This roasting batch fluctuation caused a substantial deviation in the chlorogenic acid content which is chemically converted during the roasting process, whereas caffeine is more stable during roasting (Awwad et al., 2021). Regarding Fig. 2, no significant differences in extraction kinetics were observed between the applied temperatures, as expected from the results in Section 4.1. The same was true of the cup concentration plotted in Fig. 3 for model predictions and experiments.

The error bars in Fig. 3 represent the standard deviations from
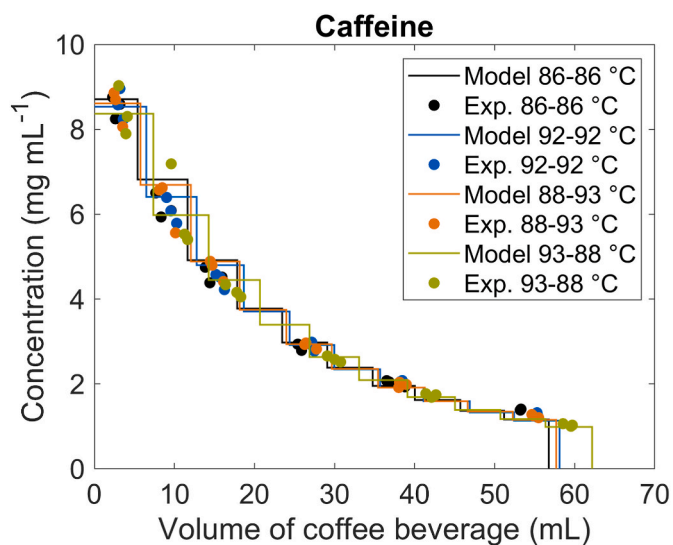

Fig. 2. Caffeine concentrations in the fractions against the accumulated volume of espresso coffee: model predictions and experiments (triplicates) at different temperature settings (input values, start-end); other settings constant: grind level 1.7, flow 2 mL s⁻¹.
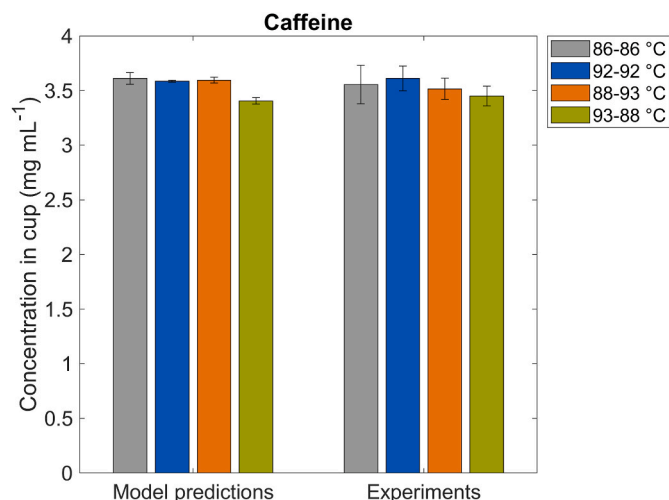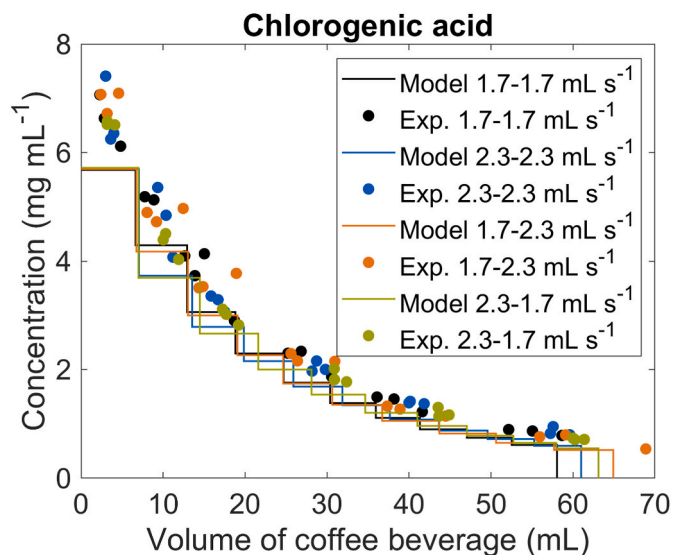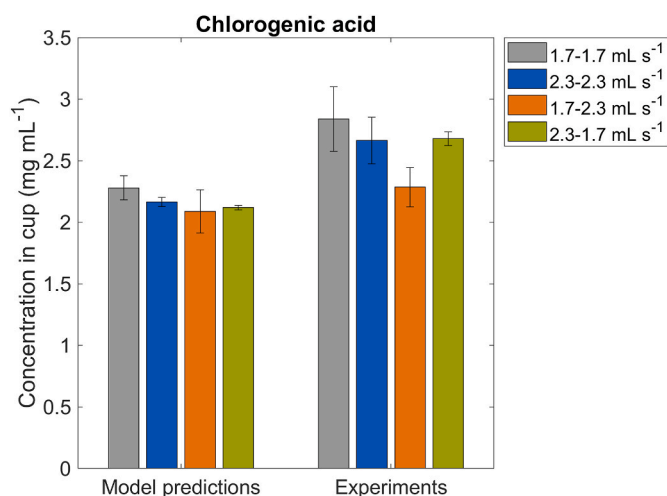

Fig. 3. Caffeine concentration in cup (volume ~60 mL) as predicted by the model vs. experimental data at different temperature settings (input values, start-end); other settings constant: grind level 1.7, flow 2 mL s⁻¹.

triplicate experiments and simulations. The model predictions are the mean values of three predictions at experimentally scattered temperatures, flow rates, and extraction times. Based on an ANOVA comparing the cup concentrations, no significant difference was identified in any investigated solute or TDS (see SM Table S6) concerning different constant temperatures and temperature gradients. However, the gradient of 93-88 °C yielded the lowest concentration of caffeine in both cases, which can be attributed to the higher cup volume of 62 mL compared to the other experiments that yielded 57–58 mL. This lack of significant differences contradicts a former study by Andueza et al. (2003). The authors found a significant increase in caffeine concentration by 0.26 mg mL⁻¹ for Arabica coffee when raising the basket temperatures from 86 °C to 92 °C, whereas it was only 0.06 mg mL⁻¹ in this study. Furthermore, Andueza et al. (2003) reported a significant increase in total dissolved solids and trigonelline and a decrease in chlorogenic acid, which is not supported by our results (see SM Figs. S16 and S18). Comparing the temperature gradients in Fig. 3, the difference in experimental mean values between 88-93 °C and 93-88 °C was 0.07 mg mL⁻¹ (not statistically significant). In contrast, Salamanca et al. (2017) reported a difference of 0.87 mg mL⁻¹, which is more than a factor of ten higher. One explanation for these contradictory results might relate to the type of flow control. Flow rate control was performed in the present research to achieve conditions consistent with the model, whereas constant pressure control was applied in (Andueza et al., 2003) and (Salamanca et al., 2017). An increase in temperature may affect the puck permeability, thus potentially leading to a change in the flow rate or homogeneity (not recorded in the literature work) and to a deviation in the final beverage volume at the set extraction time. Our results indicate that dynamic temperature control does not significantly affect the coffee composition when the flow rate and brew ratio are constant. Since only a small fraction of taste-active components has thus far been analyzed and modeled in coffee extraction research, the effect of temperature gradients on taste and aroma cannot be precluded in general. Nevertheless, a significant effect of temperature gradients on the extraction kinetics of non-volatile solutes like caffeine, trigonelline, and chlorogenic acid is questionable based on the presented results.

The prediction accuracy and impact of flow gradient control are illustrated in Figs. 4 and 5, using the example of chlorogenic acid. Plots for all other analyzed components are available in SM Figs. S19–S24. The experimental concentrations during the first half of extraction time were higher than predicted by the model (Fig. 4), resulting in an underprediction of the concentration in the final beverage (Fig. 5) with an average MAPE of 18.23 % (average of flow rate experiments). In

Fig. 4. Chlorogenic acid concentrations in the fractions against the accumulated volume of espresso coffee: model predictions and experiments (triplicates) at different flow rate settings (input values, start-end); other settings constant: grind level 1.7, temperature 90 °C.

Fig. 5. Chlorogenic acid concentration in cup (volume ~60 mL) as predicted by the model vs. experimental data at different flow rate settings (input values, start-end); other settings constant: grind level 1.7, temperature 90 °C.

comparison, trigonelline and TDS concentrations were slightly over-predicted, but caffeine matched the predictions well, according to SM Table S3. As stated above for the different temperatures, this deviation for chlorogenic acid might be explained by a variation in roasting batches. Comparing the cup concentrations of chlorogenic acid at different flow rates, a higher flow rate resulted in a lower concentration, as expected by the model. However, the only significant difference on a 5 % significance level based on an ANOVA and Tukey's HSD (honestly significant difference) test was between 1.7-1.7 mL s^{-1} (constant flow) and 1.7–2.3 mL s^{-1} (p-value for chlorogenic acid: 0.025), the concentration of the latter condition falling below the other results (see SM Table S6). Presumably, this observation is linked to an experimental error because a significant drop in concentrations was not apparent in the extraction kinetics at the gradient of 1.7–2.3 mL s^{-1} shown in Fig. 4. According to simulations, using an upward flow rate gradient or a downward gradient (at equal total extraction time) within the range tested has neither impact on the chlorogenic acid concentration in the

beverage nor the concentration of caffeine, trigonelline, or TDS. However, it was verified that the model could reasonably predict the extraction kinetics and cup concentration for both constant and time-varying process conditions.

4.3. Kinetic espresso brewing control chart

By modeling the extraction kinetics of different compounds, it is possible to predict and investigate the extract composition at any brew ratio. Comparing concentrations at more than one brew ratio is essential because the effects of extraction conditions on the component concentrations vary along with the brew ratio, as pointed out in (Schmieder et al., 2023). Fig. 6 presents a new espresso brewing control chart at brew ratio 2/3 (20 g dry coffee vs. 30 mL beverage volume). The chart is also available at other brew ratios, either in the form of a video, with each frame representing a 2 mL rise in volume, or as a graphical user interface named "Espresso Brewing Control App"; both are included for download in the data repository linked to this article (https://doi.org/10.17632/y2tz67f6ry.1). The reader is advised to examine the provided app or video because the kinetic aspect of the new brewing control chart is better observable watching the concentration evolution over time instead of studying static snapshots.

Note that the app is unsuitable for conducting simulations but visualizes interpolated data from a previously simulated data array at predefined beverage volumes (2 mL intervals) and settings. However, the data file and all MATLAB code necessary to reproduce our work are also available in the data repository. The espresso brewing control app lets users track the concentration profile along the coffee cup filling time. Each chart maps the yield Y_i of each single component i (mg solute per g of coffee powder) within the flow-temperature plane as the primary manipulable process conditions:

$$Y_i = \frac{C_{cup,i}(Q, T) \, V_{cup}}{M_0} \tag{18}$$

The variable $C_{cup,i}$ is predicted by the model via Eq. (15), integrating from $t = 0$ to $t = V_{cup}/Q$ (Q constant) and represents the concentration of a component i in the accumulated beverage volume V_{cup} with M_0 being the mass of ground coffee (default 20 g). The colors in the chart represent – like a heat map – the yield ranging from 0 (dark blue) to the maximum achieved yield per component (dark red), with the lines marking contours of equal value. The advantage of this illustration is the ability to compare the sensitivity of yield towards temperature and flow rate by comparing the contour lines and the extraction kinetics of different components by comparing the colors.

Looking at Fig. 6, an increase in caffeine and TDS yield occurred with increasing temperature, but hardly any influence was observed for trigonelline and chlorogenic acid. All solute yields increased with a decrease in flow rate to a similar extent. Although the changes of caffeine, trigonelline, chlorogenic acid, and TDS with flow rate and temperature were small, the espresso brewing control chart represents a basis that can be extended to other components of different polarity regarding which more significant influences may occur.

In addition to comparing sensitivities of component yield concerning temperature and flow rate, the espresso brewing control chart also enables a comparison of the extraction kinetics of different components. A more reddish color of the trigonelline plot in Fig. 6 indicates that trigonelline was extracted more quickly than caffeine and chlorogenic acid. This can be related to the higher polarity of trigonelline compared to caffeine and chlorogenic acid, as described in recent previous studies (Schmieder et al., 2023; Vaca Guerra et al., 2023b). Predicting the extraction kinetics of different taste- and aroma-relevant molecules using our model based on molecular polarity (using the distribution constant $K_i(T)$) opens further opportunities for understanding how the balance of taste and aroma compounds develops during espresso coffee extraction.

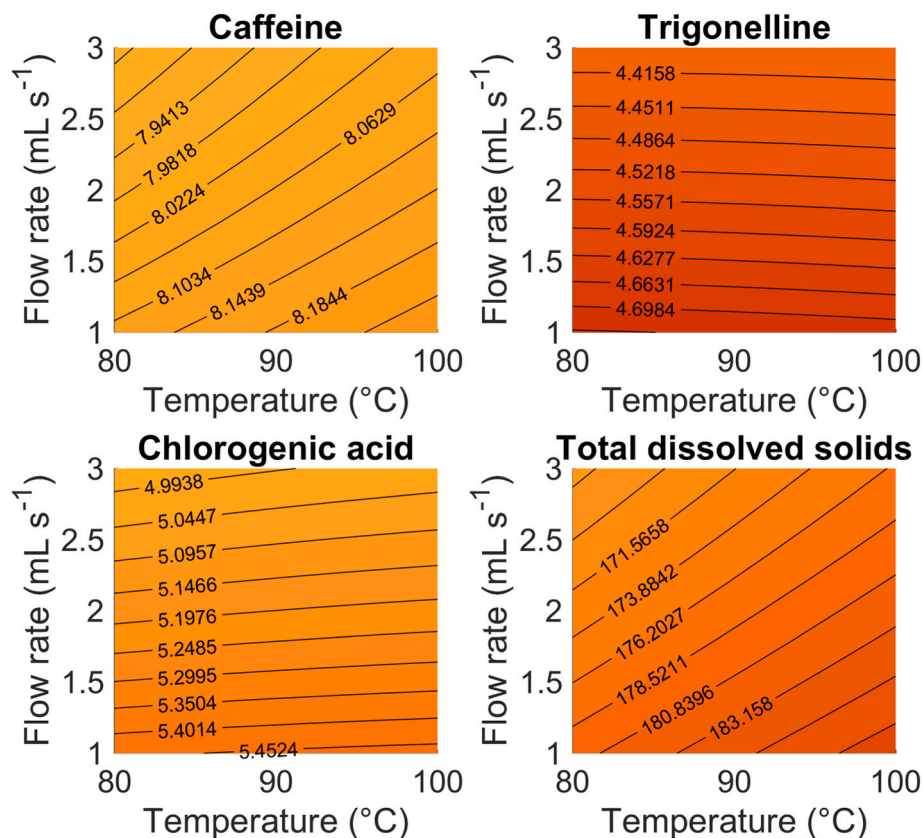The reader is advised that the results shown in the chart are limited

Fig. 6. Espresso brewing control chart at brew ratio 2/3: contour plots of yield (mg solute per g of coffee powder), color scale from ■ (zero yield) to ■ (maximum yield per component).

to the coffee and water used in this study. Any transferability to other coffee varieties, roast degrees, and water qualities is beyond the scope of this article. The same applies to human sensory analyses, which were not part of this investigation. Instead, the chart provides a quick impression of how coffee composition develops dynamically, which may aid the elucidation of otherwise misinterpreted experimental data.

5. Conclusion

Our study proposes a mechanistic espresso extraction model, based on the *two-grain model* by Moroney et al. (2019) and originating from the work by Melrose and Corrochano et al. (Corrochano, 2015; Melrose et al., 2018), which captures the influence of temperature and flow rate on the extraction kinetics of representative compounds. The model parameters were estimated using experimental extraction kinetics data from our previous study (Schmieder et al., 2023), including caffeine (bitter), trigonelline, chlorogenic acid (sour), and total dissolved solids at different temperatures (80–98 °C), flow rates (1–3 mL s^{-1}), and grind levels (1.4–2.0). The model could predict independent data during espresso brewing obtained at both constant and time-varying water flow rates and temperatures, although differences in the cup concentration were not statistically significant. A significant dependence on the choice of temperature gradients, as reported by Salamanca et al. (2017), was neither confirmed by our experiments nor by the model predictions. An interdependence between flow rate and temperature at constant pressure control due to changes in the puck permeability may explain the difference between our results and previous findings, the result of which may have been a temperature-dependent deviation in beverage volume and/or flow homogeneity. We present a kinetic espresso brewing control chart implemented as a software tool that enables users to examine and compare the influence of flow rate and temperature on the yield or concentration of different components. It is the first coffee brewing

control chart applicable to espresso coffee involving manipulable control variables and various taste-relevant components. Our findings indicate that molecular polarity can be used via the distribution constant to predict the development of taste during espresso extraction using our model. Given that the brew ratio was found to significantly impact the final yield and composition, the chart can also be applied to select optimal brew ratios based on the balance of taste-relevant components and TDS. The results are limited to the studied coffee, experimental conditions, and analyzed components. Although the estimated values of mass transfer coefficients and distribution constants captured the effects and dynamics of espresso extraction, the values of parameters may be validated by additional experiments identifying distribution constants and effective diffusion coefficients separately, e.g., in stirred suspension, to enhance their physical meaning and support the understanding of rate-controlling phenomena. Further investigations of the packed bed and intragranular diffusion are recommended for future studies to capture complex phenomena such as flow inhomogeneity and particle erosion, which were not considered in this study. Nevertheless, the approach may serve as a solid basis for future studies and can be extended as desired to other components, coffees, or control variables.

CRediT authorship contribution statement

Verena B. Pannusch: Conceptualization, Data curation, Formal analysis, Investigation, Methodology, Software, Visualization, Writing -

original draft. **Benedikt K.L. Schmieder:** Investigation, Methodology. **Lara Vannieuwenhuyse:** Investigation. **Mirjana Minceva:** Formal analysis, Funding acquisition, Resources, Supervision, Writing - review & editing. **Heiko Briesen:** Conceptualization, Formal analysis, Funding acquisition, Project administration, Supervision, Writing - review & editing.

Declaration of generative AI and AI-assisted technologies in the writing process

During the preparation of this work the authors used "Grammarly" in order to improve language and readability. After using this tool, the authors reviewed and edited the content as needed and take full responsibility for the content of the publication.

Declaration of competing interest

The authors declare the following financial interests/personal relationships which may be considered as potential competing interests:

Data availability

Data is available publicly in a data repository (https://doi.org/10.17632/y2tz67f6ry.1).

Acknowledgments

Appendix A. Supplementary data

Supplementary data to this article can be found online at https://doi.org/10.1016/j.jfoodeng.2023.111887.

Appendix B. List of Model Symbols

Table B.1
List of symbols used in the modified *two-grain model*.

Symbol	Variable	Unit
$c_{l,i}$	Concentration of solute i in liquid phase l	mg mL^{-1}
$c_{sx,i}$	Concentration of solute i in solid phase s of particle class x	mg mL^{-1}
t	Time	s
z	Spatial coordinate (top to bottom)	m
v_l	Average interstitial velocity of liquid l in z direction	m s^{-1}
$h_{slx,i}$	Solid-liquid mass transfer coefficient of solute i from particle class x	m s^{-1}
$Sh_{x,i}$	Sherwood number of particle class x and solute i	1
Re	Reynolds number for packed bed	1
Sc_i	Schmidt number of solute i	1
$A_{x,i}$	Constant correlating $Sh_{x,i}$ with Re and Sc_i	1
$B_{x,i}$	Constant correlating $Sh_{x,i}$ with Re	1
K_i	Solid-liquid distribution constant of solute i	1
$c_{s0,i}$	Initial concentration of solute i in solid phase s	mg mL^{-1}
$K_{ref,i}$	Reference distribution constant of solute i at T_{ref}	1
γ_i	Constant correlating K_i with T	K
α_l	Volume fraction of liquid phase l (bulk porosity)	1
$\alpha_{sx,k}$	Volume fraction of solid particle class x at grind level k	1
$d_{sx,k}$	Diameter of solid particle class x at grind level k	m
φ_{v2}	Volume fraction of intragranular pores/voids of solid particle class 2 (coarse particles)	1
ψ_k	Volume fraction of particle class 1 (fines) at grind level k	1
$d_{32,k}$	Sauter mean diameter at grind level k	m
T	Temperature of liquid and solid phase	K
Q	Flow rate of liquid phase	mL s^{-1}
A_{cs}	Cross section of filter basket	m^2
D_i	Diffusion coefficient of solute i	m^2 s^{-1}
ρ	Density of liquid	kg m^{-3}
η	Dynamic viscosity of liquid	kg m^{-1} s^{-1}
M_i	Molar mass of solute i	g mol^{-1}
V_i	Molar volume of solute i	cm^3 mol^{-1}

Appendix C. Rescaling of the *Two-Grain Model*

The concentrations and variables were rescaled in this study to improve the conditioning of the system of equations and avoid the impact of different component concentration scales on parameter optimization. The normalized variables used were:

$$\widetilde{c}_{l,i} = \frac{c_{l,i}}{C_{1i}} \; ; \; \widetilde{c}_{s1,i} = \frac{c_{s1,i}}{c_{s0,i}} \; ; \; \widetilde{c}_{s2,i} = \frac{c_{s2,i}}{c_{s0,i}} \quad ; \; \widetilde{t} = \frac{t}{t_c} \; ; \; \widetilde{v}_l = \frac{v_l \, t_c}{L} \; ; \; \widetilde{z} = \frac{z}{L} \tag{C.1}$$

The state C_{1i} represents the experimentally obtained concentration of solute i in fraction 1 at the respective grind, temperature, and flow rate. $c_{s0,i}$ is the initial concentration in the solid phase, t_c is a characteristic extraction time of 30 s, and L is the packed-bed height, being 15 mm.

Replacing the respective variables in Eqs. (1)–(3) yields the following equations:

$$\frac{\partial \widetilde{c}_{l,i}}{\partial \widetilde{t}} + \widetilde{v}_l \frac{\partial \widetilde{c}_{l,i}}{\partial \widetilde{z}} = \frac{6h_{sl1,i}\alpha_{s1,k}}{\alpha_l d_{s1}} t_c \left(K_i \widetilde{c}_{s1,i} \frac{c_{s0,i}}{C_{1i}} - \widetilde{c}_{l,i} \right) + \frac{6h_{sl2,i}\alpha_{s2,k}}{\alpha_l d_{s2,k}} t_c \left(K_i \widetilde{c}_{s2,i} \frac{c_{s0,i}}{C_{1i}} - \widetilde{c}_{l,i} \right) \tag{C.2}$$

$$\frac{\partial \widetilde{c}_{s1,i}}{\partial \widetilde{t}} = -\frac{6\,h_{sl1,i}}{d_{s1}} t_c \left(K_i \widetilde{c}_{s1,i} - \widetilde{c}_{l,i} \frac{C_{1i}}{c_{s0,i}} \right) \tag{C.3}$$

$$\frac{\partial \widetilde{c}_{s2,i}}{\partial \widetilde{t}} = -\frac{6\,h_{sl2,i}}{\varphi_{v2} d_{s2,k}} t_c \left(K_i \widetilde{c}_{s2,i} - \widetilde{c}_{l,i} \frac{C_{1i}}{c_{s0,i}} \right) \tag{C.4}$$

With the initial and boundary conditions:

$$\widetilde{c}_{l,i}(t=0,z) = \frac{K_i\,c_{s0,i}}{C_{1i}} \; ; \; \widetilde{c}_{s1,i}(t=0,z) = \widetilde{c}_{s2,i}(t=0,z) = 1 \; ; \; \widetilde{c}_{l,i}(t,z=0) = 0 \tag{C.5}$$

Appendix D. Numerical Solution and Parameter Estimation

The system of partial differential equations (Eqs. (1)–(12)) with initial conditions (Eq. (13)) and boundary condition (Eq. (14)) was solved in MATLAB R2020b (MathWorks, Massachusetts, USA) using a five-point-biased-upwind finite difference scheme (Bickley, 1941) for the spatial variable z with 200 nodes. The resulting system of ordinary differential equations was solved using the MATLAB "ode15s" solver. The MATLAB "lsqnonlin" function with the "trust-region-reflective" algorithm was used for nonlinear least-squares parameter estimation. All MATLAB code is available in the data repository (https://doi.org/10.17632/y2tz67f6ry.1) linked to this article.

All constant parameters not obtained from parameter estimation but from values or measurements found in the literature are listed in Table D.1. The parameters d_{PF}, L, and M_0 were set according to the experimental setup in (Schmieder et al., 2023). The bed bulk porosity α_l was determined following the methodology in (Corrochano et al., 2015) (see SM Section 3.4).

Given the large number of parameters to be identified and the specifics in the dependencies of the various parameters, we decided not to perform a global optimization of all parameters at once, instead proposing a sequential parameter estimation strategy to enhance robustness. The parameter estimation procedure applied in this study (flow chart provided in SM Fig. S37) is divided into two consecutive parts. Part 1: The component-specific parameters $A_{1,i}$, $B_{1,i}$, $A_{2,i}$, $B_{2,i}$, $K_{ref,i}$, γ_i, and $c_{s0,i}$ were estimated for each component (28 parameters in total) at medium grind level 1.7, while ψ_1 and $d_{s2,1}$ were constants selected from the PSD measurement (dry) shown in (Schmieder et al., 2023) using Eq. (5). For suitable initial guess values, an initialization step was performed beforehand in which the component-specific model parameters $h_{sl1,i}$ and $h_{sl2,i}$ were identified for individual extraction experiments, as was done in (Moroney et al., 2019), plus the relaxed parameters K_i and $c_{s0,i}$. Part 2: The non-component specific parameters ψ_k and $d_{s2,k}$ were identified for the fine and coarse grind levels 1.4 and 2.0, respectively, keeping the component-specific parameters $A_{1,i}$, $B_{1,i}$, $A_{2,i}$, $B_{2,i}$, $K_{ref,i}$, γ_i, and $c_{s0,i}$ constant, which yielded four additional parameters estimated from extraction kinetics.

Initialization strategy

Adequate initial guesses are required to limit the time for parameter estimation and to improve parameter comparability. For this purpose, the model parameters $h_{sl1,i}$, $h_{sl2,i}$, K_i, and $c_{s0,i}$ were initially estimated using the concentration data of each individual experiment (six data points each). The same procedure was performed by Moroney et al. (2019), but the parameters K_i and $c_{s0,i}$ were relaxed instead of being fixed. This initial parameter estimation yields n_1 parameters equal to the number of extraction experiments ($n = 5 * 3 = 15$) at the same grind level. The obtained parameters, representing 15 data points at specific temperatures and flow velocities, were used to estimate the parameters $A_{1,i}$, $B_{1,i}$, $A_{2,i}$, $B_{2,i}$ in Eq. (7) and $K_{ref,i}$ and γ_i in Eq. (12). The resulting values were used as initial guesses for Part 1 of the main parameter estimation.

Part 1

The experimental and simulated concentrations were normalized by dividing by the concentration of the first fraction C_{1ij} from the same extraction. The respective minimization problem of Part 1 is:

$$\min_{A_{1,i},B_{1,i},A_{2,i},B_{2,i},K_{ref,i},\gamma_i,c_{s0,i}} \sum_{j=1}^{n_1} \sum_{f=1}^{6} \left(\frac{\left(\widehat{C}_{fij}(Q_j, T_j, k=1) - C_{fij} \right)}{C_{1ij}} \right)^2 \tag{D.1}$$

The variable $\widehat{C}_{fij}(Q_j, T_j, k=1)$ denotes the simulated concentration of solute i in fraction f of experiment j derived from Eq. (15) at a specific flow rate Q_j and temperature T_j and at $k=1$ (grind level 1.7). The corresponding experimentally obtained concentration is C_{fij}. The squared residuals in Eq. (D.1) are summed up over the 6 fractions and the number of experiments n_1 at $k=1$. The parameters d_{s1}, $d_{s2,1}$, and $d_{32,1}$, were received from particle size distribution measurements (dry) (Schmieder et al., 2023), i.e., from the locations of the peaks and the d_{32} of the PSD. The fine fraction ψ_1 was determined using Eq. (5).

Part 2

The minimization problem for part 2 is:

$$\min_{\psi_k, d_{s2,k}} \sum_{i=1}^{N} \sum_{j=1}^{n_k} \sum_{f=1}^{6} \left(\frac{\left(\widehat{C}_{fij}(Q_j, T_j, k) - C_{fij} \right)}{C_{1ij}} \right)^2 \tag{D.2}$$

Which differs from Part 1 in that way that the squared residuals are not only summed up over all 6 fractions per experiment and the number of experiments at the respective grind level n_k but also over the number of components N as the parameters ψ_k and $d_{s2,k}$ are not component specific. The parameters $A_{1,i}$, $B_{1,i}$, $A_{2,i}$, $B_{2,i}$, $K_{ref,i}$, γ_i, and $c_{s0,i}$ were kept constant for each component at the optimum parameters of Part 1.

Table D.1
Constant parameters for simulations.

Symbol	Description	Value	Unit
d_{s1}	Particle diameter 1[a]	24	µm
$d_{s2,1}$	Particle diameter 2 for grind level 1.7 ($k=1$)[a]	330	µm
$d_{32,1}$	Sauter mean diameter for grind level 1.7 ($k=1$)[a]	84	µm
ψ_1	Fines volume fraction for grind level 1.7 ($k=1$)[b]	0.23	1
α_l	Volume fraction of liquid phase (bulk porosity)[c]	0.17	1
d_{PF}	Diameter of portafilter basket	5.8	cm
L	Packed-bed height	1.5	cm
φ_{v2}	Volume fraction of intragranular pores/voids[d]	0.4	1
M_0	Mass of dry ground coffee	20.0	g
ρ_l	Density of coffee extract for flow conversion[e]	0.980	g cm^{-3}

[a] From particle size distribution measurements (dry) presented in (Schmieder et al., 2023).
[b] From Eq. (5) using d_{s1}, $d_{s2,1}$, and $d_{32,1}$.
[c] From helium pycnometry measurements (see SM Section 3.4).
[d] (Pittia et al., 2011)
[e] (Kuhn et al., 2017).

Appendix E. Statistical Analyses

As shown in (Schmieder et al., 2023), the variation of solute concentrations in a cup of coffee is strongly influenced by the brew ratio, which complicates the discrimination and statistical evaluation of effects. By modeling the concentration at the same brew ratio, the variance from different brew ratios is eliminated, and an analysis of variance can be performed using the model predictions as theoretical means and the mean measurement variance of the triplicate experiments from (Schmieder et al., 2023). The concentrations of the representative components were predicted for a volume of 60 mL (brew ratio 1/3) at different temperatures, flow rates, and grind levels and compared by calculating the test statistics of an ANOVA. As the variation of the cup concentration was not accessible from experiments directly but only the variation of solute concentrations in the fractions, the cup concentration variance of each experiment was estimated from the scattering of extraction kinetics data. The mean measurement variance for the mass of a component i and an experiment j was estimated by the residual between the model simulation and the experimental data, assuming an unbiased deviation (Aster et al., 2019):

$$s_{M_{ij}}^2 = \frac{1}{n_r n_f - n_{pi}} \sum_{r=1}^{n_r} \sum_{f=1}^{n_f} \left(\widehat{M}_{fij}(Q, T, k) - M_{fij} \right)^2 \tag{E.1}$$

n_r represents the number of replicates per experiment (three for all experiments), n_f is the number of fractions per extraction (six fractions), and n_{pi} is the number of parameters estimated with respect to component i (nine parameters). Since the cup volume was equal to the sum of the 10 fractions sampled, the measurement standard deviation for the cup concentration was determined as follows according to error propagation theory:

$$s_{C_{cup,ij}} = \frac{10}{60 \ mL} * \sqrt{s_{M_{ij}}^2} \tag{E.2}$$

In prediction experiments (Section 4.2), the model parameters were not fitted to the experimental data, and especially the concentration of chlorogenic acid differed systematically from the model results due to roasting batch variation (different initial concentration). Accordingly, model predictions could not be used as estimates for the experimental mean, and the cup concentrations were determined experimentally by analyzing the mixed residues of the fractions. Classical analyses of variance (ANOVA) were performed for the triplicate measurements using the MATLAB "anova1" function and Tukey's HSD (honestly significant difference) using the "multcompare" function.

References

Andueza, S., Maeztu, L., Pascual, L., Ibáñez, C., de Peña, M.P., Cid, C., 2003. Influence of extraction temperature on the final quality of espresso coffee. J. Sci. Food Agric. 83, 240–248. https://doi.org/10.1002/jsfa.1304.

Angeloni, S., Giacomini, J., Maponi, P., Perticarini, A., Vittori, S., Cognigni, L., Fioretti, L., 2023. Computer percolation models for espresso coffee: state of the art, results and future perspectives. Appl. Sci. 13, 2688. https://doi.org/10.3390/app13042688.

Aster, R.C., Borchers, B., Thurber, C.H., 2019. Parameter Estimation and Inverse Problems, third ed. Elsevier, Amsterdam, Oxford, Cambridge, MA.

Awwad, S., Issa, R., Alnsour, L., Albals, D., Al-Momani, I., 2021. Quantification of caffeine and chlorogenic acid in green and roasted coffee samples using HPLC-DAD and evaluation of the effect of degree of roasting on their levels. Molecules 26. https://doi.org/10.3390/molecules26247502.

Bickley, W.G., 1941. Formulae for numerical differentiation. Math. Gaz. 25, 19–27. https://doi.org/10.2307/3606475.

Cameron, M.I., Morisco, D., Hofstetter, D., Uman, E., Wilkinson, J., Kennedy, Z.C., Fontenot, S.A., Lee, W.T., Hendon, C.H., Foster, J.M., 2020. Systematically improving espresso: insights from mathematical modeling and experiment. Matter 2, 631–648. https://doi.org/10.1016/j.matt.2019.12.019.

Corrochano, B.R., 2015. Advancing the Engineering Understanding of Coffee Extraction. Dissertation, Birmingham.

Corrochano, B.R., Melrose, J.R., Bentley, A.C., Fryer, P.J., Bakalis, S., 2015. A new methodology to estimate the steady-state permeability of roast and ground coffee in packed beds. J. Food Eng. 150, 106–116. https://doi.org/10.1016/j.jfoodeng.2014.11.006.

Engelhardt, U.H., Maier, H.G., 1985. Säuren des Kaffees. Z. Lebensm. Unters. Forsch. 181, 206–209. https://doi.org/10.1007/BF02425579.

Giacomini, J., Khamitova, G., Maponi, P., Vittori, S., Fioretti, L., 2020. Water flow and transport in porous media for in-silico espresso coffee. Int. J. Multiphas. Flow 126, 103252. https://doi.org/10.1016/j.ijmultiphaseflow.2020.103252.

Klade, S., 2019. Molecular and Sensory Studies on Coffee Bitter Taste. Dissertation, Freising.

Kuhn, M., Lang, S., Bezold, F., Minceva, M., Briesen, H., 2017. Time-resolved extraction of caffeine and trigonelline from finely-ground espresso coffee with varying particle sizes and tamping pressures. J. Food Eng. 206, 37–47. https://doi.org/10.1016/j.jfoodeng.2017.03.002.

Lee, W.T., Smith, A., Arshad, A., 2023. Uneven extraction in coffee brewing. Phys. Fluids 35, 054110. https://doi.org/10.1063/5.0138998.

Lockhart, E.E., 1957. The Soluble Solids in Beverage Coffee as an Index to Cup Quality. Publication (Coffee Brewing Institute, Inc.).

Melrose, J.R., Corrochano, B.R., Norton, M., Silanes-Kenny, J., Fryer, P., Bakalis, S., 2012. Optimising coffee brewing using a multiscale approach. In: Proceedings of the 24th International Conference on Coffee Science. San José, Costa Rica.

Melrose, J., Roman-Corrochano, B., Montoya-Guerra, M., Bakalis, S., 2018. Toward a new brewing control chart for the 21st century. J. Agric. Food Chem. 66, 5301–5309. https://doi.org/10.1021/acs.jafc.7b04848.

Mo, C., Johnston, R., Navarini, L., Liverani, F.S., Ellero, M., 2023. Exploring the link between coffee matrix microstructure and flow properties using combined X-ray microtomography and smoothed particle hydrodynamics simulations. Sci. Rep. 13, 16374 https://doi.org/10.1038/s41598-023-42380-y.

Moroney, K.M., Lee, W.T., O'Brien, S., Suijver, F., Marra, J., 2015. Modelling of coffee extraction during brewing using multiscale methods: an experimentally validated model. Chem. Eng. Sci. 137, 216–234. https://doi.org/10.1016/j.ces.2015.06.003.

Moroney, K.M., O'Connell, K., Meikle-Janney, P., O'Brien, S.B.G., Walker, G.M., Lee, W. T., 2019. Analysing extraction uniformity from porous coffee beds using mathematical modelling and computational fluid dynamics approaches. PLoS One 14, e0219906. https://doi.org/10.1371/journal.pone.0219906.

National Center for Biotechnology Information, 2023a. PubChem Compound Summary for CID 5570. Trigonelline. https://pubchem.ncbi.nlm.nih.gov/compound/Trigonelline. (Accessed 23 March 2023).

National Center for Biotechnology Information, 2023b. PubChem Compound Summary for CID 2519, Caffeine. https://pubchem.ncbi.nlm.nih.gov/compound/Caffeine. (Accessed 23 March 2023).

National Center for Biotechnology Information, 2023c. PubChem Compound Summary for CID 1794427. Chlorogenic Acid. https://pubchem.ncbi.nlm.nih.gov/compound/Chlorogenic-Acid. (Accessed 23 March 2023).

Pittia, P., Sacchetti, G., Mancini, L., Voltolini, M., Sodini, N., Tromba, G., Zanini, F., 2011. Evaluation of microstructural properties of coffee beans by synchrotron X-ray microtomography: a methodological approach. J. Food Sci. 76, E222–E231. https://doi.org/10.1111/j.1750-3841.2010.02009.x.

Salamanca, C.A., Fiol, N., González, C., Saez, M., Villaescusa, I., 2017. Extraction of espresso coffee by using gradient of temperature. Effect on physicochemical and sensorial characteristics of espresso. Food Chem. 214, 622–630. https://doi.org/10.1016/j.foodchem.2016.07.120.

Schmieder, B.K.L., Pannusch, V.B., Vannieuwenhuyse, L., Briesen, H., Minceva, M., 2023. Influence of flow rate, particle size, and temperature on espresso extraction kinetics. Foods 2871. https://doi.org/10.3390/foods12152871.

Spiro, M., Toumi, R., Kandiah, M., 1989. The kinetics and mechanism of caffeine infusion from coffee: the hindrance factor in intra-bean diffusion. J. Sci. Food Agric. 46, 349–356. https://doi.org/10.1002/jsfa.2740460313.

Stephan, P., Kabelac, S., Kind, M., Mewes, D., Schaber, K., Wetzel, T., 2019. VDI-waermeatlas. Springer Berlin Heidelberg, Berlin, Heidelberg.

Vaca Guerra, M., Harshe, Y.M., Fries, L., Rothberg, S., Palzer, S., Heinrich, S., 2023a. Influence of particle size distribution on espresso extraction via packed bed compression. J. Food Eng. 340, 111301 https://doi.org/10.1016/j.jfoodeng.2022.111301.

Vaca Guerra, M., Harshe, Y.M., Fries, L., Pietsch-Braune, S., Palzer, S., Heinrich, S., 2023b. Tuning the packed bed configuration for selective extraction of espresso non-volatiles based on polarity. J. Food Eng. 354, 111554 https://doi.org/10.1016/j.jfoodeng.2023.111554.

Wilke, C.R., Chang, P., 1955. Correlation of diffusion coefficients in dilute solutions. AIChE J. 1, 264–270. https://doi.org/10.1002/aic.690010222.

Wilson, E.J., Geankoplis, C.J., 1966. Liquid mass transfer at very low Reynolds numbers in packed beds. Ind. Eng. Chem. Fund. 5, 9–14. https://doi.org/10.1021/i160017a002.

B.4 Predicting the Essential Oil Composition in Supercritical Carbon Dioxide Extracts from Hop Pellets Using Mathematical Modeling

Research article

Predicting the essential oil composition in supercritical carbon dioxide extracts from hop pellets using mathematical modeling

Verena Bernadette Pannusch [a], Lukas Viebahn [b], Heiko Briesen [a], Mirjana Minceva [b, *]

[a] *Process Systems Engineering, Technical University of Munich, Freising, Germany*
[b] *Biothermodynamics, Technical University of Munich, Freising, Germany*

ARTICLE INFO

ABSTRACT

Supercritical fluid extraction from hops (*Humulus lupulus* L.) can be used to extract essential oil for the flavoring of beer. With a special focus on the oil composition being linked to the hop aroma, the influence of pressure and temperature on the extraction kinetics of seven oil components (β-myrcene, α-humulene, β-caryophyllene, 2-methylbutyl isobutyrate, undecanone, linalool, and α-pinene) is analyzed and modeled in this article.

Supercritical CO_2 extraction from hop pellets was conducted at pressure-temperature combinations of 90/100/110 bar and 40/45/50 °C. The extract composition over time, analyzed by gas chromatography, was used for the parameterization of two existing mechanistic models: an internal-mass-transfer-control (IMTC), and a broken-and-intact-cells (BIC) model. The IMTC model was found to effectively describe most extraction kinetics and hence applied in this study. In contrast to previous studies, the IMTC model parameters were not only fitted to individual extraction curves from different experiments but also correlated to temperature and pressure as a further step towards model-based prediction. Using the parameterized model, the extract composition was predicted at 95 bar/48 °C, 105 bar/42 °C, and 105 bar/48 °C.

Extraction yields were found to be higher at lower temperatures and higher pressures in general. The sensitivity towards pressure was observed to differ between components and to be particularly higher for β-myrcene compared with α-humulene. Changes of the essential oil composition with a variation in pressure and temperature were predicted correctly by the model with a mean relative deviation from experimental data of 11.7% (min. 1.2%, max. 36.2%).

1. Introduction

Due to both economic and environmental advantages, more and more industries are transitioning to the use of supercritical carbon dioxide instead of organic solvents in extraction processes [1]. In addition to its GRAS status (Generally Recognized As Safe), supercritical carbon dioxide (scCO2) also offers a couple of advantages with regard to the extraction process. Its low critical temperature of 31 °C enables extractions to be carried out in relatively mild conditions. Consequently, delicate solutes like odor-active essential oils are extracted without chemical alteration or thermal degradation [2]. Since CO_2 is gaseous in standard conditions, a drop in pressure and temperature in the collection vial suffices for an almost complete evaporation of the solvent, making additional purification steps for solvent removal unnecessary.

---

* Corresponding author.
E-mail address: mirjana.minceva@tum.de (M. Minceva).

The common hop (*Humulus lupulus* L.) has been employed in the brewing industry for centuries [3]. While they are quantitatively a minor ingredient in the process, added at the wort boiling step, they have a large impact on the aroma, taste, foam, stability, and mouthfeel of beer [4–6]. Hop products impart bitterness and a wide range of flavors to beer, including fruity, resinous, herbal, tropical, or citrus-like aroma impressions [7].

The two primary value-adding components of dried hop cones are soft resins (10–25%) and essential oils (0.4–2%). The main soft resins are α- and β-acids which impart bitterness and have a strong antimicrobial effect. The volatile essential oils comprise terpenes, sesquiterpenes and their respective oxygenated derivatives, esters, ketones as well as thiols. Some of them are highly odor-active and are responsible for the characteristic aroma of hops [8–10].

The research field of supercritical fluid extraction (SFE) of essential oil is replete with groups investigating a large number of plants and target molecules [11–14]. Recent studies shift the emphasis from the goal of maximum overall yield towards selective fractionation of the extract, e.g., by step-wise temperature [15] or pressure reduction [16]. Higher concentrations of bio-active target molecules in the fractions could be achieved by adjustment of temperature and pressure conditions in the separators [15,16]. With regard to hop cones, SFE is commonly used to produce extracts for beer hopping. Typical pressures lie between 300 and 500 bar, and temperatures range between 50 and 60 °C [17], targeting maximum yield of both bitter acids and aroma compounds. To achieve higher concentrations of aroma molecules in the extract, a more sophisticated selection of pressure and temperature is needed utilizing the specific solubility of essential oil components. Previous researchers have investigated using $scCO_2$ in novel analytical methods for hop volatiles [18,19] or the selective recovery of hop aromas for beer flavoring [20]. Nagybákay et al. [21] attempted to optimize the extraction of lipophilic antioxidants from hops.

With regard to the mathematical modeling of essential oil extraction from hops, a recent study by Bizaj et al. [22] applied a simple mathematical model to describe the extraction kinetics of total hop extract using various solvents. Kupski et al. [23] compared three different models to describe the total extract mass as a function of time with regard to $scCO_2$ extraction from ground hop. The authors found that the broken-and-intact-cells (BIC) model by Sovová [24] yielded the best fit for ground hops, one which has been successfully applied to many herbaceous raw materials like pennyroyal leaves [25], rosemary leaves [26], guava leaves [27], and many others. However, one drawback of the BIC model is the larger number of parameters to be fitted compared to other approaches, such as the internal-mass-transfer-control (IMTC) model [28]. The research presented here compares the latter two models, considering the goodness-of-fit of the models as well as their simplicity, i.e., the number of parameters to be fitted.

Former studies predominantly focused on total or essential oil yield. Considering the essential oil composition, i.e., the individual extraction kinetics of molecules, may, however, be beneficial for process design in order to enhance the extract quality and to selectively extract certain desired compounds with higher purity. Furthermore, a variety of models have accurately described $scCO_2$ extraction kinetics, but their potential for prediction and process optimization by including temperature and pressure correlations and considering the density of CO_2 in the model equations has still not been exploited.

With craft beer being globally on the rise, the demand for strong hop flavors in beer has changed the brewing industry worldwide. The focus is no longer on high α-acid utilization rates, but on a hoppy flavor achieved by "dry-hopping" procedures. Therefore, hops are not only added at the wort boiling step, but also at the end of the fermentation step and prior to the filling step at temperatures below 20 °C [29]. The subsequent separation of plant matter along with the non-isomerized α-acids inevitably results in losses of both bitter resins and beer. Technological advances will be required in order to reduce the waste of resources while increasing transfer rates of volatiles and resins. By separately extracting α-acids and essential oil using SFE with distinct operating conditions and adding them at different stages in the brewing process, both components can release their full potential while the waste of hop material is substantially reduced. For a targeted fractionation, however, the extraction behavior of the volatiles out of the complex hop matrix needs to be predictable.

The focus of this research is to investigate, model, and predict the extraction kinetics of individual essential oil components from hop pellets as functions of the operating parameters of temperature and pressure, i.e., solvent density. The results of this study may pave the way towards improved extract quality, higher yield, and less waste in the craft beer production, and in other applications of $scCO_2$ extraction from plant materials.

2. Material and methods

2.1. Materials

Hop samples (T90 pellets) from the 2020 Herkules crop were kindly supplied by Hopsteiner (Germany) in sealed vacuum packages

Table 1
List of chemicals, their purity specifications and producers.

Name	CAS Nr.	Purity, %	Supplier
β-Myrcene	123-35-3	91.8	Sigma-Aldrich (USA)
Linalool	78-70-6	98.8	Merck (Germany)
Undecanone	112-12-9	99.9	Acros Organics™ (USA)
L-Menthol	2216-51-5	99.6	Sigma-Aldrich (USA)
Ethanol abs.	64-17-5	99.98	VWR International (France)
Methyl-tert-butylether (MTBE)	1634-04-4	99.6	VWR International (France)
CO_2	124-38-9	99.7	Westfalen (Germany)

of 50.0 g. The composition as specified by the supplier is listed in Supplementary Information (SI) Table S1 online. The hop pellets had a mean density ρ_{hop} of 0.975 g cm^{-3} and were kept refrigerated until use.

All chemical substances used in this study, including their purity and supplier, are listed in Table 1.

2.2. Experimental methods

2.2.1. Supercritical fluid extraction

The extraction was carried out using an Applied Separations (USA) Spe-ed SFE Zoran extractor. The cylindrical extraction vessel has a volume of 100 mL, a length of 14.5 cm and an internal diameter of 3.0 cm. The vessel was charged by loosely filling it with 50.0 g of hop pellets and with glass wool at both ends acting as filter material. This reduced the effective bed length to 10.5 cm, resulting in a bed volume of 74 mL and a bulk density of 0.67 g cm^{-3}. The vessel was subsequently sealed, heated to the desired temperature, and filled with liquid CO_2. The pressure was then adjusted by the pump and the timer was started. The outlet valve was opened and the flow adjusted to 7 standard liters per minute (SLPM) (which is equal to a constant mass flow of 0.211 g s^{-1}) using the micro metering valve. The flow speed was measured at atmospheric pressure by an ALICAT Scientific (USA) digital flow meter and automatically corrected to 25 °C, 1.013 bar (SATP). 60 mL glass EPA vials were precooled to -27 °C in a freezer before being connected to the extractor and then cooled continuously in order to condensate any substances that might be volatile at room temperature. Samples were taken at 15 min intervals (9 samples per extraction) and all extractions were conducted in duplicates yielding 18 samples per experiment. The collected hop extract was stored at -27 °C. A flow chart of the process is shown in Fig. 1.

For analysis, the hop extract was dissolved in 10 mL of 70 vol% ethanol and 0.5 g of NaCl per 0.5 g of extract using an ultrasonic bath. The resulting extract solution was filtered using MACHEREY-NAGEL (Germany) Chromafil® PET-20/15 MS filters with a 0.20 µm pore size. The solution was kept at -27 °C in sealed tubes until further use.

2.2.2. Gas chromatography

All samples from time-resolved extract collection were analyzed via GC-FID. The hop volatiles in each extract sample were quantified by gas chromatography (GC) using a SHIMADZU (Japan) Nexis GC-2030 with flame ionization detector (FID). A SHIMADZU AOC-20i auto injector and a SHIMADZU AOC-20s Plus auto sampler were used for direct injection. The GC was equipped with a split-splitless injector which was held at 250 °C. The installed column was a Phenomenex® (USA) Zebron™ ZB5ms column (30 m length x 0.25 mm ID x 0.25 µm film thickness). A SHIMADZU P/N 221-75193 95 mm (deactivated, with wool) 3.4 mm ID liner was used. A carrier gas (helium) flow of 1.43 mL min^{-1} was maintained. The FID sampling rate was set to 40 ms and used a H_2 flow of 32 mL min^{-1} alongside a makeup flow (N_2) of 24 mL min^{-1} and an air flow of 200 mL min^{-1}. The chromatograms were analyzed using SHIMADZU LabSolutions™ software.

The samples consisted of 900 µL of filtered hop extract solution and 100 µL of menthol solution (5 mg l^{-1} dissolved in ethanol) as an internal standard (STD) whose peak does not overlap with the peaks of the characteristic essential oil components. The injected amount was 1 µL (single injection) and the split ratio was set to 1:50. The initial column temperature of 60 °C was held for 4 min before being raised to 280 °C at a rate of 10 °C min^{-1}. The final temperature was maintained for 3 min and the total time of analysis was 30 min. The FID temperature was set to 280 °C.

Given the complex nature of hop extract and possible matrix effects, STD addition was chosen as the calibration method [30]. Pure compounds of β-myrcene, linalool, and undecanone were added to a solution of commercial CO_2 hop extract provided by Hopsteiner (Germany). Additionally, each sample was spiked with an internal standard (menthol) in order to detect inconsistencies over the course of the measurements. A representative chromatogram is presented in Supplementary Fig. S37.

2.2.3. Solid density and total porosity

To determine pellet density, the mass of one pellet was measured using a precision scale. The diameter and length of the same pellet
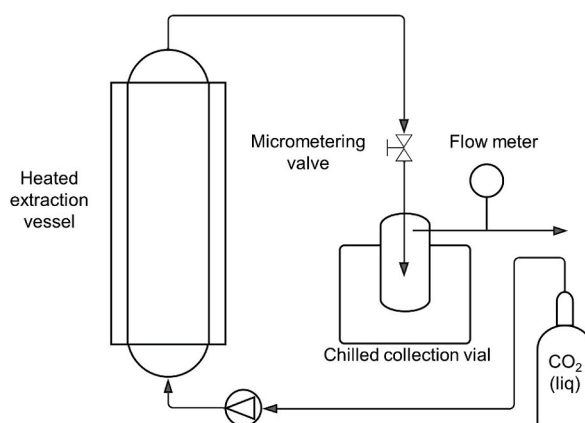
Fig. 1. Flow chart of scCO$_2$ extractor, Spe-ed SFE Zoran model (Applied Separations).

was measured using a caliper gauge and the cylinder volume determined. The mean pellet density ρ_{pellet} from 22 measurements was then calculated as:

$$\rho_{pellet} = \frac{1}{n_{pellet}} \sum_{i=1}^{n_{pellet}} \frac{m_{pellet,i}}{V_{pellet,i}} \tag{1}$$

with n_{pellet} being the number of measurements, $m_{pellet,i}$ being the mass of each pellet, and $V_{pellet,i}$ being the volume of the same pellet. The solid density ρ_s was measured in triplicate by helium pycnometry using a Micromeritics (Germany) AccuPyc 1330 pycnometer with a 10 cm^3 cylindrical measuring chamber. The inner porosity of the pellet ε_{pellet} was calculated from ρ_{pellet} (Equation (1)) as:

$$\varepsilon_{pellet} = 1 - \frac{\rho_{pellet}}{\rho_s} \tag{2}$$

The bulk porosity ε_{bulk} in the extraction column (without inner porosity ε_{pellet} of the pellets, Equation (2)) was calculated from the bulk density (mass of pellets per occupied column volume) and the pellet density as:

$$\varepsilon_{bulk} = 1 - \frac{m_0}{\frac{\pi}{4} d_i^2 L \rho_{pellet}} \tag{3}$$

with m_0 being the initial mass of hop pellets, L being the length of the extraction column, and d_i being the inner diameter of the extraction column. The total porosity ε describes the sum of the inner porosity and bulk porosity (Equation (3)):

$$\varepsilon = \varepsilon_{bulk} + (1 - \varepsilon_{bulk}) \, \varepsilon_{pellet} \tag{4}$$

The inner porosity of the pellet ε_{pellet} (Equation (2)) was analyzed both before and after 135 min of extraction at 90 bar and 45 °C in order to investigate if and to which extent a change in porosity occurred. The results are shown in the Appendix.

2.3. Mathematical modeling

The mechanistic models used in this research describe the extraction of essential oil components from a packed bed of porous pellets using supercritical CO_2 as a solvent flowing through the pores of the cylindrical packed bed. During the extraction process, species dissolve, desorb, and diffuse from the inside of the leave fractions of which the pellets consist and to the surface, where they pass through a stagnant film to the flowing fluid in the pores. The extracted mass is then transported in the direction of CO_2 flow by forced advection and collected behind the column outlet, where it is separated from the solvent by expansion and vaporization of the solvent. Fig. 2 illustrates this modeling concept and presents three different scales. On the left, the sketched column is filled with the cylindrical pellets of equal radius, with CO_2 flowing in an upward direction. In the center circle, a representative volume element can be seen, with the solid leave fragments representing the solid phase of the porous pellets. The boxes on the right side of Fig. 2 show single particles and mass transfer by diffusion for the two models compared in this article: an internal-mass-transfer-control model (IMTC model) [28], and a broken-and-intact-cells model (BIC model) [31]. For the sake of readability, we will present the main equations of both models in the following sections. Please note that, in some cases, the notation may depart slightly from the original publications in order to better compare the two models used in this research. The interested reader is referred to the original publications for a more detailed derivation.
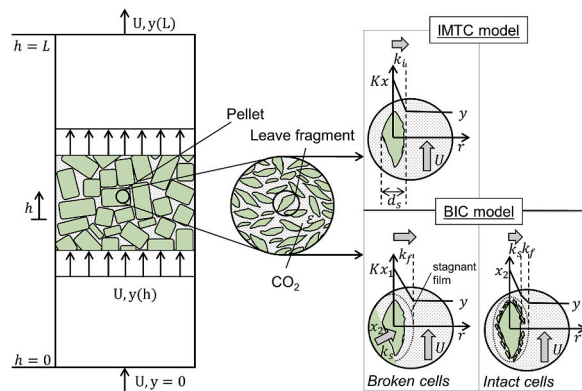
Fig. 2. Schematic illustration of the internal-mass-transfer-control model (IMTC) [28] and the broken-and-intact-cells model (BIC) [31]. Three different scales: the macroscale of the extractor column (left), a representative volume element (center), and a single leave fragment (right) with slab thickness d_s. Advection of fluid mass fraction y occurs in the direction of h along the column length L and with superficial velocity U. Mass transfer from leave fragments with solid mass fraction x is controlled by the partition coefficient K and by the internal mass transfer coefficient k_i (IMTC model) or by fluid-phase mass transfer coefficient k_f for broken cells, and by solid-phase mass transfer coefficient k_s for intact cells (BIC model). r represents the distance from the particle center.

In general, we made the following assumptions: (i) the fluid fully penetrates the pellets homogeneously, i.e., advection happens both between and inside pellets; (ii) the initial penetration and imbibition process, when CO_2 enters the extractor, displaces air, and fills the pores, is disregarded, so the porous medium is assumed to be filled with CO_2 at t = 0; (iii) structural parameters such as porosity and specific surface area (Equation (8)) remain constant; (iv) the temperature and pressure within the packed bed are constant in terms of both time and space, and (v) density and viscosity of pure CO_2 are assumed to be unaffected by the concentration of the solutes.

2.3.1. IMTC model

The IMTC model is based on the one-dimensional general diffusion model [32], with the assumption that internal mass transfer limits the extraction rate throughout the entire extraction process. This means that the external mass transfer is disregarded, and the concentration at the surface of a leaf fragment, which is modeled as a cuboid shaped slab, is expected to be the same as in the fluid bulk phase [28]. Fig. 2, at right, illustrates this assumption. The dominance of internal over external mass transfer resistance has been suggested as an appropriate assumption for extraction from leaves [33]. The IMTC model consists of the mass balance in the fluid phase:

$$\rho_f \, \varepsilon \left(\frac{\partial y}{\partial t} + U \, \frac{\partial y}{\partial h} \right) = j \tag{5}$$

and the mass balance in the solid phase:

$$\rho_s \, (1 - \varepsilon) \, \frac{\partial x}{\partial t} = -j \tag{6}$$

where x is the mass fraction of a species in the solid phase, y is the mass fraction of a species in the fluid phase, h is the spatial co-ordinate pointing upward in the direction of flow, t is the time, ρ_f is the fluid density, ρ_s is the solid density, ε is the total porosity of the packed bed of pellets (see Equation (4)), U is the superficial velocity, and j is the flux between fluid and solid phase. The volume averaged flux from the solid phase to the fluid phase neglecting external mass transfer is described by:

$$j = \rho_f \, k_i \, a \, (Kx - y) \tag{7}$$

where k_i is the internal mass transfer coefficient, a is the specific surface area of the solid phase, being:

$$a = \frac{2}{d_s} \, (1 - \varepsilon) \tag{8}$$

with slab thickness assumed to be $d_s = 21 \ \mu m$ [23] and K is the partition coefficient of a species:

$$K = \frac{y^*}{x} \tag{9}$$

The mass fraction in the fluid at equilibrium is represented by y^*. Based on the finding that plant tissue of hops swells and pores are hence filled with CO_2 [34], mass transport inside the leave fragments (thin slabs) is modeled as molecular diffusion in the intra-particle pore space. Accordingly, the driving force is the difference between the average solute concentration in the pore space of the leave fragments being y* and its concentration on the surface (equal to bulk concentration). Axial dispersion is disregarded (the relevant contributions are presented in the Supplementary Information, Equations (S.1) to (S.3), available online).

The initial conditions for a solute mass fraction in the fluid and solid phase, respectively, are:

$$y|_{t=0} = 0 \; ; \quad x|_{t=0} = x_0 \tag{10}$$

where x_0 is the initial solute mass fraction in the solid phase. Please note that we assume the initial concentration in the fluid phase to be zero, i.e., the pore space is filled with pure $scCO_2$. The boundary condition at the inlet of the extractor is defined by:

$$y|_{h=0} = 0 \tag{11}$$

The cumulated extracted solute mass E in the CO_2 extract is obtained by:

$$E = \rho_{f,out} \, Q_{CO_2} \int_0^t y|_{h=L} \, dt' \tag{12}$$

where Q_{CO_2} is the volume flow of CO_2, $\rho_{f,out}$ is the fluid density at the outlet pressure of 1 bar (after expansion) and a temperature of 20 °C. The respective yield Y is:

$$Y = \frac{E}{m_0} \tag{13}$$

with m_0 being the total mass of hop pellets at the beginning of extraction ($t = 0$).

The above model has been transformed into dimensionless form and normalized for numerical solution, which is shown in the Supplementary Information online (Equations (S.4) to (S.9)).

2.3.2. BIC model

With regard to the BIC model, it is expected that two extraction stages exist, the former being controlled by the solution equilibrium of a solute in CO_2 (see Equation (9)) due to quick fluid-phase (external) mass transfer from broken cells, and the latter being limited by the solid-phase (internal) mass transfer resistance in intact cells [31]. In contrast with the IMTC model, it is in this case assumed that, in addition to intact cells with internal mass transfer control, a second solid phase of broken cells also exists at the surface of intact cells which is controlled by external mass transfer only. As a result, diffusion occurs from intact cells to broken cells and from broken cells into the fluid. The two sketches at the lower right of Fig. 2 illustrate these relations.

The BIC model equations by Sovová [31] consist of the mass balance of solutes in the fluid phase:

$$\rho_f \, \varepsilon \left(\frac{\partial y}{\partial t} + U \, \frac{\partial y}{\partial h} \right) = j_f \tag{14}$$

the mass balance in broken cells:

$$r \, \rho_s \, (1 - \varepsilon) \frac{\partial x_1}{\partial t} = j_s - j_f \tag{15}$$

and the mass balance in intact cells:

$$(1 - r) \, \rho_s \, (1 - \varepsilon) \frac{\partial x_2}{\partial t} = - j_s \tag{16}$$

In the above model, there are two fluxes, j_f describing the flux from the broken cells to the fluid and j_s being the flux from the intact cells to the broken cells. The mass fraction of a species in broken cells is represented by x_1, the mass fraction in intact cells is x_2.

Parameter r stands for the volume fraction of broken cells. The flux from broken cells to the fluid is described by:

$$j_f = k_f \, a \, \rho_f \, \left(y^* - y \right) = k_f \, a \, \rho_f \, \left(K \, x_1 - y \right) \tag{17}$$

where k_f represents the fluid-phase mass transfer coefficient and the flux from the intact cells to the broken cells is:

$$j_s = k_s \, a \, \rho_s \, (x_2 - x_1) \tag{18}$$

with k_s being the solid-phase mass transfer coefficient.

The initial and boundary conditions for this set of partial differential equations are:

$$y|_{t=0} = y_0 \; ; \quad x_1|_{t=0} = x_{1,0} \; ; \quad x_2|_{t=0} = x_{2,0} \; ; \quad y|_{h=0} = 0 \tag{19}$$

The initial mass fraction in the broken cells is $x_{1,0}$ and the initial mass fraction in the intact cells is $x_{2,0}$. The extracted mass of a solute at time t is calculated by Equation (12), similar to the IMTC model.

Regarding the fluxes j_f and j_s, Sovová [31] proposes different terms, depending on the initial concentration of a solute. A type D extraction (Sovová's classification: initial equilibrium below saturation concentration), suitable for essential oil extraction from leaves and flowers, was selected in this case as the initial condition for the fluid phase:

$$y_0 = y^* \left(x_{1,0} \right) = K \, x_{1,0} \tag{20}$$

The type D equilibrium was selected based on the shape of extraction curves observed in this study (smooth transition between stages) and on the fact that the operational solubility determined from the initial slope was lower than the theoretical solubility of essential oil components [35,36]. The initial amount of free solute in the broken and intact cells is described by:

$$x_{1,0} = \frac{r \, x_u}{r + \gamma \, K} \; ; \quad x_{2,0} = x_u \tag{21}$$

The parameter x_u defines the mass fraction of a species in the insoluble solid and γ is:

$$\gamma = \frac{\rho_f \, \varepsilon}{\rho_s \, (1 - \varepsilon)} \tag{22}$$

The model equations are transformed into dimensionless form as described in Ref. [31].

2.4. Numerical solution and parameter fitting

All computations were performed on a computer with the following specifications: Intel(R) Core(TM) i7-8700 CPU @ 3.20 GHz, 3.19 GHz, 16.0 GB RAM memory, equipped with a NVIDIA GeForce GT 1030 graphic card and a Microsoft Windows 10 Enterprise operating system.

The systems of partial differential equations for both models were solved numerically using finite differences. A five-point biased upwind scheme was used for the spatial coordinate [37]. The solution of the resulting ordinary differential equations and algebraic equations was implemented in MATLAB® R2020b (MathWorks, Massachusetts, USA) using the "ode15s" function.

For parameter fitting, the non-linear least squares solver "lsqnonlin" and the linear fit solver "robustfit" were used, and the sum of

squared residuals between the experimental and simulated cumulated mass of extract (Equation (12)) was minimized. The fitting procedure applied in this research for achieving predictions of extraction kinetics as a function of extraction temperature and pressure is divided into four steps: I) fitting model parameters to data from single extraction experiments; II) model selection; III) correlations of model parameters with temperature and pressure; IV) fitting correlation parameters to all experimental data using fitted parameters from step 3 partially as starting values for the numerical iterations and partially as constants.

2.4.1. Fitting model parameters to single experiments

Regarding the IMTC model, three unknown model parameters were fitted: $k_i a$, $y^*(x_0)$, and x_0. In order to more closely approach a global minimum, three start values for $k_i a$ were investigated: 0.01, 0.001, and 0.0001. The goodness-of-fit was evaluated by the mean absolute percentage error (MAPE, %):

$$MAPE = \frac{1}{n}\sum_{i=1}^{n} abs\left(\frac{E_{i,exp} - E_{i,sim}}{E_{i,exp}}\right) * 100 \tag{23}$$

The combinations of parameters exhibiting the lowest MAPE were selected and used for the subsequent fitting steps.

As for the BIC model, the procedure presented in Ref. [31] was applied. The unknown parameters in this model to be fitted are $y^*(x_{1,0})$, r, $k_s a$, $k_f a$. The initial solid-phase mass fraction necessary for this model (Equation (21) and (22)) was determined by either using the supplier's information (see SI Table S1 online), or, if no data was available, the maximum yield from experiments. The respective data are included in SI Table S2 online. In a first step, the operational solubility (initial outlet concentration in case of equilibrium conditions and free solute, Equation (20)) was determined by defining the initial slope of the extraction curve from the derivative of a fitted 6th degree polynomial at $t = 0$. Start values for r and $k_s a$, as well as the value of K were calculated as described in Ref. [31]. A reasonable initial guess for k_f was determined from a correlation found in the literature (by Puiggené et al. [38]), which defines the Sherwood number:

$$Sh = 0.206\, Re^{0.80} Sc^{1/3} \tag{24}$$

where Re is the particle Reynolds number and Sc is the Schmidt number. This yields the fluid-phase mass transfer coefficient:

$$k_f = \frac{Sh\, D_{12}}{d_s} \tag{25}$$

with D_{12} being the binary diffusion coefficient of the respective essential oil compound. $D_{12}(p, T)$ was approximated by using the correlation by Catchpole and King [39]. The density and viscosity of supercritical CO_2 for the respective temperature and pressure, which are necessary to calculate Re, Sh (Equation (24)), and k_f (Equation (25)), were calculated from thermodynamic correlations [40, 41].

After all of the start values were determined, r was fitted to all experimental data, individually for each substance. Although it might be assumed that r is not substance-specific, fitting r to all substance data at once yielded unsatisfactory results. The resulting value of r was subsequently taken as a constant, and the parameters $k_s a$ and $k_f a$ were fitted to each individual experimental run.

2.4.2. Model selection

The IMTC model and the BIC model were compared using a modified Akaike criterion (AIC$_c$) for sample numbers less than 40 [42]:

$$AIC_c = n\left[\ln\left(\frac{RSS}{n}\right)\right] + 2g + \frac{2g(g+1)}{n-g-1} \tag{26}$$

In this case, n is the number of samples, RSS is the residual sum of squares, and g is the number of fitted parameters which is three for the IMTC model ($k_i a$, $y^*(x_0)$, and x_0) and four in the BIC model ($k_f a$, $k_s a$, $y^*(x_{1,0})$, and r). The model identified as preferable at most conditions was selected for further use in order to cover the range of temperature and pressure conditions.

2.4.3. Correlations of model parameters with temperature and pressure

The correlation equations used to describe the model parameters (fitted in step I) for the selected model as functions of temperature and pressure are presented in the following. The three correlation equations with fitting parameters, specified as $\boldsymbol{\alpha}$, $\boldsymbol{\beta}$, and $\boldsymbol{\gamma}$, were fitted to the model parameters obtained in fitting step (I). Vectors of fitting parameters are subsequently highlighted in bold.

With regard to the equilibrium concentration $y^*(x_0)$ in supercritical CO_2, a correlation equation by Chrastil [43] was used which is based on the reaction kinetics of the solvato complex formation between a molecule and a gas and is defined by:

$$c^*(p, T) = \rho_f(p, T)^{\alpha_1}\; e^{\left(\frac{\alpha_2}{T} + \alpha_3\right)} \tag{27}$$

In this case, the fitting parameters are α_1, α_2, and α_3; p and T are the extraction pressure in MPa and temperature in Kelvin, c^* is the equilibrium concentration in g dm^{-3}, and ρ_f is the fluid density in g dm^{-3}. The relation between volume-based equilibrium concentration c^* (mass per volume CO_2) and mass fraction y^* (mass per mass CO_2) is given by:

$$y^*(p,T) = \frac{c^*(p,T)}{\rho_f(p,T)} \tag{28}$$

Temperature is directly included in Equation (27), whereas the influence of pressure is included in its impact on the fluid density. The pressure and temperature function of CO_2 density is received from Ref. [40].

According to Ref. [44], the internal mass transfer coefficient k_i is related to the effective diffusion coefficient D_e in the solid phase by:

$$D_e(p,T) = \frac{k_i \, d_s}{6 \, (1 - \varepsilon)} \tag{29}$$

which is furthermore related to the binary diffusion coefficient of a species by:

$$F_M(p,T) = \frac{D_{12}(p,T)}{D_e(p,T)} \tag{30}$$

with F_M being a microstructural factor which includes diffusion hindrance as well as interactions with the solid matrix. A correlation of D_{12} for each substance with pressure and temperature was determined using a method by Catchpole and King [39]. To account for changes of F_M with pressure and temperature, a second-order model was used:

$$F_M(p,T) = \beta_1 + \beta_2 p + \beta_3 T + \beta_4 p^2 + \beta_5 T^2 + \beta_6 pT \tag{31}$$

Six fitting parameters are required, represented by the vector $\boldsymbol{\beta}$. The above type of correlation, with up to second order expressions, is commonly used for the description of response surfaces from two factors.

The initial mass fraction x_0 was also found to change with pressure and temperature. The dependence of x_0 on the latter variables is as well described by a second-order model applying to all components except α-pinene:

$$x_0(p,T) = \gamma_1 + \gamma_2 p + \gamma_3 T + \gamma_4 p^2 + \gamma_5 T^2 + \gamma_6 pT \tag{32}$$

With respect to α-pinene, a first-order correlation of the type:

$$x_0(p,T) = \gamma_1 + \gamma_2 p + \gamma_3 T \tag{33}$$

was applied because a second-order correlation would have over-estimated curvature and yielded negative values in the area of small concentrations without significantly improving the goodness-of-fit.

2.4.4. Fitting correlation parameters to all experiments

In the last fitting step, the correlation vectors $\boldsymbol{\beta}$, and $\boldsymbol{\gamma}$, fitted in step III were kept constant, and the vector $\boldsymbol{\alpha}$ describing the dependence of $y^*(x_0)$ on temperature and pressure was fitted to all 18 experiments (index i) , including all 9 sampling times (index j) for each of the essential oil components analyzed and for the total mass of extract. The regression problem is then:

$$\min_{\boldsymbol{\alpha}} \sum_{i=1}^{18} \sum_{j=1}^{9} \left(E(\boldsymbol{\alpha},\boldsymbol{\beta},\boldsymbol{\gamma},p_i,T_i,t_j) - E_{exp,i,j} \right)^2 \tag{34}$$

The fitted $\boldsymbol{\alpha}$ from step 3 was used as an initial guess.

3. Results and discussion

The results of this study will be presented in three sections: 1) selection of a model for the description of extraction kinetics; 2) study of the influence of pressure and temperature on the extraction kinetics, extract yield, and composition; and 3) prediction of the latter using the selected and parameterized model. Seven volatiles were investigated in the scope of this research: β-myrcene, α-humulene, β-caryophyllene, 2-methylbutyl isobutyrate (2-MBIB), undecanone, linalool, and α-pinene (in decreasing order of content). Additionally, the total mass of extract was assessed for the evaluation of yield and extract composition. For the sake of brevity, the parameter fitting results are shown subsequently for (a) β-myrcene as a representative monoterpene, (b) α-humulene as a representative sesquiterpene, and (c) total mass of extract. These three representative extraction curves are adequate for demonstrating both the development of extract composition and the overall yield. A full factorial design of experiments was applied with three settings each for extraction pressure and temperature: 90, 100, and 110 bar and 40, 45, and 50 °C.

3.1. Model selection and parameterization

The IMTC model (Equations (5) to (7)) with the initial and boundary conditions presented in Equations (10) and (11) and the BIC model (Equations (14) to (18)), with initial and boundary conditions described by Equation (19), were compared with respect to their goodness-of-fit and numbers of fitting parameters. Simulations of extraction yield, calculated by Equation (13), for both fitted models are depicted in Fig. 3 together with the experimental data. β-Myrcene, α-humulene, and total mass yield are shown at a representative condition of T = 40 °C and p = 100 bar which is equivalent to a density of about 629 kg m^{-3}. Plots of all other investigated pressure-

temperature combinations are presented in the Supplementary Information (SI) Figs. S1–S8 online. The experimentally derived value for total porosity ε is included in Appendix A.

Table 2 lists the respective fitted parameters of both models for T = 40 °C and p = 100 bar, as well as the MAPE (Equation (23)) and AIC_c (Equation (26)). The results for MAPE and AIC_c in all other analyzed experimental conditions and volatiles are available in SI Table S3 online. With respect to these conditions, it is evident that the values of MAPE and AIC_c for the IMTC fit are lower than those for the BIC fit. Particularly for β-myrcene, a lack of fit is visible when using the BIC model, as shown in Fig. 3. Although this is not the case in all experimental conditions (see SI Table S3 online), the mean AIC_c values across all experiments (shown in Table 3) are lower for the majority of components in the case of the IMTC model. This indicates that the IMTC model is superior to the BIC model for this process because it requires fewer parameters and leads to a comparable or even better fit. In addition to the foregoing argument, the fitted value of the BIC parameter r describing the volume fraction of broken cells varies for different substances, indicating a lack of identifiability, and is rather low, in particular for total mass, at 0.0149. This supports the assumption that the impact of a broken cells phase characterized by a high mass transfer rate is negligible for the system investigated. Consequently, the IMTC model was selected and subsequently used to correlate model parameters with temperature and pressure (respective fitted and experimental extraction curves at all operating conditions available in SI Figs. S9-S15 online). Although internal mass transfer has been shown to control SFE from hops in CFD simulations [45], the IMTC model has not yet been proposed for modeling SFE kinetics from hops [23]. According to the high goodness-of-fit achieved (MAPE <5%, presented in Table 2), the IMTC model may serve as a model of choice in the scope of essential oil extraction from hops.

3.2. Influence of pressure and temperature on extraction kinetics

The specific influence of extraction pressure and temperature on the essential oil profile is unknown *a priori*. Accordingly, relations of the kinetic model parameters as functions of pressure and temperature are required in order to predict extraction under different conditions. As a first step, the IMTC model was fitted to the single extraction curves. Based on the results, it was observed that all model parameters, i.e., $y^*(x_0)$, $k_i a$, and x_o changed with temperature and pressure. These relations to T and p can be described by the functions $c^*(\alpha, p, T)$ (see Equation (27)), $F_M(\beta, p, T)$ (see Equation (31)), and $x_0(\gamma, p, T)$ (see Equations (32) and (33)), respectively. The parameters β (6 parameters) and γ (6 or 3 parameters in case of α-pinene) were each fitted to all 18 fitted model parameters (see Figs. 4 and 5). Thereupon, α (3 parameters) was fitted to the extracted solute mass data $E(t)$ at all of the 9 pressure-temperature combinations investigated (162 data points in total; see Equation (34)), keeping β and γ constant.

The microstructural factor F_M, characteristic for the intraparticle diffusion hindrance, was calculated for each value of k_i and the parameter vector β, correlating F_M to pressure and temperature, was fitted (see Equations (29)–(31)). A plot of the fitted model function $F_M(p, T)$ is shown in Fig. 4 together with the 18 data points it was fitted to. The corresponding second-order models are:

$$\begin{pmatrix} F_{M,myrcene} \\ F_{M,humulene} \\ F_{M,total\ mass} \end{pmatrix} = \begin{pmatrix} \boldsymbol{\beta_{myrcene}} \\ \boldsymbol{\beta_{humulene}} \\ \boldsymbol{\beta_{total\ mass}} \end{pmatrix} \bullet \begin{pmatrix} 1 \\ p \\ T \\ p^2 \\ T^2 \\ pT \end{pmatrix} = \begin{pmatrix} 2.12e08 & 4.33e05 & -1.49e06 & -329 & 2.54e03 & -1.17e03 \\ -1.81e06 & 1.35e04 & 6.05e03 & 28.7 & 2.78 & -62.9 \\ -2.00e06 & 1.39e04 & 9.35e03 & 46.6 & -5.31 & -70.9 \end{pmatrix} \bullet \begin{pmatrix} 1 \\ p \\ T \\ p^2 \\ T^2 \\ pT \end{pmatrix} \quad (35)$$
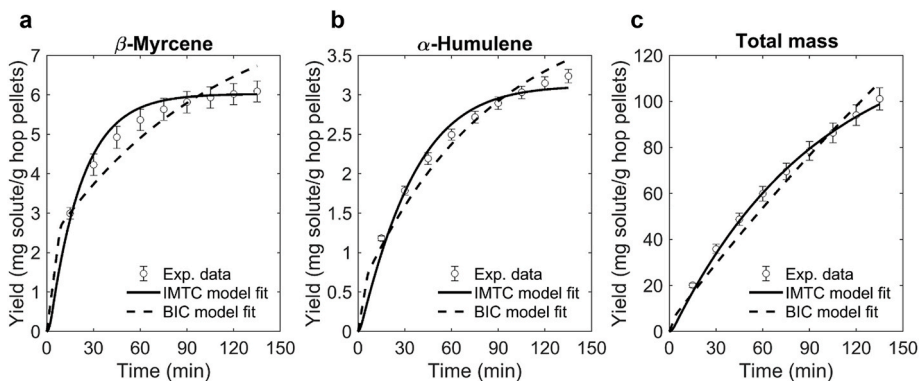

Fig. 3. Comparison of IMTC and BIC model fit for β-myrcene (a), α-humulene (b), and the total mass of extract (c) at 40 °C and 100 bar with standard deviation (duplicates).

Table 2

Model parameters of the IMTC and BIC model fitted to experimental data and respective mean absolute percentage error (MAPE) for condition T = 40 °C and p = 100 bar.

	β-Myrcene	α-Humulene	Total mass
IMTC model			
$k_i a$ (s^{-1})	8.66×10^{-4}	4.97×10^{-3}	1.25×10^{-3}
$y^*(x_0)$ (g g^{-1})	3.62×10^{-3}	3.73×10^{-4}	1.29×10^{-2}
x_0 (g g^{-1})	3.09×10^{-3}	1.60×10^{-3}	6.62×10^{-2}
MAPE (%)	3.67	4.57	3.18
AIC$_c$ (1)	48.30	36.96	84.27
BIC model			
r (1)	0.309	0.168	0.0149
$k_s a$ (s^{-1})	5.84×10^{-5}	9.76×10^{-5}	2.06×10^{-5}
$k_f a$ (s^{-1})	0.988	0.928	0.676
$y^*(x_{1,0})$ (g g^{-1})	1.18×10^{-3}	4.37×10^{-4}	6.09×10^{-3}
MAPE (%)	6.50	5.52	8.97
AIC$_c$ (1)	72.24	52.85	117.6

Table 3

Mean values of mean absolute percentage error (MAPE) and Akaike criterion (AIC$_c$) across all experimental conditions for each volatile and total mass analyzed.

	MAPE (%)		AIC$_c$ (1)	
	IMTC	BIC	IMTC	BIC
β-Myrcene	3.72	9.10	40.42	65.17
α-Humulene	6.45	4.48	35.47	43.21
2-Methylbutyl isobutyrate	4.71	4.04	−7.07	1.51
β-Caryophyllene	6.53	4.35	13.22	19.97
Undecanone	8.15	8.86	−27.24	−14.91
Linalool	9.50	4.43	−32.63	−33.73
α-Pinene	17.56	11.15	−51.33	−47.82
Total mass	4.22	5.85	77.38	95.75

$$
\begin{pmatrix} x_{0,myrcene} \\ x_{0,humulene} \\ x_{0,total\ mass} \end{pmatrix} = \begin{pmatrix} \gamma_{myrcene} \\ \gamma_{humulene} \\ \gamma_{total\ mass} \end{pmatrix} \cdot \begin{pmatrix} 1 \\ p \\ T \\ p^2 \\ T^2 \\ pT \end{pmatrix} = \begin{pmatrix} -19.4 & -0.738 & 0.467 & -3.26e-03 & -1.65e-03 & 4.63e-03 \\ -138 & 0.432 & 0.739 & 1.93e-05 & -9.38e-04 & -1.37e-03 \\ -1.23e04 & -8.57 & 82.5 & -3.33e-02 & -0.143 & 5.40e-02 \end{pmatrix} \cdot \begin{pmatrix} 1 \\ p \\ T \\ p^2 \\ T^2 \\ pT \end{pmatrix}
$$

(36)

The fitted parameters of β for all compounds are available in SI Table S4 online. Fig. 4 shows that the dependence of F_M on pressure and temperature differs for β-myrcene, α-humulene, and total mass. All of the other compounds exhibit a behavior similar to α-humulene, as can be seen in SI Figures S16-S20 online. An overall decrease of F_M is observed at increasing pressure and decreasing temperature for most essential oil components, a result which might be attributed to the increased co-extraction of cuticular waxes [12, 46]. It has been demonstrated by Gaspar [46] that an increased extraction of cuticular waxes at higher pressures leads to a simultaneous increase in essential oil extraction. The reduction of this wax barrier contributes to a decrease in intra-particle diffusion hindrance and an increase in exposure area of essential oils. Moreover, an enhanced disruption of glandular trichomes in which the major monoterpenes and sesquiterpenes are enclosed might explain this effect [47,48]. With regard to total mass, the tendency is the opposite, which might be linked to the selection of the pseudo-solute for the D_{12} correlation in this case (weighted average of representative compounds α-humulene, isohumulone, and lupulone according to Ref. [44]) or other model simplifications [12].

Surprisingly, the fitted initial mass fraction x_0 was found to systematically change with pressure and temperature, a behavior which was unexpected and which might be attributed to unrevealed physical or chemical phenomena not covered by the model assumptions, or mutual dependence of parameters. Please note that the approaches used by the authors employing a constant value of x_0 for all p-T conditions did not yield satisfactory fitting results. The fitted function of x_0 over pressure and temperature is depicted in Fig. 5, along with the parameters of γ listed in SI Table S4 online. The fitted function increases at increasing pressure and decreases at increasing temperature with respect to β-myrcene and total mass. This is also the case for 2-MBIB and α-pinene (see SI Figures S22 and S25 online). In contrast, α-humulene, β-caryophyllene (SI Figure S21 online), undecanone (SI Figure S23 online), and linalool (SI Figure S24 online) exhibit a different correlation, especially at high temperatures. Basically, changes in the initial molecular mass fractions with pressure and temperature might be attributed to a change in the accessibility of essential oil due to the removal of cuticular waxes [46] (increased exposure at higher pressure), the physical integrity of glandular trichomes [47], or due to other structural changes, such as swelling [34]. It should, however, be considered that the changes of x_0 might also be a consequence of parameter fitting and hence should be interpreted with caution in the absence of experimental evidence for this behavior.

a

b

c
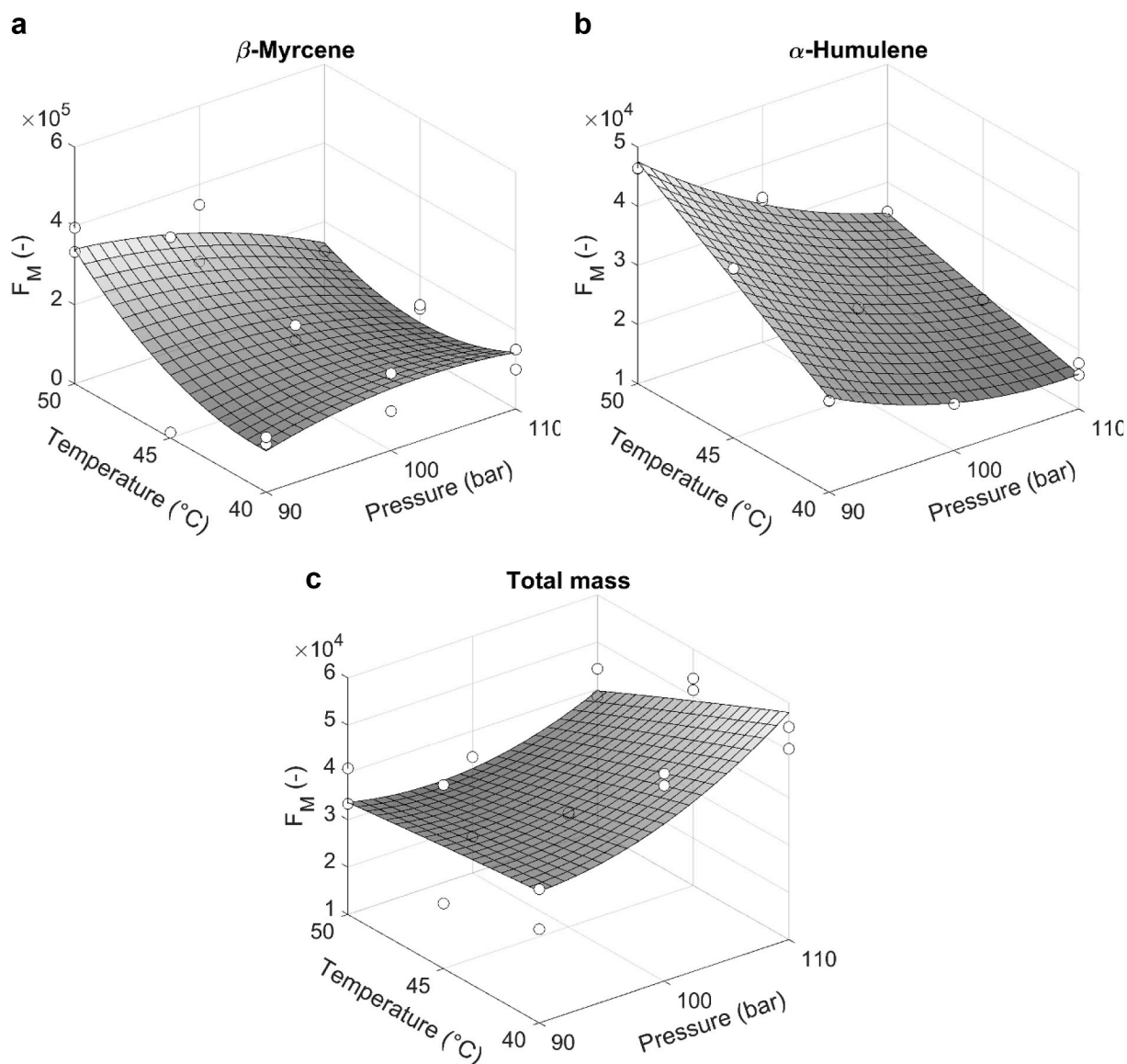
Fig. 4. Fits of microstructural factor F_M for β-myrcene (a), α-humulene (b), and the total mass of extract (c) as a function of temperature and pressure; surface plots of second-order model fitted to values of F_M obtained from fits to single experiments (◯).

Correlations of equilibrium mass fraction $y^*(x_0)$ with pressure and temperature conditions are described by the parameter vector $\boldsymbol{\alpha}$ (3 parameters; see Equations (27) and (28)). The results of $\boldsymbol{\alpha}$ are listed in Table 4 together with the MAPE average across all experiments. According to our results, the equilibrium concentrations increase with increasing pressure (α_1 positive) and decrease with increasing temperature (α_2 and α_3 negative) for all components. In other words, within the analyzed range, the lowest temperature (40 °C) and highest pressure (110 bar) were preferable for achieving the maximum essential oil yield.

This result is also evident from the extraction yield curves plotted in Figs. 6-8. Lines represent the simulated extraction kinetics of β-myrcene, α-humulene, and total mass, based on the parameterized IMTC model, whereas circles specify experimental data points (plots for other compounds available in SI Figures S26-S30 online). The highest yield is observed at 110 bar and 40 °C for most components (except linalool and undecanone; see SI Figures S11-12 online, attributed to experimental error). In a similar manner, the lowest total yield of the compounds analyzed in this research resulted from an extraction at 50 °C and 90 bar, i.e., the highest temperature and lowest pressure. Looking at yield vs. time, the highest extraction rates (slope of the curve) are always observed within the first 15 min, after which the rate of extraction decreased continuously until the end of the experiment, at 135 min. This result is in contrast to the findings by Van Opstaele et al. [20] and Langezaal et al. [49], who extracted hop oil components from hop powder and hop cones/leaves, respectively. The authors claimed that the extraction rates of some components (e.g., β-caryophyllene) can increase over time, which was not observed in our case. Comparing the sensitivity of the total extraction yield to temperature and pressure, the
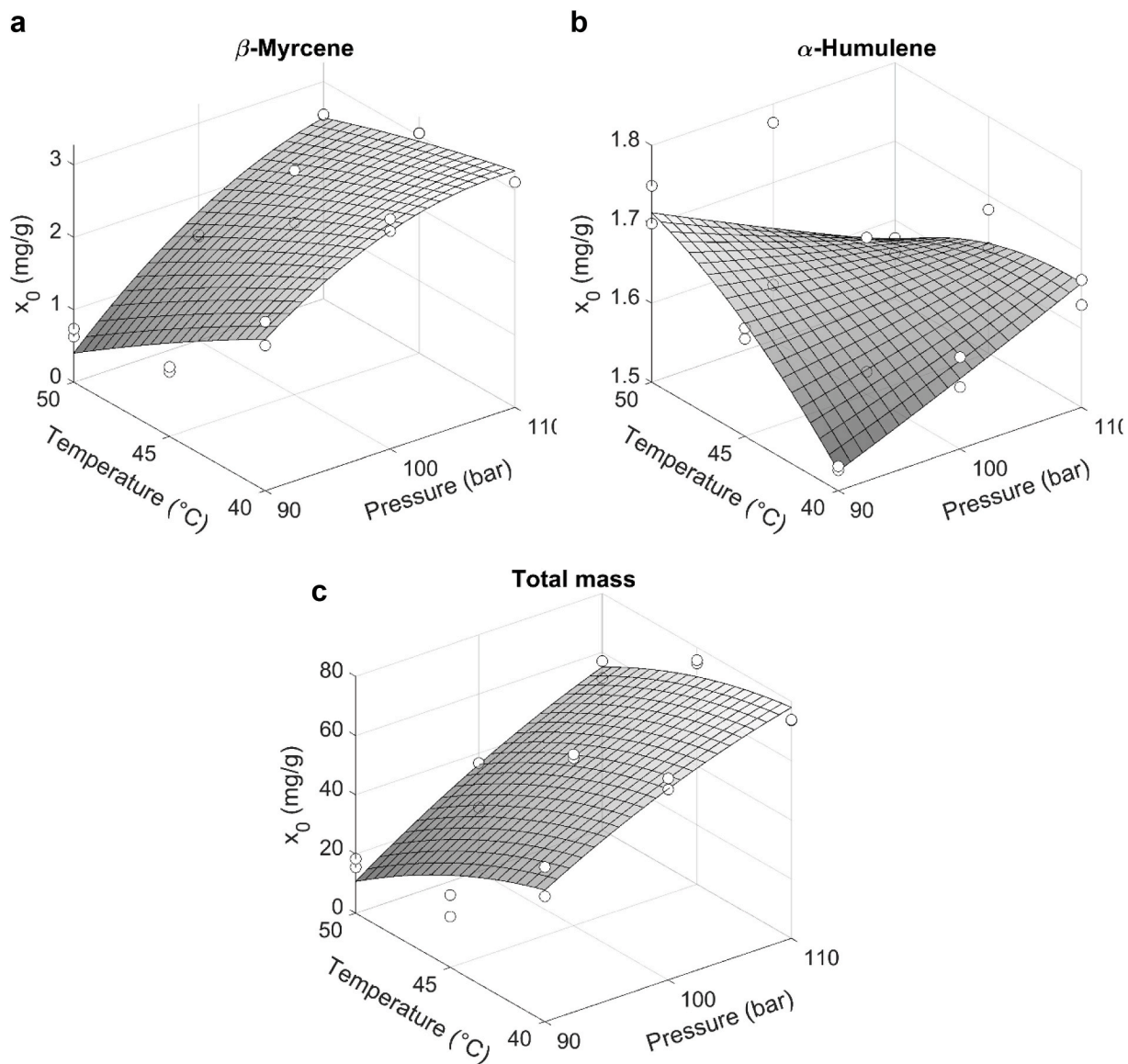
Fig. 5. Fits of initial solid-phase mass fraction x_0 for β-myrcene (a), α-humulene (b), and the total mass of extract (c) as a function of temperature and pressure; surface plots of second-order model fitted to values of x_0 obtained from fits to single experiments (○).

Table 4

Parameters of y*(x_0) as a function of temperature and pressure, fitted to all experimental data and the mean absolute percentage error (MAPE, average across all experiments).

Component	α_1	α_2	α_3	MAPE (%)
β-Myrcene	3.065	−2.638	−10.548	13.44
α-Humulene	2.822	−2.351	−12.194	8.38
β-Caryophyllene	2.789	−2.169	−13.801	8.11
2-Methylbutyl isobutyrate	2.005	−1.595	−11.218	7.29
Undecanone	2.547	−2.848	−12.746	12.40
Linalool	2.687	−0.575	−21.183	11.70
α-Pinene	2.784	−1.531	−20.034	26.75
Total mass	5.215	−2.745	−22.784	13.50
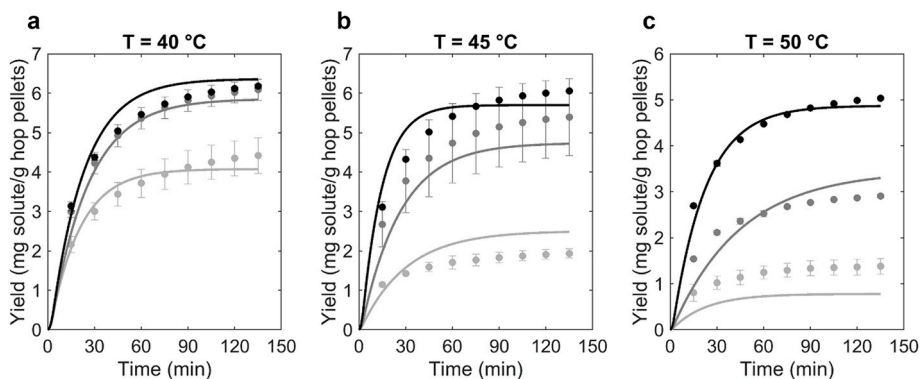
Fig. 6. Fitted extraction curves of β-myrcene (IMTC model) as functions of pressure and temperature at T = 40 °C (a), T = 45 °C (b), and T = 50 °C (c). Experimental data at p = 90 bar (●), p = 100 bar (●), and p = 110 bar (●) with standard deviation (duplicates) and IMTC model fits at p = 90 bar (−), p = 100 bar (−), and p = 110 bar (−).

effect of pressure variation is observed to be basically higher than the effect of temperature variation within the investigated range (see Figs. 6-8).

Regarding the goodness-of-fit, Table 4 shows the average MAPE values ranging between 7.29% for 2-MBIB and 26.75% for α-pinene. The results of MAPE for all individual experimental conditions are available in SI Table S5 online. For most components, the best goodness-of-fit was obtained at high pressures and low temperatures, corresponding to the highest yield. At high temperatures and low pressures, i.e., 50 °C and 90 bar, the goodness-of-fit was poor for most compounds, as was 45 °C and 90 bar, a partial explanation for which was the high standard deviation of measurements. Nevertheless, the authors are concluding that changes of scCO$_2$ extraction from hop pellets with temperature and pressure variation were able to be described appropriately for most experimental conditions and essential oil components.

The small nonpolar monoterpenes β-myrcene (Fig. 6) and α-pinene (SI Figure S30 online) extracted fastest for all tested conditions. In contrast, the large sesquiterpenes α-humulene (Fig. 7) and β-caryophyllene (SI Figure S26 online) both exhibited moderate extraction rates over the entire extraction time. This result agreed with the findings by Wei et al. [50], who investigated the SFE of α-humulene from clove oil. Molecules with intermediate molar mass (2-MBIB, undecanone, linalool), presented in SI Figures S27, S28, and S29 (available online), respectively, exhibit extraction behaviors in-between those of monoterpenes and sesquiterpenes. 2-MBIB shares similarities with the monoterpenes, undergoing a rather quick and exhaustive extraction. Linalool and undecanone are extracted more slowly. According to all these observations, extraction kinetics vary with different molecular structure and size: the smaller the molecule, the quicker it seems to be extracted.

In general, it was observed for all compounds that small variations in the operating conditions (5 °C or 10 bar) resulted in large changes in the extraction rate and essential oil composition. This result can be explained by the high compressibility of CO$_2$ in the pressure-temperature range under investigation, as well as the resulting variation in solvent capacity. Overall, the increase in yield at an increasing pressure and a decreasing temperature is variously pronounced for the aroma compounds. More precisely, a change in temperature, pressure, or extraction time leads to a change in the final extract composition. Comparing Figs. 6 and 7, this is particularly applicable to β-myrcene and α-humulene since the variation of yield with a change in pressure is considerably higher for β-myrcene than it is for α-humulene, i.e., pressure is expected to influence the mass ratio of these two components.
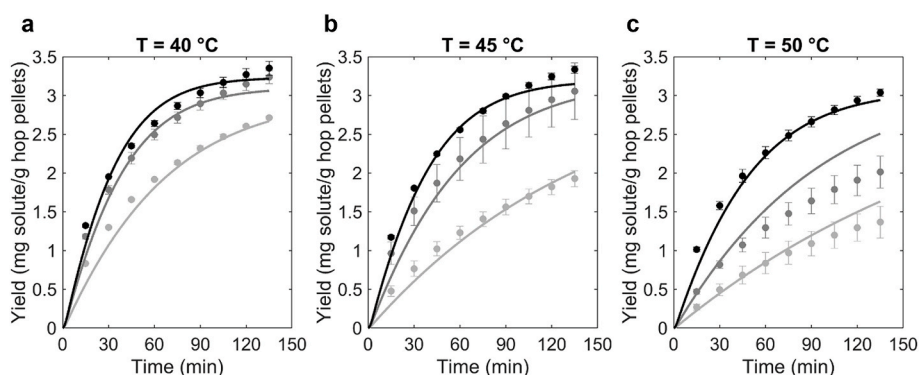
Fig. 7. Fitted extraction curves of α-humulene (IMTC model) as functions of pressure and temperature at T = 40 °C (a), T = 45 °C (b), and T = 50 °C (c). Experimental data at p = 90 bar (●), p = 100 bar (●), and p = 110 bar (●) with standard deviation (duplicates) and IMTC model fits at p = 90 bar (−), p = 100 bar (−), and p = 110 bar (−).
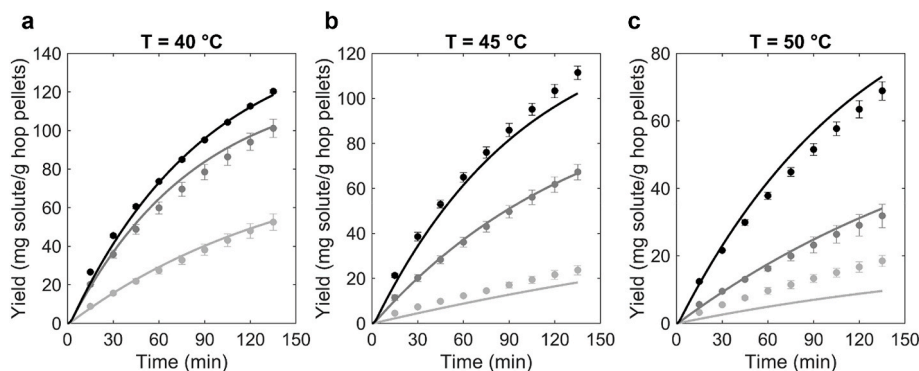
Fig. 8. Fitted extraction curves of total mass (IMTC model) as functions of pressure and temperature at T = 40 °C (a), T = 45 °C (b), and T = 50 °C (c). Experimental data at p = 90 bar (●), p = 100 bar (●), and p = 110 bar (●) with standard deviation (duplicates) and IMTC model fits at p = 90 bar (—), p = 100 bar (—), and p = 110 bar (—).

To the best of the authors' knowledge, this is the first research investigating the extraction kinetics of various different essential oil components extracted from hops and their sensitivity towards pressure and temperature. In a recent study by Nagybákay et al. (2021) [21], response surface methodology was applied to the total extract yield of SFE from hops. However, the essential oil composition of those extracts was only determined at four conditions without evaluating the kinetics of different compounds. In this study, the presented approach combines the correlation analysis of the response surface methodology regarding temperature and pressure with mechanistic modeling of extraction kinetics, and hence allows a better understanding of how aroma composition develops in the course of time.

3.3. Prediction and model validation

In order to evaluate the IMTC model prediction using the determined correlations of $k_i a(p, T)$ (based on Equations (8), (29), (30) and (35)), $y^*(p, T)$ (Equations (27) and (28)), and $x_0(p, T)$ (Equation (36)), additional extraction experiments were performed at (i) 95 bar and 48 °C, (ii) 105 bar and 42 °C, and (iii) 105 bar and 48 °C. In Fig. 9, the three simulated extraction curves are plotted together with experimental data for β-myrcene, α-humulene, and total mass. The plots for all other analyzed volatiles are available in SI Figures S31-S35 online; respective MAPE values are listed in SI Table S6 online. A good agreement of extraction kinetics is observed for α-humulene and total mass, whereas β-myrcene lacks prediction accuracy, especially at the end of extraction. An overprediction of yield after 30 min is observed for all experiments in this case. Comparing the relative deviation between predictions and experiments for all compounds, as presented in Table 5, the large sesquiterpenes α-humulene and β-caryophyllene, as well as 2-MBIB, exhibit the highest overall prediction accuracy, with a relative error between 1.5% (α-humulene at 105 bar and 42 °C and 48 °C) and 17.3% (β-caryophyllene at 95 bar and 48 °C). In contrast, the small monoterpenes β-myrcene and α-pinene are furthest from the experimental results, with a deviation of up to 44.1% (α-pinene at 105 bar and 48 °C after 30 min). One reason for this lack of predictability might have been a higher variation in the concentrations of monoterpenes. A lower overall content of β-myrcene after, in this case, approximately 5 months of storage due to chemical reactions or differences in phase partitioning could explain the overprediction in yield. The predicted qualitative changes are, however, correct for these compounds. At a high pressure and low temperature, i.e., at a higher CO$_2$ density, the overall error is lower for most components, which agreed with the former fitting results. From the economical perspective of an industrial user, conditions leading to higher total essential oil yields should be more attractive for application. Given that the region of interest is then the region at higher pressures, which is represented well by the IMTC model for most components and total mass (see Table 5, center and right column), we consider these limitations on accuracy to be acceptable and recommend using the model for pressures between 100 and 110 bar and temperatures between 40 and 45 °C.

Fig. 10 presents the essential oil profile of the four major oil components β-myrcene, α-humulene, β-caryophyllene, and 2-MBIB as prediction plots with different markers. The total amount of oil is approximated in this case by the sum of all seven quantified essential oil components. Values for compound content after 30 min of extraction are shown in grey, and the final content after 135 min is depicted in black. The predicted and measured contents matched well for the major components β-myrcene, α-humulene, β-caryophyllene, and 2-MBIB under all of the experimental conditions tested. Moreover, the plots highlight the differences in the extraction kinetics of monoterpenes and sesquiterpenes, and it is evident that the content of β-myrcene was much higher after 30 min than after 135 min, when the β-myrcene and α-humulene contents converged and were almost equal at 95 bar and 48 °C. This result again demonstrates that the extraction time represents another important variable to be optimized, e.g., for maximizing β-myrcene content.

Overall, the results prove that the proposed modeling approach, taking into account the parameterization for seven volatiles, is appropriate to predict the aroma composition within the experimental space of 90–110 bar and 40–50 °C. The suggested parameter fitting method applied in this scope is especially useful for components which are not freely available, e.g. due to their entrapment in glandular trichomes, and thus cannot be predicted solely by solubility models [51]. To apply the obtained results on a larger scale, it is, however, recommended to compare qualitative changes predicted by the model with large-scale experimental results, as the scope of validation is limited to the laboratory scale and the setting described in Section 2.2.1.
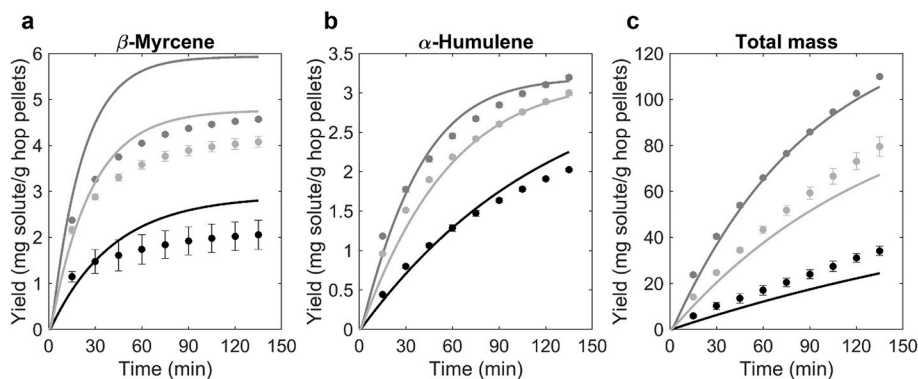
Fig. 9. IMTC model predictions of β-myrcene (a), α-humulene (b), and total mass (c) vs. experiments. Experimental data at 105 bar and 48 °C (●), 105 bar and 42 °C (●), 95 bar and 48 °C (●) with standard deviation (duplicates) and IMTC model predictions at 105 bar and 48 °C (—), 105 bar and 42 °C (—), and 95 bar and 48 °C (—).

Table 5
Relative deviation between predicted and measured extracted mass of solute after 30 min and 135 min at three different pressure and temperature conditions.

Component	Relative deviation of predicted solute mass from experiments (%)					
	95 bar and 48 °C		105 bar and 42 °C		105 bar and 48 °C	
	30 min	135 min	30 min	135 min	30 min	135 min
β-Myrcene	1.0	36.2	37.7	29.6	11.1	16.3
α-Humulene	11.3	11.2	2.9	1.5	15.0	1.5
β-Caryophyllene	3.9	17.3	5.1	4.3	9.3	3.2
2-Methylbutyl isobutyrate	9.4	6.4	15.6	9.6	3.4	1.9
Undecanone	14.9	7.1	2.9	6.6	8.6	4.0
Linalool	29.8	1.2	10.4	19.9	16.8	14.6
α-Pinene	27.4	3.8	29.2	7.4	44.1	28.7
Total mass	38.7	28.4	8.9	4.0	17.8	15.4
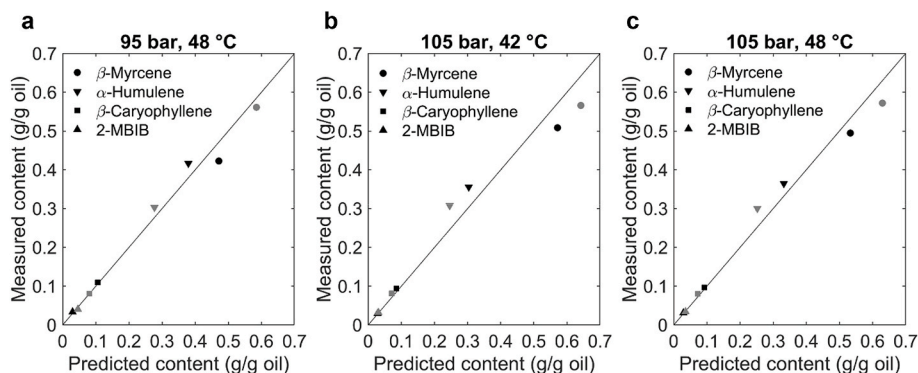
Fig. 10. Comparison of predicted and measured contents in the oil fraction of β-myrcene, α-humulene, β-caryophyllene, and 2-methylbutyl iso-butyrate (2-MBIB) at 95 bar/48 °C (a), 105 bar/42 °C (b), and 105 bar/48 °C (c) after 135 min (●, ▼, ■, ▲) and 30 min (●, ▼, ■, ▲). The solid line marks zero prediction error.

4. Conclusions

The research presented herein demonstrates, through the example of hop pellet extraction using supercritical CO_2, that a com-bination of mechanistic modeling and fitting the model parameters as functions of temperature and pressure to experimental data enables the prediction of essential oil yield and composition. Our research found the internal-mass-transfer-control (IMTC) model [28] to be preferable over the broken-and-intact-cells model [31] (based on the modified Akaike criterion). The IMTC model was found to describe the extraction kinetics of all essential oil compounds adequately allowing the modeling of essential oil composition at different extraction times within the maximum extraction time evaluated. Three model parameters – mass transfer coefficient, initial

equilibrium concentration, and initial solid-phase concentration – were successfully described as functions of temperature and pressure by least-squares parameter fitting to the extraction kinetics of essential oil components. Unexpected changes of the solid-phase concentration with pressure and temperature were determined by parameter fitting which indicates that the physical meaning of this parameter should be interpreted with caution and might be attributed to parameter interdependence. Our results show that the yield of essential oil components increases with a rise in pressure and decreases with a rise in temperature in the range of 90–110 bar and 40–50 °C, respectively. This behavior could be described by the parameterized solubility model by Chrastil [43]. Quite different extraction kinetics and pressure sensitivities of the monoterpene β-myrcene and the sesquiterpene α-humulene highlight the fact that extract composition is adjustable through a systematic selection of processing conditions. The predictive performance of the parameterized IMTC model was shown to be excellent for sesquiterpenes, whereas the prediction of the monoterpene extraction was unsatisfactory, possibly due to evaporation when storing the material, or due to effects not considered by the model assumptions. Nonetheless, the essential oil composition was able to be predicted with a generally high level of accuracy, which represents a quick and low-cost alternative to the experimental trial-and-error strategies. Upscaling and transferability studies to other operating conditions and raw materials are beyond the scope of this article and may be investigated in future studies.

Prospectively, our findings may pave the way for process optimization with respect to temperature, pressure, and time of extraction. In order to further improve both prediction performance and generalizability, and to investigate the validity of model assumptions, additional analyses of flow and solute partitioning are recommended in the future. Potential industrial applications include the production of tailored hop aroma extracts using supercritical fluid extraction, for which model-based optimization can be applied. The aroma-intense extract can be used for the flavoring and standardization of beer in the cold stage prior to filling as an alternative to dry hopping methods. This would enable a reduction in raw material consumption and provide new products with elevated sensory quality.

Author contribution statement

Verena Bernadette Pannusch: Performed the experiments; Analyzed and interpreted the data; Contributed reagents, materials, analysis tools or data; Wrote the paper.

Lukas Viebahn: Conceived and designed the experiments; Performed the experiments; Analyzed and interpreted the data; Wrote the paper.

Heiko Briesen: Analyzed and interpreted the data.

Mirjana Minceva: Conceived and designed the experiments; Analyzed and interpreted the data; Contributed reagents, materials, analysis tools or data.

Data availability statement

Data will be made available on request.

Declaration of interest's statement

The authors declare no competing interests.

Appendix A. Solid density and porosity

The solid density ρ_s measured by helium pycnometry before extraction was 1312 kg m^{-3} ± 2 kg m^{-3} and 1316 kg m^{-3} ± 10 kg m^{-3} after 135 min of extraction at 90 bar and 45 °C. Given that the change of density throughout extraction proved to be within the standard deviation, the solid density value after extraction was used as a parameter for the simulations of extraction kinetics and assumed to be constant throughout extraction. The total porosity ε, calculated according to Equation (4) was found to be 0.49 before and 0.50 after 135 min of extraction at 90 bar and 45 °C. Due to this very small change, a constant porosity of $\varepsilon = 0.50$ was defined for simulations.

Appendix B. Supplementary data

Supplementary data related to this article can be found at https://doi.org/10.1016/j.heliyon.2023.e13030.

References

[1] M. Herrero, et al., Supercritical fluid extraction: recent advances and applications, J. Chromatogr. A 1217 (16) (2010) 2495–2511.

[2] V. Illés, et al., Extraction of coriander seed oil by CO_2 and propane at super-and subcritical conditions, J. Supercrit. Fluids 17 (2) (2000) 177–186.

[3] D.G. Wilson, Plant remains from the Graveney boat and the early history of *Humulus lupulus* L. in W. Europe, New Phytol. 75 (3) (1975) 627–648.

[4] K. Goiris, et al., The flavoring potential of hop polyphenols in beer, J. Am. Soc. Brew. Chem. 72 (2) (2014) 135–142.

[5] W.J. Simpson, P.S. Hughes, Stabilization of Foams by Hop-Derived Bitter Acids. Chemical Interactions in Beer Foam, Cerevisia and Biotechnology, Belgium), 1994.

[6] C. Almaguer, et al., Humulus lupulus - a story that begs to be told. A review, J. Inst. Brew. 120 (4) (2014) 289–314.

[7] N. Rettberg, M. Biendl, L.-A. Garbe, Hop aroma and hoppy beer flavor: chemical backgrounds and analytical tools - a review, J. Am. Soc. Brew. Chem. 76 (1) (2018) 1–20.

[8] F. Sharpe, D. Laws, The essential oil of hops a review, J. Inst. Brew. 87 (2) (1981) 96–107.

[9] M. Biendl, et al., 1, Fachverlag Hans Carl. (2015) 53–54.

[10] Y. Liu, et al., Antioxidant activities of hops (*Humulus lupulus*) and their products, J. Am. Soc. Brew. Chem. 65 (2) (2007) 116–121.

[11] T. Fornari, et al., Isolation of essential oil from different plants and herbs by supercritical fluid extraction, J. Chromatogr. A 1250 (2012) 34–48.

[12] K. Araus, E. Uquiche, J.M. del Valle, Matrix effects in supercritical CO_2 extraction of essential oils from plant material, J. Food Eng. 92 (4) (2009) 438–447.

[13] S.M. Pourmortazavi, S.S. Hajimirsadeghi, Supercritical fluid extraction in plant essential and volatile oil analysis, J. Chromatogr. A 1163 (1–2) (2007) 2–24.

[14] M.M.R. de Melo, A.J.D. Silvestre, C.M. Silva, Supercritical fluid extraction of vegetable matrices: applications, trends and future perspectives of a convincing green technology, J. Supercrit. Fluids 92 (2014) 115–176.

[15] L. Baldino, R. Adami, E. Reverchon, Concentration of Ruta graveolens active compounds using SC-CO_2 extraction coupled with fractional separation, J. Supercrit. Fluids 131 (2018) 82–86.

[16] L.C. dos Santos, et al., Integrated supercritical CO_2 extraction and fractionation of passion fruit (Passiflora edulis Sims) by-products, J. Supercrit. Fluids (2021) 168.

[17] A. Forster, et al., Advances in hop extraction with supercritical carbon dioxide, Brauwelt Int. 5 (2020) 324–330.

[18] D. De Kjujkeleire, et al., Automated reporting on the quality of hops and hop products, J. Inst. Brew. 104 (2) (1998) 75–82.

[19] M. Verschuere, P. Sandra, F. David, Fractionation by SFE and microcolumn analysis of the essential oil and the bitter principles of hops, J. Chromatogr. Sci. 30 (10) (1992) 388–391.

[20] F. Van Opstaele, et al., Production of novel varietal hop aromas by supercritical fluid extraction of hop pellets - Part 2: preparation of single variety floral, citrus, and spicy hop oil essences by density programmed supercritical fluid extraction, J. Supercrit. Fluids 71 (2012) 147–161.

[21] N.E. Nagybákay, et al., Optimized supercritical CO_2 extraction enhances the recovery of valuable lipophilic antioxidants and other constituents from dual-purpose hop (*Humulus lupulus* L.) variety ella, Antioxidants 10 (918) (2021).

[22] K. Bizaj, et al., Sub-and supercritical extraction of slovenian hops (Humulus lupulus L.) aurora variety using different solvents, Plants 10 (6) (2021) 1137.

[23] S.C. Kupski, et al., Mathematical modeling of supercritical CO_2 extraction of hops (*Humulus lupulus* L.), J. Supercrit. Fluids 130 (2017) 347–356.

[24] H. Sovová, Rate of the vegetable oil extraction with supercritical CO_2 - I. Modelling of extraction curves, Chem. Eng. Sci. 49 (3) (1994) 409–414.

[25] E.M.C. Reis-Vasco, et al., Mathematical modelling and simulation of pennyroyal essential oil supercritical extraction, Chem. Eng. Sci. 55 (15) (2000) 2917–2922.

[26] M.R. García-Risco, et al., Kinetic study of pilot-scale supercritical CO_2 extraction of rosemary (Rosmarinus officinalis) leaves, J. Supercrit. Fluids 55 (3) (2011) 971–976.

[27] P.M. Moura, et al., Supercritical fluid extraction from guava (Psidium guajava) leaves: global yield, composition and kinetic data, J. Supercrit. Fluids 62 (2012) 116–122.

[28] J.M. del Valle, P. Napolitano, N. Fuentes, Estimation of relevant mass transfer parameters for the extraction of packed substrate beds using supercritical fluids, Ind. Eng. Chem. Res. 39 (12) (2000) 4720–4728.

[29] K. Verschueren, Dry hopping process challenges, Brauwelt Int. 2 (2019) 127–129.

[30] D. Saison, et al., Optimisation of a complete method for the analysis of volatiles involved in the flavour stability of beer by solid-phase microextraction in combination with gas chromatography and mass spectrometry, J. Chromatogr. A 1190 (1–2) (2008) 342–349.

[31] H. Sovová, Mathematical model for supercritical fluid extraction of natural products and extraction curve evaluation, J. Supercrit. Fluids 33 (1) (2005) 35–52.

[32] E. Reverchon, C. Marrone, Supercritical extraction of clove bud essential oil: isolation and mathematical modeling, Chem. Eng. Sci. 52 (20) (1997) 3421–3428.

[33] E. Reverchon, Mathematical modeling of supercritical extraction of sage oil, AIChE J. 42 (6) (1996) 1765–1771.

[34] M. Stamenic, et al., Swelling of plant material in supercritical carbon dioxide, J. Supercrit. Fluids 52 (1) (2010) 125–133.

[35] A. Berna, A. Cháfer, J.B. Montón, Solubilities of essential oil components of orange in supercritical carbon dioxide, J. Chem. Eng. Data 45 (5) (2000) 724–727.

[36] J. da Cruz Francisco, B. Sivik, Solubility of three monoterpenes, their mixtures and eucalyptus leaf oils in dense carbon dioxide, J. Supercrit. Fluids 23 (1) (2002) 11–19.

[37] W.G. Bickley, Formulae for numerical differentiation, Math. Gaz. 25 (263) (2016) 19–27.

[38] J. Puiggené, M.A. Larrayoz, F. Recasens, Free liquid-to-supercritical fluid mass transfer in packed beds, Chem. Eng. Sci. 52 (2) (1997) 195–212.

[39] O.J. Catchpole, M.B. King, Measurement and correlation of binary diffusion coefficients in near critical fluids, Ind. Eng. Chem. Res. 33 (7) (1994) 1828–1837.

[40] R. Span, W. Wagner, A new equation of state for carbon dioxide covering the fluid region from the triple-point temperature to 1100 K at pressures up to 800 MPa, J. Phys. Chem. Ref. Data 25 (6) (1996) 1509–1596.

[41] A. Laesecke, C.D. Muzny, Reference correlation for the viscosity of carbon dioxide, J. Phys. Chem. Ref. Data 46 (1) (2017).

[42] M.R.E. Symonds, A. Moussalli, A brief guide to model selection, multimodel inference and model averaging in behavioural ecology using Akaike's information criterion, Behav. Ecol. Sociobiol. 65 (1) (2010) 13–21.

[43] J. Chrastil, Solubility of solids and liquids in supercritical gases, J. Phys. Chem. 86 (15) (1982) 3016–3021.

[44] J.M. del Valle, et al., *Mass transfer and equilibrium parameters on high-pressure CO_2 extraction of plant essential oils*, in: Food Engineering Interfaces, Springer, 2010, pp. 393–470.

[45] A. Formato, et al., Supercritical fluid extraction of α-and β-acids from hops compared to cyclically pressurized solid–liquid extraction, J. Supercrit. Fluids 84 (2013) 113–120.

[46] F. Gaspar, *Extraction of essential oils and cuticular waxes with compressed CO_2: Effect of extraction pressure and temperature*, Ind. Eng. Chem. Res. 41 (10) (2002) 2497–2503.

[47] F. Gaspar, R. Santos, M.B. King, Disruption of glandular trichomes with compressed CO_2: alternative matrix pre-treatment for CO_2 extraction of essential oils, J. Supercrit. Fluids 21 (1) (2001) 11–22.

[48] G. Wang, et al., Terpene biosynthesis in glandular trichomes of hop, Plant Physiol. 148 (3) (2008) 1254–1266.

[49] C.R. Langezaal, et al., Analysis of supercritical carbon dioxide extracts from cones and leaves of a *Humulus lupulus* L cultivar, J. Sci. Food Agric. 53 (4) (1990) 455–463.

[50] M.-C. Wei, J. Xiao, Y.-C. Yang, Extraction of a-humulene-enriched oil from clove using ultrasound-assisted supercritical carbon dioxide extraction and studies of its fictitious solubility, Food Chem. 210 (2016) 172–181.

[51] L.M. Valenzuela, A.G. Reveco-Chilla, J.M. del Valle, Modeling solubility in supercritical carbon dioxide using quantitative structure–property relationships, J. Supercrit. Fluids 94 (2014) 113–122.